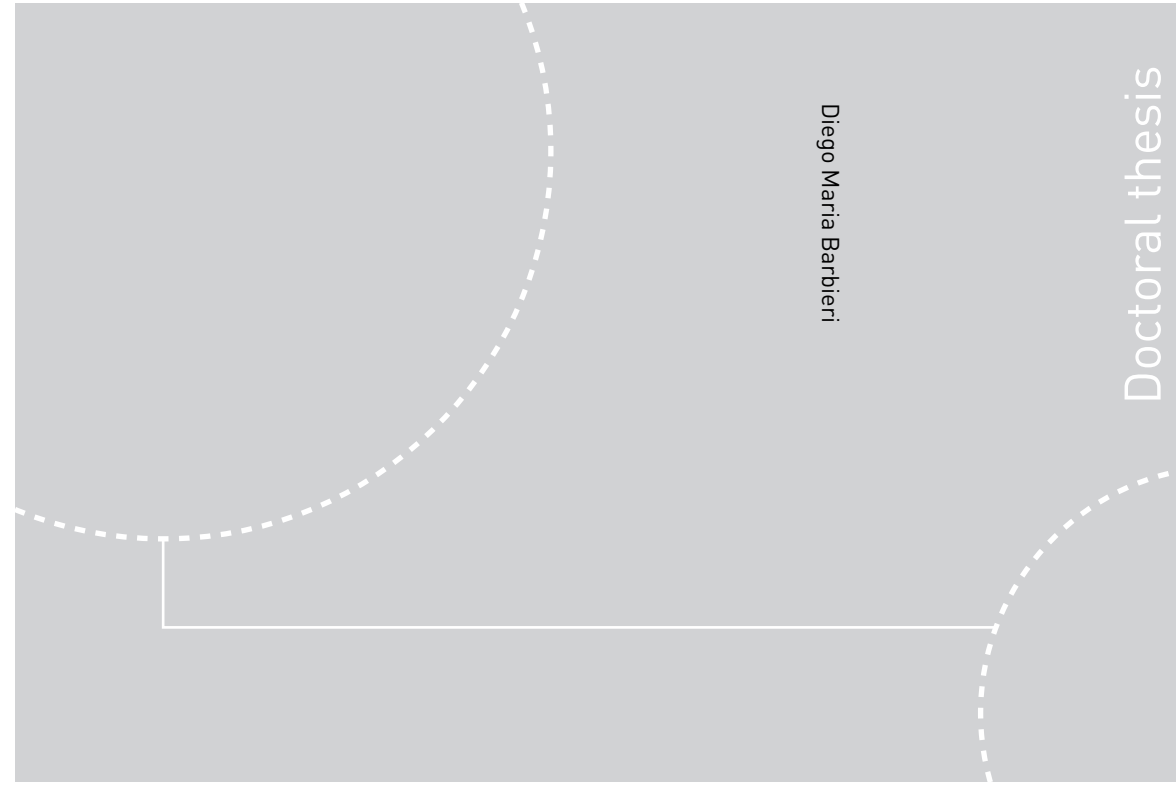


ISBN 978-82-326-3622-8 (printed ver.)
ISBN 978-82-326-3623-5 (electronic ver.)
ISSN 1503-8181



Doctoral theses at NTNU, 2019:28

Diego Maria Barbieri

USE OF LOCAL MATERIALS FOR ROAD CONSTRUCTION

Innovative Stabilization Techniques for
Crushed Rocks

 **NTNU**
Norwegian University of
Science and Technology

Doctoral theses at NTNU, 2019:28

NTNU
Norwegian University of Science and Technology
Thesis for the Degree of
Philosophiae Doctor
Faculty of Engineering
Department of Civil and Environmental
Engineering

 NTNU

 **NTNU**
Norwegian University of
Science and Technology

Diego Maria Barbieri

USE OF LOCAL MATERIALS FOR ROAD CONSTRUCTION

Innovative Stabilization Techniques for Crushed
Rocks

Thesis for the Degree of Philosophiae Doctor

Trondheim, January 2019

Norwegian University of Science and Technology
Faculty of Engineering
Department of Civil and Environmental Engineering



Norwegian University of
Science and Technology

NTNU

Norwegian University of Science and Technology

Thesis for the Degree of Philosophiae Doctor

Faculty of Engineering

Department of Civil and Environmental Engineering

© Diego Maria Barbieri

ISBN 978-82-326-3622-8 (printed ver.)

ISBN 978-82-326-3623-5 (electronic ver.)

ISSN 1503-8181

Doctoral theses at NTNU, 2019:28

Printed by NTNU Grafisk senter

USE OF LOCAL MATERIALS FOR ROAD CONSTRUCTION

Innovative Stabilization Techniques for Crushed Rocks

Diego Maria Barbieri

Thesis submitted to the
Department of Civil and Environmental Engineering,
Faculty of Engineering Science and Technology,
Norwegian University of Science and Technology (NTNU),
in partial fulfilment of the requirements for the degree of philosophiae doctor.

Trondheim
October, 2018

*For all the stone, which is mill-stone and hard by nature,
Appius quarried in another place far away and brought there;
for it is not found anywhere in that district.*

Procopius of Caesarea (History of the Wars, V, xiv 7-14)

ACKNOWLEDGEMENTS

This Ph.D. project has been carried out at the Norwegian University of Science and Technology (NTNU), Department of Civil and Environmental Engineering. This Ph.D. thesis is part of the major project “Ferry-free coastal highway route E39” promoted by Norwegian Public Roads Administration, which is greatly acknowledged for having established and financed such a challenging research mission.

First of all, I wish to express my most sincere appreciation and profound gratitude to my supervisor Professor Inge Hoff (NTNU) for his insightful guidance, constructive dialogues and inspiring attitude; I have been able to delve into a stimulating and exciting research project under his guidance. I am deeply grateful to my co-supervisor Dr. Lillian Mathisen Uthus (Veidekke Industry) for her precious suggestion and continuous support. I also wish to express my deep gratitude to Professor Chun-Hsing Ho and thank him for having arranged a three-month stay at Northern Arizona University (NAU), Civil and Environmental, Flagstaff, USA.

The research has involved many individuals from several parts and industries, they have eagerly and constantly contributed. Dr. Carl Thodesen (NTNU), Professor Helge Mork (NTNU), Professor Mai Britt Engeness Mørk (NTNU), laboratory assistants Lisbeth Johansen (SINTEF), Bent Lervik (NTNU) and Jan Erik Molde (NTNU) are greatly acknowledged for their invaluable suggestion, discussions and ideas. Their constant support has been crucial to the accomplishment of this work. Furthermore, I would like to thank all my friends and research fellows who have enriched the Ph.D. experience and inspired the work in many ways.

The precious cooperation kindly offered by Sparks AS (Asker, Norway), Zydex Industries (Vadodara, India), Borregaard AS (Sarpsborg, Norway), Franzefoss Pukkverk avd. Vassfjell (Heimdal, Norway) and Veidekke Industry (Trondheim, Norway) has been truly appreciated.

Last but not least, I would like to extend my thanks to my parents Ivo and Claudia, siblings Saverio and Aurora for their love, patience and encouragement throughout my studies. This has been a long and challenging journey and none of these could have been possible without them.

Trondheim, October 2018
Diego Maria Barbieri

SUMMARY

The Norwegian Public Roads Administration is currently running the “Ferry-free coastal route E39” project, which reduces the travel time along the Norwegian highway E39 connecting Trondheim to Kristiansand. The plan includes the creation of several long tunnels, which will generate a surplus of blasted rocks; these unbound granular materials are often damaged from the intensive blasting and will in many cases fail the strict criteria stated in the pavement design guidelines. However, they could be used in the road unbound layers close to the place of production, entailing a sustainable cost-benefit application.

The geology encountered along the E39 road alignment is mapped: several rock types (igneous, sedimentary and metamorphic) are spread in the locations of the tunnelling operations. The existing code defines requirements for road unbound layers in terms of Los Angeles (LA) and micro-Deval (MDE) tests. The major part of the rocks has igneous origin and fulfils the standard check procedures (“strong” rocks); anyway, a considerable quantity of the rocks having different origin does not (“weak” rocks). The materials collected and used for the research mission are characterized by means of thin-section microscopy, X-Ray Diffractometry (XRD), X-Ray Fluorescence (XRF) and Scanning Electron Microscope (SEM). Moreover, the crushability of some different rock types connected to the road construction phase and service life phase is analysed.

The research investigates how to promote the use of the “weak” rocks using some possible techniques in the laboratory. The first approach is the mixture between the various types of rocks available in situ. The second approach is additive application; two different non-traditional additive types are examined: one is polymer-based, the other one is lignin-based. Repeated Triaxial Load Tests (RTL) are used to assess the additives’ effectiveness. The results are interpreted according to some models available in literature and a finite element model is developed to simulate the repeated triaxial load test and compare its results.

Finally, the research investigates the performance of the additives in the field. Three typical base layer sections are built and added with water (no treatment), water and polymer-based additive, water and lignin-based additive, respectively. The development of the layers’ stiffness and deformation properties are mainly assessed by means of Light Weight Deflectometer (LWD). Dynamic Cone Penetrometer (DCP) and rutting formation evaluation also contribute to investigate the field performance.

The results of laboratory and field test campaigns indicate that both the polymer-based and lignin-based products can enhance the mechanical properties of the “weak” crushed rocks.

SAMMENDRAG (in Norwegian)

Statens Vegvesen driver for tiden med veiprojektet «Ferjefri E39», som skal redusere reisetiden langs den norske motorveien E39 som knytter Trondheim til Kristiansand. Planen omfatter byggingen av flere lange tunneller, som vil føre til et overskudd av sprengt stein; disse ubundne granulære materialene blir ofte skadet fra intensiv sprengning og i mange tilfeller kan de ikke tilfredsstillende strenge kravene i veinormalene. Om de kan brukes likevel i de ubundne lagene i nærheten av produksjonsstedet kan det gi en bærekraftig og kostnadseffektiv anvendelse.

Geologien langs E39 er kartlagt: det finnes flere bergarter (eruptive, sedimentære, metamorfe) på de stedene hvor tunnelsprengning gjennomføres. Den nåværende normalen stiller krav til de ubundne veilagene i forhold til Los Angeles (LA) og micro-Deval (MDE) tester. Bergartene er hovedsakelig eruptive og oppfyller standard kontroll prosedyrer (“sterke” bergarter). Uansett er en betydelig mengde bergarter preget av en annen geologisk opprinnelse og oppfyller ikke kravene (“svake” bergarter). Materialene som samles og brukes til undersøkelsen karakteriseres ved tynnslip analyse, røntgenkrystallografi (XRD), røntgenfluorescens (XRF) og sveipelektronmikroskop (SEM). I tillegg blir knusingsegenskaper av granulære materialer undersøkt, både i konstruksjonsfasen og levetidsfasen til en vei.

Forskningen blir utført på laboratoriet med formål å finne ut hvordan man kan benytte seg av de “svake” bergartene ved å undersøke noen mulige teknikker. Den første tilnærmingen er å blande de forskjellige bergartene som befinner seg på stedet. Den andre tilnærmingen er å bruke tilsetningsstoff; to forskjellige ikke-tradisjonelle stoff benyttes: ett er polymerbasert og ett er ligninbasert. Treksialforsøk (RTL) brukes for å vurdere effekten av tilsetningsstoffene. Resultatene blir tolket basert på flere modeller som er tilgjengelige i litteratur og element-modeller blir utviklet for å beskrive treksialforsøk og sammenligne resultatene.

Til slutt blir ytelsen til tilsetningsstoffene i felt undersøkt. Tre typiske bærelag blir bygd opp og tilsatt henholdsvis vann (ingen behandling), vann og polymer basert tilsetningsstoff, vann og ligninbasert tilsetningsstoff. Forløpet av stivhet- og deformasjonsegenskaper blir overvåket hovedsakelig med lett fallodd (FWD). Dynamic Cone Penetrometer (DCP) og spordannelse evaluering bidrar også til å bedømme ytelsen på feltet.

Resultatene til lab- og felttester framhever at både de polymerbaserte og ligninbaserte tilsetningsstoffene kan forbedre de mekaniske egenskapene av de “svake” bergartene.

概要 (in Chinese)

挪威交通部目前正在进行“无渡轮沿海 E39 路线”项目。该项目连接特隆赫姆市与到克里斯蒂安桑市，主要目的是缩短行程时间。本项目将会沿着 E39 路线建造许多长隧道，在隧道施工及爆破过程中会生产许多碎石。密集爆破过程会损坏原始岩石构造，因此在很多情况下，这些爆破的碎石材料无法满足规范的严格要求。然而，将这些碎石材料回收后当作路面基层或底层（未黏结层），将可增加可持续性 & 达到经济的效益。

本研究针对 E39 路线的地质情况进行测绘工作，调查发现有许多岩石类型（火山岩，沉积岩与变质岩）存在隧道施工的位置。现行道路工程技术标准对碎石材料的性能要求以洛杉矶试验（LA）与微狄法尔试验（MDE）来测试。碎石料大多是火山岩，而且经标准程序调查过后却认为“硬质”碎石；与此同时，相当数量且不同来源的碎石，经判断后属于“弱质”碎石。所有碎石材料都经过薄切片显微镜，X 射线绕线试验（XRD）与 X 射线荧光试验（XRF），及电镜扫描（SEM）来了解材料的特性。此外，碎石材料的破碎性质及应用在道路建造阶段及往后的服务阶段一并分析探讨。

本研究利用许多技术性的实验方法来探究如何开展“弱质”碎石的用途。第一方法是混合法，亦即混合施工现场现有的不同碎石，来达到符合规范要求。第二方法是添加剂法。本研究采用两种非传统的添加剂：一个是聚合物基，一个是木质素基。掺入添加剂后的材料，进行反复性三轴试验（RTL），用来评估添加剂对碎石材料的效应。试验的结果跟目前文献上的方程式进行差异比较。本研究也建立有限元分析模型来模拟反复性三轴试验的过程及结果。

最后，本研究在现场建造三个测试路段用来调查该添加剂的性能。每一路段分别添加不同方法来滚压夯实：水分，水分与聚合物基，水分与木质素基。三个测试路段皆进行手持式落锤弯沉仪（LWD），用来采集基层劲度与变形数据。同时进行动态圆锥贯入仪（DCP）及观测表面车辙情形，用来综合评估两种添加剂的性能。

本研究经过实验室与现场的实验证明后，发现添加聚合物基与木质素基在碎石材料后，可以大幅度的提高该“弱质”碎石的力学性能。

RIASSUNTO (in Italian)

L'Ente Nazionale Norvegese per le Strade gestisce attualmente il progetto "Autostrada costiera E39 libera dalle connessioni traghettuali", lo scopo è quello di ridurre il tempo di percorrenza lungo l'autostrada norvegese E39 che collega Trondheim a Kristiansand. Il piano prevede la creazione di un esteso sistema di gallerie, il cui scavo genera un significativo volume di rocce; questi materiali granulari sono spesso danneggiati dalle intensive operazioni di esplosione ed in molti casi non rispondono ai rigidi criteri stabiliti dalle linee guida della progettazione stradale. Tuttavia, potrebbero essere utilizzati negli strati non legati delle strade vicine ai luoghi di apertura delle gallerie, comportando una soluzione ecosostenibile.

La geologia presente lungo l'allineamento stradale E39 è mappata: diversi tipi di rocce (igneo, sedimentarie e metamorfiche) sono diffuse lungo le aree interessate dalle operazioni di scavo. La normativa esistente prescrive i requisiti per gli strati non legati delle pavimentazioni stradali in base ai test Los Angeles (LA) e micro-Deval (MDE). La maggior parte delle rocce ha origine ignea e soddisfa queste procedure standard di controllo (rocce "forti"); d'altro canto, una considerevole quantità di rocce di diversa origine non ottempera a tali requisiti (rocce "deboli"). I materiali raccolti ed utilizzati per la ricerca sono caratterizzati tramite microscopia in sezione sottile, diffrattometria a raggi X (XRD), fluorescenza a raggi X (XRF) e microscopio elettronico a scansione (SEM). Inoltre, viene studiata la propensione delle rocce ad essere frantumate durante la fase di costruzione e durante la fase di servizio della pavimentazione.

La ricerca indaga in laboratorio come consentire l'uso delle rocce "deboli" considerando alcune possibili tecniche. Il primo approccio è mescolare opportunamente i vari tipi di rocce disponibili in situ. Il secondo approccio è applicare additivi; si esaminano due diversi tipi di additivi non tradizionali: uno è derivato da polimeri, l'altro è derivato da lignina. Prove di carico ripetute in cella triassiale (RTL) sono impiegate per valutare l'efficacia degli additivi. I risultati sono interpretati secondo equazioni disponibili in letteratura; inoltre, un modello ad elementi finiti è sviluppato per simulare il suddetto test di laboratorio e confrontare i risultati.

Infine, la ricerca indaga le prestazioni degli additivi sul campo. Tre strati di base sono costruiti e sono rispettivamente trattati con acqua (senza stabilizzazione), acqua e additivo a base polimerica, acqua e additivo a base di lignina. Lo sviluppo della rigidità e deformazione è principalmente valutato tramite il deflettometro leggero (LWD). Il penetrometro dinamico a cono (DCP) e la misurazione di ornaamenti caratterizzano ulteriormente le prestazioni.

I risultati delle campagne sperimentali, sia in laboratorio che in campo, indicano che entrambi i prodotti di stabilizzazione migliorano le proprietà meccaniche delle rocce "deboli".

TABLE OF CONTENTS

ACKNOWLEDGEMENTS	V
SUMMARY	VI
TABLE OF CONTENTS	XII
LIST OF PAPERS.....	XV
LIST OF SYMBOLS	XVI
LIST OF ABBREVIATIONS	XVIII
LIST OF FIGURES.....	XIX
LIST OF TABLES	XXII
1. INTRODUCTION.....	1
1.1. THE “FERRY-FREE COASTAL ROUTE E39” PROJECT.....	1
1.2. OBJECTIVES AND SCOPE OF THE RESEARCH.....	2
1.3. AN EXAMPLE ABOUT THE BENEFICIAL IMPACT.....	5
1.4. STRUCTURE OF THE THESIS	7
2. MECHANICAL PROPERTIES OF UNBOUND GRANULAR MATERIALS	9
2.1. REPEATED TRIAXIAL LOAD TEST	9
2.2. RESILIENT MODULUS	11
2.2.1. Hicks and Monismith model	12
2.2.2. Uzan model	13
2.2.3. Uzan and Witczak model	13
2.3. PERMANENT DEFORMATION.....	13
2.3.1. Barksdale model.....	14
2.3.2. Sweere model	14
2.3.3. Hyde model	15
2.3.4. Shenton model.....	15
2.3.5. Time hardening approach for Barksdale and Sweere models	15
2.3.6. The shakedown approach	16
2.3.7. The Coulomb approach	17
3. DISCUSSION	19
3.1. GEOLOGY ALONG E39 ALIGNMENT.....	19

3.1.1.	Thin section microscopy	20
3.1.2.	XRD analysis.....	22
3.1.3.	XRF analysis	23
3.1.4.	Standard tests characterization	23
3.2.	CRUSHABILITY OF ROCKS	25
3.2.1.	Scope and preparation of the test	25
3.2.2.	Crushability assessment in laboratory and in field.....	28
3.3.	POLYMER-BASED ADDITIVE STABILIZATION	31
3.4.	LIGNIN-BASED ADDITIVE STABILIZATION.....	32
3.5.	CRUSHED ROCKS STABILIZATION: LABORATORY TESTS.....	33
3.5.1.	Mixture of the rocks available in situ.....	33
3.5.2.	Polymer-based additive application	34
3.5.3.	Lignin-based additive application	37
3.5.4.	Overheating	39
3.6.	CRUSHED ROCKS STABILIZATION: MODELLING	40
3.6.1.	Resilient modulus.....	40
3.6.2.	Accumulation of permanent vertical deformation	41
3.6.3.	RTL finite element simulation.....	44
3.7.	CRUSHED ROCKS STABILIZATION: FIELD TESTS.....	47
3.7.1.	Field test preparation.....	47
3.7.2.	Measurement procedures.....	51
3.7.3.	Field test results.....	52
4.	FINAL CONSIDERATIONS	59
4.1.	CONCLUSIONS AND PRACTICAL CONSEQUENCES.....	59
4.2.	LIMITATIONS OF THE RESEARCH AND INPUTS FOR DEVELOPMENTS ..	60
5.	REFERENCES.....	62
	PAPER I.....	74
	PAPER II.....	84
	PAPER III	106
	PAPER IV	116
	PAPER V.....	138

PAPER VI.....	174
APPENDIX A	218
APPENDIX B	224
APPENDIX C	232

LIST OF PAPERS

The following papers are included in the thesis.

Paper I (conference proceedings)

Barbieri, D. M., Hoff, I., and Mork, H. (2017). “Laboratory investigation on unbound materials used in a highway with premature damage.” 10th International Conference on the Bearing Capacity of Roads, Railways and Airfields.

Paper II (conference proceedings)

Barbieri, D. M., Hoff, I., and Mørk, M. B. E. (2019). “Mechanical assessment of crushed rocks derived from tunnelling operations.” W.-C. Cheng, J. Yang, and J. Wang, eds., Springer International Publishing, 225–241. GeoChina 2018.

Paper III (conference proceedings)

Barbieri, D. M., Mofid, S. A., Hoff, I., and Jelle, B. P. (2018). “Nanoscale technology enhancement of crushed rocks ’ mechanical properties for pavement applications.” 6th International Symposium on Nanotechnology in Construction.

Paper IV (journal manuscript)

Barbieri, D. M., Hoff, I., and Mørk, M. B. E. “Innovative stabilization techniques for weak crushed rocks used in road unbound layers: a laboratory investigation.” Transportation Geotechnics. Submitted.

Paper V (journal manuscript)

Barbieri, D. M., Hoff, I., and Ho, C. S. “Innovative stabilization techniques for weak crushed rocks used in road unbound layers: a numerical investigation.” Construction and Building Materials. Submitted.

Paper VI (journal manuscript)

Barbieri, D. M., Hoff, I., and Mørk, M. B. E. “Innovative stabilization techniques for weak crushed rocks used in road unbound layers: a field investigation.” Journal of Transportation Engineering, Part B Pavements. Submitted.

LIST OF SYMBOLS

A	creep rate coefficient
a	apparent attraction
a _{BA}	first regression parameter, Barksdale model
a _{HY}	regression parameter, Hyde model
a _{SH}	first regression parameter, Shenton model
a _{SW}	first regression parameter, Sweere model
B ₁₀	particle breakage factor
b _{BA}	second regression parameter, Barksdale model
b _{SH}	second regression parameter, Shenton model
b _{SW}	second regression parameter, Sweere model
C _c	coefficient of curvature
C _u	coefficient of uniformity
D ₁₀	grain diameter at 10% passing
D ₃₀	grain diameter at 30% passing
D ₆₀	grain diameter at 60% passing
E _{LWD}	dynamic modulus measured by light weight deflectometer
k ₁	first regression parameter, Hicks and Monismith model
k ₁₁	first regression parameter, Uzan model
k ₁₁₁	first regression parameter, Uzan and Witczak model
k ₂	second regression parameter, Hicks and Monismith model
k ₂₂	second regression parameter, Uzan model
k ₂₂₂	second regression parameter, Uzan and Witczak model
k ₃₃	third regression parameter, Uzan model
k ₃₃₃	third regression parameter, Uzan and Witczak model
Log	decimal logarithm
M _R	resilient modulus
N	number of load cycles
n	creep stress rate exponent
p	mean bulk stress
q	mean deviatoric stress
R ²	coefficient of determination for goodness of fit

S_m	average settlement measured by light weight deflectometer
w	gravimetric moisture content
α	parameter connecting LA to B_{10}
β	parameter connecting MDE to B_{10}
$\dot{\epsilon}$	strain rate
ϵ_r	residual (or recoverable or elastic) strain
$\epsilon_{r,v}$	residual (or recoverable or elastic) vertical strain
ϵ_p	permanent (or not recoverable or residual) strain
$\epsilon_{p,v}$	permanent (or not recoverable or residual) vertical strain
ζ	optimum vertical translation from pre-compaction to post-compaction curve
θ	bulk stress
ν	Poisson's ratio
ρ	mobilized angle of friction
ρ_b	bulk density
ρ_d	dry density
σ_1	major principal stress
σ_2	intermediate principal stress
σ_3	minor principal stress
σ_a	reference pressure
σ_d	deviatoric stress
$\sigma_{d,dyn}$	dynamic deviatoric stress
σ_t	triaxial (or confining) pressure
τ_{oct}	octahedral shear stress
φ	mobilized angle of failure

LIST OF ABBREVIATIONS

AC	Asphalt Concrete
ASTM	American Society for Testing and Materials
CBR	California Bearing Ratio
CEN	Comité Européen de Normalisation
DCP	Dynamic Cone Penetrometer
FE	Finite Element
IBC	Intermediate Bulk Container
KPG	Kvalitet av Pukk- og Grusindustriens produkter (quality of aggregate products)
LA	Los Angeles (test)
LVDT	Linear Variable Differential Transducer
LWD	Light Weight Deflectometer
MDE	micro-Deval (test)
MS HSL	Multi-Stage High Stress Level
MS LSL	Multi-Stage Low Stress Level
NPRA	Norwegian Public Roads Administration
NTNU	Norwegian University of Science and Technology
SS HSL	Single-Stage High Stress Level
SS LSL	Single-Stage Low Stress Level
UGM	Unbound Granular Material
XRD	X-Ray Diffractometry
XRF	X-Ray Fluorescence

LIST OF FIGURES

Figure 1 Map of Norway (a) and position of E39 highway alignment (b).....	1
Figure 2 Tunnelling operations: blasting (a), transporting (b) and stockpiling (c) rocks	2
Figure 3 Flexible pavement structure with unbound layers highlighted (Thom 2014).....	4
Figure 4 Tunnel profile considered to assess the beneficial impact of using blasted rocks	5
Figure 5 Highway profile considered to assess the beneficial impact of using blasted rocks ..	6
Figure 6 Relations between the papers and the topics discussed in the thesis	8
Figure 7 RTLT specimen preparation phases.....	10
Figure 8 Loading sequences for the MS LSL procedure.....	11
Figure 9 Strains in UGMs during one cycle of load application (Lekarp et al. 2000a)	12
Figure 10 UGMs permanent deformation behaviour according to the shakedown approach (Werkmeister et al. 2004).....	16
Figure 11 Degrees of shear strengths according to Coulomb approach.....	17
Figure 12 Bedrock geology of southern Norway and E39 highway alignment	19
Figure 13 Mineralogy and grain sizes of M1 (a, b), M2 (c, d), M3 (e, f) and M4 (g, h). Mineral abbreviations: Am/amphibole, Ca/calcite, Chl/chlorite, Ep/epidote, Fs/feldspar, Mi/mica/biotite, Pl/plagioclase laths, Q/quartz, Zo/zoisite (optical micrographs, transmitted plane-polarized light, 1 mm scale bar).....	21
Figure 14 Bulk mineralogy of the investigated crushed rocks	22
Figure 15 Spectrum of M1, M2, M3 and M4 chemical composition (percentage of the total solid mass). Element abbreviations: Si/silicon, Al/aluminium, Ti/titanium, Fe/iron, Mn/manganese, Mg/magnesium, Ca/calcium, Na/sodium, K/potassium, P/phosphorus.....	23
Figure 16 Grain size distribution limit curves for base layer	24
Figure 17 Los Angeles and micro-Deval values of investigated materials	24
Figure 18 Layout of the field test to assess rocks crushability (dimensions in mm)	25
Figure 19 Main stages of the field test to assess rocks crushability.....	26
Figure 20 Bulk density of the unbound layer before and after roller compaction	27
Figure 21 Sieving curves referring to pre-compaction and post-compaction action	28
Figure 22 Particle breakage factor of the calculated sieving curves	29
Figure 23 Sieving curves referring to pre-load and post-load action.....	30
Figure 24 Particle breakage factor of the sieving curves	31

Figure 25 Polymer-based stabilization: siloxane linkages (a) (Ugwu et al. 2013) and formation of hydrophobic alkyl siloxane layer (b)	32
Figure 26 LA and MDE results and linear trend distributions for mixtures made of M2 and M1 (a), M3 and M1 (b).....	33
Figure 27 M1, M2 and M3 bulk density and dry density at OMC w=5% (a), M2 and M3 bulk density after additive application with P1, P2 proportions (b).....	35
Figure 28 M1, M2 and M3 resilient modulus at OMC w=5% (a), M2 and M3 resilient modulus after additive application with P1, P2 proportions (b)	35
Figure 29 Mobilized angle of friction ρ and failure angle ϕ of M2 (a) and M3 (b) for untreated and additive-treated conditions	36
Figure 30 Coating effect provided by the polymer-based additive assessed by standard procedures: LA test (a), MDE test (b).....	36
Figure 31 M1, M2 and M3 bulk density and dry density at w=1% (a), M2 and M3 bulk density after additive application (b)	37
Figure 32 M1, M2 and M3 resilient modulus at w=1% (a), M2 and M3 resilient modulus after additive application (b).....	38
Figure 33 Mobilized angle of friction ρ and failure angle ϕ of M2 (a) and M3 (b) for untreated and additive-treated conditions	38
Figure 34 Coating effect provided by the lignin-based additive assessed by standard procedures: LA test (a), MDE test (b)	39
Figure 35 MDE values after overheating M2 (b) and M3 (b).....	39
Figure 36 Resilient modulus according to Uzan model: polymer-based additive (a) and lignin-based additive (b)	40
Figure 37 Resilient modulus according to Uzan and Witczak model: polymer-based additive (a) and lignin-based additive (b)	41
Figure 38 Accumulated vertical permanent deformation, Barskdale model: polymer-based additive (a) and lignin-based additive (b)	42
Figure 39 Accumulated vertical permanent deformation, Sweere model: polymer-based additive (a) and lignin-based additive (b)	42
Figure 40 Accumulated vertical permanent deformation, Hyde model: polymer-based additive (a) and lignin-based additive (b)	43
Figure 41 Accumulated vertical permanent deformation, Shenton model: polymer-based additive (a) and lignin-based additive (b)	43

Figure 42 Mesh of the FEM RTL model	44
Figure 43 Accumulated vertical permanent deformation, Tresca plasticity model: polymer-based additive (a) and lignin-based additive (b)	46
Figure 44 Accumulated vertical permanent deformation, Von Mises plasticity model: polymer-based additive (a) and lignin-based additive (b)	46
Figure 45 Accumulated vertical permanent deformation, Shenton model: polymer-based additive (a) and lignin-based additive (b)	47
Figure 46 Grain size distribution curve (base layer) used in the investigations carried out in laboratory and in field	48
Figure 47 Construction of the first 15-cm part of the base layer: laying of the material (a), spreading water (b), spreading polymer-based additive (c), spreading lignin-based additive (d), mixing (e) and compacting (f).....	50
Figure 48 Construction completion of the road base sections: with water (L0), with polymer-based additive (L1) and with lignin-based additive (L2)	50
Figure 49 Bulk density (a), dry density (b) and water content (c) for materials tested in the field after construction and after 115 days	53
Figure 50 Surface appearance after 50 days: untreated (a), with polymer-based additive (b) and with lignin-based additive (c).....	54
Figure 51 Weather conditions in the field during the first 50 days after construction: average, minimum, maximum temperature and precipitation	54
Figure 52 LWD measurements results during the first 50 days after construction: dynamic modulus E_{LWD} (a) and settlement S_{LWD} (b)	56
Figure 53 Polymer-based additive: water poured on the top does not seem to penetrate (a); lignin-based additive: “crust” effect (b), “droplet” effect (c) and dissolution with water (d)..	57
Figure 54 Average depth from layers’ surfaces with increasing number of DCP blows	57
Figure 55 Average number of DCP blows necessary to reach the layers’ bottoms	58
Figure 56 Rutting formation: stimulating procedure (a) and measured values (b)	58

LIST OF TABLES

Table 1 Use of blasted rocks: from tunnelling blasting to road construction.....	6
Table 2 Mobile jaw crusher and mobile cone crusher used to crush blasted rocks.....	6
Table 3 Price for 1 tonne of crushed rocks: use of blasted rocks vs quarry production ...	7
Table 4 Shakedown approach: permanent strain rates and the ranges of material behaviour.	17
Table 5 Coulomb approach: permanent strain rates and the ranges of material behaviour.....	18
Table 6 Quantity of water and additives used in each investigated location.....	49

1. INTRODUCTION

1.1. THE “FERRY-FREE COASTAL ROUTE E39” PROJECT

The Norwegian Public Roads Administration (NPRA) is currently running the “Ferry-free coastal route E39” project, which aims to reduce the travel time along the Norwegian highway E39 connecting Trondheim to Kristiansand (**Figure 1**); this will be achieved by replacing ferries with bridges and tunnels, in addition to upgrading a number of road sections on land. After construction completion, the estimated travel time will be reduced from 21 h to 11 h, the route running Trondheim to Kristiansand is approximately 1100 km long (NPRA 2017a). The project has a remarkable national relevance as the industries located along the route generate about half of Norway’s traditional export. More rapid transport of people and goods, both locally and regionally, will better tie the involved areas and contribute to more efficient industries (Dunham 2016).

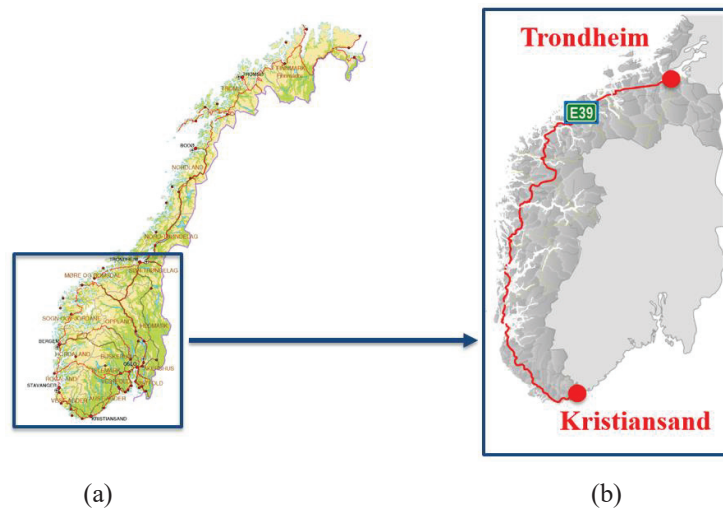


Figure 1 Map of Norway (a) and position of E39 highway alignment (b)

The plan includes the construction of several long tunnels, which will generate a very large surplus of blasted rocks.

1.2. OBJECTIVES AND SCOPE OF THE RESEARCH

The tunnelling operations bringing to the production of the blasted rocks are reported in **Figure 2**: the explosives are positioned by means of drilling jumbos (a), the blasted rocks are transported to a predetermined site (c) and are successively stockpiled (c). There are different techniques for the drill and blasting operations, the dimensions of the obtained rocks depends on several parameters, e.g. rock density, angle cut, drilling pattern, firing pattern and velocity of detonation (Natvik 1998; Zare 2006).



Figure 2 Tunnelling operations: blasting (a), transporting (b) and stockpiling (c) rocks

The blasted rocks could be used as viable substitutes for aggregates in the road unbound layers close to the place of production. Using excavated geomaterials is beneficial from economic, environmental and social points of views (Chittoori et al. 2012; Riviera et al. 2014); energy consumption reduction and limited greenhouse gas emissions are the most beneficial advantages (Aatheesan et al. 2008; Arulrajah et al. 2013; Gomes Correia et al. 2016; Haritonovs et al. 2016; Núñez et al. 2008; Onyango et al. 2007; Otto et al. 2015). Furthermore, the concern about environmentally-friendly policies and the public awareness regarding the use of natural resources are turning into more and more relevant topics in Norway, as it pledges to become climate neutral by 2030 (Petkovic 2005; Teknologirådet 2012).

The Norwegian pavement design guide (NPRA 2014a) underlines the importance of recycling and reusing: these activities must be prioritized according to the local resources and environmental considerations (“*gjenvinning og gjenbruk skal prioriteres ut fra ressurs- og miljøhensyn [...] redusere avfallsmengdene og fremme en bedre behandling av avfall*”).

In Norway the production of natural aggregates has been declining since 1997, while the production of crushed rocks has been increasing since 2003. In 2015 almost 70 million

tonne of crushed rocks were produced in Norway. The average yearly aggregate consumption per capita is 11 tonne; approximately half part of this figure is used for road construction (Erichsen and Aasly 2015; NGU 2015). At the end of the 20th century the Norwegian project “Quality of aggregate products” (*Kvalitet av Pukk- og Grusindustriens produkter* KPG) focused on characterizing the properties of crushed rocks compared to natural gravel (Bakløkk et al. 1998; Hansen and Hansen 1998).

Recent experience regarding the recycling strategies of tunnel excavation materials highlights the importance of this challenge for construction management and economics. The following rock classification in three classes has been suggested regarding the excavations in the Alpine regions (Lieb 2009): rocks for concrete aggregates (class 1), for soil surrogates in embankments (class 2) and finally for disposal (class 3). This classification aims to identify the most suitable lithology for each application. The value of the raw materials increases as the application context changes from embankments to subgrades, subbase and bituminous/cementitious mixtures and the quality requirements become more and more stringent (Burdin and Monin 2009; Haritonovs et al. 2016; Resch et al. 2009; Sybilski et al. 2010).

The use of blasted and crushed materials in pavement applications is a sustainable solution to minimise the waste and lower carbon footprints while reducing the demand for scarce quarried materials, activity which is resource intensive and consumes large amounts of energy (Fladvad et al. 2017). The transport distance of the blasted materials should be within 20 - 30 km to represent a competitive solution compared to the purchase of quarry virgin aggregates (Berger 1978; Neeb 1992).

The blasted rocks can be reduced in size by action of crushing (comminution); particular size distributions can be obtained by a multi-stage crushing to guarantee a marketable product (Rothery and Mellor 2007). The blasted rocks can be comminuted in situ by means of mobile crushers to obtain crushed rocks. They could be used in the unbound layers of highways and roads as Unbound Granular Materials (UGMs); the use of UGMs close to the place of production represents a sustainable cost-benefit application. **Figure 3** represents a typical flexible pavement structure. The unbound layers are highlighted and correspond to base, subbase and capping layers; furthermore, an additional “frost protection layer” can be found in Norwegian roads, UGMs may be used in this course as well.

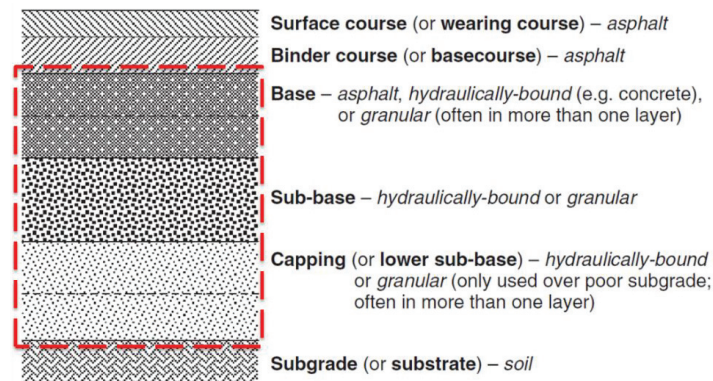


Figure 3 Flexible pavement structure with unbound layers highlighted (Thom 2014)

UGMs have been used in roads since the beginning of pavement infrastructure construction. The layers composing the most important Roman roads (called *viae lapidibus stratae*) comprised four layers from the bottom: statumen, rudus, nucleus and pavementum; the use of suitable stones and aggregates played an important role (Ray 1999). Broadly speaking, the granular layers have the following roles: contribute to spreading the vehicle loads to a magnitude that does not damage the subgrade, provide an adequate stiff layer for the compaction of overlaying courses, e.g. asphalt concrete (AC), and support them during the pavement service phase (Araya 2011; Douglas 2017; Huang 2004; Mallick and El-Korchi 2013; Thom 2014).

The Norwegian road design manual “Håndbok N200” (NPRA 2014a) defines requirements for road unbound layers in terms of grading curve, flakiness index, Los Angeles (LA) and micro-Deval (MDE) tests (CEN 2010, 2011, 2012a; b). Tunnel blasting induces significant weakening of the rocks from microcracks due to the high energy released in a confined situation (Raina et al. 2000). Some rocks available along the E39 alignment fulfill these standard check procedures (“strong” rocks); anyway, some rocks do not (“weak” rocks). The scope of the Ph.D. research is to investigate sustainable and non-traditional stabilization methods to improve the mechanical properties of the “weak” rocks.

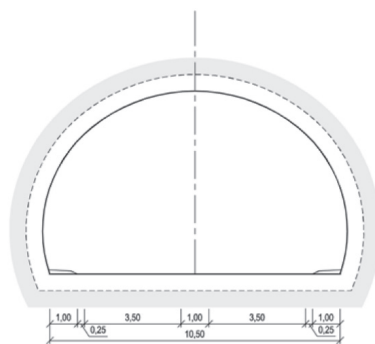
Some traditional stabilization methods already exist for coarse pavement layers, e.g. cement and bitumen. However, these stabilization agents may bring to highly alkaline and sometimes corrosive chemical admixtures (Jiang and Fan 2013; Myre 2014; NPRA 2014b; Siripun et al. 2010). Furthermore, traditional stabilizers like cement, lime, flyash and gypsum can cause excessive brittle failure (Behnood 2018). The research investigates two innovative

non-traditional stabilization admixtures and may bring to a wider acceptance of the products. The investigation comprises laboratory experiments, numerical modelling and field tests.

1.3. AN EXAMPLE ABOUT THE BENEFICIAL IMPACT

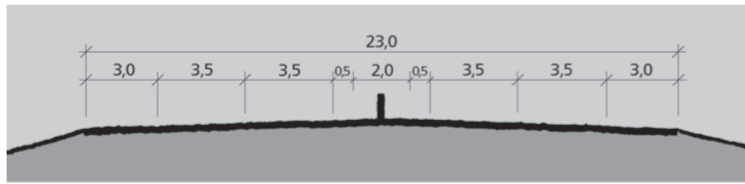
Let us take into consideration the excavation of a 4-km twin-tube tunnel with profile T10.5 as displayed in **Figure 4** (NPRA 2016); its cross section area is 75 m^2 , the specific weight of the mountain rock is assumed to be 1.6 t/m^3 . Therefore, the total blasted volume is around $600\,000 \text{ m}^3$ and its total weight is approximately $1 \cdot 10^6 \text{ t}$. The excavated materials are to be used in the unbound layers of a F-class highway positioned nearby; the cross section comprises 4 lanes and the total width of the road is 23 m (NPRA 2013), as shown in **Figure 5**.

Two subgrade scenarios may be taken into consideration as reported in **Table 1**: one corresponds to a strong subgrade, e.g. mountain cut, the other one corresponds to a weak subgrade, e.g. silt. The thicknesses of the two road unbound courses, namely base course (paved crushed rocks) and subbase course (crushed rocks), are evaluated. It would be possible to use the rocks up to 50 km and 20 km for strong subgrade and weak subgrade, respectively. Even if this approximated calculation has assumed that all the blasted rocks can be suitably crushed to obtain the grading curves needed for each unbound layer, the beneficial potential for blasted rocks use appears unequivocal.



Figur V1.9 Tunnelprofil T10.5 (mål i m)

Figure 4 Tunnel profile considered to assess the beneficial impact of using blasted rocks (dimensions in m)



Figur C.11: Tverrprofil H9, 23 m vegbredde (mål i m)

Figure 5 Highway profile considered to assess the beneficial impact of using blasted rocks (dimensions in m)

Table 1 Use of blasted rocks: from tunnelling blasting to road construction

	STRONG SUBGRADE	WEAK SUBGRADE
Base layer thickness (cm)	25	25
Subbase layer thickness (cm)	30	120
Unbound layers cross section (m²)	13	34
Estimate road length (km)	50	20

Estimating the tonne price of the used crushed rocks compared to the purchase of quarry virgin crushed rocks is also crucial to understand the beneficial economic impact of the project. **Table 2** displays the features of the mobile jaw crusher and the mobile cone crusher considered to properly crush the blasted rocks (Sandvik 2018).

Table 2 Mobile jaw crusher and mobile cone crusher used to crush blasted rocks

	Mobile jaw crusher	Mobile cone crusher
price (USD)	600 000	600 000
throughput capacity (t/h)	400	500
diesel consumption (l/h)	50	50

Table 3 illustrates the main costs that make up the price for a single tonne of crushed rocks for the two mentioned scenarios: use of crushed rocks from tunnelling operations and purchase of quarry crushed rocks (Forset Grus 2018; Franzefoss 2018; Velde 2018), respectively. The aim of this comparison is to show the great potential of using the crushed rocks, a painstaking economic study could be useful to reach a more accurate estimate.

Table 3 Price for 1 tonne of crushed rocks: use of blasted rocks vs quarry production

COSTS FROM BLASTING (referring to 1·10 ⁶ t, then divided)		COSTS FROM QUARRYING (directly per tonne)	
mobile crushers	1 200 000	quarry price	10
two workers, 2500 h	180 000	transit, 20 km	4
fuel, 125 000 l	190 000	rocks removal	5
PRICE (USD/t)	~2	PRICE (USD/t)	~19

This section has highlighted the beneficial economic impact and the importance from the sustainability point of view of using the blasted rocks derived from tunnelling operations as pavement construction materials in the form of crushed rocks. They can represent "short travelled rocks" (*"kortreist stein"*).

1.4. STRUCTURE OF THE THESIS

The thesis is divided in chapters. Chapter 1 has introduced the Ph.D. research background and scope. Chapter 2 describes the UGMs mechanical properties, namely resilient modulus and resistance to permanent deformation. It deals with the laboratory devices used to assess these properties and how to model them. Chapter 3 is the core of the research, as it illustrates the non-traditional stabilization technologies. It is further subdivided into subsections that describe the criteria adopted for laboratory tests, FE modelling and full-scale field test. Chapter 4 discusses the results of the Ph.D. research as well as its limitations, it also presents inputs for further investigations. Chapter 5 contains references and literature. Appendix A displays four conference posters. Appendices B and C show two models of MATLAB script used to evaluate resilient modulus and permanent vertical deformation, respectively.

Six papers are reported in the thesis section following the chapters. Paper I deals with the mechanical properties of UGMs and it describes some key research procedures largely employed successively. Paper II maps the geology encountered along the E39 alignment and discusses rocks' crushability. Paper III illustrates the effect of the stabilizing additives from a macroscale and nanoscale points of view. Paper IV, Paper V and Paper VI accurately describe the laboratory tests, FE modelling and full-scale field test, respectively; these investigations have been carried out to assess soundly the stabilizing products (**Figure 6**).

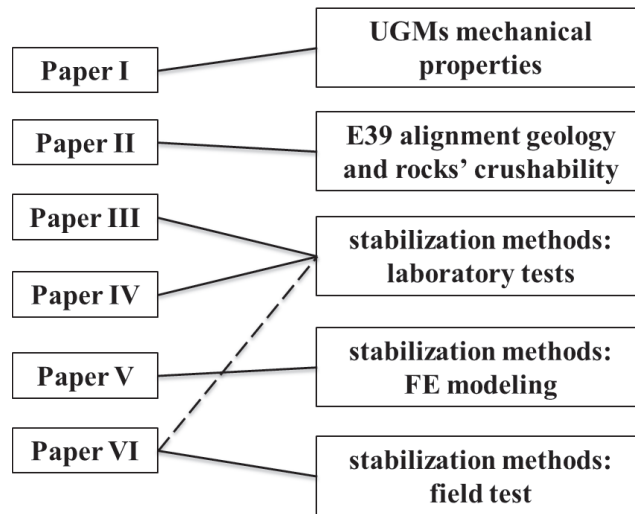


Figure 6 Relations between the papers and the topics discussed in the thesis

2. MECHANICAL PROPERTIES OF UNBOUND GRANULAR MATERIALS

2.1. REPEATED TRIAXIAL LOAD TEST

The Repeated Triaxial Load Test (RTLTL) gives a comprehensive insight into the properties of materials by assessing the stiffness and the resistance to permanent deformation (Hoff 1999; Huang 2004; Kolisoja 1997). RTLTL (also referred to as Repeated Load Triaxial Test, RLTT) is one of the best methods available for laboratory simulation of traffic loading on UGMs; it reproduces the stress conditions in flexible pavements more adequately than other available methods like the California Bearing Ratio (CBR) test (Barksdale 1971).

Hicks and Monismith (1971), Lekarp et al. (2000a, b), Li and Selig (1994) and Seed (1962) presented a thorough state-of-the-art of the mechanical behaviour. They found that the resilient modulus and the permanent deformation were mainly influenced by the same factors (Uthus 2007; Uthus et al. 2007): stress level, moisture content, dry density, grading and mineralogy, etc.

The triaxial apparatus used in the research was developed at Norwegian University of Science and Technology (NTNU) during the seventies, the equipment has been gradually upgraded (Hoff 1999; Horvli 1979; Uthus 2007). The triaxial chamber is made of plexiglass, water is used as a confining medium. The loading procedures applied on all the materials are to be found in the European code EN 13286-7 (CEN 2004); the multi-stage low stress level (MS LSL) procedure is used for all samples. The MS loading procedure is designed to avoid too large permanent deformations in the materials and it is possible to obtain information about the mechanical properties from one sample (Gidel et al. 2001). The LSL procedure has been adopted in this research to have enough load steps also for the “weak” rocks and by this make it easier to compare with the “strong” rocks.

Figure 7 shows the preparation procedure for the RTLTL specimen. 7300 g of material are initially prepared, the crushed rocks are selected according to a grading curve distribution (a). The desired amount of water and additive, if needed, is added to the testing material, which rests for 24 h to let the moisture distribute uniformly (b). A Kango 950X vibratory hammer (total weight 35 kg, frequency 25 ÷ 60 Hz, amplitude 5 mm) compacts the specimen layers for 30 s each (c); the bulk density and dry density are assessed as specified by EN 13286-4 (CEN

2003). The specimen is fully compacted inside the steel mould (d); afterwards, it is extracted vertically by means of a dedicated ejecting tool and the specimen is encapsulated in a latex membrane (e). All the samples have a diameter of 150 mm and the final height varies between 170 and 190 mm. The sample height differs from the indication given by the code, where the height is recommended to be twice the diameter of the sample (CEN 2004). Research regarding the influence of the height to diameter ratio with respect both to resilient modulus and permanent deformations has demonstrated that samples with a ratio ranging from 1:1 to 1.5:1 show little differences (Dongmo-Engeland 2005). Finally, the sample is covered by means of another latex membrane, end metal plates, plastic rings and hose clamps to avoid water penetration (f). Two and three LVDTs (Linear Variable Differential Transducers) measure the axial and radial deformations, respectively (g). The test is ready to be run (h).

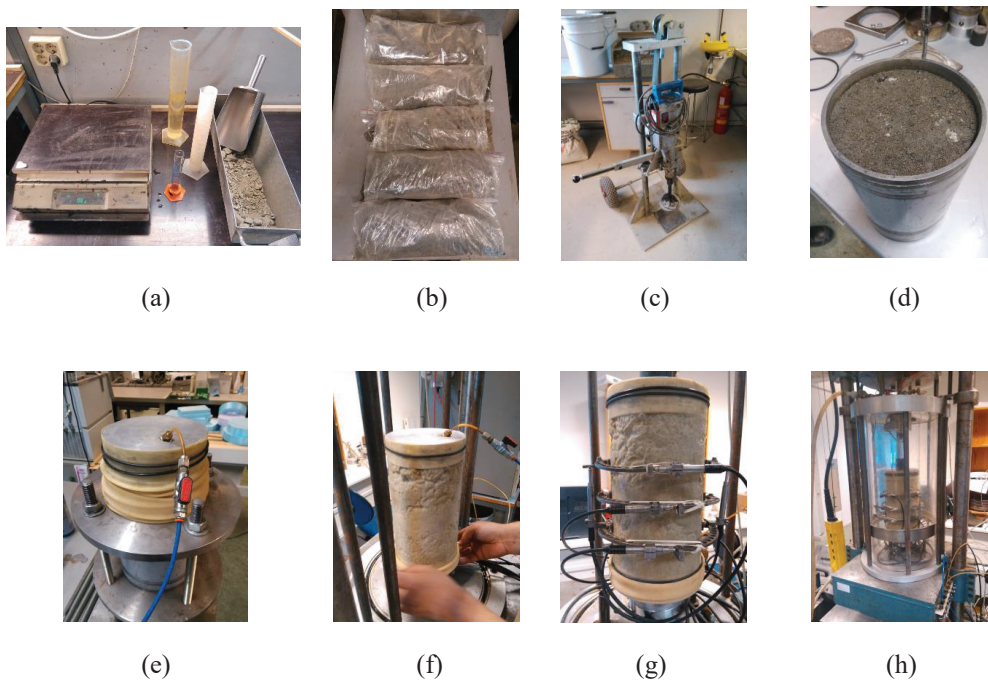


Figure 7 RTLT specimen preparation phases

RTLT apparatus exerts a uniform confining pressure in all the directions (σ_t , triaxial or confining stress) and an additional vertical dynamic stress (σ_d , deviatoric stress), which stepwise increases at different levels of σ_t . This type of triaxial test is also referred to as “biaxial

testing” as σ_2 and σ_3 , namely the intermediate and minor principal stresses, have the same value and correspond to σ_t . The triaxial test comprising $\sigma_2 \neq \sigma_3$ is also referred to as “true triaxial testing”. The RTLTL apparatus performs the MS LSL loading procedure: five sequences are associated with five different σ_t values ($\sigma_t = 20, 45, 70, 100, 150$ kPa). In addition, six steps associated to six given σ_d values form each sequence (CEN 2004).

The five loading sequences and the respective loading steps according to bulk stress θ ($\theta = \sigma_1 + \sigma_2 + \sigma_3 = \sigma_d + 3\sigma_t$; $\sigma_1, \sigma_2, \sigma_3$ are the principal stresses) and σ_d are displayed in **Figure 8**. Each load step consists of 10000 load pulses at 10 Hz frequency. A loading sequence is interrupted if the axial permanent deformation reaches 0.5%. Pressurised water is the confining medium; a hydraulic jack exerts σ_d according to a sinusoidal pattern, a minimum value of 5 kPa assures contact between the specimen end plate and the jack.

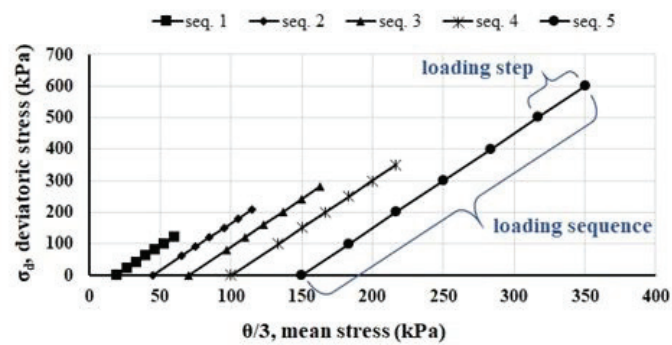


Figure 8 Loading sequences for the MS LSL procedure.

2.2. RESILIENT MODULUS

The deformation response of UGMs under a loading action is often conveniently separated into two deformation types: one resilient ϵ_r (recoverable or elastic) and one permanent ϵ_p (not recoverable or residual) as shown in **Figure 9**. In this figure the permanent strain is exaggerated for clarity’s sake, since commonly $\epsilon_r \gg \epsilon_p$.

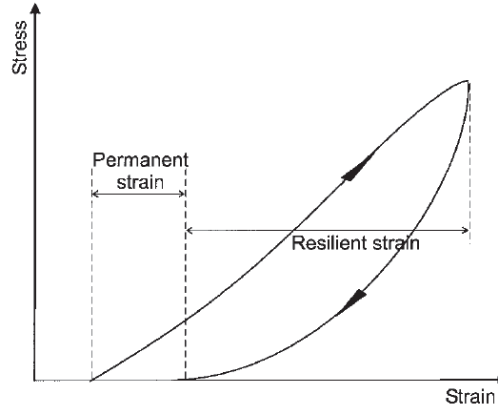


Figure 9 Strains in UGMs during one cycle of load application (Lekarp et al. 2000a)

The resilient modulus M_R expresses the stiffness of the material. The resilient modulus associated with a change in the dynamic deviatoric stress $\sigma_{d,dyn}$ and a constant confining pressure σ_t is

$$M_R = \frac{\Delta\sigma_{d,dyn}}{\varepsilon_{r,v}}, \quad (\text{Eq. 01})$$

where $\varepsilon_{r,v}$ is the axial resilient vertical strain. The resilient modulus represents the UGMs behaviour under repeated traffic loading and is a critical parameter for any mechanistically based design (Ghadimi and Nikraz 2017; Hoff et al. 2005; Zhalehjo et al. 2018). Several non-linear relationships have been developed to describe M_R with reference to different parameters (Lekarp et al. 2000a). All the regression parameters are assessed through least-square regression.

2.2.1. Hicks and Monismith model

Hicks and Monismith have proposed a simple and effective connection between the resilient modulus M_R and the bulk stress θ (Hicks and Monismith 1971)

$$M_R = k_1 \sigma_a \left(\frac{\theta}{\sigma_a} \right)^{k_2}, \quad (\text{Eq. 02})$$

where σ_a is a reference pressure (100 kPa) and k_1, k_2 are regression parameters. This relationship enables a clear comparison in a two-dimensional $M_R - \theta$ plot; due to its simplicity, this is the most used model to interpret resilient modulus of UGMs (Lekarp et al. 2000a).

2.2.2. Uzan model

Uzan model establishes a relationship between three parameters: resilient modulus M_R , bulk stress θ and deviatoric stress σ_d (Uzan 1985)

$$M_R = k_{111} \sigma_a \left(\frac{\theta}{\sigma_a} \right)^{k_{222}} \left(\frac{\sigma_d}{\sigma_a} \right)^{k_{333}}, \quad (\text{Eq. 03})$$

where σ_a is a reference pressure (100 kPa) and $k_{111}, k_{222}, k_{333}$ are regression parameters. Compared to Hicks and Monismith model, Uzan model has the advantage to take into consideration both bulk stress and deviatoric stress, which are the two most important factors affecting UGMs resilient modulus (Lekarp et al. 2000a).

2.2.3. Uzan and Witczak model

Uzan and Witczak model is a generalization of Uzan model, since the former takes into consideration the octahedral shear stress instead τ_{oct} of deviatoric stress σ_d in order to include full three-dimensional conditions (Uzan and Witczak 1988)

$$M_R = k_{111} \sigma_a \left(\frac{\theta}{\sigma_a} \right)^{k_{222}} \left(\frac{\tau_{oct}}{\sigma_a} \right)^{k_{333}}, \quad (\text{Eq. 04})$$

where σ_a is a reference pressure (100 kPa) and $k_{111}, k_{222}, k_{333}$ are regression parameters.

2.3. PERMANENT DEFORMATION

As stated in the previous section, UGMs deformational response can be divided into two parts: one is resilient and the other one is permanent. The latter is the result of further compaction, particle crushing or material migration; plastic deformation is responsible for rutting and other long-term pavement distresses (Lekarp et al. 2000b). Moreover, UGMs permanent deformation

consists of two phases. In the first phase, there is a rapid increase in permanent strain with load applications; in the second phase, the deformation rate becomes constant and is characterized by volume change (Werkmeister et al. 2004). Permanent deformation increases with the moisture content, as water reduces the effective stress and friction (Erlingsson et al. 2017).

A number of models have been developed to describe the accumulation of permanent vertical deformation $\varepsilon_{p,v}$ as a function of the applied load pulses N or as a combination of one or more of the following parameters: mean bulk stress p ($p = \theta/3$), mean deviatoric stress q ($q = (\sigma_1 - \sigma_3)/2$) and resilient vertical deformation $\varepsilon_{r,v}$ (Gidel et al. 2001)

$$\varepsilon_{p,v} = f_1(N)f_2(p, q, \varepsilon_{r,v}). \quad (\text{Eq. 05})$$

2.3.1. Barksdale model

Barksdale has found that the accumulation of vertical permanent strain $\varepsilon_{p,v}$ is proportional to the logarithm of the number N of load cycles (Barksdale 1972) as follows

$$\varepsilon_{p,v} = a_{BA} + b_{BA}\text{Log}(N), \quad (\text{Eq. 06})$$

where a_{BA} and b_{BA} are regression parameters.

2.3.2. Sweere model

Sweere has also performed a series of tests on UGMs, he has found that the logarithm of vertical permanent strain $\varepsilon_{p,v}$ is proportional to the logarithm of the number N of load cycles (Sweere 1990) as follows

$$\text{Log}(\varepsilon_{p,v}) = a_{SW} + b_{SW}\text{Log}(N), \quad (\text{Eq. 07})$$

where a_{SW} and b_{SW} are regression parameters.

2.3.3. Hyde model

Hyde model establishes a relationship between the vertical permanent strain $\varepsilon_{p,v}$, mean deviatoric stress q and triaxial stress σ_3 (Hyde 1974) as follows

$$\varepsilon_{p,v} = a_{HY} \frac{q}{\sigma_3}, \quad (\text{Eq. 08})$$

where a_{HY} is a regression parameter.

2.3.4. Shenton model

Shenton model establishes a relationship between the vertical permanent strain $\varepsilon_{p,v}$, maximum mean deviatoric stress q_{\max} and triaxial stress σ_3 (Shenton 1975) as follows

$$\varepsilon_{p,v} = a_{SH} \left(\frac{q_{\max}}{\sigma_3} \right)^{b_{SH}}, \quad (\text{Eq. 09})$$

where a_{SH} and b_{SH} are regression parameters.

2.3.5. Time hardening approach for Barksdale and Sweere models

Both Barksdale and Sweere models have been developed to fit the data of a single-stage (SS) RTLT. Their results are displayed in a graph having the number N of load repetitions along the x-axis and the accumulated permanent vertical deformation $\varepsilon_{p,v}$ along the y-axis, where the first value is equal to zero. As the research uses MS RTLT, the time hardening approach is adopted to describe the experimental data (Erlingsson and Rahman 2013; Rahman 2015; Rahman and Erlingsson 2015): the first y-value of each loading step is different from zero (except for the very first RTLT step). According to the time hardening approach, the accumulated vertical permanent deformation values corresponding to each step are treated as the last part of as many curves; each of them ideally corresponds to a SS RTLT, in which the first y-value is zero. This study calculates 30 curves (one for each loading step), each curve is assessed with the least-square method with a third-order polynomial expression; the data used to retrieve this third-order polynomial curve are the vertical permanent deformation values for the specific step.

Finally, for each loading step, the parameters of the chosen model (a_{BA} , b_{BA} for Barksdale model or a_{SW} , b_{SW} for Sweere model) are calculated through least-square regression considering the permanent vertical deformation values of a specific step and the first point of the ideal curve (having the first y-value equal to zero) of the same step.

2.3.6. The shakedown approach

The permanent deformation behaviour of UGMs can be described according to three ranges. Range A is the plastic shakedown range: the response is plastic for a finite number of load applications, no further permanent strain occurs after post-compaction; therefore, the pavement in such a condition is said to “shake down”. Range C is the incremental collapse range, it defines the increment in plastic strain with each load cycle. Range B is the plastic creep, it is an intermediate response between range A and range C; the plastic strains are higher during the first load cycles, at a later stage the strain rate reaches a nearly constant level (Werkmeister 2003; Werkmeister et al. 2004, 2005). **Figure 10** shows these three ranges of permanent deformation.

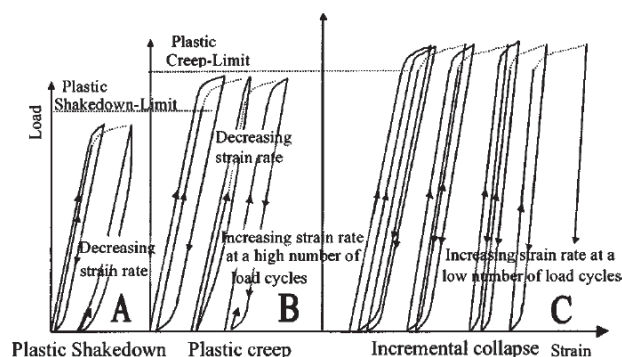


Figure 10 UGMs permanent deformation behaviour according to the shakedown approach
(Werkmeister et al. 2004)

The three ranges are identified based on the accumulation of axial permanent vertical strain rate $\dot{\epsilon}_{v,p}$ as shown in **Table 4**, being $\dot{\epsilon}_{v,p, 5000}$ and $\dot{\epsilon}_{v,p, 3000}$ the accumulated vertical strain at 5000 and 3000 load cycles with a given deviatoric stress, respectively.

Table 4 Shakedown approach: permanent strain rates and the ranges of material behaviour

Permanent strain rate	Range
$\dot{\epsilon}_{v,p, 5000} - \dot{\epsilon}_{v,p, 3000} < 4.5 \cdot 10^{-5}$	elastic zone
$4.5 \cdot 10^{-5} < \dot{\epsilon}_{v,p, 5000} - \dot{\epsilon}_{v,p, 3000} < 4.0 \cdot 10^{-4}$	elastoplastic zone
$\dot{\epsilon}_{v,p} > 4.0 \cdot 10^{-4}$	plastic (failure) zone

2.3.7. The Coulomb approach

The Coulomb criterion relates the mobilized shear strength to the development of permanent deformations and the maximum shear strength to failure (Hoff et al. 2003). The mobilized angle of friction ρ and the failure angle φ , respectively, express the degree of mobilized shear strength and the maximum shear strength. The mobilized angle of friction is

$$\sin \rho = \frac{\sigma_1 - \sigma_3}{\sigma_1 + \sigma_3 + 2a}, \quad (\text{Eq. 10})$$

where a is the apparent attraction of the material. The angle of friction and of failure identify three different ranges of material behaviour: elastic, elastoplastic and failure. The Coulomb criterion is shown in **Figure 11** in a σ - τ plot.

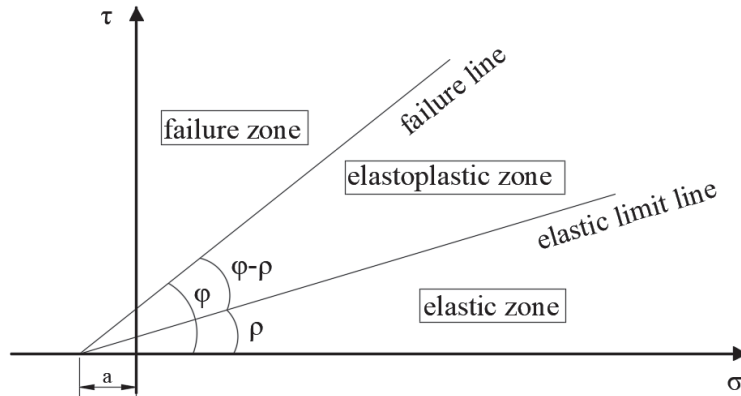


Figure 11 Degrees of shear strengths according to Coulomb approach

The strain rate $\dot{\epsilon}$ is a measure of the speed of the permanent deformation per cycle and is used as the parameter to define failure. **Table 5** defines the two boundary lines between the three ranges (**Figure 11**): each load step is categorized considering the average strain rate for the last 5000 to 10000 cycles.

Table 5 Coulomb approach: permanent strain rates and the ranges of material behaviour

Permanent strain rate	Range
$\dot{\epsilon}_{v,p} < 2.5 \cdot 10^{-8}$	elastic zone
$2.5 \cdot 10^{-8} < \dot{\epsilon}_{v,p} < 1.0 \cdot 10^{-7}$	elastoplastic zone
$\dot{\epsilon}_{v,p} > 1.0 \cdot 10^{-7}$	plastic (failure) zone

The equations for the elastic limit line and failure line are, respectively

$$\sigma_d = \frac{2 \sin \rho (\sigma_3 + a)}{1 - \sin \rho}, \quad (\text{Eq. 11})$$

$$\sigma_d = \frac{2 \sin \varphi (\sigma_3 + a)}{1 - \sin \varphi}. \quad (\text{Eq. 12})$$

A regression analysis is used to find the two best fit boundary lines. As a simplification, the apparent attraction is interpreted to be 20 kPa for all the samples.

3. DISCUSSION

3.1. GEOLOGY ALONG E39 ALIGNMENT

Knowledge about the geology encountered by the tunnelling operations is needed to map the origin and distribution of the materials (NGU 2017; Ramberg et al. 2013). **Figure 12** displays the geology of the southern part of Norway and the alignment of E39 highway. On the other hand, the most accurate geological information is obtained during the construction operations.

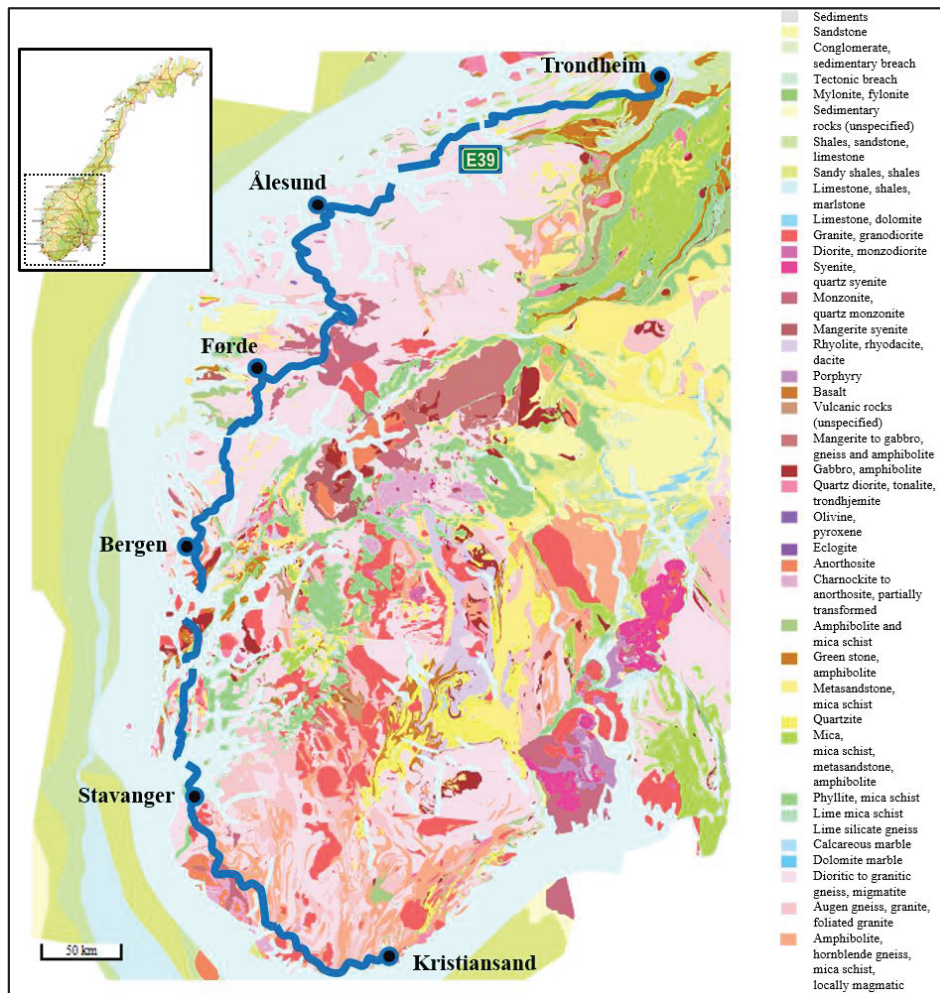


Figure 12 Bedrock geology of southern Norway and E39 highway alignment

The E39 highway alignment comes across different types of bedrocks (NGU, 2017; Ramberg et al., 2013). The major part of the rocks is igneous and supracrustal of Precambrian ages (1700 - 900·106 years) variably influenced by metamorphism and deformation related to the Caledonian orogeny. They mainly comprise granite, granodiorite and granitic to dioritic gneiss. There are also areas with Caledonian rocks; these locations are anyway at maximum 20 - 30 km far from the most widespread aforementioned geology. Metamorphic rocks occur close to Bergen (gabbro and augen gneiss). Zones of foliated Caledonian metamorphic rocks (e.g. mica-schist and phyllite) are locally present, in particular around Boknafjord area close to Stavanger.

Four rock materials are collected and used in the Ph.D. research; they are here referred to as M1, M2, M3 and M4, respectively. They adequately represent the variety in the geology spread along the entire highway alignment. M1, M2 and M3 come from the construction site “Svegatjørn-Rådal”: tunnel connections will improve the traffic condition between Bergen and Os (NPRA 2018). These materials are collected from Lyshorn tunnel, designed to connect the locality of Endelausmarka (Os municipality) to Rådal with a length of 9.3 km. M4 comes from Vassfjellet, this area is located in close to Trondheim and has several quarries (Grenne et al. 1980; Wolff 1976). M1, M2 and M3 are used for the laboratory test campaign, M4 is used for the field test campaign.

- Material M1. Mafic igneous origin, partly modified by metamorphism (amphibolite), minor amounts of felsic gneisses and mica-schist.
- Material M2. Metamorphic origin, fine-grained felsic and micaceous rocks.
- Material M3. Metamorphic origin, very fine-grained felsic and micaceous rocks.
- Material M4. Magmatic and metamorphic origin, mainly greenschist and gabbro.

3.1.1. Thin section microscopy

Thin-section microscopy images of selected rock samples show mineralogy and grain sizes (**Figure 13**). Igneous rocks M1 are modified by metamorphism, e.g. amphibolization and replacement of coarse igneous feldspar by aggregates of fine epidote and feldspar. Finer-grained felsic and micaceous rocks appear more dominant in M2 and especially in M3 and M4. Metamorphic reactions regarding M4 caused replacement of igneous pyroxene by amphibole, and growth of epidote/zoisite within the igneous plagioclase laths. The M4 samples also include small amounts of fine-grained metagabbro/meta-dolerite varieties.

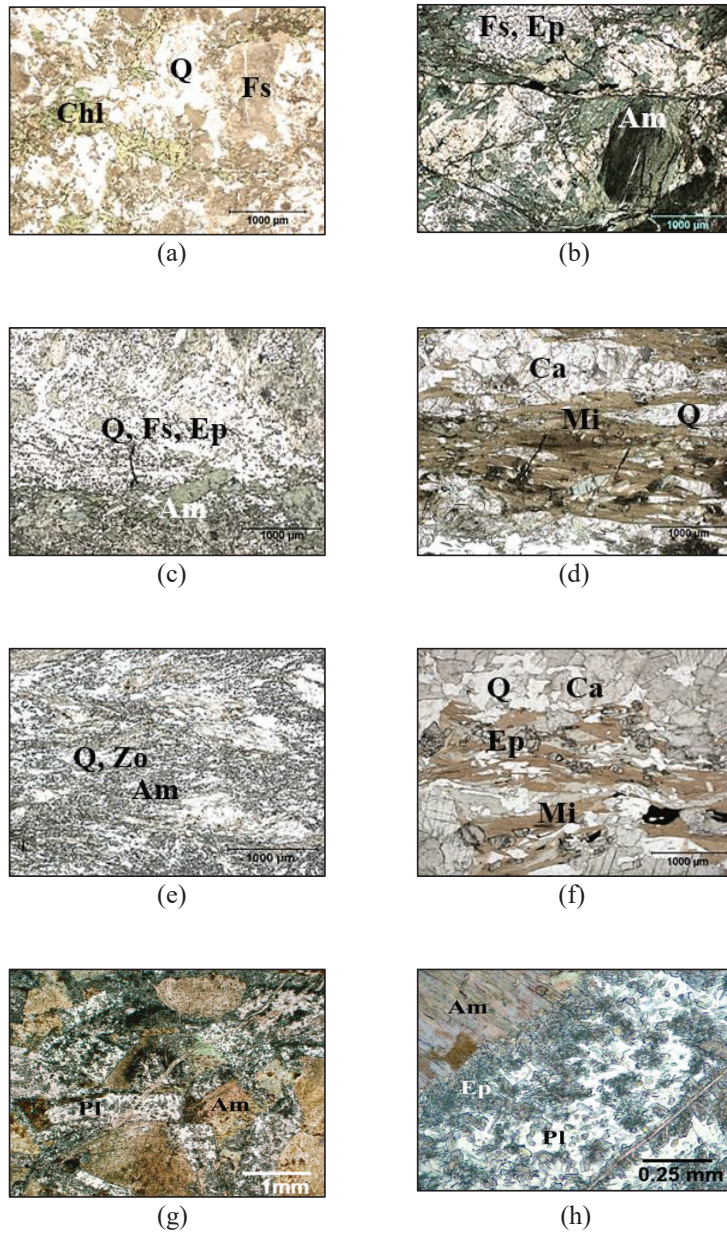


Figure 13 Mineralogy and grain sizes of M1 (a, b), M2 (c, d), M3 (e, f) and M4 (g, h).

Mineral abbreviations: Am/amphibole, Ca/calcite, Chl/chlorite, Ep/epidote, Fs/feldspar, Mi/mica/biotite, Pl/plagioclase laths, Q/quartz, Zo/zoisite (optical micrographs, transmitted plane-polarized light, 1 mm scale bar)

3.1.2. XRD analysis

X-Ray Diffractometry (XRD) analyses show the mineralogical composition for each material type according to Rietveld mineral quantification. Samples are crushed, split, milled to 10 μ m and analysed as powder prepare in the XRD diffractometer. The semi-quantitative weight proportions of the most abundant minerals are displayed in **Figure 14**.

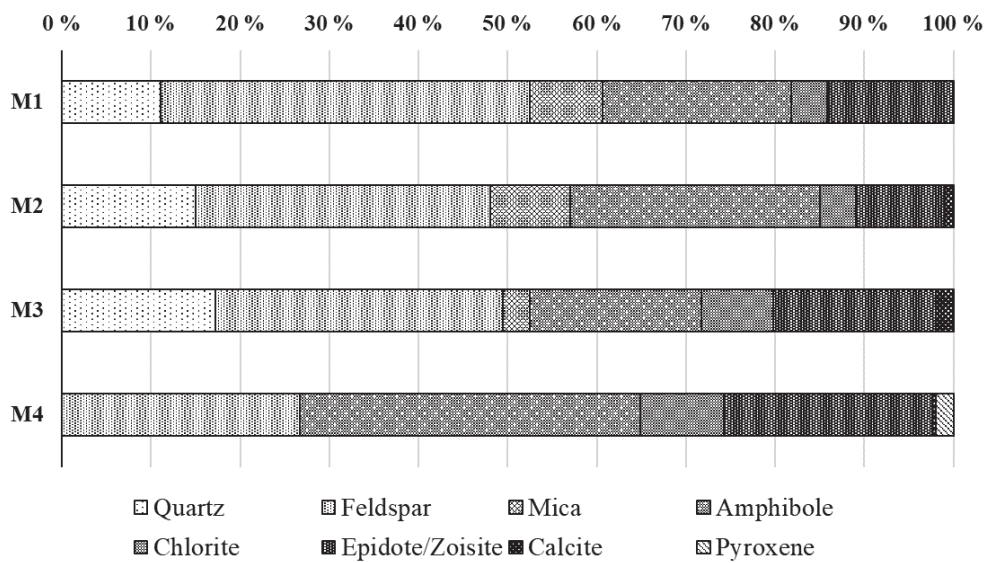


Figure 14 Bulk mineralogy of the investigated crushed rocks

Feldspar and amphibole are the predominant minerals in all M1, M2, M3 and M4 mixtures. M3 is richer in chlorite, epidote-zoisite and calcite compared to M1 and M2. Moreover, M3 has a higher content of foliated felsic rocks: networks of fine epidote-zoisite particles partly replace feldspars. Finer-grained felsic and micaceous rocks appear more dominant in M2 and especially in M3. Epidote/zoisite are present in major quantity in M4 compared to M1, M2 and M3; furthermore, M4 does not contain quartz. Compared to M1, M2 and M3 compositions, the M4 mineralogy deviates by higher content of mafic (iron-bearing) silicate minerals.

3.1.3. XRF analysis

X-Ray Fluorescence (XRF) bulk chemical analyses display the chemical composition of the rocks as a percentage of the total mass, samples are grinded and ignited to 550°C. Silicon is the major component for all M1, M2, M3 and M4 (**Figure 15**).

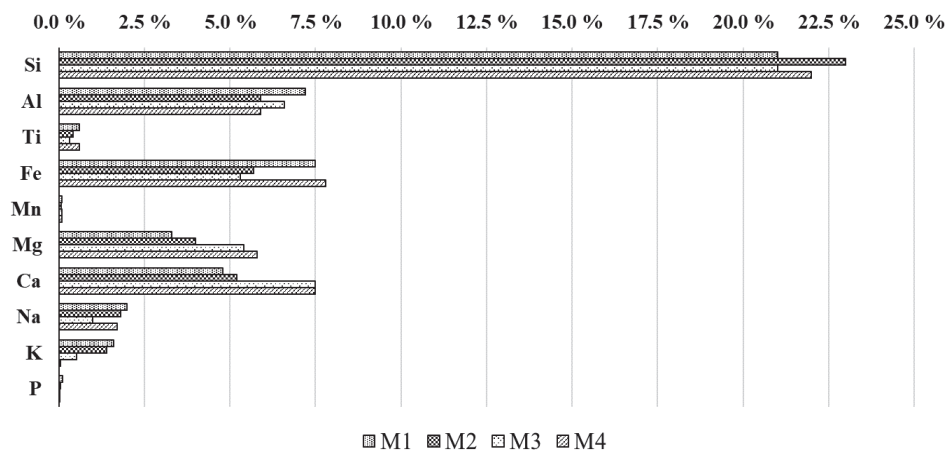


Figure 15 Spectrum of M1, M2, M3 and M4 chemical composition

(percentage of the total solid mass). Element abbreviations:

Si/silicon, Al/aluminium, Ti/titanium, Fe/iron, Mn/manganese, Mg/magnesium,
Ca/calcium, Na/sodium, K/potassium, P/phosphorus

3.1.4. Standard tests characterization

The pavement design manual “Håndbok N200” (NPRA 2014a) sets requirements for the use of crushed rocks. It is possible to use this resource in the road base layer as paved crushed rocks and in the road subbase layer as unsorted crushed rocks if Los-Angeles standard test (LA value) and micro-Deval standard test (MDE value) are fulfilled. The LA limit values are respectively 30 and 35 for base layer and subbase layer, the MDE limit value is 15 for both of them. Further requirements in terms of upper and lower grain size distribution curve are demanded for the base layer (**Figure 16**). The distribution curve of the subbase layer must be within 20/120 mm; this is one of the most common grain shapes defined in the design guidelines (NPRA 2014a).

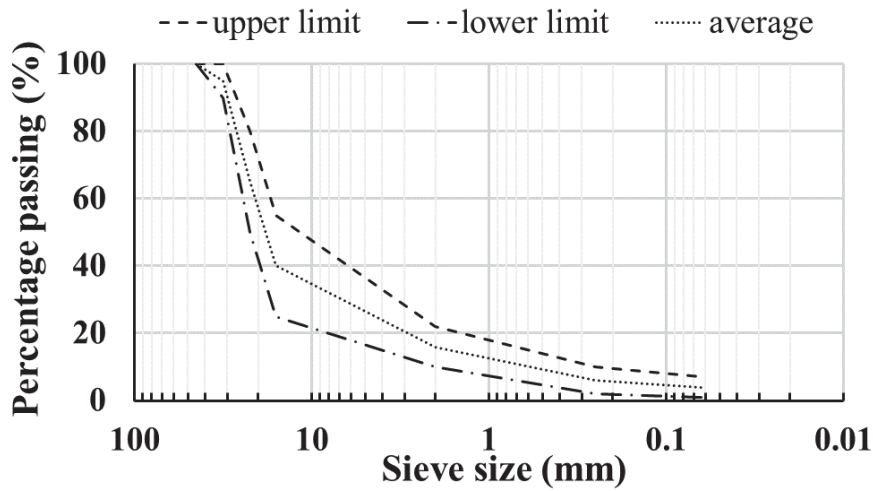


Figure 16 Grain size distribution limit curves for base layer

Figure 17 displays the materials values related to LA and MDE standard check procedures. Materials M1 and M4 fulfil the code requirements. Both materials M2 and M3 have LA values lying close to the limit, and exceed the threshold regarding MDE values. Materials M1 and M4 are designated as “strong”, while materials M2 and M3 are designated as “weak” in the research.

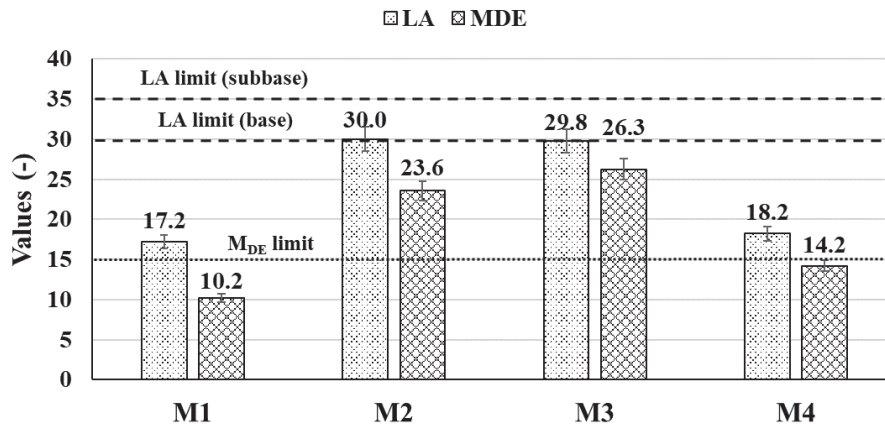


Figure 17 Los Angeles and micro-Deval values of investigated materials

3.2. CRUSHABILITY OF ROCKS

3.2.1. Scope and preparation of the test

The crushing and variation in grain size of UGMs is investigated during the two phases attaining a road pavement structure. They are construction phase, simulated by a full scale testing to assess aggregate soundness after rolling, and service life phase, simulated with the triaxial cell apparatus. The construction phase often reduces the service life of a road; furthermore, this investigation can bring to a better understanding of the relationship between the standard tests (LA, MDE) and the behaviour of the crushed rocks in situ. The crushing of a subbase layer is investigated for this purpose. The sieving curves referring to before and after the external actions are compared.

The materials M1, M2 and M3 used in the construction phase have gradation 20/120 mm. They are placed in three areas close to each other: each area is made of about 15 t of rocks and is approximately 7 m long, 5 m wide and 300 mm high. The compactor exerts its action just on one side of the rocks, as shown in **Figure 18**.

It is assumed that, before the compacting action takes place, the grain size distribution associated with the not compacted stripe (marked in blue) is the same of the compacted stripe (marked in red). Four portions are identified in each area: two do not undergo compaction and two undergo compaction. Each portion is 1 m wide, 1 m long, 300 mm high and weighs about 200 kg; portions are numbered from 1 to 12. Bomag BW 213 DH is the single steel drum roller used in the construction phase. Its weight is 12.3 t, the drum axle load is 7.6 t, the wheel axle load is 5.2 t, the static linear load is 35.5 kg/cm and the working width is 2.1 m.

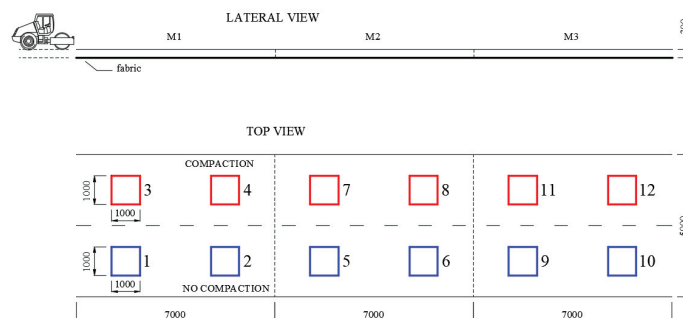


Figure 18 Layout of the field test to assess rocks crushability (dimensions in mm)

Figure 19 depicts the main stages of the test fulfilment: firstly, the existing surface is compacted with a single steel drum roller and operators lay out a polypropylene not woven geotextile (a), which prevents losing the small fractions produced during the test. The materials are tipped from a truck and distributed uniformly with the help of a gravedigger. The single steel drum roller Bomag BW 213 DH then compacts one side of the placed crushed rocks (b), it accomplishes four passages as specified in the manual code (NPRA 2014a). **Figure 20** displays the bulk densities of the layer before and after the roller compaction. The construction phase is completed and the twelve portions are highlighted with coloured spray (c). The rocks are collected from these portions by hand to keep the gradation as unaltered as possible and moved into plastic bags (d); finally, the material is sieved.



(a)



(b)



(c)



(d)

Figure 19 Main stages of the field test to assess rocks crushability

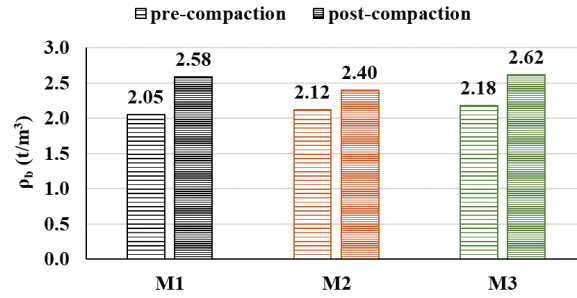


Figure 20 Bulk density of the unbound layer before and after roller compaction

Researchers have used various parameters or measures to represent the amount of particle breakage that takes place during loading (Gupta 2016); either as the variation of a particular grain diameter (Lade et al. 1996; Marsal 1967; Miura and O-hara 1979) or as the shift of the whole grain size distribution curve (Hardin and Asce 1985). The research refers to coefficient of uniformity C_u , coefficient of curvature C_c and particle breakage factor B_{10} (Lade et al. 1996). These parameters are defined as

$$C_u = \frac{D_{10}}{D_{60}}, \quad (\text{Eq. 13})$$

$$C_c = \frac{D_{30}^2}{D_{10}D_{60}}, \quad (\text{Eq. 14})$$

$$B_{10} = 1 - \frac{D_{10,f}}{D_{10,i}}; \quad (\text{Eq. 15})$$

where D_{10} , D_{30} , D_{60} are respectively the grain diameter at 10%, 30%, 60% passing, subscripts f and i respectively stand for final and initial gradation.

According to the pavement design manual N200, traffic class F entails at least 10 million repetitions of 10-tonne standard axle load (NPRA 2014a). The RTLT equipment is used to reproduce the average stress state in the subbase: 20 kPa and 120 kPa are the pressures respectively set in the horizontal and vertical directions in the triaxial cell (Floss 2001; Gorman and Mooney 2003; Mooney and Adam 2007; Yoo and Selig 1980). COMSOL software is used to simulate the two mentioned stages to assess the stress level and distribution. The modelling

highlights a remarkable difference in the stress state; during the construction phase rocks are expected to experience a state of stress which is larger than the one expected during the service life phase (Kwon et al. 2008).

Two specimens are tested for each material M1, M2 and M3 in the RTLT. All the samples have a diameter of 150 mm and height of 240 mm. The lower size of the subbase investigated in situ is 20 mm; moreover, it is recommended the maximum testing particle size to be smaller than one fifth of the specimen diameter (CEN 2004): the specimens are made of crushed rocks 20/30 mm in size. All the materials are washed and dried before the testing in the triaxial cell. The specimens are subjected to one million load repetitions, since this amount is sufficient to highlight discrepancies among the three materials.

3.2.2. Crushability assessment in laboratory and in field

The crushed rocks coming from the twelve field portions are sieved. The steel drum roller exerts its action just along a stripe which comprises six portions. It is assumed that, before the compaction takes place, the grain size distribution referring to the not compacted stripe is the same of the compacted stripe. In total twelve sieving curves are assessed. Therefore for each material type there is a set of two portions subjected to the same treatment (compacted or not compacted), for each set the average curve is assessed: **Figure 21** depicts six sieving curves. The amount of particle breakage during compaction can be visualized thanks to the particle size distribution curves measured before and after the external action.

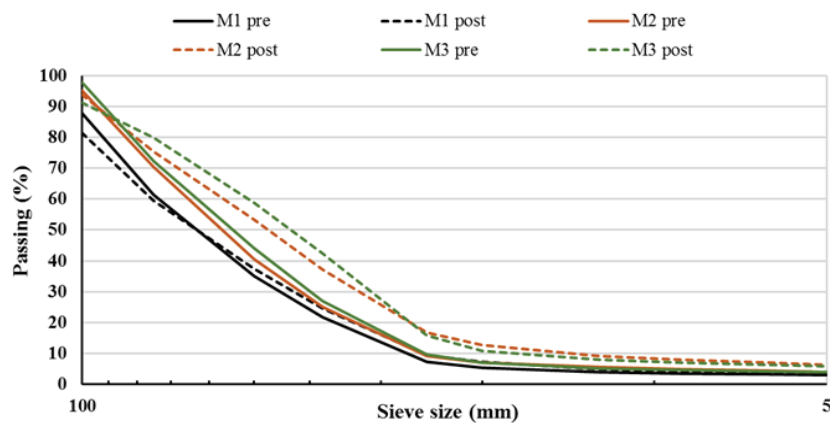


Figure 21 Sieving curves referring to pre-compaction and post-compaction action

From **Figure 21** it is apparent that there is a slight change in the grain size for material M1, while both materials M2 and M3 undergo substantial crushing. There is an unexpected crossing of lines between 100 mm and 75 mm regarding pre- and post-compaction: the assumption that the grading curve of the not compacted stripe is the same of the compacted stripe before the roller action turns out to be not completely exact; although this hypothesis is necessary in order not to sieve all the materials placed in situ (about 45 t). Each sieving curve is fitted by a third-order equation of the type

$$ax^3 + bx^2 + cx + d = 0, \quad (\text{Eq. 16})$$

six polynomial expressions are calculated based on the sieving curves. Considering these new calculated particle size distribution curves, it is possible to have a better estimation of the coefficient of uniformity C_u , coefficient of curvature C_c and particle breakage factor B_{10} . In addition, the optimum vertical translation of the pre-compaction curve towards the post-compaction curve is estimated with the least square methods; the value ζ quantifies this translation and also contributes to evaluating the overall difference in the curve shapes. **Figure 22** displays the coefficient particle breakage factor for each material, material M1 experiences the smallest modifications.

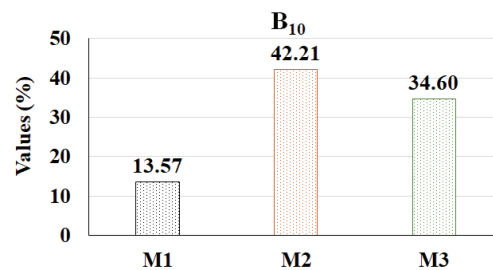


Figure 22 Particle breakage factor of the calculated sieving curves

It is possible to establish a relationship between the standard tests and the particle breakage factor as follows

$$LA = \alpha B_{10} , \quad (\text{Eq. 17})$$

$$M_{DE} = \beta B_{10} , \quad (\text{Eq. 18})$$

the best fitting values for parameters α , β in this case are $\alpha = 0.95$ and $\beta = 0.69$. The displacement along the y-axis of the pre-compaction curve assessed with the least square method is $\zeta = -0.14$ for M1, $\zeta = 6.68$ for M2 and $\zeta = 7.3$ for M3. The pre- and post-compaction curves for material M1 are much closer compared to the ones concerning materials M2 and M3. There is a good correlation between the crushing standard tests and the crushing taking place in situ.

Specimens made of crushed rocks M1, M2 and M3 in size 20/30 mm are tested in the triaxial cell. A set of two specimens for each type is tested and sieved both before and after the load action, therefore twelve sieving curves are assessed. Average curves are estimated: **Figure 23** depicts six sieving curves. The trends of pre- and post-load curves are very similar for all the material types.

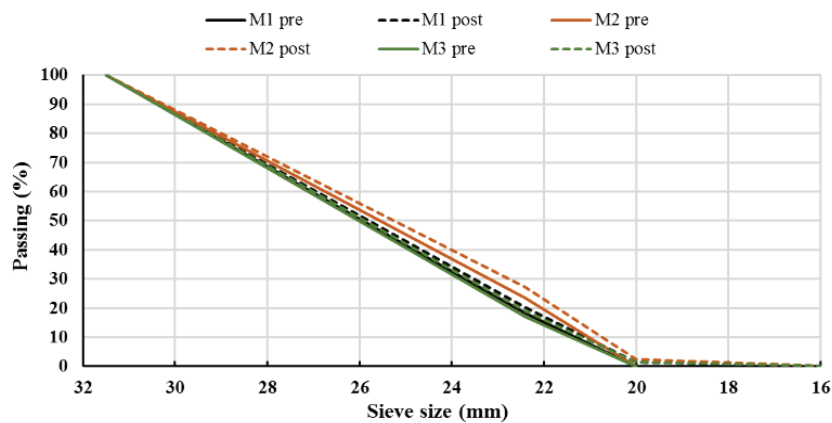


Figure 23 Sieving curves referring to pre-load and post-load action

Figure 24 shows the particle breakage factors, their values are very close to the lower limit zero, which would imply no particle breakage. The curves are considerably close to each other for all the materials and the loading action does not bring to significant crushing.

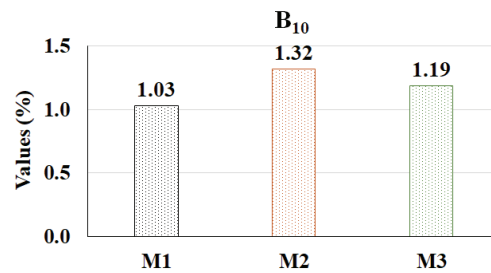


Figure 24 Particle breakage factor of the sieving curves

No significant differences in grain size are observed due to the service life phase loading: all the materials perform similarly in this scenario.

3.3. POLYMER-BASED ADDITIVE STABILIZATION

The polymer-based additive used in the research is water-soluble, non-leachable and UV, heat stable. The additive is a nanoscale technology and is made of two components C1 and C2; the modification taking place at nanoscale dimension entails major changes at a relative larger scale (Huang and Wang 2016; Paul and Robeson 2008).

Component C1 is an acrylic co-polymer emulsion based on acetic acid and methanol. The particle size is lower than 90 nm and has almost the same number of polymer particles as soil particles. Component C2 is a polymeric dispersion based on propylene glycol and alkoxy-alkyl silyl. **Figure 25** shows the stabilization process. After hydrolysis, the formed silanol (Si-OH) group can condense with another silanol group belonging to the silicate-containing surface of the rocks and form a siloxane linkage (= Si-O-Si=), namely a strong chemical covalent polar bond (a). Therefore, component C2 converts the water absorbing silanol groups presented on the rocks surface to a 4-6 nm layer of hydrophobic alkyl siloxane (b); this takes place thanks to the organic group having a long alkyl chain (C₁₈H₃₇).

Components C1 and C2 impart water resistance, better lubrication for compaction and bonding action at ambient temperature. The existing positive and limited experience refers to silty and clayey soils tested in laboratory (Daniels and Hourani 2009; Ugwu et al. 2013) and in field (Kumar et al. 2017), therefore the research experiments with a new application context. The additive loses its effect in conditions that are seldom achieved in road construction:

prolonged exposure to base (Wasserman et al., 1989) or air temperature above 200°C (Kim et al., 2003).

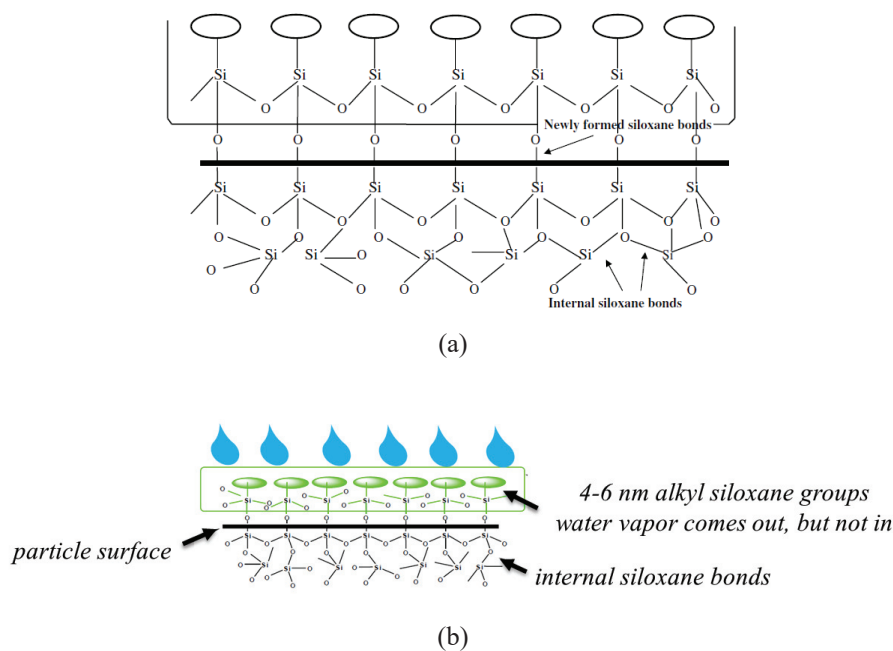


Figure 25 Polymer-based stabilization: siloxane linkages (a) (Ugwu et al. 2013) and formation of hydrophobic alkyl siloxane layer (b)

The use of this nanotechnology product shows how construction materials can be engineered to make them meet the quality requirements. Furthermore, the major areas of nanotechnology application are currently biomedicine and electronic engineering. Application in design and construction processes, including concrete technology and general civil structures, represents a field with new opportunities (Roco 2003; Sobolev and Shah 2015; Ugwu et al. 2013).

3.4. LIGNIN-BASED ADDITIVE STABILIZATION

The lignin-based additive (also referred to as lignosulfonate) is a renewable product of timber and pulp industry. It comes from lignin, which is generated by extracting fiber and wood pulp from plant biomass; lignin global annual production is approximately equal to 50 million tonne

(Angenent et al. 2004). Lignosulfonate is an organic polymer that consists of both hydrophilic and hydrophobic groups; it is a non-corrosive and non-toxic chemical (Alazigha et al. 2018).

Previous experiments investigating the strength and density modification of unpaved road using lignosulfonate showed promising outcomes for silty and clayey soils both in laboratory (Alazigha et al. 2018; Chen et al. 2014; Santoni et al. 2002; Ta'negonbadi and Noorzad 2018; Zhang et al. 2018) and in field (Hoff 2004; NPRA 2017b; Zhang et al. 2017). As in the case for the polymer-based additive, the product application to crushed rocks could bring to a wider acceptance of this admixture.

3.5. CRUSHED ROCKS STABILIZATION: LABORATORY TESTS

3.5.1. Mixture of the rocks available in situ

The major part of the rocks spread along the highway alignment has mafic igneous origin and is suitable for road construction; therefore, a convenient solution could be to mix appropriately the different rock types that are available in situ. Material M1 is mixed with materials M2 or M3 according to three proportions in mass (25%, 50%, 75%). LA and MDE tests respectively express resistance against fragmentation and wearing (Erichsen et al. 2011; Nälsund 2014).

Figure 26 displays the results for M1 mixed with M2 (a) and for M1 mixed with M3 (b).

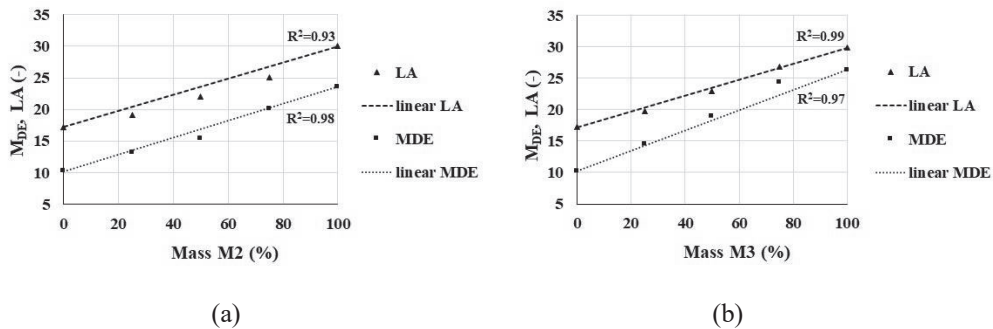


Figure 26 LA and MDE results and linear trend distributions for mixtures made of M2 and M1 (a), M3 and M1 (b)

The results distribution highlights a linear trend regarding both LA and MDE tests. The following equations describe the observed data in a mixture made of two materials i and j

$$LA_{i+j} = LA_i \frac{m_i}{m_i+m_j} + LA_j \frac{m_j}{m_i+m_j}, \quad (\text{Eq. 19})$$

$$M_{DE,i+j} = M_{DE,i} \frac{m_i}{m_i+m_j} + M_{DE,j} \frac{m_j}{m_i+m_j} \quad (\text{Eq. 20})$$

where m_i , m_j are the masses and LA_i , LA_j , $M_{DE,i}$, $M_{DE,j}$ are the standard test values assessed for materials i , j . A proper mixture of different crushed rocks types is an effective method to meet the code requirements and, possibly, to maximize the use of the “weak” material.

This requires an extra processing step and space to store the two (or more) qualities of rock; on the other hand, the clear linear results for different combinations should bolster a stable production: the economic feasibility has to be evaluated depending on local conditions. The mixed materials are not tested in the RTLTL device, but it is reasonable to believe that the mechanical properties show similar linear trend relationships.

3.5.2. Polymer-based additive application

The product is mixed at OMC and added to M2 or M3. Two different additive proportions are tested: 1 kg C1 + 1 kg C2 for 200 l water (proportion P1) and 10 kg C1 + 10 kg C2 for 200 l water (proportion P2), no special curing procedures are necessary. Proportion P2 has been studied after the initial proportion P1 suggested by the product supplier, since the results regarding P1-treated materials have not been too different from the untreated materials (especially for M3). The materials M2 and M3 enhanced performances are assessed by RTLTLs. The behaviour of untreated M1, M2 and M3 serves as a comparison basis. **Figure 27** displays the bulk density and dry density at OMC (a), the bulk density after the addition of the polymer-based product according to proportions P1, P2 (b).

Resilient modulus k - θ relationships are evaluated according to Hicks and Monismith model through data regression, **Figure 28** displays the results. It shows the performance of M1, M2 and M3 at OMC without additive; material M1 is stiffer than materials M2 and M3 (a). It also illustrates the enhanced behaviour of M2 and M3: they become stiffer and stiffer when changing from proportion P1 to proportion P2; the “weak” rocks performance becomes comparable with the “strong” rocks behaviour (b). The results show that the product is more effective on M2 than M3 probably because of the geological composition. The additive performance is dependent on the quantity of silicate minerals on the rocks surface. M2 and M3

have similar content of quartz and feldspar, but M2 is richer in amphibole and with a more distinct content of mica. M3 has a higher content of epidote-zoisite, which has lower Si-contents, as well as calcite (CaCO_3), which does not contain silicon.

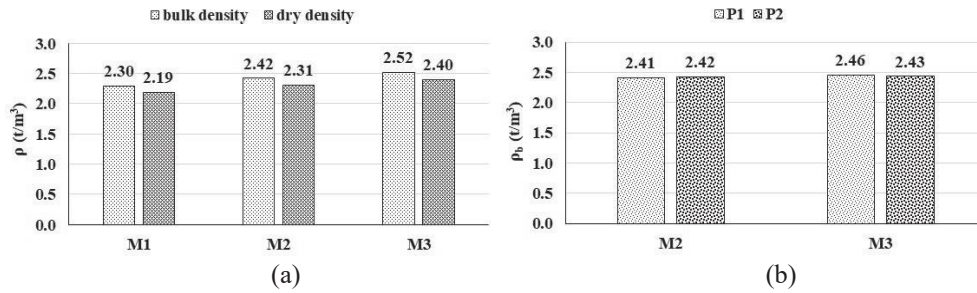


Figure 27 M1, M2 and M3 bulk density and dry density at OMC $w=5\%$ (a), M2 and M3 bulk density after additive application with P1, P2 proportions (b)

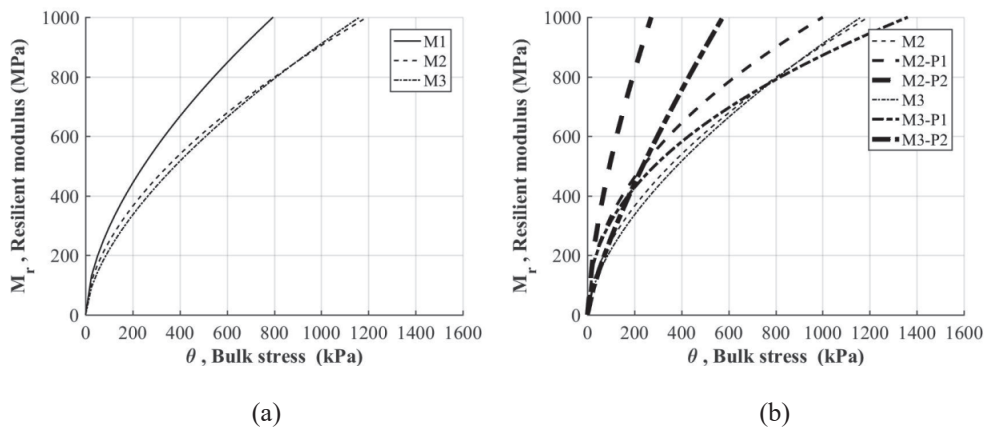


Figure 28 M1, M2 and M3 resilient modulus at OMC $w=5\%$ (a), M2 and M3 resilient modulus after additive application with P1, P2 proportions (b)

The additive effects also pertain to the deformation properties of the materials. **Figure 29** depicts the mobilized angle of friction ρ and the failure angle ϕ for the crushed rocks without and with the polymer-based stabilization, the additive application enhances both the angles.

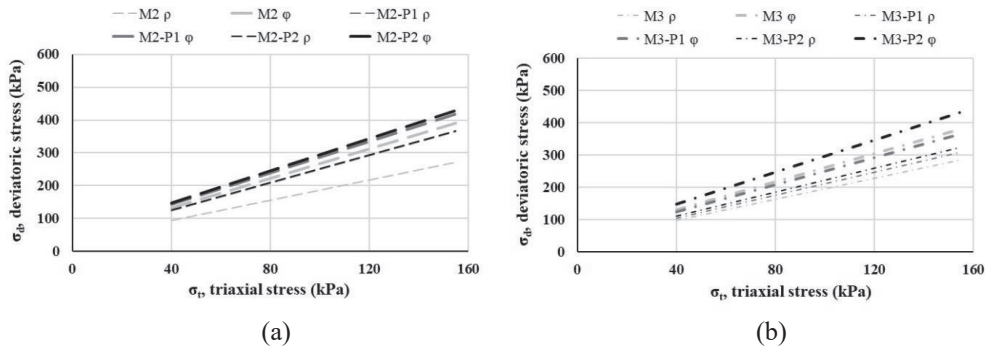


Figure 29 Mobilized angle of friction ρ and failure angle ϕ of M2 (a) and M3 (b) for untreated and additive-treated conditions

Proportion P2 is considered in the rest of the research. Furthermore, the beneficial coating effect promoted by the additive is evaluated by the standard procedures in terms of resistance against fragmentation (LA test) and wearing (MDE test). In this case, materials M2 and M3 are soaked with the additive (50% C1, 50% C2) and tested after 24 hours to let the crushed rocks dry. **Figure 30** shows that the additive supplies a significant beneficial effect when it comes to MDE wearing, it also provides a lesser benefit regarding the LA fragmentation. The steel balls used in the LA test imply higher impact loads compared to MDE test; therefore, the thin coating protection is more effective in the latter case.

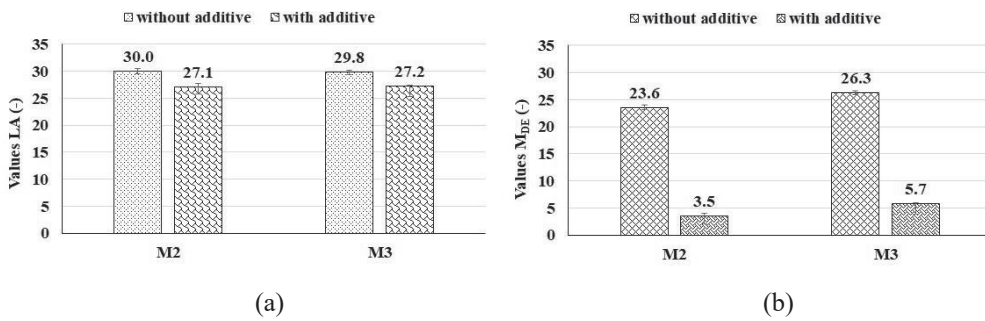


Figure 30 Coating effect provided by the polymer-based additive assessed by standard procedures: LA test (a), MDE test (b)

3.5.3. Lignin-based additive application

The product is mixed at OMC and added to M2 or M3; the mass percentage of lignosulfonate added to the crushed rocks is 1.5%. RLTs assess the materials M2 and M3 enhanced performances. Lignosulfonate needs a curing time to dry in order to become effective and attach properly to the material particles (Santoni et al., 2002). To simulate a long field curing process, each RLT sample is firstly conditioned at 50°C for 24 hours and then at 22°C (room temperature) for 24 hours before testing. The measured water contents after the curing process are between 2% and 2.5%. The behaviour of the untreated materials at $w=1\%$ serves as a comparison basis, this is a cautious comparison since M_R gradually reduces as w increases (Erlingsson et al. 2017). **Figure 31** displays the bulk density and dry density at $w=1\%$ (a) and the bulk density relative to the main stages of the curing process after additive application (b).

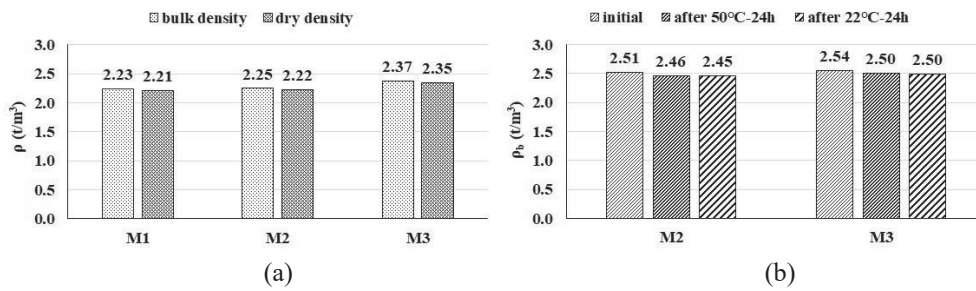


Figure 31 M1, M2 and M3 bulk density and dry density at $w=1\%$ (a),
M2 and M3 bulk density after additive application (b)

Resilient modulus k - θ relationships are evaluated according to Hicks and Monismith model through data regression, **Figure 32** displays the results. It shows the performance for M1, M2 and M3 at $w=1\%$ (a); material M1 is stiffer than M2 and M3; it also illustrates the enhanced stiffer resilient curves of materials M2 and M3 (b). The additive effects also pertain to the deformation properties of the materials. **Figure 33** depicts the mobilized angle of friction ρ and the failure angle ϕ for the crushed rocks without and with the lignin-based stabilization, the additive application enhances both the angles.

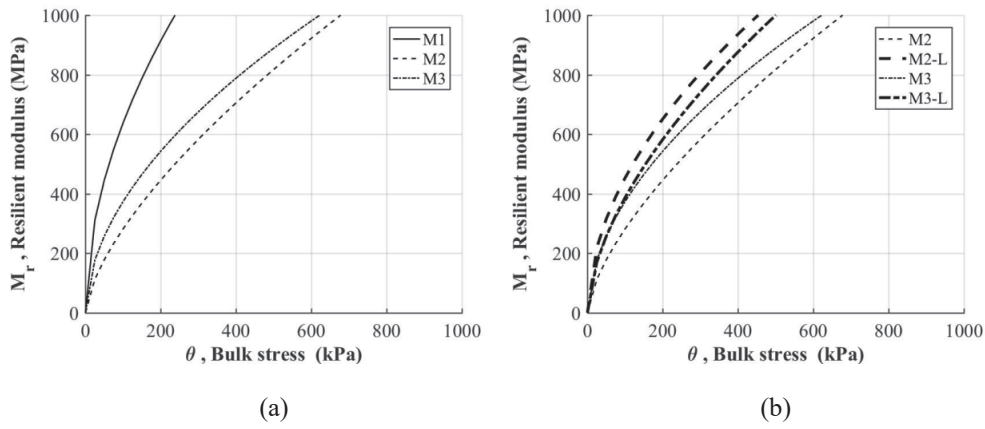


Figure 32 M1, M2 and M3 resilient modulus at $w=1\%$ (a), M2 and M3 resilient modulus after additive application (b)

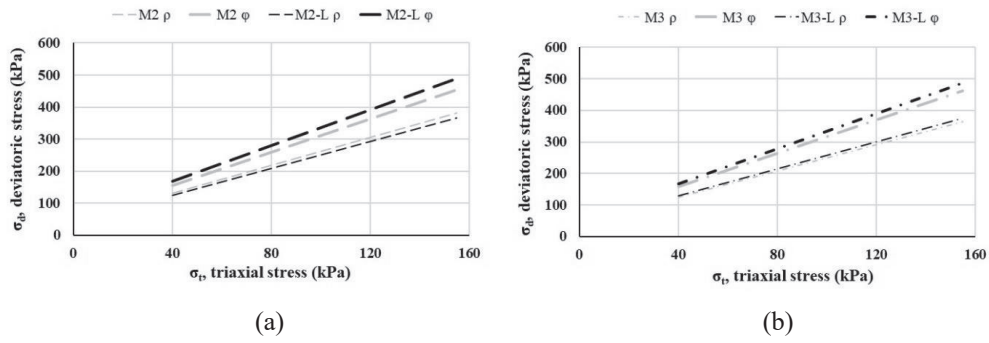


Figure 33 Mobilized angle of friction ρ and failure angle ϕ of M2 (a) and M3 (b) for untreated and additive-treated conditions

LA and MDE tests assess the beneficial coating effect provided by the lignin-based additive. Materials M2 and M3 are soaked with the product and undergo the same curing procedure describe for the RTLTLT specimens preparations. LA and MDE standard tests are used to assess the coating effect when soaked with the lignin-based additive. **Figure 34** shows that the product provides a beneficial effect in terms of LA fragmentation; there is also a small enhancement in terms of MDE wearing. The improvement in MDE values is not as pronounced as one would

expect because lignosulfonate is highly moisture susceptible (Santoni et al. 2002); this property is especially relevant when referring to running water, as in the case of MDE test.

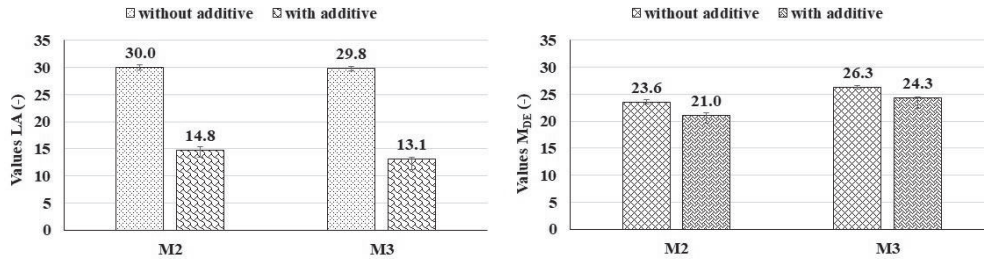


Figure 34 Coating effect provided by the lignin-based additive assessed by standard procedures: LA test (a), MDE test (b)

3.5.4. Overheating

Materials M2 and M3 are tested with the MDE procedure to assess if the overheating can induce modifications in the mineralogical structure, which may strengthen the rocks and improve the MDE results (Obert et al. 1946; Simpson and Fergus 1968; Zhang et al. 2009). The values of the three tested conditioning temperatures (105°C, 175°C, 250°C) do not seem to exert a major influence. On the other hand, the duration of the overheating seems to be a more relevant factor, as the results connected to the 48-hour conditioning are better than those connected to the 24-hour conditioning, as shown in **Figure 35**. Even so, the induced improvement is sensibly limited as the highest observed decrease among the original MDE values is equal to approximately two units. The tested conditioning temperatures do not significantly improve the weak materials to make them meet the code requirements. Anyway, overheating the crushed rocks would demand an intensive energy use even if a small beneficial effect was found.

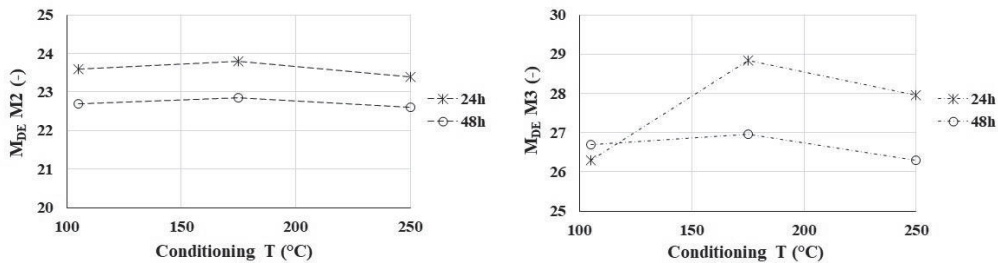


Figure 35 MDE values after overheating M2 (a) and M3 (b)

3.6. CRUSHED ROCKS STABILIZATION: MODELLING

3.6.1. Resilient modulus

The models presented in sections 2.2 are among the most used to describe the UGMs resilient modulus. The results obtained in the previous subsections 3.5.2 and 3.5.3 are here considered for the least-square regression analyses. The model MATLAB script used to carry out these calculations is reported in Appendix B.

Hicks and Monismith model enables a clear comparison between treated and untreated material in a two-dimensional plot, this has been already reported in subsections 3.5.2 and 3.5.3. Compared to Hicks and Monismith model, Uzan model takes into consideration the deviatoric stress as a further parameter to characterize resilient modulus. The 3D graphs reported in **Figure 36** refer to polymer-based additive (a) and lignin-based additive (b).

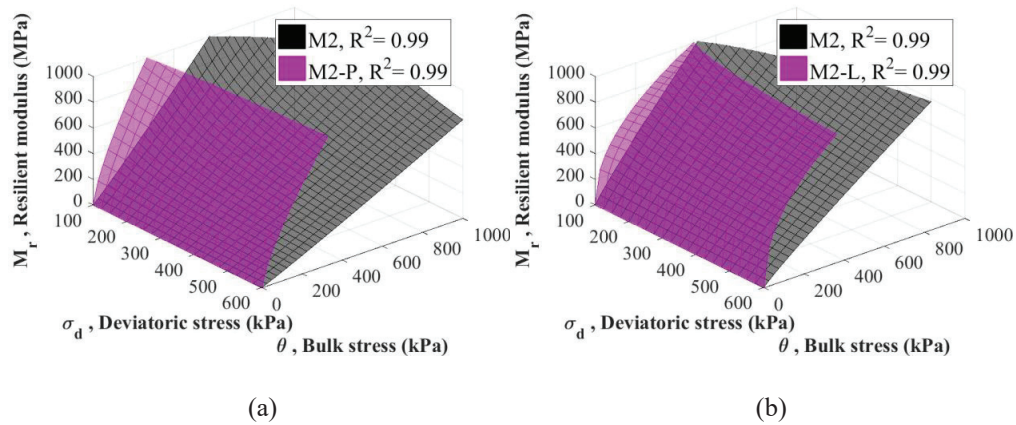


Figure 36 Resilient modulus according to Uzan model: polymer-based additive (a) and lignin-based additive (b)

Compared to Hicks and Monismith model, Uzan and Witczak model takes into consideration the octahedral stress as a further parameter to characterize resilient modulus. The 3D graphs displayed in **Figure 37** refer to polymer-based additive (a) and lignin-based additive (b).

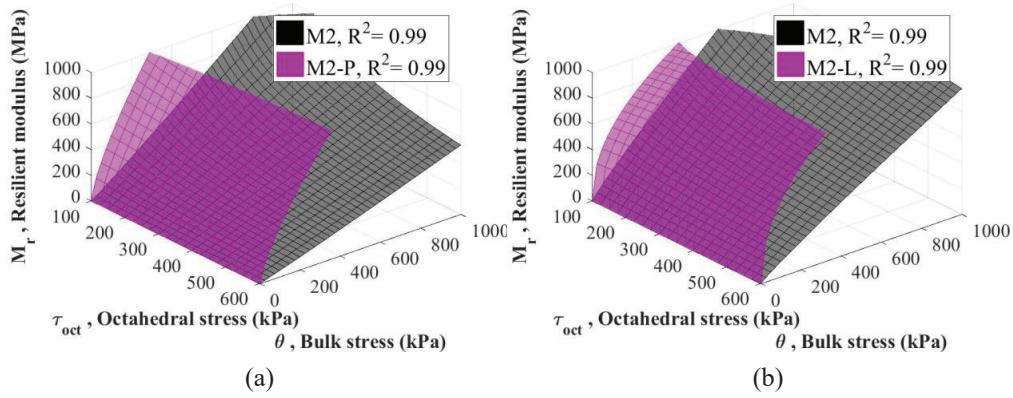


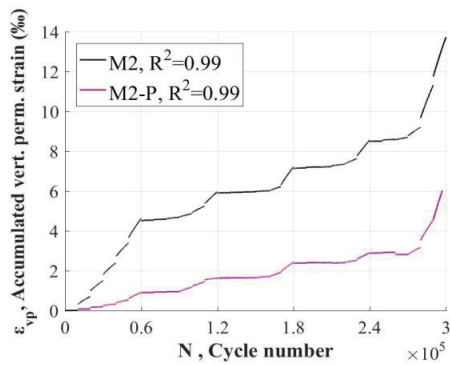
Figure 37 Resilient modulus according to Uzan and Witczak model:
 polymer-based additive (a) and lignin-based additive (b)

All the models clearly show that the additive application brings to higher values of resilient modulus M_R ; therefore, the additive application seems to be an effective solution to increase the material stiffness.

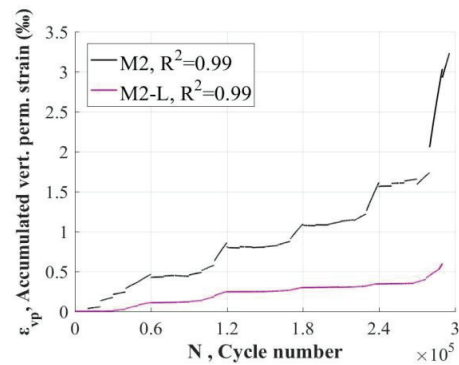
3.6.2. Accumulation of permanent vertical deformation

The models presented in sections 2.3 describe the UGMs accumulation of vertical permanent deformation. The results obtained in the previous subsections 3.5.2 and 3.5.3 are here taken into consideration for the least-square regression analyses. The model MATLAB script used to carry out these calculations is reported in Appendix C.

The first two considered models are Barksdale (**Figure 38**) and Sweere (**Figure 39**). These models fit the data corresponding to each single loading step considering the time hardening approach discussed above. The treated materials show considerable less deformation than the untreated materials.

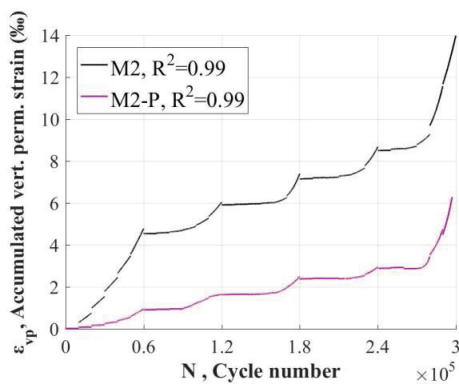


(a)

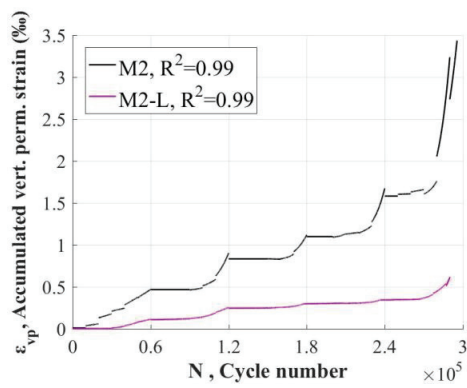


(b)

Figure 38 Accumulated vertical permanent deformation, Barksdale model:
polymer-based additive (a) and lignin-based additive (b)



(a)



(b)

Figure 39 Accumulated vertical permanent deformation, Sweere model:
polymer-based additive (a) and lignin-based additive (b)

Hyde model results are displayed in **Figure 40** for polymer-based additive (a) and lignin-based additive (b). Each loading sequence corresponds to a straight line, therefore, five straight lines correspond to the MS LSL RTLT. As the Barksdale and Sweere representations, also Hyde model highlights that the treated materials have better resistance to permanent deformation.

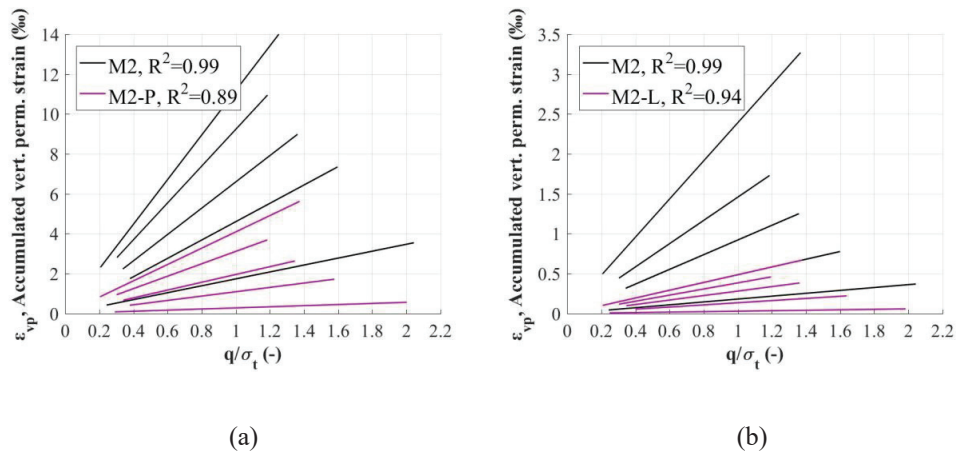


Figure 40 Accumulated vertical permanent deformation, Hyde model:
 polymer-based additive (a) and lignin-based additive (b)

Shenton model results are displayed in **Figure 41** for polymer-based additive (a) and lignin-based additive (b). Each loading sequence corresponds to a curve, therefore, five curves correspond to the MS LSL RTLTL. As well as the three previous representations, Shenton model also highlights the effectiveness of the product: the curves of the treated materials correspond to smaller vertical permanent deformations.

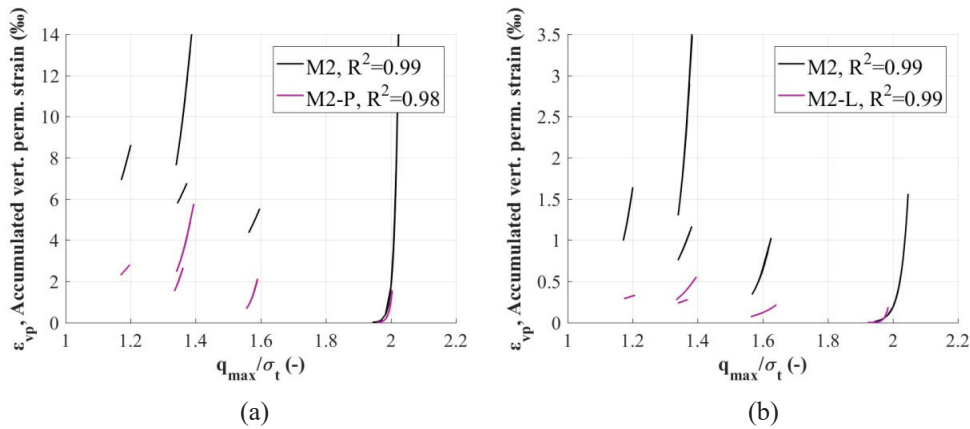


Figure 41 Accumulated vertical permanent deformation, Shenton model:
 polymer-based additive (a) and lignin-based additive (b)

3.6.3. *RTLTL finite element simulation*

Researchers have carried out numerical analyses to study the UGMs behaviour: they have considered linear and non-linear elastic and plastic relationships in the attempt to describe properly the material behaviour (Ghadimi and Nikraz 2017). This study compares numerical and experimental results in terms of vertical permanent deformation by implementing non-linear elastic, plastic and viscous constitutive relationships.

The RTLTL is modelled by using COMSOL Multiphysics software (COMSOL 2017). The goal of the modelling is to implement a constitutive relationship able to describe properly the accumulation of vertical permanent deformation: numerical and experimental results are compared. **Figure 42** displays a portion of the model, the problem is two-dimensional axisymmetric and quadrilateral elements are used in the mesh (height 180 mm, radius 75 mm, Poisson's ratio 0.3 and density 2300 kg/m³). A fixed boundary constraint is applied at the bottom.

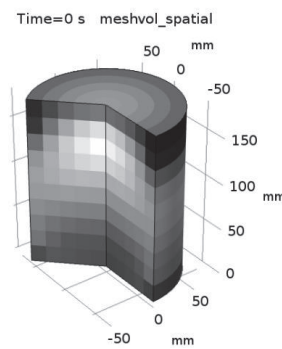


Figure 42 Mesh of the FEM RTLTL model

Different models can describe the UGM behaviour: non-linear elastic (Ghadimi and Nikraz 2017; Kim et al. 2009), plastic (Chazallon et al. 2006; Hornych et al. 2007) and creep (David et al. 2005) relationships have been used by researchers to interpret the UGMs' behaviour.

A time-dependent analysis is performed (as this enables a creep study), the total time is 30000 s and it corresponds to the actual duration of the RTLTL. Each loading step, as reported in section 2.1, corresponds to a specific combination of external triaxial and deviatoric stress and lasts for 1000 s; no deviatoric pulse repetitions are considered. COMSOL Multiphysics enables to implement a non-linear elastic model by specifying the elastic modulus trend. The

resilient moduli obtained by Hicks and Monismith, Uzan and Uzan and Witzak models are implemented.

Tresca and Von Mises yield criteria are used to specify associated flow plasticity. Each model requires the definition of two parameters, namely initial yield stress and plastic tangent modulus to define linear isotropic hardening. The initial yield stress is equal to the deviatoric stress of each loading step, since every step implies plastic deformation from the beginning. The plastic tangent modulus is evaluated as a secant value using the least-square method in a graph displaying $\sigma_1 - \sigma_3$ along y-axis and $\epsilon_{p,v}$ along x-axis for Tresca model or $(2/3) \cdot \epsilon_{p,v}$ along x-axis for Von Mises model.

UGMs are not considered to be viscous in the sense that applying a constant load does not bring about a time-dependent deformation, but models for viscosity could be adapted to account for the gradual increase in $\epsilon_{p,v}$ per load cycle. Norton power law is used to describe the viscosity associated with the duration of each loading step (1000 s) as a means to take into consideration the load pulse repetitions taking place in the actual RTLT. The creep rate is defined as

$$\dot{\epsilon}_{cr} = A\sigma^n, \quad (\text{Eq. 21})$$

where A is the creep rate coefficient and n is the stress exponent.

The aim of the modelling is to evaluate the permanent vertical deformations and compare the results with the experimental outcomes. The first modelling attempt considers Tresca plasticity model. All the examined non-linear elastic models (Hicks and Monismith, Uzan, Uzan and Witzak) are implemented. **Figure 43** displays the results for the polymer-based additive (a) and the lignin-based additive (b).

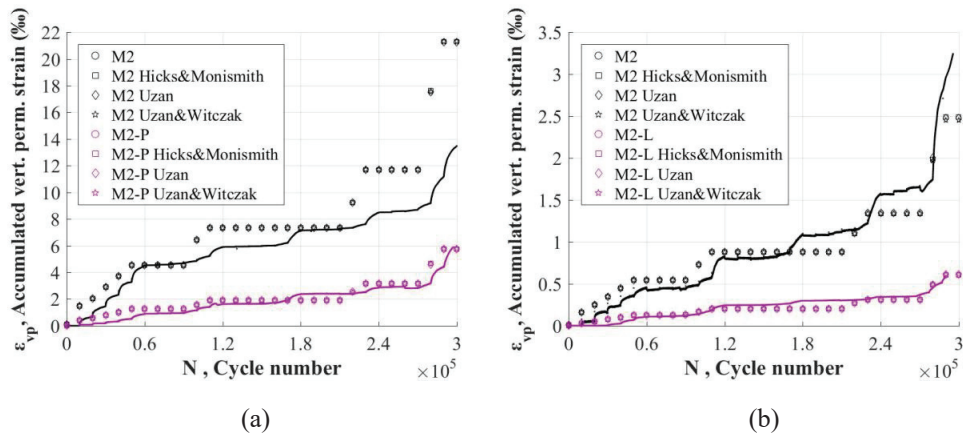


Figure 43 Accumulated vertical permanent deformation, Tresca plasticity model: polymer-based additive (a) and lignin-based additive (b)

The second modelling attempt considers Von Mises plasticity, all the non-linear elastic laws previously mentioned are implemented. **Figure 44** displays the results for the polymer-based additive (a) and the lignin-based additive (b).

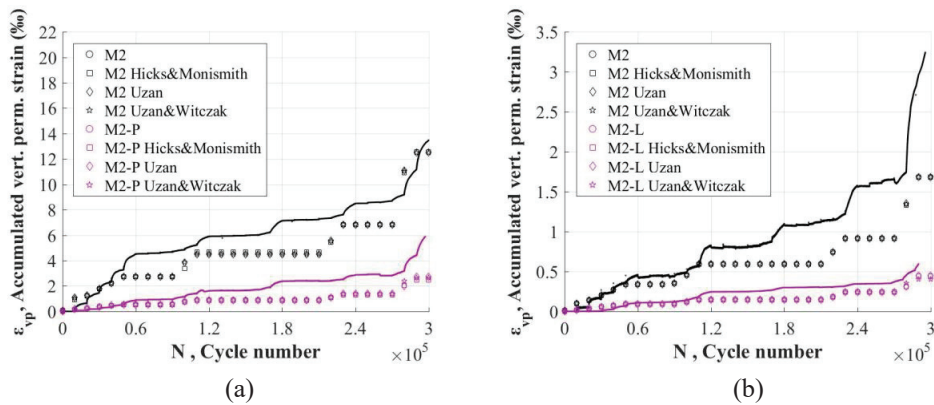


Figure 44 Accumulated vertical permanent deformation, Von Mises plasticity model: polymer-based additive (a) and lignin-based additive (b)

Comparing Figure 18 and Figure 19, Tresca plasticity model tends to overestimate the results, while Von Mises plasticity model tends to underestimate them. Moreover, all the considered non-linear elastic models bring to results very close to each other.

Since Von Mises model underestimates the actual experimental results, viscous behaviour is added to the material model. The considered non-linear elastic law associated with creep is only Hicks and Monismith, since the choice of the elastic law does not seem to play a significant role as just observed. A parametric analysis has been performed to find the best fitting values of the creep rate coefficient A and the stress exponent n . **Figure 45** displays the results for the polymer-based additive (a) and the lignin-based additive (b). Adding viscosity to Von Mises plasticity provides a better description of the experimental results. The finite element model could be further extended to comprise analyses of actual roads.

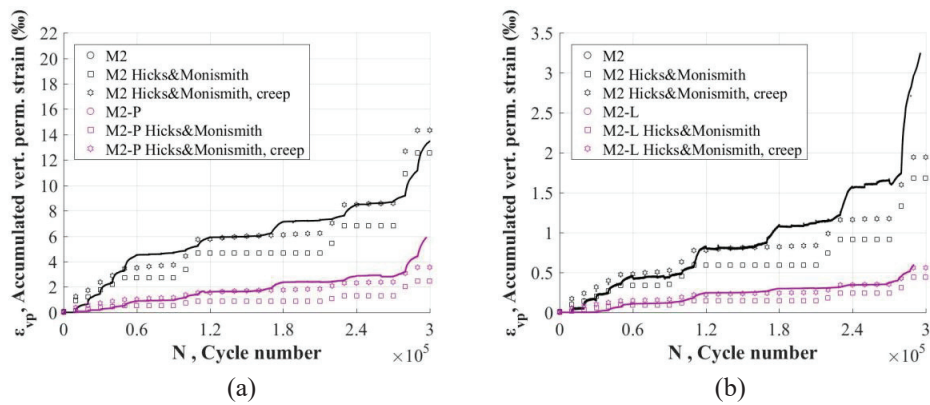


Figure 45 Accumulated vertical permanent deformation, Shenton model: polymer-based additive (a) and lignin-based additive (b)

3.7. CRUSHED ROCKS STABILIZATION: FIELD TESTS

3.7.1. Field test preparation

The field test is located in a large area available inside a quarry in Vassfjellet. Material M4 is a “strong” material, in the sense that it does fulfil the design guide requirements. Arranging the field test using a “weak” material has not been possible for practical and economic reasons, since it has not been easy to find enough quantities from quarries. On the other hand, this does

not hinder the general purpose of the research, namely to investigate whether the use of the additives can improve the mechanical properties of a given type of crushed rocks at a full-scale level.

The grain size distribution curve used for this investigation is displayed in solid line (“laboratory and in-field initial”) in **Figure 46**; the same figure also shows in dashed line (“in-field final”) the grading curve attained after the mixing and compaction actions necessary for the construction of the field test sections. The two distribution curves are very close as expected due to the good LA value. They are also very close to the grading curve used for the laboratory experiences (**Figure 16**), OMC is equal to 5%.

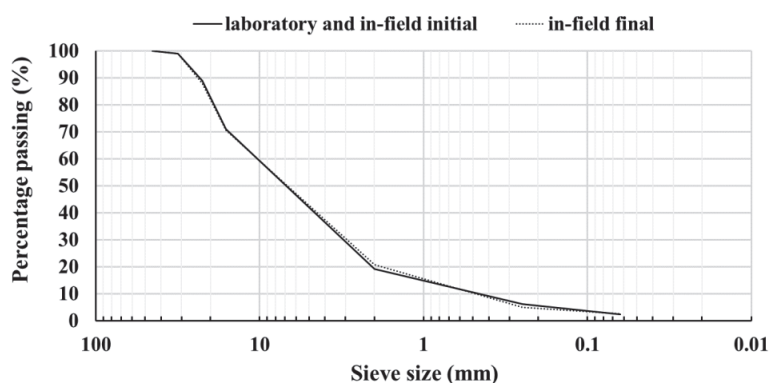


Figure 46 Grain size distribution curve (base layer) used in the investigations carried out in laboratory and in field

Three 0/32 base layer sections are built, they correspond to three locations which undergo different treatments: water use (location L0), polymer-based additive (location L1), lignin-based additive (location L2); each section is 30 cm thick (before compaction), 3.5 m wide and 10 m long. As a first step, the existing subgrade is covered by a 0/8 mm capping layer, its thickness varies between 50 cm and 60 cm. Since the zone of influence of the LWD is found to be 1.5 to 2 times the 30-cm diameter of the LWD plate (Elhakim et al. 2014), the chosen value of the capping layer thickness appears reasonable. Afterwards, a roller compactor compacts the capping layer, Bomag BW 177 D-4 is the single steel drum roller used for this purpose. Its weight is 7.5 t, the drum axle load is 4.2 t, the wheel axle load is 3.3 t, the static linear load is 24.9 kg/cm and the working width is 1.7 m; the roller compactor accomplishes seven passages as specified in the manual code (NPRA 2014a).

Figure 47 displays the main steps of the first 15-cm construction. 10 tonne of 0/32 crushed rocks are placed in each location (a). Water and additives are transported to the field thanks to Intermediate Bulk Containers (IBCs); before pumping out their contents, operators use of a mixing drill to attain more homogeneous solutions. Each location is treated according to the proportions already used in laboratory as reported in subsections 3.5.2 and 3.5.3 (b, c, d). Afterwards, a light recycler machine operates achieving two passages (e). The teeth of the shifting rotor gently blend rocks, water and additives up to a depth of 15 cm. Finally, the roller compactor Bomag BW 177 D-4 compacts each location with five passages as specified in the manual code (NPRA 2014a) (f). Successively, the second 15-cm part of the 30-cm thick base layer is placed and undergoes the same procedure. **Table 6** reports the total quantity of the admixtures totally used in each location.

Table 6 Quantity of water and additives used in each investigated location

Location	water (kg)	P-based additive (kg)		L-based additive (kg)
		component C1	component C2	
L0	1000	0	0	0
L1	1000	52	52	0
L2	1000	0	0	300

Therefore, the liquids amount used in L2 is bigger than in L0 and L1. The final thickness after the compaction procedures is about 17 cm; the construction processes do not significantly alter the grain size distribution curve as reported in Figure 4. **Figure 48** shows the completion of the three road base sections.



Figure 47 Construction of the first 15-cm part of the base layer: laying of the material (a), spreading water (b), spreading polymer-based additive (c), spreading lignin-based additive (d), mixing (e) and compacting (f)



Figure 48 Construction completion of the road base sections: with water (L0), with polymer-based additive (L1) and with lignin-based additive (L2)

3.7.2. Measurement procedures

The main device adopted in the field to assess the additives' effectiveness is the Light Weight Deflectometer (LWD). LWD is used for the determination of bearing capacity and compaction quality of soils and unbound materials (ASTM International 2015); it is currently gaining more and more interest in several countries, as it is a portable spot-testing device for quality control (Mooney and Miller 2009). The LWD uses the same technology of the Falling Weight Deflectometer (FWD) equipment: the major differences are the reduced load pulse duration and reduced maximum applied force (Fleming et al. 2007).

Several types of LWD are available, but are similar in principle; the research is performed using the LWD produced by HMP company (HMP-LFG 2018). The test consists in subjecting the road base layer to a pulse load applied via a steel plate, a geophone records the speed of the plate movement and assesses its acceleration and settlement. The maximum impact force is 7.07 kN, the duration of the impact is 17.0 ± 1.5 ms and the settlement range measured is 0.1 to 2.0 mm ± 0.02 mm. After completion of three measurements, the average settlement S_m and the dynamic modulus E_{LWD} are evaluated. E_{LWD} is determined via circular plate on half-space theory assuming homogeneous, isotropic, linear elastic soil behaviour (Boussinesq 1885; HMP-LFG 2017; Vennapusa and White 2009). The goal of the research lies more on comparing the LWD results for the three investigated locations than in obtaining absolute values for each location. Measurements are carried out daily up to 50 days after construction completion.

Another instrument used to evaluate the additives' performances is the Dynamic Cone Penetrometer (DCP), the test provides a measure of the material's in situ resistance to penetration. The test is performed by driving a metal cone into the ground with a 8 kg weight dropped from a distance of 575 mm (ASTM International 2018). Test results might be correlated to other properties, e. g. resilient modulus and bearing capacity (Chen et al. 2005, 1999; Siekmeier et al. 2000). DCP device is used in the research as a further practical and easy method to assess the additives' performances in addition to LWD. Finally, the resistance against permanent deformation is assessed by measuring the rutting formation due to a single vehicle's passages. The front axle of a truck is driven back and forth on the three locations for a determined number of times, the front axle weight is 6 t and the axle length is 1.7 m.

LWD measurements are taken on a daily basis up to 50 days, they approximately correspond to May and June 2018; the first measurements are taken 48 h after construction. In case of precipitation, the measurements are carried out after it has stopped raining. Average,

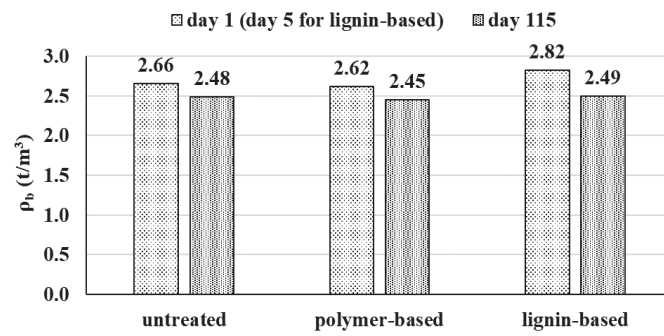
minimum, maximum temperature and precipitation are daily recorded in the two closest weather stations: Skjetlein station and Saupstad station, both of them are approximately located 5 km away from the test site (Norwegian Meteorological Institute 2018). The average values are assessed thanks to the National Weather Service distance weighting method (US National Weather Service 2018). In order to study a longer term behaviour, after 60 days new LWD measurements are carried out for 5 days (namely from day 110 to day 115 after construction completion); the operations regarding DCP and rutting formations take place during last day 115.

3.7.3. Field test results

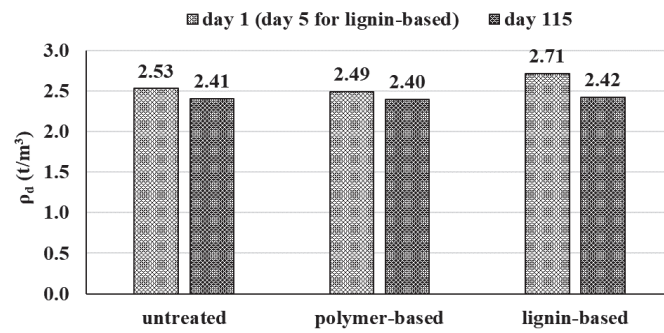
The in situ density is assessed thanks to the excavation method (CEN 2017), two areas for each location are investigated and average values are presented; **Figure 49** displays the bulk density (a), dry density (b) and water content (c). The area treated with lignin-based additive has the highest density, this can be partly due to the fact that the lignosulfonate density (approximately 0.05 t/m^3) is included. The liquid quantity used for location L2 has been significantly higher than in the other two locations L0 and L1; therefore, L2 has been clearly oversaturated after construction and the first water content measurements have been carried out after 120 h. As an input for further research, mixing proportions containing lower water percentages may be tested.

Figure 50 displays the appearance of the surfaces after 50 days. Compared to the untreated location L0 (a), both the polymer-based and the lignin-based products seem to promote a more bounded layer at location L1 (b) and at location L2 (c), respectively.

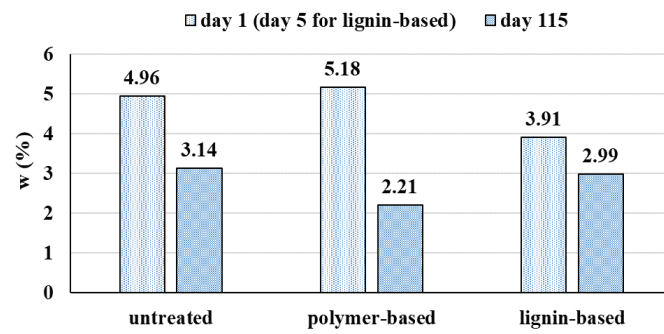
Figure 51 displays the weather conditions during the first 50 days after construction completion. The average temperature varies between $5 \text{ }^\circ\text{C}$ and $20 \text{ }^\circ\text{C}$, rain starts to take place approximately every day from day 24; the trend is exceptionally warm and dry in the Norwegian context (Norsk rikskringkasting AS 2018). After the initial 50 days, no measurements are taken for a period of 60 days. During this interval the average values of average, minimum and maximum temperature have been $14.9 \text{ }^\circ\text{C}$, $10.3 \text{ }^\circ\text{C}$ and $20.6 \text{ }^\circ\text{C}$, respectively; the cumulated precipitation has been 199.9 mm.



(a)



(b)



(c)

Figure 49 Bulk density (a), dry density (b) and water content (c) for materials tested in the field after construction and after 115 days

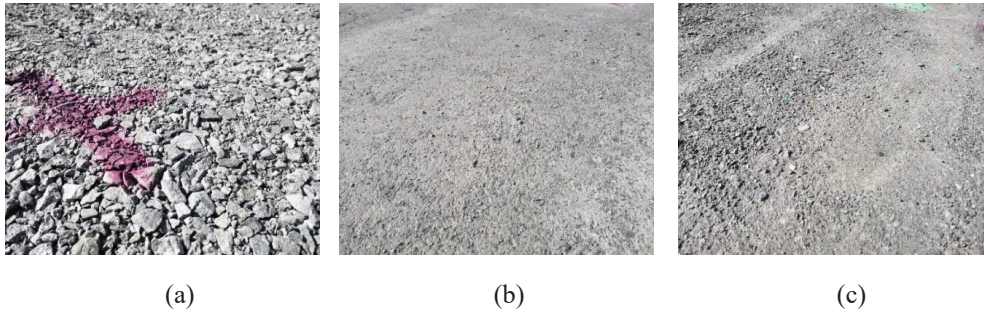


Figure 50 Surface appearance after 50 days:
 untreated (a), with polymer-based additive (b) and with lignin-based additive (c)

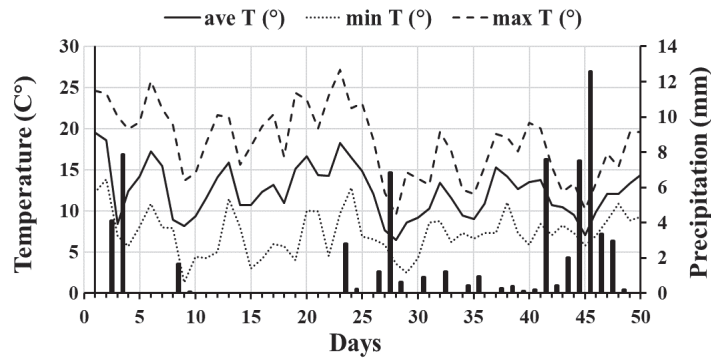


Figure 51 Weather conditions in the field during the first 50 days after construction:
 average, minimum, maximum temperature and precipitation

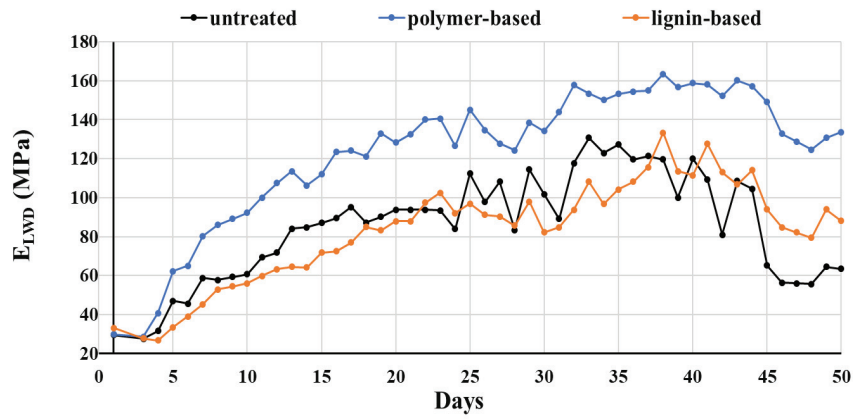
Figure 52 shows the LWD results regarding the dynamic modulus E_{LWD} (a) and the settlement S_{LWD} (b). During the initial 50 days after construction, the polymer-based additive brings to the highest E_{LWD} value (163.5 MPa) and the lowest S_{LWD} value (0.14 mm) for location L1. The improvement of the lignin-based treated area takes place at a slower pace. The performance of location L2 becomes better than the untreated location L0 after 23 days, this may be also connected to the oversaturation of location L2. The lignin-based additive reaches 133.4 MPa as the highest E_{LWD} value and 0.18 as the lowest S_{LWD} . Both the treated areas L1 and L2 reach their best performance values on day 38.

Figure 53 displays some relevant pictures worth to be discussed. The polymer-based additive treated location L1 becomes very little sensitive to water (a): some water, which is

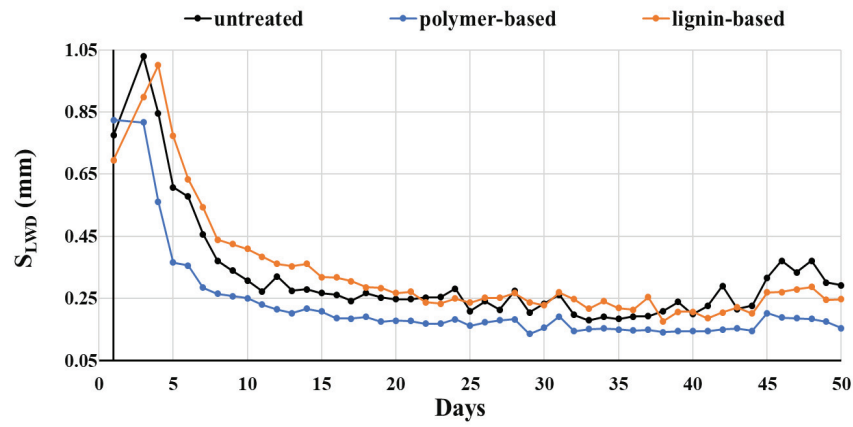
poured on the top of the layer on purpose, does not seem to penetrate. Some observations regarding the lignin-based additive can be drawn: while the lignosulfonate on the outermost part of layer is hardened forming a bonded “crust” with very few pores, the internal part still needs time to dry and attach to the material particles, as found by excavating some centimetres below the surface (b). Most likely, this is the reason why it is possible to see some lignosulfonate “droplets” reaching the surface during sunny days (c); moreover, this may also imply that improving the E_{LWD} values for location L2 takes a longer time. The “crust” effect would probably decrease if less water had been added to the test site, i.e. a higher concentrated solution of lignosulfonate; therefore, this may be an input for further research, both in laboratory and in field.

Lignosulfonate is water-soluble and dissolves in case of precipitation (d); therefore, the LWD results are affected by the rain, which takes place almost every day after day 24. In addition, the untreated location L0 is the area most vulnerable to water because there are meaningful changes in its E_{LWD} and S_{LWD} values from day to day. On the other hand, even if the locations have not been graded to have a cross profile to lead the water away, the changes due to precipitation for location L1 and L2 are smaller. During day 50 the E_{LWD} values are 63.5 MPa for location L0, 133.7 MPa (2.1 times $E_{LWD, L0}$) for location L1 and 88.1 MPa for location 2 (1.4 times $E_{LWD, L0}$).

The DCP measurements follow this procedure: 7 sequences composed of 3 blows are carried out, the increasing depth from the layer surface is recorded at the end of each sequence, **Figure 54** shows the average results for each location. The outcomes referring to the untreated location L0 are reported up to 4 sequences (i.e. 12 blows), because a higher number of blows is sufficient to reach the layer’s bottom in the major part of the measurement points. Both the treated locations L1 and L2 perform better than the untreated location L0. Furthermore, there is a switch in the trend of penetration rate between the polymer-based and lignin-based areas: the latter is stiffer up to 5 sequences (i.e. 15 blows), which approximately correspond to 5.5 cm. For a larger number of blows, namely for a major depth, the former achieves better results. This can be connected to the “crust” effect of the lignin-based treatment previously discussed.



(a)



(b)

Figure 52 LWD measurements results during the first 50 days after construction: dynamic modulus E_{LWD} (a) and settlement S_{LWD} (b)

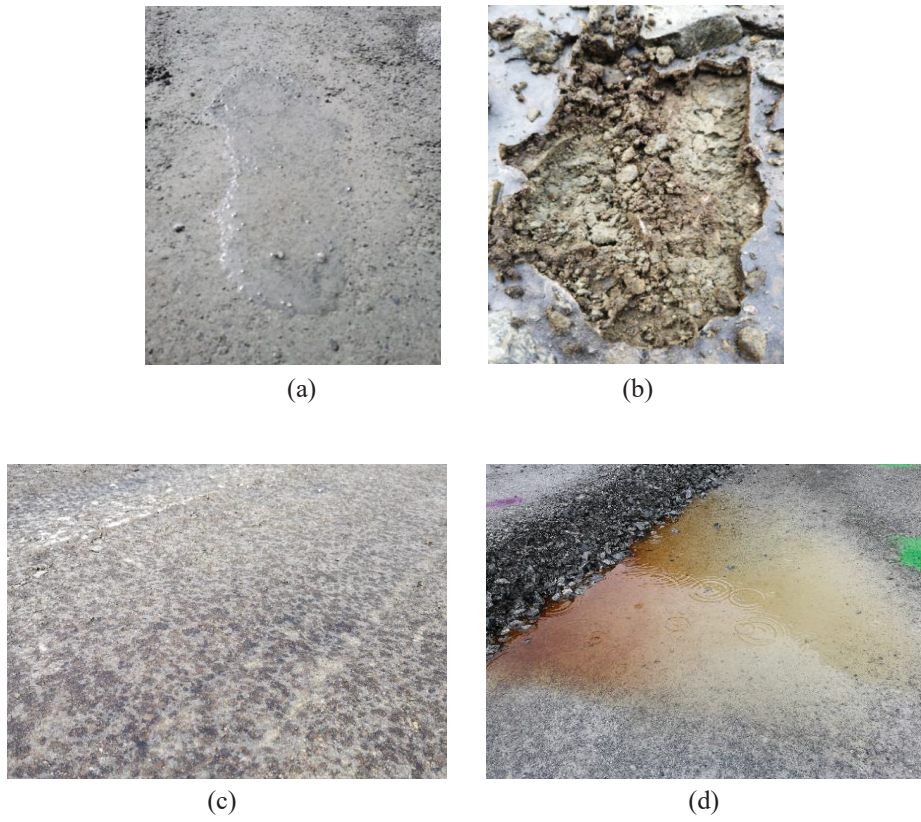


Figure 53 Polymer-based additive: water poured on the top does not seem to penetrate (a); lignin-based additive: “crust” effect (b), “droplet” effect (c) and dissolution with water (d)

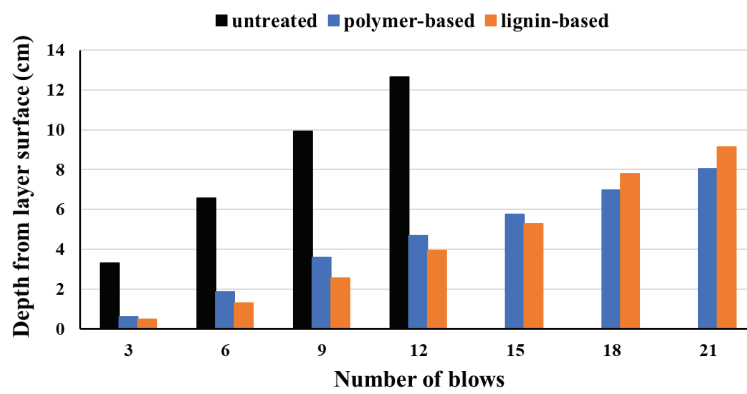


Figure 54 Average depth from layers’ surfaces with increasing number of DCP blows

Figure 55 shows the average total number of blows necessary to reach the layers' bottoms, namely approximately 17 cm below their surfaces. The treated locations are significantly harder than the untreated location. The polymer-based additive achieves the highest number of blows.

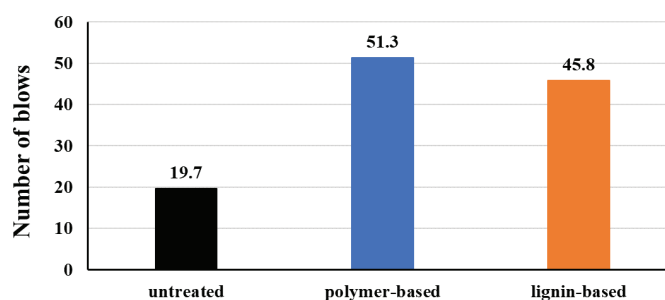
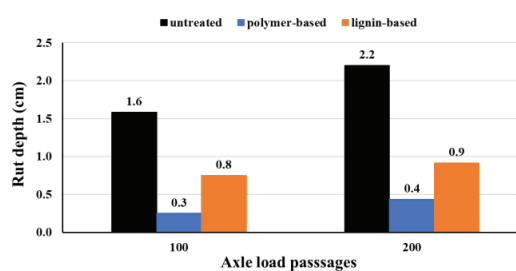


Figure 55 Average number of DCP blows necessary to reach the layers' bottoms

Figure 56 deals with the permanent deformation evaluation. The front 6-ton axle of a truck is driven back and forth to cause the rutting formation (a). Measurements after 100 passages and 200 passages prove the effectiveness of the additive products. The average rut depths for each location L0, L1 and L2 are assessed (b). The polymer-based treated area L1 achieves the smallest rut depths, the lignin-based treated area L2 achieves slightly higher values; this may be due to the hardening time demand previously discussed. Even if both stress level and number of passages are not necessarily the same as in e.g. a base layer of a real road, however, this test is used for relative ranking between the three test sections.



(a)



(b)

Figure 56 Rutting formation: stimulating procedure (a) and measured values (b)

4. FINAL CONSIDERATIONS

The research has investigated different approaches and technologies to improve the mechanical properties of crushed rocks to be used in the road unbound layers. This can open opportunities to use abundant local materials that would not meet performance specifications in their natural state. Among the studied solutions, two stabilizing additives have been investigated, one is polymer-based and the other one is lignin-based. Laboratory and field tests have been fulfilled to characterize their performance. Notwithstanding some research limitations, the investigation has led to positive results.

4.1. CONCLUSIONS AND PRACTICAL CONSEQUENCES

Four types of crushed rocks M1, M2, M3 and M4 have been tested. The investigation has been developed based on laboratory experiments (Repeated Triaxial Load Tests RTLTs, Los Angeles LA test and micro-Deval MDE test), FE modelling and field full-scale test (with Light Weight Deflectometer LWD and Dynamic Cone Penetrometer DCP). The following conclusions can be drawn both for practicing engineers and researchers:

- (1) RTLTL, LA and MDE tests identify that materials M1 and M4 have a better performance than materials M2 and M3. RTLTLs can also assess the beneficial effect provided by additives; on the other hand, there are no standard LA and MDE test procedures concerning an additive application.
- (2) Both polymer-based additive and lignin-based additive are non-traditional stabilization technologies, which improve the mechanical properties of crushed rocks and enable their use in the pavement unbound layers. All the adopted laboratory and field testing methods prove the effectiveness of the admixtures.
- (3) All the models used to interpret the experimental data referring to resilient modulus (Hicks and Monismith, Uzan and Uzan and Witczak) and vertical permanent deformation (Barksdale, Sweere, Hyde and Shenton) highlight that the use of the additives is an effective method to improve the mechanical properties of the crushed rocks.

(4) The field test demonstrates that the polymer-based additive has a rapid effect. Furthermore, the polymer-based additive apparently creates an impermeable layer. The field test also demonstrates that the lignin-based additive needs time to become effective; 23 days are necessary for the treated materials to exceed the untreated materials' performance. On the other hand, the liquids amount used in laboratory and field have led to oversaturation and "crust" formation in field.

(5) The lignin-based additive is water-soluble; the engineer needs to bear in mind this feature in the road design and construction phases. A suitable solution could be to apply the admixture during days without rainfall and then cover the treated layer with a top (e.g. bituminous) layer. When dealing with gravel roads, another option could be to make sure that the water can properly drain (e.g. good profile and well-maintained ditches).

(6) In the FE simulation of RTLs, all the non-linear elastic relationships (Hicks and Monismith, Uzan and Uzan and Witzak) bring to close results in terms of accumulated permanent vertical deformation. Norton exponential creep law added to Von Mises plasticity model can describe the experimental results better than the Von Mises plasticity model alone.

(7) An appropriate mixture of the crushed rocks available in situ is a convenient solution to fulfil LA and MDE requirements. The LA and MDE values of the mixture can be evaluated by a linear relationship based on the mass quantity of each employed material.

(8) The ability of the crushed rocks to withstand compaction and trafficking has been investigated during the construction phase and during service life phase. The crushing is substantially more significant in the former stage than in the latter stage for all the materials.

4.2. LIMITATIONS OF THE RESEARCH AND INPUTS FOR DEVELOPMENTS

There are some characteristics which may have impacted the research findings and their interpretation. The following criteria may be useful to overcome the limitations and expand the research:

(i) The research has dealt with four types of crushed rocks. Even if the results have been positive and highly promising, these outcomes could be generalized even more by further testing of other rock types.

(ii) The amount of water used in combination with lignin-based additive have led to oversaturation and “crust” formation in field; therefore, mixing proportions containing lower water percentages may be investigated.

(iii) Repeating the field measurements in the future could be useful to assess the long-term response of the stabilizing products and attain a more comprehensive knowledge about their performances compared to the properties of the untreated materials.

(iv) The FE model has been developed to simulate the RTLTL and the model parameters have been adjusted to fit the actual results. This work may be expanded in order to analyse the use of the additive products in actual roads.

(v) The general scope of the research has dealt with the local use of crushed rocks in the road unbound layers to provide a sustainable and cost-benefit application. This mission could be extended and investigate the potential use of the crushed rocks in the road bounded layers.

5. REFERENCES

- Aatheesan, T., Arulrajah, A., Wilson, J., and Bo, M. W. (2008). "Beneficial use of brick rubble as pavement sub-base material." *Advances in Transportation Geotechnics*, Taylor & Francis, London, 695–699.
- Alazigha, D. P., Indraratna, B., and Vinod, J. S. (2018). "Mechanisms of stabilization of expansive soil with lignosulfonate admixture." *Transportation Geotechnics*, Elsevier, 14, 81–92.
- Angenent, L. T., Karim, K., Al-Dahhan, M. H., Wrenn, B. A., and Domínguez-Espinosa, R. (2004). "Production of bioenergy and biochemicals from industrial and agricultural wastewater." *Trends in Biotechnology*, 22(9), 477–485.
- Araya, A. A. (2011). "Characterization of unbound granular materials for pavements." Delft University of Technology.
- Arulrajah, A., Piratheepan, J., Disfani, M. M., and Bo, M. W. (2013). "Geotechnical and geoenvironmental properties of recycled construction and demolition materials in pavement subbase applications." *Journal of Materials in Civil Engineering*, 25(8), 1077–1088.
- ASTM International. (2015). *Standard test method for measuring deflections using a portable impulse plate load test device*. USA.
- ASTM International. (2018). *Standard test method for use of the dynamic cone penetrometer in shallow pavement applications*. USA.
- Baklökk, L. J., Hoff, I., and Nordal, R. S. (1998). "A study of methods for ranking unbound granular materials in pavement construction." *5th International Conference on the Bearing Capacity of Roads and Airfields*, R. S. Nordal and G. Refsdal, eds., Tapir, Trondheim, 1361–1370.
- Barksdale, R. D. (1971). "Compressive stress pulse times in flexible pavements for use in dynamic testing." *Highway Research Record*, 32–44.
- Barksdale, R. D. (1972). "Laboratory evaluation of rutting in basecourse materials." *3rd Conference on the Structural Design of Asphalt Pavements*, London, 161–174.
- Behnood, A. (2018). "Soil and clay stabilization with calcium- and non-calcium-based additives: a state-of-the-art review of challenges, approaches and techniques." *Transportation Geotechnics*, Elsevier, 17, 14–32.
- Berger, A. (1978). "Massedeponering. Beregning av kostnadsminimale tranportmønstre for

- planering av fjell- og jordmasser ved bygging av veier.” Norwegian University of Science and Technology.
- Boussinesq, J. (1885). *Application des potentiels a l'étude de l'équilibre et du mouvement des Solids Elastiques*. Gauthier-Villars, Paris.
- Burdin, J., and Monin, N. (2009). “The management of excavated materials from the Lyon-Turin rail link project.” *Geomechanik und Tunnelbau*, 2(5), 652–662.
- CEN. (2003). *Unbound and hydraulically bound mixtures. Part 4: test methods for laboratory reference density and water content. Vibrating hammer*.
- CEN. (2004). *Cyclic load triaxial test for unbound mixture*.
- CEN. (2010). *Tests for mechanical and physical properties of aggregates. Part 2: methods for the determination of resistance to fragmentation*.
- CEN. (2011). *Tests for mechanical and physical properties of aggregates. Part 1: determination of the resistance to wear (micro-Deval)*.
- CEN. (2012a). *Tests for geometrical properties of aggregates. Part 1: determination of particle size distribution. Sieving method*.
- CEN. (2012b). *Tests for mechanical and physical properties of aggregates. Part 3: determination of particle shape - flakiness index*.
- CEN. (2017). *Soil quality - Determination of dry bulk density*.
- Chazallon, C., Hornych, P., and Mouhoubi, S. (2006). “Elastoplastic model for the long-term behavior modeling of unbound granular materials in flexible pavements.” *International Journal of Geomechanics*, 6(4), 279–289.
- Chen, D. H., Lin, D., Liau, P., and Bilyeu, J. (2005). “A correlation between dynamic cone penetrometer values and pavement layer moduli.” *Geotechnical Testing Journal*, 28(1).
- Chen, J., Hossain, M., and Latorella, T. (1999). “Use of falling weight deflectometer and dynamic cone penetrometer in pavement evaluation.” *Transportation Research Record*, Transportation Research Board, 1655, 145–151.
- Chen, Q., Indraratna, B., Carter, J., and Rujikiatkamjorn, C. (2014). “A theoretical and experimental study on the behaviour of lignosulfonate-treated sandy silt.” *Computers and Geotechnics*, Elsevier, 61, 316–327.
- Chittoori, B., Puppala, A. J., Reddy, R., and Marshall, D. (2012). “Sustainable reutilization of excavated trench material.” *GeoCongress 2012*, 4280–4289.
- COMSOL. (2017). “COMSOL Multiphysics 5.3 reference manual.”
- Daniels, J., and Hourani, M. S. (2009). “Soil improvement with organo-silane.” *U.S.-China*

- Workshop on Ground Improvement Technologies 2009*, Orlando.
- David, C. T., García-Rojo, R., Herrmann, H. J., and Luding, S. (2005). "Hysteresis and creep in powders and grains." *Powders and Grains 2005*, 291–294.
- Dongmo-Engeland, B. (2005). *GARAP, Influence of sample's height on the development of permanent deformation*. Trondheim.
- Douglas, R. A. (2017). *Low-volume road engineering*. CRC Press, Boca Raton.
- Dunham, K. K. (2016). "Coastal Highway Route E39 - Extreme crossings." *Transportation Research Procedia*, Elsevier, 14(2352), 494–498.
- Elhakim, A. F., Elbaz, K., and Amer, M. I. (2014). "The use of light weight deflectometer for in situ evaluation of sand degree of compaction." *HBRC Journal*, 10(3), 298–307.
- Erichsen, E., and Aasly, A. (2015). *Mineralressurser i Norge 2015. Mineralstatistikk og bergindustriberetning*. Trondheim.
- Erichsen, E., Ulvik, A., and Sævik, K. (2011). "Mechanical degradation of aggregate by the Los Angeles-, the micro-Deval- and the nordic test methods." *Rock Mechanics and Rock Engineering*, 44(3), 333–337.
- Erlingsson, S., and Rahman, M. S. (2013). "Evaluation of permanent deformation characteristics of unbound granular materials by means of multistage repeated-load triaxial tests." *Transportation Research Record: Journal of the Transportation Research Board*, 2369, 11–19.
- Erlingsson, S., Rahman, M. S., and Salour, F. (2017). "Characteristic of unbound granular materials and subgrades based on multi stage RLT testing." *Transportation Geotechnics*, 13, 28–42.
- Fladvad, M., Aurstad, J., and Wigum, B. J. (2017). "Comparison of practice for aggregate use in road construction - results from an international survey." *10th International Conference on the Bearing Capacity of Roads, Railways and Airfields*.
- Fleming, P., Frost, M., and Lambert, J. (2007). "Review of lightweight deflectometer for routine in situ assessment of pavement material stiffness." *Transportation Research Record: Journal of the Transportation Research Board*, Transportation Research Board, 2004, 80–87.
- Floss, R. (2001). *Compaction technology in earthwork, highway and transportation engineering, volume 1*. BOMAG GmbH & Co., Boppard.
- Forset Grus. (2018). "Pukk." <<https://www.forset.no/produkter/pukk/>> (Sep. 10, 2018).
- Franzefoss. (2018). "Pukk." <<https://www.franzefoss.no/pukk/pukk/>> (Sep. 10, 2018).

- Ghadimi, B., and Nikraz, H. (2017). "A comparison of implementation of linear and nonlinear constitutive models in numerical analysis of layered flexible pavement." *Road Materials and Pavement Design*, 18(3), 550–572.
- Gidel, G., Hornych, P., Chauvin, J.-J., Breysse, D., and Denis, A. (2001). "A new approach for investigating the permanent deformation behaviour of unbound granular material using the repeated load triaxial apparatus." *Bulletin des Laboratoires des Pont et Chaussées*, 233(July-August), 5–21.
- Gomes Correia, A., Winter, M. G., and Puppala, A. J. (2016). "A review of sustainable approaches in transport infrastructure geotechnics." *Transportation Geotechnics*, Elsevier, 7, 21–28.
- Gorman, P. B., and Mooney, M. A. (2003). "Monitoring Roller Vibration During Compaction of Crushed Rock." *20th International Association for Automation and Robotic in Construction*.
- Grenne, T., Grammelvedt, G., and Vokes, F. M. (1980). "Ophiolites type sulphide deposits in the western Trondheim district, central Norwegian caledonides." *International Ophiolite Symposium*, Cyprus, Geological Survey Department, Cyprus, 727–743.
- Gupta, A. K. (2016). "Effects of particle size and confining pressure on breakage factor of rockfill materials using medium triaxial test." *Journal of Rock Mechanics and Geotechnical Engineering*, 8, 378–388.
- Hansen, E. K., and Hansen, G. (1998). "Quality of crushed rock aggregates for pavement structures." *5th International Conference on the Bearing Capacity of Roads and Airfields*, R. S. Nordal and G. Refsdal, eds., Tapir, Trondheim, 1325–1330.
- Hardin, B. B. O., and Asce, F. (1985). "Crushing of soil particles." *Journal of Geotechnical Engineering*, 111(10), 1177–1192.
- Haritonovs, V., Tihonovs, J., and Smirnovs, J. (2016). "High modulus asphalt concrete with dolomite aggregates." *Transportation Research Procedia*, Elsevier, 14, 3485–3492.
- Hicks, R. G., and Monismith, C. L. (1971). "Factors influencing the resilient properties of granular materials." *Highway Research Record*, 15–31.
- HMP-LFG. (2017). *HMP-LFG4 Instruction manual*. Magdeburg.
- HMP-LFG. (2018). "The light drop weight tester. Magdeburg prüfgeratebau GmbH." <<https://www.hmp-online.com/en/>> (Sep. 10, 2018).
- Hoff, I. (1999). "Material properties of unbound aggregates for pavement structures." Norwegian University of Science and Technology.

- Hoff, I. (2004). *Dypstabilisering med fres - feltforsøk i Budalen*. Trondheim.
- Hoff, I., Arvidsson, H., Erlingson, S., Houben, L. J. M., Kolisoja, P., and Schwartz, C. W. (2005). "Round robin investigation on the cyclic triaxial test for unbound granular materials." *7th International Conference on the Bearing Capacity of Roads, Railways and Airfields*, R. S. Nordal and G. Refsdal, eds., Tapir, Trondheim.
- Hoff, I., Bakløkk, L. J., and Aurstad, J. (2003). "Influence of laboratory compaction method on unbound granular materials." *6th International Symposium on Pavements Unbound*.
- Hornych, P., El Abd, A., Chazallon, C., and Allou, F. (2007). "Prediction of permanent deformations of unbound granular materials in low traffic pavements." *Road Materials and Pavement Design*, 8(4), 643–666.
- Horvli, I. (1979). "Dynamisk prøving av leire for dimensjonering av veger." Norwegian University of Science and Technology.
- Huang, Y. H. (2004). *Pavement Analysis and design*. (Pearson, ed.), Upper Saddle River.
- Huang, Y., and Wang, L. (2016). "Experimental studies on nanomaterials for soil improvement: a review." *Environmental Earth Sciences*, Springer, 75(6), 497.
- Hyde, A. F. L. (1974). "Repeated load triaxial testing of soils." University of Nottingham.
- Jiang, Y. J., and Fan, L. F. (2013). "An investigation of mechanical behavior of cement-stabilized crushed rock material using different compaction methods." *Construction and Building Materials*, Elsevier, 48, 208–515.
- Kim, M., Tutumluer, E., and Kwon, J. (2009). "Nonlinear pavement foundation modeling for three-dimensional finite-element analysis of flexible pavements." *International Journal of Geomechanics*, 9(5), 195–208.
- Kolisoja, P. (1997). "Resilient deformation characteristics of granular materials." Tampere University of Technology.
- Kumar, R., Adigopula, V. K., and Guzzarlapudi, S. D. (2017). "Stiffness-based quality control evaluation of modified subgrade soil using lightweight deflectometer." *Journal of Materials in Civil Engineering*, 29(9).
- Kwon, J., Tutumluer, E., and Konietzky, H. (2008). "Aggregate base residual stresses affecting geogrid reinforced flexible pavement response." *International Journal of Pavement Engineering*, 9(4), 275–285.
- Lade, P. V., Yamamuro, J. A., and Bopp, P. A. (1996). "Significance of particle crushing in granular materials." *Journal of Geotechnical and Geoenvironmental Engineering*, 122(4), 309–316.

- Lekarp, F., Isacsson, U., and Dawson, A. (2000a). "State of the art. I: resilient response of unbound aggregates." *Journal of Transportation Engineering*, 126(1), 66–75.
- Lekarp, F., Isacsson, U., and Dawson, A. (2000b). "State of the art. II: permanent strain response of unbound aggregates." *Journal of Transportation Engineering*, 126(1), 76–83.
- Lieb, R. (2009). "Materials management at the Gotthard base tunnel - experience from 15 years of construction." *Geomechanik und Tunnelbau*, 2(5), 619–626.
- Mallick, R. B., and El-Korchi, T. (2013). *Pavement engineering. Principles and practice*. CRC Press, Boca Raton.
- Marsal, R. J. (1967). "Large-scale testing of rockfill materials." *Journal of the Soil Mechanics and Foundations Division*, 93(2), 27–43.
- Miura, N., and O-hara, S. (1979). "Particle crushing of a decomposed granite soil under shear stresses." *Soils and Foundations*, 19(3), 1–14.
- Mooney, M. A., and Adam, D. (2007). "Vibratory roller integrated measurement of earthwork compaction." *7th International Symposium on Field Measurements in Geomechanics*, D. Jerry and P. Osborn, eds., Boston.
- Mooney, M. A., and Miller, P. (2009). "Analysis of lightweight deflectometer test based on in situ stress and strain response." *Journal of Geotechnical and Geoenvironmental Engineering*, American Society of Civil Engineers, 135(2), 199–208.
- Myre, J. (2014). "The use of cold bitumen stabilized base course mixes in Norway." 1–14.
- Nålsund, R. (2014). "Railway ballast characteristics, selection criteria and performance." Norwegian University of Science and Technology.
- Natvik, J. (1998). "Alternative testmetoder i undersøkelser av tilslagsmaterialer." Norwegian University of Science and Technology.
- Neeb, P.-R. (1992). *Byggeråstoff*. Tapir, Trondheim.
- NGU. (2015). "Sand, grus og pukk som byggeråstoff." <<http://www.ngu.no/emne/sand-grus-og-pukk-som-byggeråstoff>> (Sep. 10, 2018).
- NGU. (2017). "Norges Geologiske Undersøkelse (Geological Survey of Norway)." <<http://www.ngu.no/>> (Sep. 10, 2018).
- Norsk rikskringkasting AS. (2018). "Varmerekord i Sør-Norge i mai." <<https://www.nrk.no/hordaland/varmerekord-i-sor-norge-i-mai-1.14054641>> (Sep. 10, 2018).
- Norwegian Meteorological Institute. (2018). "eKlima." <http://sharki.oslo.dnmi.no/portal/page?_pageid=73,39035,73_39049&_dad=portal&_sc

- hema=PORTAL> (Sep. 10, 2018).
- NPRA. (2013). *Håndbok N100 veg- og gateutforming*. Vegdirektoratet, Norway.
- NPRA. (2014a). *Håndbok N200 vegbygging*. Vegdirektoratet, Norway.
- NPRA. (2014b). *Kalde bitumen- stabiliserte bærelag*. Vegdirektoratet, Norway.
- NPRA. (2016). *Håndbok N500 vegtunneler*. Vegdirektoratet, Norway.
- NPRA. (2017a). “The E39 coastal highway route.”
<<https://www.vegvesen.no/en/roads/Roads+and+bridges/Road+projects/e39coastalhighwayroute;jsessionid=99D143CB28F87A072777C744BBCA31E8?lang=nn>> (Sep. 10, 2018).
- NPRA. (2017b). *Stabilisering av bærelag med DUSTEX, oppfølging av FOU rapport nr. 2008003393-I*.
- NPRA. (2018). “E39 Svegatjørn–Rådal.”
<<https://www.vegvesen.no/vegprosjekter/e39svegatjornradal>> (Sep. 10, 2018).
- Núñez, W. P., Ceratti, J. A., Malysz, R., and Retore, T. S. (2008). “Using unbound aggregates resulting from amethyst mining in low volume roads.” *Advances in Transportation Geotechnics*, Taylor & Francis, London, 219–225.
- Obert, L., Windes, S. L., and Duvall, W. I. (1946). *Standardized tests for determining the physical properties of mine rock*.
- Onyango, M., Macha, I., and Busch, C. (2007). “Use of naturally occurring pozzolans for road construction in Tanzania.” *Transportation Research Record: Journal of the Transportation Research Board*, 2(1989), 169–177.
- Otto, A., Endale, A. A., and Greening, P. A. K. (2015). “Method for increasing the use of locally available materials for road construction in Ethiopia by allowing for climatic variations.” *Transportation Research Record: Journal of the Transportation Research Board*, 2474(2474), 108–115.
- Paul, D. R., and Robeson, L. M. (2008). “Polymer nanotechnology: nanocomposites.” *Polymer*, Elsevier, 49(15), 3187–3204.
- Petkovic, G. (2005). “Recycling in Norwegian conditions.” *5th International Conference on the Bearing Capacity of Roads and Airfields*, R. S. Nordal and G. Refsdal, eds., Tapir, Trondheim.
- Rahman, M. S. (2015). “Characterising the deformation behaviour of unbound granular materials in pavement structures.” Royal Institute of Technology, Stockholm.
- Rahman, M. S., and Erlingsson, S. (2015). “Predicting permanent deformation behaviour of

- unbound granular materials.” *International Journal of Pavement Engineering*, 16(7), 587–601.
- Raina, A., Chakraborty, A. K., Ramulu, M., and Jethwa, J. L. (2000). “Rock mass damage from underground blasting, a literature review, and lab- and full scale tests to estimate crack depth by ultrasonic method.” *Fragblast International Journal for Blasting and Fragmentation*, 4(2), 103–125.
- Ramberg, I. B., Bryhni, I., Nøttvedt, A., and Rangnes, K. (2013). *Landet blir til*. (Norsk Geologisk Forening, ed.), Trondheim.
- Ray, L. (1999). *The roads of Roman Italy*. Routledge.
- Resch, D., Lassnig, K., Galler, R., and Ebner, F. (2009). “Tunnel excavation material - high value raw material.” *Geomechanik und Tunnelbau*, 2(5), 612–618.
- Riviera, P. P., Bellopede, R., Marini, P., and Bassani, M. (2014). “Performance-based re-use of tunnel muck as granular material for subgrade and sub-base formation in road construction.” *Tunnelling and Underground Space Technology*, Elsevier, 40, 160–173.
- Roco, M. C. (2003). “Broader societal issues of nanotechnology.” *Journal of Nanoparticle Research*, 5, 181–189.
- Rothery, K., and Mellor, S. (2007). *Crushing and screening*. Institute of Quarrying, Nottingham, UK.
- Sandvik. (2018). “Sandvik mobile crushers and screens.” <<https://www.rocktechnology.sandvik/en/products/mobile-crushers-and-screens/>> (Sep. 10, 2018).
- Santoni, R. L., Tingle, J. S., and Webster, S. L. (2002). “Stabilization of silty sand with nontraditional additives.” *Transportation Research Record*, 61–70.
- Shenton, M. J. (1975). “Deformation of railway ballast under repeated loading.” *Symposium on Railroad Track Mechanics*, Princeton University, New Jersey.
- Siekmeier, J., Young, D., and Beberg, D. (2000). “Comparison of the dynamic cone penetrometer with other tests during subgrade and granular base characterization in Minnesota.” *Nondestructive Testing of Pavements and Backcalculation of Moduli: 3rd volume*, S. D. Tayabji and E. O. Lukanen, eds., American Society for Testing and Materials, West Conshohocken, PA.
- Simpson, D. R., and Fergus, J. H. (1968). “The effect of water on the compressive strength of diabase.” 73(20), 6591–6594.
- Siripun, K., Jitsangiam, P., and Nikraz, H. (2010). “Characterization analysis and design of

- hydrated cement treated crushed rock base as a road base material in Western Australia.” *International Journal of Pavement Research and Technology*, 10(1), 39–47.
- Sobolev, K., and Shah, S. P. (2015). “Nanotechnology in construction.” *Proceedings of NICOM5*, K. Sobolev and S. P. Shah, eds., Springer, 509.
- Sweere, G. T. H. (1990). “Unbound granular bases for roads.” University of Delft.
- Sybilski, D., Bankowski, W., and Krajewski, M. (2010). “High modulus asphalt concrete with limestone aggregate.” *International Journal of Pavement Research and Technology*, 3(2), 96–101.
- Ta’negonbadi, B., and Noorzad, R. (2018). “Physical and geotechnical long-term properties of lignosulfonate-stabilized clay: An experimental investigation.” *Transportation Geotechnics*, Elsevier, 17, 41–50.
- Teknologirådet. (2012). “Teknologirådet | Norge 2030 arkiver.” <<https://teknologiradet.no/norge-2030/>> (Sep. 10, 2018).
- Thom, N. (2014). *Principles of pavement engineering*. ICE, Lon.
- Ugwu, O. O., Arop, J. B., Nwoji, C. U., and Osadebe, N. N. (2013). “Nanotechnology as a preventive engineering solution to highway infrastructure failures.” *Journal of Construction Engineering and Management*, 139(8), 987–993.
- US National Weather Service. (2018). “Precipitation measurements.” US National Weather Service, <<https://www.weather.gov/abr/c/map>> (Sep. 10, 2018).
- Uthus, L. (2007). “Deformation properties of unbound granular aggregate.” Norwegian University of Science and Technology.
- Uthus, L., Tutumluer, E., Horvli, I., and Hoff, I. (2007). “Influence of grain shape and texture on the deformation properties of unbound aggregates in pavements.” *International Journal of Pavements*, 6(1).
- Uzan, J. (1985). “Characterization of granular material.” *Transportation Research Record*, (1022), 52–59.
- Uzan, J., and Witzak, M. W. (1988). *The universal airport pavement design system, report I of IV: granular material characterization*.
- Velde. (2018). “Pukk og grus.” <<https://www.veldeas.no/stein>> (Sep. 10, 2018).
- Vennapusa, P., and White, D. (2009). “Comparison of light weight deflectometer measurements for pavement foundation materials.” *Geotechnical Testing Journal*, 32(3).
- Werkmeister, S. (2003). “Permanent deformation behaviour of unbound granular materials in pavement constructions.” Dresden University of Technology.

- Werkmeister, S., Dawson, A. R., and Wellner, F. (2004). "Pavement design model for unbound granular materials." *Journal of Transportation Engineering*, 130(5), 665–674.
- Werkmeister, S., Dawson, A., and Wellner, F. (2005). "Permanent deformation behavior of granular materials and the shakedown concept." *Transportation Research Record*, 1757, 75–81.
- Wolff, F. C. (1976). *Geologisk kart over Norge, berggrunnskart TRONDHEIM 1:250.000*. Trondheim.
- Yoo, T.-S., and Selig, E. T. (1980). "Dynamics of vibratory-roller compaction." *International Journal of Rock Mechanics and Mining Sciences and Geomechanics*, 1211–1231.
- Zare, S. (2006). "Drill and blast tunneling blast design." Norwegian University of Science and Technology.
- Zhalehjoo, N., Tolooiyan, A., Mackay, R., and Bodin, D. (2018). "The effect of instrumentation on the determination of the resilient modulus of unbound granular materials using advanced repeated load triaxial testing." *Transportation Geotechnics*, Elsevier, 14, 190–201.
- Zhang, L., Mao, X., and Lu, A. (2009). "Experimental study on the mechanical properties of rocks at high temperature." *Science in China, Series E: Technological Sciences*, 52(3), 641–646.
- Zhang, T., Cai, G., and Liu, S. (2017). "Application of lignin-based by-product stabilized silty soil in highway subgrade: a field investigation." *Journal of Cleaner Production*, Elsevier, 142, 4243–4257.
- Zhang, T., Cai, G., and Liu, S. (2018). "Application of lignin-stabilized silty soil in highway subgrade: A macroscale laboratory study." *Journal of Materials in Civil Engineering*, 30(4).

PAPER I

Barbieri, D. M., Hoff, I., and Mork, H. (2017). "Laboratory investigation on unbound materials used in a highway with premature damage." 10th International Conference on the Bearing Capacity of Roads, Railways and Airfields.

Laboratory investigation on unbound materials used in a highway with premature damage

D. M. Barbieri & I. Hoff & H. Mork

Norwegian University of Science and Technology, Trondheim, Norway

ABSTRACT: A highway road section was built from 2004 to 2006 in the southern part of Norway. Soon after the opening significant damage in form of alligator cracking and rutting occurred. The aim of the research described in this paper is to characterize the behaviour of the pavement unbound layers that may have possibly caused the issue.

At a first stage, a collaboration among different partners carried out field surveys and samplings in five locations with and without visible surface damage.

At a second stage, laboratory analyses investigated the properties of the base layer and especially focused on repeated triaxial load testing. The specimens were analysed with varying moisture content and degree of compaction. These laboratory tests gave significantly lower stiffness and resistance to permanent deformation for the damaged sections; this could partly explain why distresses are more evident just on some parts of the road.

1 INTRODUCTION

The research described in this paper focuses on a highway section situated in the southern part of Norway. The new road link was built in 2004; the length is about 17.5 km, including a bridge and several tunnels.

Damage in form of both alligator cracking and rutting occurred soon after the opening to traffic in 2006: a series of interconnecting cracks developed along the wheel paths.

This type of damage is uncommon in new asphalt pavements in Norway: excessive rutting and unevenness are the typical damage sometimes seen early in a pavement life.

A collaboration comprising NTNU (Norwegian University of Science and Technology), NPRA (Norwegian Public Roads Administration) and the contractor organized a field investigation in September 2014 in five areas. Three locations had clear distresses: site I (km 0.844), site II (km 1.195), site III (km 1.547). Alligator cracking was distinctly visible and the fracture pattern was approximately 10×10 cm.

Two locations had no visible distresses: site IV (km 8.709), site V (km 9.720). Table 1 describes the road pavement structure designed according to the pavement design manual in use at the time (Statens Vegvesen 1998).

Table 1. Section designs as derived from Handbook 018. Construction of the wearing course was postponed.

<i>Layer</i>	<i>Thickness (mm)</i>	<i>Material</i>
wearing course	35	hot-mixed asphalt
binder course	45	hot-mixed asphalt
upper base	50	paved gravel
lower base	150	crushed rock
subbase	550	blasted rock

The aim of the research presented is to analyse the mechanical behaviour of the unbound layers in the pavement and highlight any possible relationships between their properties and the premature damage encountered. RTLT (Repeated Triaxial Load Test) was used to characterize the materials.

2 METHODOLOGY

2.1 Material sampling

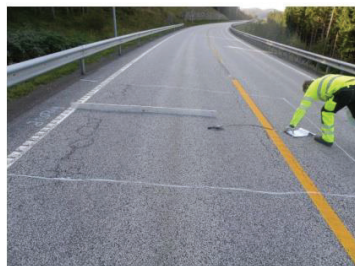
Figure 1 portrays the condition of the wearing course related to sites I, II, III, V.



site I (damaged)



site II (damaged)



site III (damaged)



site V (not damaged)

Figure 1. Road surface condition of the surveyed sites.

The ruts along the wheel paths were measured using a three-meter straightedge. The condition of the road pavement was inspected according to a preset excavation pattern (Figure 2).

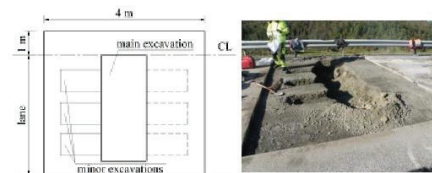


Figure 2. Framework of excavation and its fulfilment.

The excavation surface was rectangular with 4 m x 5 m in size. The asphalt layer was sawn with a diamond blade and removed using an excavator. A transversal excavation ca. 0.5 m deep took place in the central area to examine both base and subbase layers. There were also some lesser digs extending longitudinally from the main excavation to compare the base course materials along the inner and outer as well as between the wheel-paths.

The lower base course material was so hard to displace that the use of a pneumatic drill was necessary. This action could have generated some extra fines. However, it is believed that this did not significantly change the grain size distribution; it is reasonable to assume any crushing happened in the same proportion for all the sites.

2.2 Sieving analysis

Laboratory tests enabled a more careful examination of the materials extracted from each location, the unbound lower base course (crushed rock) were studied.

The sieving analysis identifies the grain sizes and highlights possible significant discrepancies among the five locations and the grading envelope specified by the code Handbook 018 (also defined in EN 933-1, CEN 2012).

2.3 RTL (Repeated Triaxial Load Test)

RTL is the main testing procedure used in this research. It gives a comprehensive insight into the properties of the material by assessing the stiffness (resilient modulus, which replaces the modulus of elasticity to indicate the nonlinearity of the behaviour) and the resistance to permanent deformation.

Barksdale (1971) found that the RTL is one of the best methods available for laboratory simulation of traffic loading on unbound materials. It reproduces the stress conditions in flexible pavements more adequately than other available methods like the CBR test.

A confining pressure and a vertical load are the actions exerted on the specimen. For unbound granular

aggregates, it is often convenient to separate deformations into two types: one elastic (recoverable or resilient) and one permanent (not recoverable or residual). Rutting is the most common damage caused by permanent deformations.

Seed et al. (1962) and Hicks & Monismith (1971) discussed the main factors influencing the stiffness and the deformation for unbound materials; Lekarp et al. (2000a, b) presented a thorough state-of-the-art of the mechanical behaviour. They found that the resilient modulus and the permanent deformation were mainly influenced by the same factors (Uthus 2009): mineralogy, stress level, moisture content, dry density, grading, particle size and fines content.

2.3.1 Sample preparation

Stress level, moisture content and dry density are the input parameters used in this research to analyse the sensitivity of the collected materials. The amount of water in the samples varies between 3%, 5% and 7%. A Kango 950X vibratory hammer (total weight 35 kg, frequency 25 ÷ 60 Hz, amplitude 5 mm) compacts the specimen layers for 20 s or 40 s leading to different densities. Both the mineralogy and the grading are given.

In order to prepare the sample, the desired amount of water is added to the testing material, which rests for 24 h to let the moisture distribute uniformly. Five equal layers are compacted with the vibratory hammer according to the desired time. The bulk density and dry density are assessed as specified by EN 13286-4 (CEN 2003).

All the samples have a diameter of 150 mm and the height of the mould is 240 mm. This parameter differs from the indication given by EN 13286-7 (CEN 2004) where the height is recommended to be twice the diameter of the sample. Dongmo-Engeland (2005) studied the influence of the height to diameter ratio with respect both to resilient modulus and the resistance against permanent deformations. It was concluded that samples with a ratio ranging from 1:1 to 1.5:1 showed little difference.

Water is the confining medium, the triaxial chamber is made of plexiglass. There is one metal plate at each end of the specimen, two rubber membranes surround it and prevent the entrance of water.

2.3.2 Loading procedure

Two and three LVDTs (Linear Variable Differential Transducer) measure the axial and radial deformations, respectively.

The code EN 13286-7 (CEN 2004) specifies different ways to apply the load. The multi-stage loading procedure gathers data regarding the resistance against permanent deformation and the resilient properties from one sample. The alternative of testing one sample for each stress combination would be very time consuming (Gidel et al. 2001).

The confining medium applies a uniform constant pressure in all directions (σ_c , triaxial or confining stress). The hydraulic jack exerts an additional vertical dynamic stress (σ_d , deviatoric stress), which stepwise increases at different levels of confining stress.

The triaxial test apparatus performs the multi-stage loading procedure in five different sequences with different confining stresses ($\sigma_c = 20, 45, 70, 100, 150$ kPa). In addition, six steps form a given sequence and each of them has a different increasing deviator stress. Table 2 contains the five loading sequences and the respective loading steps (combination of confining and deviatoric stresses). The hydraulic jack applies the deviatoric stress according to a sinusoidal pattern. It ranges from a minimum value of 5 kPa to assure contact between the end plate and the jack itself to the maximum values specified in Table 2. Each load step consists of 10,000 load pulses at 10 Hz frequency. A loading sequence is interrupted if the axial permanent deformation reaches 0.5%; the operator then continues with the next loading sequence.

Table 2. Loading sequences for the multi-stage low stress procedure (data in kPa).

Seq. 1		Seq. 2		Seq. 3		Seq. 4		Seq. 5	
σ_c	σ_d	σ_c	σ_d	σ_c	σ_d	σ_c	σ_d	σ_c	σ_d
20	20	45	60	70	80	100	100	150	100
20	40	45	90	70	120	100	150	150	200
20	60	45	120	70	160	100	200	150	300
20	80	45	150	70	200	100	250	150	400
20	100	45	180	70	240	100	300	150	500
20	120	45	210	70	280	100	350	150	600

2.3.3 Interpretation of results

The resilient modulus M_R expresses the stiffness of the material. The resilient modulus associated with a change in the dynamic deviatoric stress σ_d^{dyn} and a constant confining pressure σ_c is:

$$M_R = \frac{\Delta \sigma_d^{dyn}}{\epsilon_a^{el}} \quad (1)$$

where ϵ_a^{el} is the axial resilient strain.

There are models describing the relationship between the resilient modulus and the applied stress. The k- θ model is a well-known curve-fitting equation based on the sum of principal stresses or bulk stress. The k- θ model is a non-linear, stress-dependent power function model described by Hicks & Monismith (1971). The model is given as follows in its dimensionless form:

$$M_R = k_1 \sigma_a \left(\frac{\theta}{\sigma_a} \right)^{k_2} \quad (2)$$

where θ is the bulk stress sum of the principal stresses, σ_a is a reference pressure (100 kPa) and k_1

and k_2 are model parameters assessed from the regression of the test results.

Figure 3 is a typical RTLT output. The resilient modulus is evaluated as expressed by equation 1.

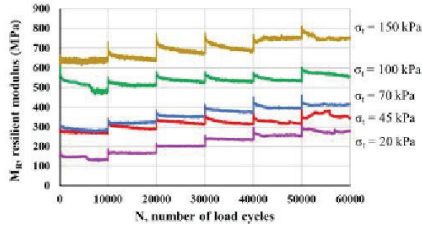


Figure 3. Example of resilient modulus data obtained from a repeated triaxial load test.

Figure 4 portrays a distribution of the resilient moduli obtained when using the bulk stress as the abscissa. The continuous line is the general trend obtained from the k- θ model (Equation 2) adopted as the regression curve.

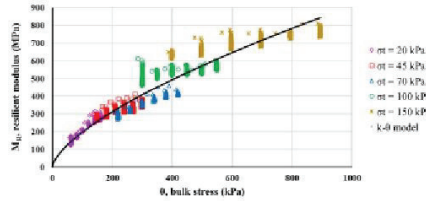


Figure 4. Example of a k- θ regression curve from the resilient modulus data obtained from a repeated triaxial load test.

There are several models used to interpret the permanent deformation behaviour of an unbound granular material tested in a cyclic load apparatus; the shakedown approach (Werkmeister et al. 2001) and the Coulomb approach (Hoff et al. 2003) are two of them. The Coulomb criterion relates the mobilized shear strength to the development of permanent deformations and the maximum shear strength to failure. The mobilized angle of friction ρ and the failure angle ϕ , respectively, express the degree of mobilized shear strength and the maximum shear strength. The mobilized angle of friction is:

$$\sin \rho = \frac{\sigma_1 - \sigma_3}{\sigma_1 + \sigma_3 + 2a} \quad (3)$$

where σ_1 is the maximum principal stress, σ_3 is the minimum principal stress and a is the apparent attraction of the material. The angle of friction and of failure identify three different ranges of material behaviour: elastic, elasto-plastic and failure. The Coulomb criterion is shown in Figure 5 in a σ - τ plot.

The strain rate $\dot{\epsilon}$ is a measure of the speed of the permanent deformation and is used as the parameter

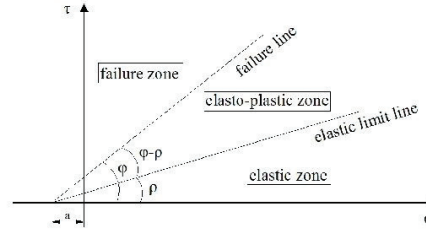


Figure 5. Degrees of mobilized shear strength ρ and maximum shear strength ϕ : different ranges of material behaviour.

to define failure. The strain rate $\dot{\epsilon}$ here refers to the development of permanent deformation per cycle.

Table 3 defines the two boundary lines between the three ranges (Figure 5): each load step is categorized considering the average strain rate for the last 5000 to 10,000 cycles (Hoff et al. 2003).

Table 3. Permanent strain rate values defining the ranges of material behaviour.

Permanent strain rate	Range
$\dot{\epsilon} < 2.5 \cdot 10^{-8}$	elastic zone
$2.5 \cdot 10^{-8} < \dot{\epsilon} < 1.0 \cdot 10^{-7}$	elasto-plastic zone
$\dot{\epsilon} > 1.0 \cdot 10^{-7}$	plastic (failure) zone

The equations for the elastic limit line and failure line are, respectively:

$$\sigma_d = \frac{2 \sin \rho \cdot (\sigma_3 + a)}{1 - \sin \rho} \quad (4)$$

$$\sigma_d = \frac{2 \sin \phi \cdot (\sigma_3 + a)}{1 - \sin \phi} \quad (5)$$

A regression analysis is used to find the two best fit boundary lines. As a simplification, the apparent attraction is interpreted to be 20 kPa for all the samples to make comparison easier between them.

Unbound granular materials develop some permanent deformations at each load step. Figure 6 shows a typical output obtained from a RTLT. The permanent deformation is assessed at every load step of each load sequence. The strain rate is normally highest for the first few pulses of loading and then decreases gradually. There are five loading sequences corresponding to five confining (triaxial) stresses. It is quite common to have extra permanent deformation for the first load sequence indicating that the following sequences are influenced by the load history of the previous steps.

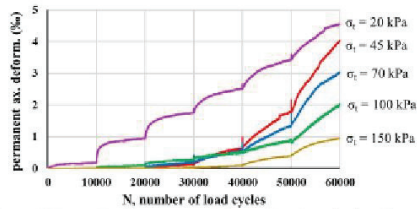


Figure 6. Example of permanent deformation data obtained from a repeated triaxial load test.

The limits given in Table 3 are the criteria defining the boundaries between the different ranges according to the Coulomb approach. The steps in the elastic, elasto-plastic and failure range are respectively marked by square, triangle and circle symbols. The first load sequence is interpreted as part of the compaction procedure of the material, thus only the other four load sequences contribute to the assessment of the boundary lines (Uthus et al. 2007). Figure 7 portrays a typical output.

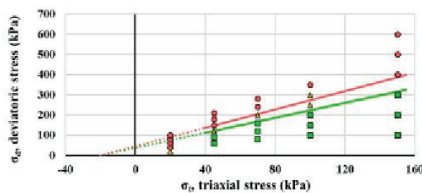


Figure 7. Example of permanent deformation data treatment according to the Coulomb approach. The shapes of the points (square, triangle, circle) stand for the deformation range. The two boundary lines corresponds to the degree of mobilized shear strength ϕ and degree of maximum shear strength ϕ .

3 RESULTS AND DISCUSSION

3.1 Material sampling

Table 4 lists the results obtained from the field investigations.

Table 4. Field surveys data collection.

Site	Condition	Wheel path depth (mm)		Asphalt layer (mm)	Lower sub-base (mm)
		inner	outer		
I	damage	24	17	80	135
II	damage	24	20	84	158
III	damage	13	13	96	123
IV	no damage	17	15	101	95
V	no damage	15	16	94	148

3.2 Sieving analysis

The sieving test describes the grain dimensions of the lower base relating to all the five inspected sites. The

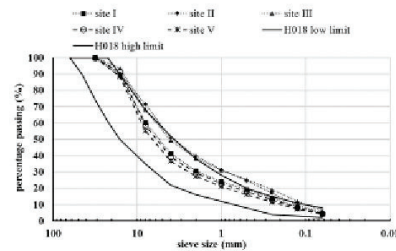


Figure 8. Sieving test of the materials.

The grain sizes for the base layer are between the oversize and the undersize specified by Handbook 018 (Statens Vegvesen 1998) for site I, IV and V. The grain size distribution for sites II and III is very close to the oversize limit, and the quantity of material smaller than 2 mm is higher than the allowed limit. Even if these grain size distributions were somewhat outside of requirements for some of the samples, it was difficult to explain the difference in performance among the five sites from these tests.

3.3 RLT, resilient modulus

The first RLTs inspect the materials coming from site I and from site IV to establish some initial comparisons between a damaged site and a not damaged site. The compression time (t_c) is 20 s and the water contents are 3%, 5% and 7%. Figure 9 portrays the dry density corresponding to each water content after compaction.

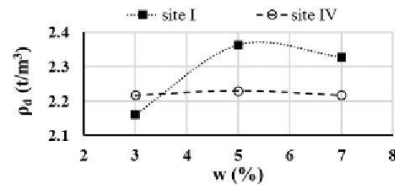


Figure 9. Dry densities for samples coming from site I, IV; $w = 3\%, 5\%, 7\%$; $t_c = 20$ s.

Both site I and IV show a little variation in density and the optimum water content determined from these samples is around 5%. The field densities were not measured.

The k - θ regression curves for site I are displayed in Figure 10. Table 5 specifies the k_1 and k_2 parameters corresponding to the curves.

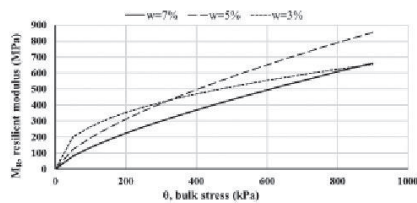


Figure 10. k - θ regression curves for site I; $w = 3\%$, 5% , 7% ; $t_c = 20$ s.

Table 5. Model parameters k_1 and k_2 for site I; $t_c = 20$ s.

Site	w (%)	k_1	k_2
I	7	1.4	0.7
I	5	2.0	0.7
I	3	2.7	0.4

The k - θ regression curves for site IV are displayed in Figure 11. Table 6 specifies the k_1 and k_2 parameters corresponding to the curves.

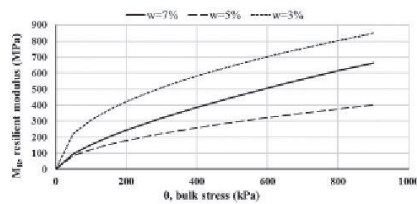


Figure 11. k - θ regression curves for site IV; $w = 3\%$, 5% , 7% ; $t_c = 20$ s.

Table 6. Model parameters k_1 and k_2 for site IV; $t_c = 20$ s.

Site	w (%)	k_1	k_2
IV	7	1.5	0.7
IV	5	1.2	0.5
IV	3	3.1	0.5

The resilient moduli data from site I and IV show a sensitivity to water content. Further analyses are considering just $w = 7\%$ because this is sufficient to highlight discrepancies among the five sites; moreover, running RTLs with further water content values would be quite time consuming. The specimens from sites II and III reach the maximum permanent deformation of 0.5% just after some tens of cycles. Figure 12 shows the different k - θ regression curves with

compaction time of 20 s. Table 7 specifies the k_1 and k_2 parameters corresponding to the curves.

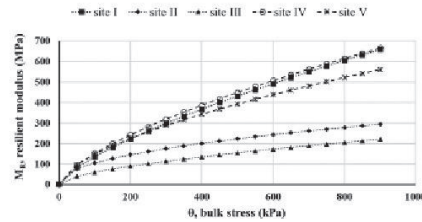


Figure 12. k - θ regression curves for site I, II, III, IV, V; $w = 7\%$; $t_c = 20$ s.

Table 7. Model parameters k_1 and k_2 for site I, II, III, IV, V; $w = 7\%$.

Site	t_c (s)	k_1	k_2
I	20	1.4	0.7
II	20	1.1	0.5
III	20	0.6	0.6
IV	20	1.5	0.7
V	20	1.5	0.6

Figure 13 shows the different k - θ regression curves with compaction time of 40 s. Table 8 specifies the k_1 and k_2 parameters corresponding to the curves.

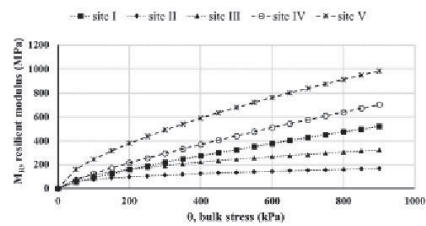


Figure 13. k - θ regression curves for site I, II, III, IV, V; $w = 7\%$; $t_c = 40$ s.

Table 8. Model parameters k_1 and k_2 for site I, II, III, IV, V; $w = 7\%$.

Site	t_c (s)	k_1	k_2
I	40	0.9	0.8
II	40	0.8	0.4
III	40	1.1	0.5
IV	40	1.2	0.8
V	40	2.5	0.6

The stiffness values in Figure 12 and 13 underline a significant variation in the resilient properties of the materials. The specimens from sites II and III have the lowest curves throughout the bulk stress range: their resilient modulus values are almost one third of

those belonging to the other sites when $t_c = 20$ s. The not damaged sites IV and V always have the highest stiffness values, the damaged site I presents high values when the compaction time is 20 s.

3.4 RTLT, permanent deformation

As specified in section 3.3, the specimens coming from sites I and IV are tested initially with compression time (t_c) of 20 s and water contents equal to 3%, 5% and 7%. The elastic limit line and the failure line for site I are displayed in Figure 14. Table 9 specifies the angle of mobilization ρ and the angle of failure φ corresponding to site I.

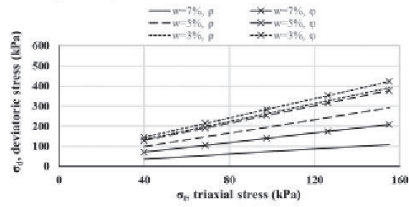


Figure 14. Range boundary lines for site I; $w = 7\%$, 5% , 3% ; $t_c = 20$ s.

Table 9. Angle of mobilization ρ and angle of failure φ for site I; $t_c = 20$ s.

Site	w (%)	ρ (°)	φ (°)
I	7	32	50
I	5	59	65
I	3	66	68

The elastic limit line and the failure line for site IV are displayed in Figure 15. Table 10 specifies the angle of mobilization ρ and the angle of failure φ corresponding to site IV.

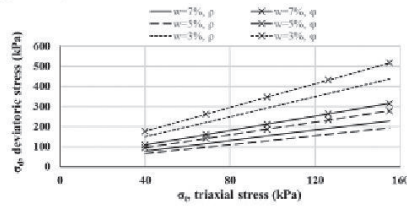


Figure 15. Range boundary lines for site IV; $w = 7\%$, 5% , 3% ; $t_c = 20$ s.

Table 10. Angle of mobilization ρ and angle of failure φ for site IV; $t_c = 20$ s.

Site	w (%)	ρ (°)	φ (°)
IV	7	53	61
IV	5	48	58
IV	3	68	71

The permanent deformation data from site I and IV also show a sensitivity to water content. Moreover, the specimen from site IV has higher range boundary limits than specimens from site I. As for the resilient modulus, further analyses are performed just considering $w = 7\%$. The specimens from sites II and III reach the maximum permanent deformation of 0.5% just after some tens of cycles. The analyses regarding these two locations are not given because they reach the failure very quickly (they would lie along the X axis). Figure 16 shows the different range boundary lines with compaction time of 20 s. Table 11 specifies the corresponding angle of mobilization ρ and angle of failure φ .

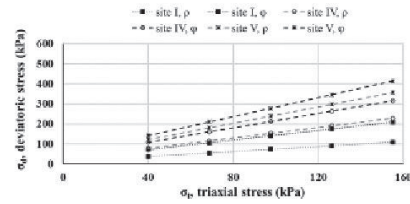


Figure 16. Range boundary lines for site I, IV, V; $w = 7\%$; $t_c = 20$ s.

Table 11. Angle of mobilization ρ and angle of failure φ for site I, IV, V; $w = 7\%$.

Site	t_c (s)	ρ (°)	φ (°)
I	20	32	50
IV	20	53	61
V	20	64	67

Figure 17 shows the different range boundary lines with compaction time of 40 s. Table 12 specifies the corresponding angle of mobilization ρ and angle of failure φ .

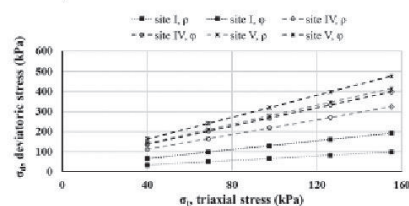


Figure 17. Range boundary lines for site I, IV, V; $w = 7\%$; $t_c = 40$ s.

Table 12. Angle of mobilization ρ and angle of failure φ for site I, IV, V; $w = 7\%$.

Site	t_c (s)	ρ (°)	φ (°)
I	40	29	48
IV	40	62	66
V	40	67	70

Figures 16 and 17 show a significant variation in the permanent deformation. The performances of sites IV and V are similar. The angle of mobilization from site I is approximately 50% of the corresponding value of sites IV and V, the ratio becomes approximately 15% when considering the angle of failure. The specimens from sites II and III reaches the 0.5% limit very quickly and they are not reported in the graphs.

4 CONCLUSION

This research has dealt with the road distresses which occurred in a highway in southern part of Norway. Five locations with and without visible damage were chosen to survey the conditions. Laboratory tests evaluated the properties of the unbound base layer. Specimens from two sites contained somewhat more material smaller than 2 mm than allowed in the design guidelines.

The curves resulting from the $k-\theta$ regression model highlighted that the base layers of not damaged locations were much stiffer than the ones from damaged areas.

The permanent deformation results also underlined a significant discrepancy in damaged and not damaged sites: both the angle of mobilization and of failure from site I were lower than the respective ones from sites IV and V. Sites II and III reached the maximum permanent deformation of 0.5% just after some tens of cycles in the triaxial test apparatus.

The overall performance of the damaged sites proved to be significantly different from the ones which did not undergo distresses.

However, the differences in stiffness and resistance against permanent deformation in the base materials are not likely to represent the only explanation for the distresses observed. The research could be extended by inspecting more areas of the road and testing the fatigue properties of the asphalt mix. The estimation of the stress and strain levels for the total structure could be a basis for deciding on the best rehabilitation strategy.

REFERENCES

Barksdale, R. 1971. Compressive stress pulse times in flexible pavements for use in dynamic testing. *Highway Research Record* 345: 32-44. Washington DC: Highway Research Board.

CEN 2003. *EN 13286-4 Unbound and hydraulically bound mixtures. Part 4: test methods for laboratory reference density and water content. Vibrating hammer*. Brussels: CEN.

CEN 2004. *EN 13286-7 Unbound and hydraulically bound mixtures. Part 7: cyclic load triaxial test for unbound mixtures*. Brussels: CEN.

CEN 2012. *EN 933-1 Tests for geometrical properties of aggregates. Part 1: determination of particle size distribution. Sieving method*. Brussels: CEN.

Dongmo-Engeland, B. 2005. *GARAP, Influence of sample's height on the development of permanent deformation*. Rapport STF50 A05075. Trondheim: SINTEF.

Gidel, G. & Hornych, P. & Chauvin, J.J. & Breysse, D. & Denis, A. 2001. A new approach for investigating the permanent deformation behaviour of unbound granular material using the repeated load triaxial apparatus. *Bulletin des Laboratoires des Ponts et Chaussées* 233: 5-21. Champs-sur-Marne: IFSTTAR.

Hicks, R.G. & Monismith, C.L. 1971. Factors influencing the resilient response of granular materials. *Highway Research Record* 345: 15-31. Washington DC: Highway Research Board.

Hoff, I. & Baklökk, L. & Aurstad, J. 2003. Influence of laboratory compaction method on unbound granular materials. *Proceedings for the 6th International Symposium on Pavements Unbound*: CD-ROM. Nottingham: University of Nottingham.

Lekarp, F. & Isacsson, U. & Dawson, A. 2000a. State of the Art. I: Resilient response of unbound aggregates. *Journal of Transportation Engineering* 126(1): 66-75. Reston: ASCE.

Lekarp, F. & Isacsson, U. & Dawson, A. 2000b. State of the Art. II: Permanent strain response of unbound aggregates. *Journal of Transportation Engineering* 126(1): 76-83. Reston: ASCE.

Seed, H. B. & Chan, C. K. & Lee, C.E. 1962. Resilience characteristics of subgrade soils and their relations to fatigue in asphalt pavements. *Proceedings of International Conference on Structural Design of Asphalt Pavements* 1: 611-636. Ann Arbor: University of Michigan.

Statens Vegvesen 1998. *Håndbok 018 Vegbygging*. Oslo: Vegdirektoratet.

Uthus, L. & Tutumluer, E. & Horvli, I. & Hoff I. 2007. Influence of grain shape and surface texture on the deformation properties of unbound aggregates in pavements. *International Journal of Pavements* 6(1). United Kingdom: Abingdon.

Uthus, L. 2009. Effect of grading and moisture on the deformation properties of unbound granular aggregates. *8th International Conference on the Bearing Capacity of Roads, Railways and Airfields* 8: 167-177. Rotterdam: Balkema.

Werkmeister, S. & Dawson, A. & Wellner, F. 2001. Permanent deformation behaviour of granular materials and the shake-down concept. *Transportation Research Record* 1757: 75-81. Washington DC: Highway Research Board.

PAPER II

Barbieri, D. M., Hoff, I., and Mørk, M. B. E. (2019). “Mechanical assessment of crushed rocks derived from tunnelling operations.” W.-C. Cheng, J. Yang, and J. Wang, eds., Springer International Publishing, 225–241. GeoChina 2018.

Mechanical assessment of crushed rocks derived from tunnelling operations

Diego Maria Barbieri¹, Inge Hoff², PhD and Mai Britt Engeness Mørk³, PhD

¹ PhD candidate, NTNU, Department of Civil and Environmental Engineering, Trondheim, Norway, diego.barbieri@ntnu.no.

² Professor, NTNU, Department of Civil and Environmental Engineering, Trondheim, Norway, inge.hoff@ntnu.no.

³ Professor, NTNU, Department of Geosciences and Petroleum, Trondheim, Norway, mai.britt.mork@ntnu.no.

ABSTRACT: The Norwegian Public Roads Administration is currently running the “Ferry-free coastal route E39” project, which reduces the travel time along the Norwegian coast from Trondheim to Kristiansand. The plan includes the creation of several long tunnels, which will generate a surplus of blasted rocks; these could be used in the road unbound layers close to the place of production. The research presented here has three goals. The first aim is to map the geology encountered along the E39 road alignment. The second aim is to check whether the rocks fulfil the existing code requirements for road unbound layers, defined in terms of Los Angeles and micro-Deval limit values. The third aim is to investigate the crushing and the variation in grain size of the unbound materials during both construction phase and service life phase. The construction stage is achieved by a full scale testing to assess rock soundness after rolling, the service life stage is simulated by the repetition of a specific load in the triaxial cell apparatus. The current tunnelling operations located south of Bergen are producing blasted rocks, they adequately represent the geology spread along the entire E39 alignment. Three types of crushed rocks are selected and tested. The major part of the rocks excavated are suitable for direct use in pavement unbound layers. The most significant modification in grain size distribution curve takes place during the compaction phase for all the materials.

INTRODUCTION AND BACKGROUND

Norwegian Public Roads Administration (NPRA) is currently running the “Ferry-free coastal route E39” project, which improves the viability along the Norwegian coast for a total length of about 1100 km from Trondheim to Kristiansand (NPRA 2017; Dunham 2016). The project includes the building of several bridges and tunnels, while aiming for creating a sustainable infrastructure. The extended tunnelling systems will generate a surplus of blasted rocks. They could be used as viable substitutes for natural aggregates in the road unbound layers close to the place of production. This is beneficial from both economic and environmental point of views (Aatheesan et al. 2008; Arulrajah et al. 2013; Núñez et al. 2008; Onyango et al. 2007; Otto et al. 2015). The usage of demolition materials in pavement applications is a sustainable option to minimise the waste while reducing the demand for scarce quarried materials and lowering carbon footprints

(Fladvad et al. 2017). The transport distance should be within 20 - 30 km to represent a competitive solution (Neeb 1992).

The need for recycling and reusing materials is a topic of global interest and concern. In Norway the production of natural aggregate has been declining since 1997, while the production of crushed rocks has been increasing since 2003. In 2015 almost 70 million tons of crushed rocks were produced in Norway. The average yearly aggregate consumption per capita is 11 tons; approximately half part of this figure is used for road construction (Erichsen and Aasly 2016).

The existing requirements for road unbound layers are connected to relatively simple tests: the Norwegian pavement design manual N200 (NPRA 2014) sets limits in terms of sieving curve (CEN 2012), Los Angeles (CEN 2010) and micro-Deval (CEN 2011) values. By respecting the specified thresholds, the road should perform adequately without encountering premature damage (Barbieri et al. 2017).

The research presented here has three goals. In the first place, the geology encountered along the E39 road alignment is mapped, this task is essential to identify the bedrock distribution where the tunnels are excavated. In the second place, the study investigates whether the blasted rocks fulfil the existing requirements for road unbound layers established by the design manual. In the third place, the crushing and variation in grain size of unbound materials is investigated during both construction phase and service life phase. The grain size distribution curve is closely connected to the material performance in terms of resilient modulus and deformation (Hicks and Monismith 1971, Lekarp et al. 2000a, Lekarp et al. 2000b, Li and Selig 1994), therefore the variation in grain size largely affects the material behaviour. Furthermore, this investigation could bring to a better understanding between the mentioned standard tests and the behaviour of the crushed rocks in situ.

The building site "Svegatjørn-Rådal" is located south of Bergen and the current tunnelling operations are producing blasted rocks; which adequately represent the geology spread along the entire E39 alignment. Three types of crushed rocks (designated as material M1, M2, M3) are selected and tested.

METHODOLOGY

Geology and materials

Knowledge about the geology encountered by the tunnelling operations is needed to map the origin and distribution of the materials (NGU 2017, Ramberg et al. 2013). Figure 1 displays the geology of the southern part of Norway and the alignment of E39 highway. The highway alignment comes across different types of bedrocks. The major part of the rocks is igneous and supracrustal of Precambrian ages (1700 - 900- 10⁶ years); they mainly comprise granite, granodiorite and granitic to dioritic gneiss. There are also areas with Caledonian rocks, these locations are anyway at maximum 20 - 30 km far from the most widespread geology aforementioned. Igneous and metamorphic rocks occur close to Bergen, where various brownish and red colours stand for gabbro, diorite, anorthosite,

granite and augen gneiss. Low grade metamorphic rocks such as phyllite occur in the Boknafjord area close to Stavanger.

NPRA is responsible for the current operations in the construction site "Svegatjørn-Rådal": tunnel connections will improve the traffic condition between Bergen and Os. Tunnels are excavated with means of explosive slurry injected by drilling jumbos. The blasted rocks are in size up to one meter. The material is then crushed by mobile impact crushers, sieved and stored in large areas. The blasted rocks derived from this building site adequately represent the variety in the geology spread along the entire highway alignment.

The materials collected come from Lyshorn tunnel, designed to connect the locality of Endelausmarka (Os municipality) to Rådal with a length of 9.3 km. Three types of rocks are selected and tested.

- Material M1. Mafic igneous origin, partly modified by metamorphism (amphibolite);
- Material M2. Metamorphic origin, fine-grained felsic and micaceous rocks;
- Material M3. Metamorphic origin, very fine-grained felsic and micaceous rocks.

Thin-section microscopy images of selected rock samples show mineralogy and grain sizes (Figure 2). Igneous rocks M1 are modified by metamorphism, e.g. amphibolization and replacement of coarse igneous feldspar by aggregates of fine epidote and feldspar. Finer-grained felsic and micaceous rocks appear more dominant in M2 and especially in M3.

Standard tests for road unbound layers materials

The pavement design manual N200 (NPRA 2014) allows for the use of crushed rocks. It is possible to use this resource in the road base layer as paved crushed rocks and in the road subbase layer as unsorted crushed rocks if Los-Angeles standard test (LA value) and micro-Deval standard test (MDE value) are fulfilled. The LA limit values are respectively 30 and 35 for base layer and subbase layer, the MDE limit value is 15 for both of them.

Further requirements in terms of upper and lower grain size distribution curve are demanded for the base layer (Figure 3). The distribution curve of the subbase layer must be within 20/120 mm. The major part of the E39 highway corresponds to traffic class F, which is associated to a minimum of 10 million repetitions of 10-ton equivalent standard axle load.

Materials M1, M2, M3 are tested according to the Los Angeles standard test (CEN 2010) and the micro-Deval standard test (CEN 2011).

Modelling construction phase and service life phase

The crushed rocks behaviour is studied according to two phases: construction phase and service life phase. These steps are respectively represented by the compaction action of a drum roller and the repetition of a 10-ton standard axle load. The variation in grain size

due to crushing largely affects the most important engineering properties of granular materials in terms of resilient modulus and deformation.

The crushing of a subbase layer is investigated for this purpose. Materials M1, M2, M3 have gradation 20/120 mm.

Bomag BW 213 DH is the single steel drum roller taken into consideration for the construction phase. Its weight is 12.3 t, the drum axle load is 7.6 t, the wheel axle load is 5.2 t, the static linear load is 3.55 kg/mm and the working width is 2.1 m. The compactor is interpreted with a one-degree-of-freedom lumped parameter scheme (Figure 4). m_d and m_f are the drum and frame masses, F_C is the centrifugal force, F_s is the contact force between drum and soil and g is the acceleration of gravity, frame inertia is neglected (Mooney and Dietmar 2007; Yoo and Selig 1980). For the compactor considered, the parameters are $m_d = 7560$ kg, $m_f = 1475$ kg, $F_C = 284$ kN. The drum acceleration a_d varies, a cautious value of $3 \cdot g$ is considered (Gorman and Mooney 2003). The contact force F_s is then assessed per equilibrium of forces and it is equal to 150 kN.

COMSOL software is used to simulate the two mentioned stages to assess the stress distribution; during the construction phase rocks are expected to experience a state of stress which is larger than the one expected during the service life phase (Kwon et al. 2008).

In the former stage, the subbase is subjected to the compaction load. The layer is 300 mm thick, 3 m wide, 0.5 m long and the drum is 2.1 m wide; the drum contact area is rectangular. The widths are halved thanks to the symmetry of the problem (Figure 5a).

In the second stage, the subbase and the other layers of the road are subjected to the vehicle loads, these are considered as repetitions of the 10-ton standard axle load. This configuration is modelled by adding a base layer and a top layer, respectively 100 mm and 200 mm thick, on the previous subbase layer. The distance between the axes of the wheels is 1.7 m and the tyre contact area is circular. The model parameters for the top layer are Young's modulus $E = 3$ GPa, Poisson's ratio $\nu = 0.4$ and density $\rho = 2300$ kg/m³. The problem is symmetric so the widths are halved (Figure 5b).

Both subbase and base are unbound layers and their mechanical behaviour can be properly described by a non-linear law defining the resilient modulus M_R . The $k-\theta$ model is a non-linear, stress dependent power function (Hicks and Monismith 1971). The model is given as follows in its dimensionless form:

$$M_R = k_1 \sigma_a \left(\frac{\theta}{\sigma_a} \right)^{k_2}, \quad (1)$$

where θ is the bulk stress sum of the principal stresses, σ_a is a reference pressure (100 kPa) and k_1 and k_2 are model parameters assessed from the regression of the test results.

Repeated Triaxial Load Test (RTLTL) can define the resilient modulus parameter. The RTLTL equipment available can be used to test materials up to 30 mm in size: all the samples are prepared according to the sieving curve reported as dashed line in Figure 3, which corresponds to a base layer. In order to prepare a specimen, the desired amount of water is added to the material and rests for 24 h to let the moisture distribute uniformly.

Four equal layers are compacted with the vibratory hammer. Each material set comprises two specimens, they have a diameter of 150 mm and height of 240 mm, the amount of water is 1%. A Kango 950X vibratory hammer (total weight 35 kg, frequency $25 \div 60$ Hz, amplitude 5 mm) is used to compact the specimen layers for 30 s. Figure 6 displays the average bulk density for each material set (CEN 2003). RTLs are performed according to the multi-stage loading procedure in five different sequences with different confining stresses (CEN 2004). Water is the confining medium and applies a uniform constant pressure in all directions (triaxial or confining stress), a hydraulic jack exerts an additional vertical dynamic stress (deviatoric stress), which stepwise increases at different levels of confining stress. Two and three Linear Variable Differential Transducers (LVDTs) measure the axial and radial deformations, respectively. Figure 7 displays the resilient modulus curves and the values of k_1 , k_2 parameters for the three materials under investigation.

Road construction phase

Field operations investigate the crushing of the materials M1, M2, M3: the sieving curves referring to before and after drum roller action are compared. The crushing of a subbase layer is studied: materials M1, M2, M3 have dimension 20/120 mm. They are placed in three areas close to each other: each area is approximately 7 m long, 5 m wide and 300 mm high, it is made of about 15 t of rocks. The compactor exerts its action just on one side of the rocks (Figure 8). It is assumed that, before the compacting action takes place, the grain size distribution associated with the not compacted stripe (marked in blue) is the same of the compacted stripe (marked in red). Four portions are identified in each area: two do not undergo compaction and two undergo compaction. Each portion is 1 m wide, 1 m width, 300 mm high, weighs about 200 kg and numbered from 1 to 12.

Figure 9 depicts the main stages of the test fulfilment: firstly, the existing surface is compacted with a single steel drum roller and operators lay out a polypropylene not woven geotextile (Figure 9a), which prevents losing the small fractions produced during the test. The materials are tipped from a truck and distributed uniformly with the help of a grader. A single steel drum roller then compacts one side of the placed crushed rocks (Figure 9b). Bomag BW 213 DH accomplishes four passages as specified in the manual code (NPRA 2014).

Figure 10 displays the bulk densities of the layer before and after the roller compaction. The construction phase is completed and the twelve portions are highlighted with coloured spray (Figure 9c). The rocks are collected from these portions by hand to keep the gradation as unaltered as possible and moved into plastic bags (Figure 9d); finally, the material is sieved. Researchers have used various parameters or measures to represent the amount of particle breakage that takes place during loading (Gupta 2016); either as the variation of a particular grain diameter (Lade et al. 1996) or as the shift of the whole grain size distribution curve (Hardin 1985). This research refers to coefficient of uniformity C_u , coefficient of curvature C_c and particle breakage factor B_{10} (Lade et al. 1996). These parameters are respectively defined as

$$C_u = \frac{D_{10}}{D_{60}}, \quad (2)$$

$$C_c = \frac{D_{30}^2}{D_{10}D_{60}}, \quad (3)$$

$$B_{10} = 1 - \frac{D_{10f}}{D_{10i}}; \quad (4)$$

where D_{10} , D_{30} , D_{60} are respectively the grain diameter at 10%, 30%, 60% passing, subscript f and i respectively stand for final and initial gradation.

Road service life phase

According to the pavement design manual N200, traffic class F entails at least 10 million repetitions of 10-ton standard axle load (NPRA 2014). The RTL equipment is used to reproduce the average stress state in the subbase: 20 kPa and 120 kPa are the pressures respectively set in the horizontal and vertical directions in the triaxial cell. These values derive from the modelling outcomes referring to service life scenario (Figure 12d, 12e, 12f).

Two specimens are tested for each material M1, M2, M3. All the samples have a diameter of 150 mm and height of 240 mm.

The lower size of the subbase investigated in situ is 20 mm; moreover, it is recommended the maximum testing particle size to be smaller than one fifth of the specimen diameter (CEN 2004): the specimens are made of crushed rocks 20/30 mm in size. All the materials are washed and dried before the testing in the triaxial cell. The specimens are subjected to one million load repetitions, since this figure is sufficient enough to highlight discrepancies among the three materials.

TEST RESULTS AND DISCUSSION

Standard acceptance tests outcomes

Los Angeles and micro-Deval are the standard tests when it comes to accept crushed rocks as building materials in the pavement unbound layers. Three and two specimens for each material are respectively tested, Figure 11 displays the average results with standard deviation.

Material M1 fulfils the code requirements, therefore it can be directly used for road construction. Both material M2 and M3 have LA values lying close to the limit, but both of them exceed the threshold when it comes to MDE values.

Stress magnitudes during construction phase and service life phase

The contact length between the drum and the soil is the remaining parameter to be defined for modelling purposes. Figure 12 displays the vertical stress in the symmetry plane for respectively 25 mm (a), 75 mm (b) and 125 mm (c).

The vehicle load is the 10-ton standard axle load: each wheel exerts 5 ton. Figure 12 shows the vertical stress in the subbase plane under the wheel for different lengths of tyre contact radius: 130 mm (d), 150 mm (e) and 170 mm (f).

The stress distributions depicted in Figure 12 refer to M1 resilient curve, as the results connected to M2, M3 resilient curves are highly similar.

The subbase experiences the largest stresses during the compaction phase, moreover, the roller-soil contact length has a large impact on the results regarding stress distribution.

The stress values connected to the service life phase are one order of magnitude smaller; in addition, they are not particularly sensible to the tyre contact radius: major crushing is expected to take place during the former stage than during the latter stage (Gupta 2016).

Crushed rocks performance during construction phase

The crushed rocks coming from the twelve field portions are sieved. The steel drum roller exerts its action just along a stripe which comprises six portions. It is assumed that, before the compaction takes place, the grain size distribution referring to the not compacted stripe is the same of the compacted stripe. In total twelve sieving curves are assessed. Therefore for each material type there is a set of two portions subjected to the same treatment (compacted or not compacted), for each set the average curve is assessed: Figure 13 depicts six sieving curves. The amount of particle breakage during compaction can be visualized thanks to the particle size distribution curves measured before and after the external action.

From Figure 13 it is apparent that there is a slight change in the grain size for material M1, while both materials M2 and M3 undergo substantial crushing. There is an unexpected crossing of lines between 100 mm and 75 mm regarding pre- and post-compaction: the assumption that the grading curve of the not compacted stripe is the same of the compacted stripe before the roller action turns out to be not completely exact; although this hypothesis is necessary in order not to sieve all the materials placed in situ (about 45 t).

Figure 14 displays the increment in passing for each sieve size used in the sieve analyses; the increment is assessed as the difference in passing values between post-compaction curve and pre-compaction curve, divided by the passing value referring to pre-compaction curve. The maximum increment for material M1 is 31.6 % referring to sieve size 20 mm, both materials M2 and M3 have much higher maximum increment, respectively 83.1 % and 64.3 % referring to sieve size 25 mm. Material M1 crushes less than the other two materials M2 and M3 under compaction load. Each sieving curve is fitted by a third-order equation

$$ax^3 + bx^2 + cx + d = 0, \quad (5)$$

six polynomial expressions are calculated based on the sieving curves. Considering these new calculated particle size distribution curves, it is possible to have a better estimation of the coefficient of uniformity C_u , coefficient of curvature C_c and particle breakage factor B_{10} .

In addition, the optimum vertical translation of the pre-compaction curve towards the post-compaction curve is estimated with the least square methods; the value ζ quantifies this translation and also contributes to evaluating the overall difference in the curve shapes.

Figure 15 displays the coefficient of uniformity, coefficient of curvature and particle breakage factor for each material. Material M1 experiences the lesser modifications in coefficient of uniformity and curvature, its particle breakage factor is smaller than the values referring to M2, M3.

It is possible to establish a relationship between the standard tests and the particle breakage factor as follows

$$LA = \alpha B_{10}, \quad (6)$$

$$M_{DE} = \beta B_{10}, \quad (7)$$

the best fitting α , β parameters values in this case are $\alpha = 0.95$ and $\beta = 0.69$. The displacement along the y-axis of the pre-compaction curve assessed with the least square method is $\zeta = -0.14$ for M1, $\zeta = 6.68$ for M2 and $\zeta = 7.3$ for M3. The pre- and post-compaction curves for material M1 are much closer compared to the ones concerning materials M2, M3.

Crushed rocks performance during service life phase

Specimens made of crushed rocks M1, M2, M3 in size 20/30 mm are tested in the triaxial cell. A set of two specimens for each type is tested and sieved both before and after the load action, therefore twelve sieving curves are assessed. Average curves are estimated: Figure 16 depicts six sieving curves. The trends of pre- and post-load curves are very similar for all the material types.

Figure 17 shows the passing values after the loading action. It generates new grain sizes (smaller than 20 mm) with approximately the same percentage for all the materials, even if M1 crushes less than M2, M3. Figure 18 shows the coefficient of uniformity, coefficient of curvature and particle breakage factor. The first two parameters do not undergo remarkable changes due to the loading action. The particle breakage factors are close to the lower limit zero, which would imply no particle breakage. The curves are considerably close to each other for all the materials and the loading action does not bring to significative crushing.

CONCLUSIONS

The research has focused on the mechanical assessment of crushed rocks derived from blasted rock surplus as a result of tunnel installations along E39 highway. Possible use in the road unbound layers close to the place of production would provide a sustainable cost-benefit application. Three material types M1, M2, M3 have been chosen to represent adequately the bedrock geologies encountered along the entire highway alignment. Material M1 complies with the requirements set by the pavement design manual N200 in terms of Los Angeles and micro-Deval limit values; vice versa materials M2 and M3 do not fulfil them. Material M1 stands for the major part of the geology encountered along the highway, therefore there is a huge potential for the excavated rocks to be directly used in pavement unbound layers.

The research has also investigated the ability of the three materials to withstand compaction and trafficking while used in the unbound layers of a road structure. The crushing process of the materials is investigated during the construction phase, achieved by a full scale testing to assess aggregate soundness after rolling, and during service life phase, simulated with the triaxial cell apparatus. The modelling connected to these two scenarios highlights a remarkable difference in the stress state. The crushing is substantially more significant in the former stage than in the latter stage for all the materials.

Coefficient of uniformity C_u , coefficient of curvature C_c , particle breakage factor B_{10} and optimum vertical translation ζ are the parameters selected to describe the grain size distribution curves before and after drum roller compaction. There is a good correlation between the crushing standard tests and the crushing taking place in situ. Moreover, two relationships involving Los Angeles value, micro-Deval value and particle breakage factor have been proposed. These parameters clearly show material M1 performs better than materials M2, M3.

No significant differences in grain size have been observed due to the service life phase loading: all the materials perform similarly in this scenario.

REFERENCES

- Aatheesan, T. *et al.* (2008). Beneficial use of brick rubble as pavement subbase material. *Advances in Transportation Geotechnics*.
<https://doi.org/10.1201/9780203885949.pt10>
- Arulrajah, A. *et al.* (2013). Geotechnical and geoenvironmental properties of recycled construction and demolition materials in pavement subbase applications. *Journal of Materials in Civil Engineering*.
[https://doi.org/10.1061/\(ASCE\)MT.1943-5533.0000652](https://doi.org/10.1061/(ASCE)MT.1943-5533.0000652)
- Barbieri, D. M. *et al.* (2017). Laboratory investigation on unbound materials used in a highway with premature damage. *Bearing capacity of Roads, Railways and Airfields*.
- CEN (2003). EN 13286-4. Unbound and hydraulically bound mixtures. Part 4: test methods for laboratory reference density and water content. Vibrating hammer.
- CEN (2004). Unbound and hydraulically bound mixtures. Part 7: cyclic load triaxial test for unbound mixtures.
- CEN (2010). EN 1097-2. Tests for mechanical and physical properties of aggregates. Part 2: methods for the determination of resistance to fragmentation.
- CEN (2011). EN 1097-1. Tests for mechanical and physical properties of aggregates. Part 1: determination of the resistance to wear (micro-Deval).
- CEN (2012). EN 933-1. Tests for geometrical properties of aggregates. Part 1: determination of particle size distribution. Sieving method.
- Dunham, K. K. (2016). Coastal highway route E39 - extreme crossings. *Transportation Research Procedia*. <https://doi.org/10.1016/j.trpro.2016.05.102>
- Erichsen, E. and Aasly, A. (2016). Mineralressurser i Norge 2015. *Mineralstatistikk og bergindustriberetning*. (In Norwegian).
- Fladvad, M. *et al.* (2017). Comparison of practice for aggregate use in road construction - results from an international survey. *Bearing Capacity of Roads, Railways and Airfields*.
- Gorman, P. B. and Mooney, M. A. (2003). Monitoring roller vibration during compaction of crushed rock. *20th International Association for Automation and Robotic in Construction*.

- Gupta, A. K. (2016). Effects of particle size and confining pressure on breakage factor of rockfill materials using medium triaxial test. *Journal of Rock Mechanics and Geotechnical Engineering*. <https://doi.org/10.1016/j.jrmge.2015.12.005>
- Hardin, B. O. (1985). Crushing of soil particles. *Journal of Geotechnical Engineering*. [https://doi.org/10.1061/\(ASCE\)0733-9410\(1985\)111:10\(1177\)](https://doi.org/10.1061/(ASCE)0733-9410(1985)111:10(1177))
- Hicks, R.G. and Monismith, C. L. (1971). Factors influencing the resilient response of granular materials. *Highway Research Record*.
- Kwon, J. *et al.* (2008). Aggregate base residual stresses affecting geogrid reinforced flexible pavement response. *International Journal of Pavement Engineering*. <http://dx.doi.org/10.1080/10298430701582347>
- Lade, P. V. *et al.* (1996). Significance of particle crushing in granular materials. *Journal of Geotechnical Engineering*. [https://doi.org/10.1061/\(ASCE\)0733-9410\(1996\)122:4\(309\)](https://doi.org/10.1061/(ASCE)0733-9410(1996)122:4(309))
- Lekarp, F. *et al.* (2000). State of the art. I: resilient response of unbound aggregates. *Journal of Transportation Engineering*. [https://doi.org/10.1061/\(ASCE\)0733-947X\(2000\)126:1\(66\)](https://doi.org/10.1061/(ASCE)0733-947X(2000)126:1(66))
- Lekarp, F. *et al.* (2000). State of the art. II: permanent strain response of unbound aggregates. *Journal of Transportation Engineering*. [https://doi.org/10.1061/\(ASCE\)0733-947X\(2000\)126:1\(76\)](https://doi.org/10.1061/(ASCE)0733-947X(2000)126:1(76))
- Li, D. and Selig, E. T. (1994). Resilient modulus for fine-grained subgrade soils. *Journal of Geotechnical Engineering*. [https://doi.org/10.1061/\(ASCE\)0733-9410\(1994\)120:6\(939\)](https://doi.org/10.1061/(ASCE)0733-9410(1994)120:6(939))
- Mooney, M. and Dietmar, A. (2007). Vibratory roller integrated measurement of earthwork compaction: an overview. *Seventh International Symposium on Field Measurements in Geomechanics*. [https://doi.org/10.1061/40940\(307\)80](https://doi.org/10.1061/40940(307)80)
- Neeb, P. R. (1992). Byggeråstoffer. (In Norwegian).
- NGU (Norges Geologiske Undersøkelse, Geological Survey of Norway). Accessed 1 October 2017. <http://www.ngu.no/>
- NPRA, Norwegian Public Roads Administration (2014). Håndbok N200 Vegbygging. (In Norwegian).

- NPRA, Norwegian Public Roads Administration (2017). The E39 Coastal Highway Route. 10 May 2017, accessed 1 October 2017.
<http://www.vegvesen.no/vegprosjekter/ferjefriE39/English>
- Núñez, W. P. *et al.* (2008). Using unbound aggregates resulting from amethyst mining in low volume roads. *Advances in Transportation Geotechnics*.
<https://doi.org/10.1201/9780203885949.ch28>
- Onyango, M. and Busch, C. (2007). Use of naturally occurring pozzolans for road construction in Tanzania. *Transportation Research Record: Journal of the Transportation Research Board*. <https://doi.org/10.3141/1989-61>
- Otto, A. *et al.* (2015). Method for increasing the use of locally available materials for road construction in Ethiopia by allowing for climatic variations. *Transportation Research Record: Journal of the Transportation Research Board*.
<https://doi.org/10.3141/2474-13>
- Ramberg, I. B. *et al.* (2013). Landet blir til. (In Norwegian).
- Yoo, T. S. and Selig, E. T. (1980). Dynamics of vibratory-roller compaction. *International Journal of Rock Mechanics and Mining Sciences and Geomechanics*.

FIGURES

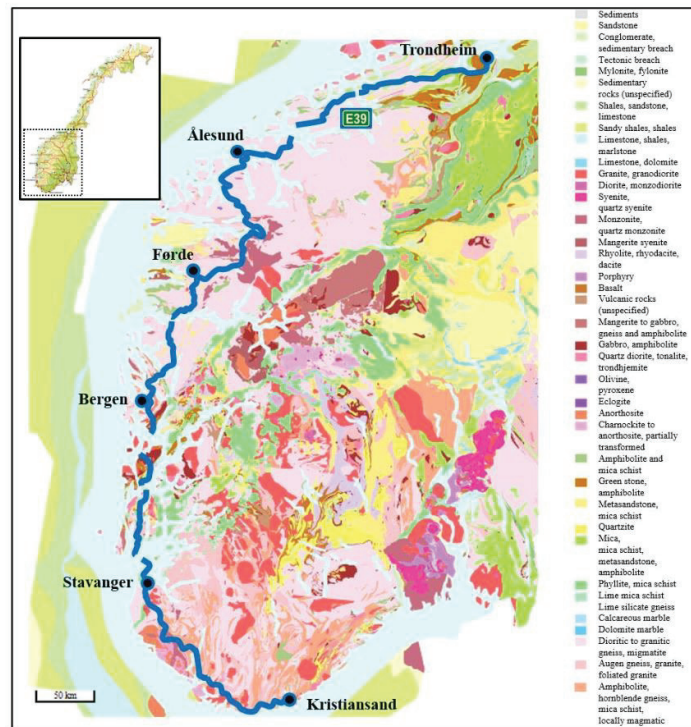


FIG. 1. Bedrock geology of southern Norway and alignment of E39 highway

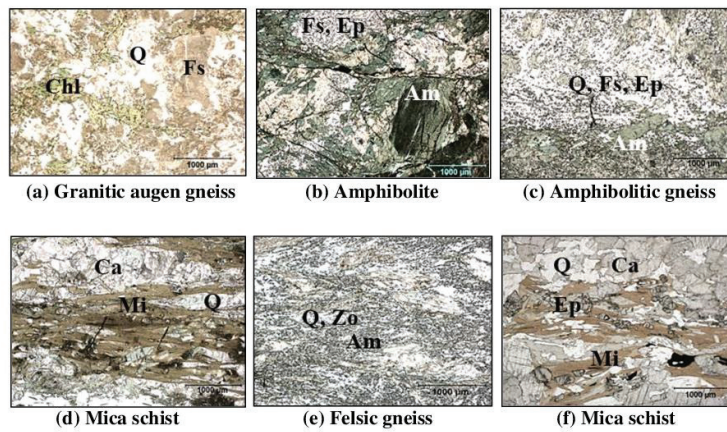


FIG. 2. Mineralogy and grain sizes M1 (a, b), M2 (c,d), M3 (e,f). Mineral abbreviations: Am/amphibole, Ca/calcite, Chl/chlorite, Ep/epidote, Fs/feldspar, Q/quartz, Mi/mica/biotite, Zo/zoisite (optical micrographs, transmitted plane-polarized light, 1 mm scale bar)

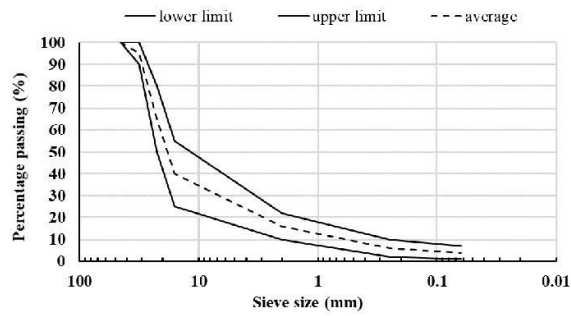


FIG. 3. Grain size distribution curve for base layer

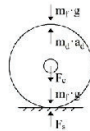


FIG. 4. Drum roller one-degree-of-freedom scheme (after Yoo and Selig 1980)

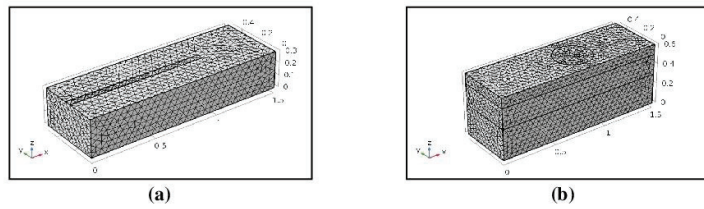


FIG. 5. Modelling of the subbase (a) and subbase, base, top layers (b)

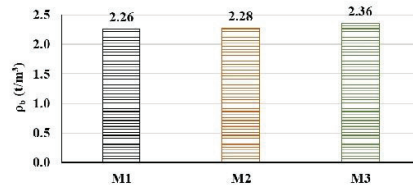


FIG. 6. Bulk density of the specimens tested with RTL

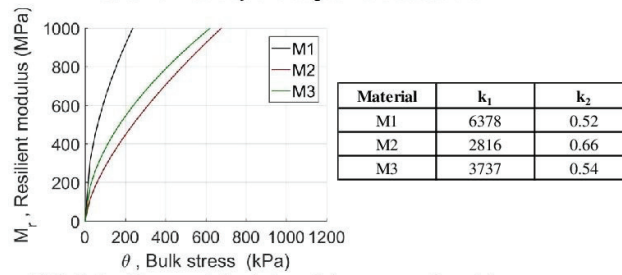


FIG. 7. Resilient modulus k- θ model: curves and model parameters

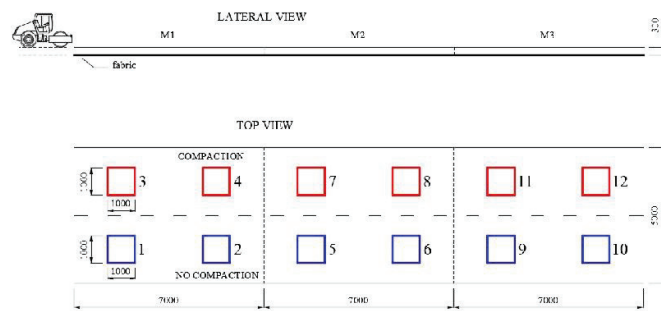


FIG. 8. Layout of the field test (dimensions in mm)

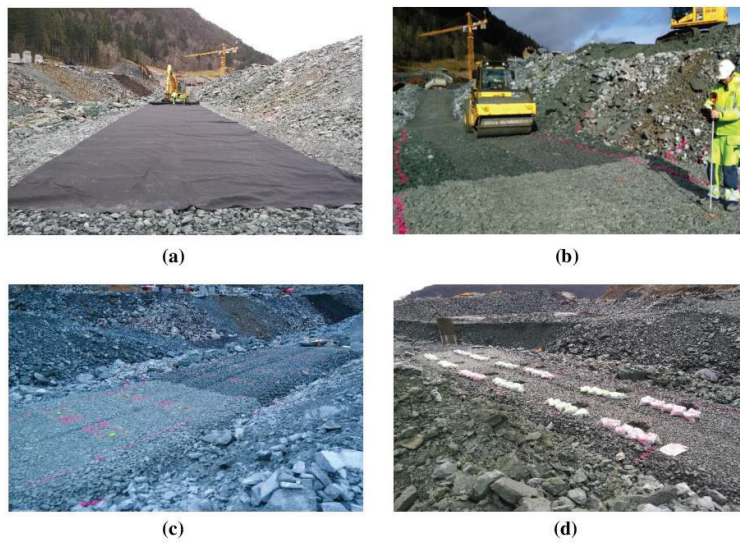


FIG. 9. Main stages of the field test

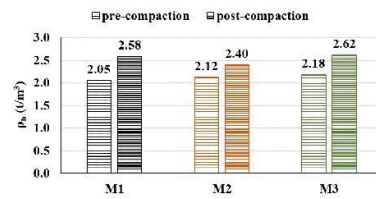


FIG. 10. Bulk density of the unbound layer before and after roller compaction

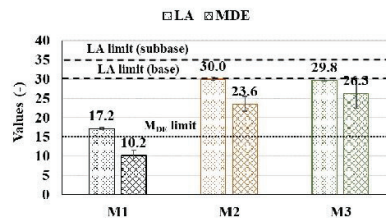


FIG. 11. Los Angeles and micro-Deval values

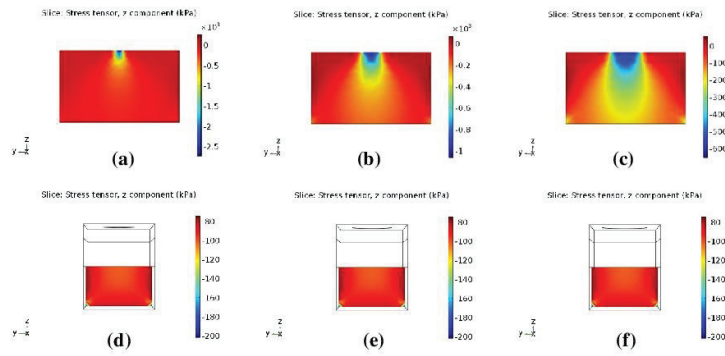


FIG. 12. Vertical stress in the subbase (kPa);
for different values of drum contact length: 25 mm (a), 75 mm (b), 125 mm (c);
for different values of tyre contact radius: 130 mm (d), 150 mm (e), 170 mm (f)

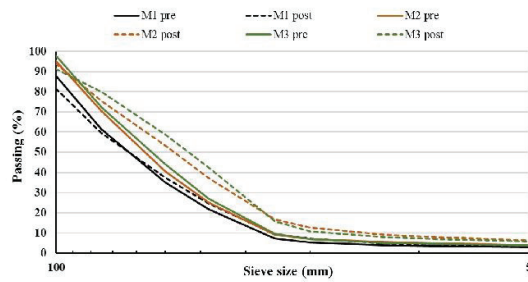


FIG. 13. Sieving curves referring to pre-compaction and post-compaction action

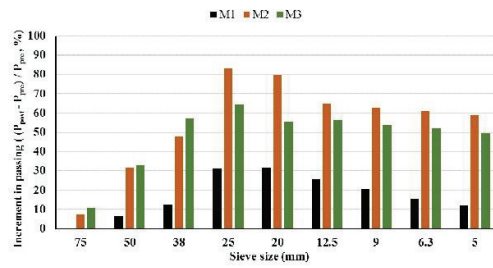


FIG. 14. Increment in passing for each sieve size after compaction

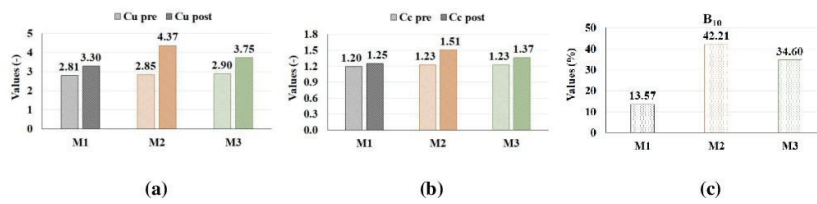


FIG. 15. Coefficient of uniformity (a), coefficient of curvature (b) and particle breakage factor (c) of the calculated sieving curves before and after compaction

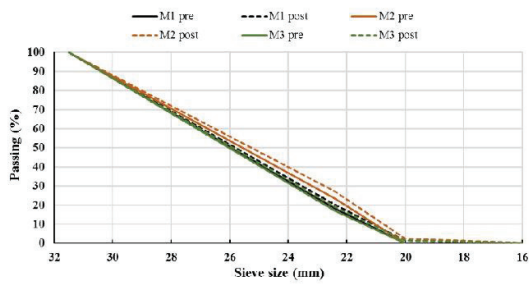


FIG. 16. Sieving curves referring to pre-load and post-load action

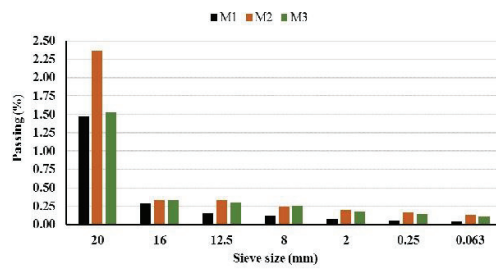


FIG. 17. Passing of the grain sizes generated during the load action

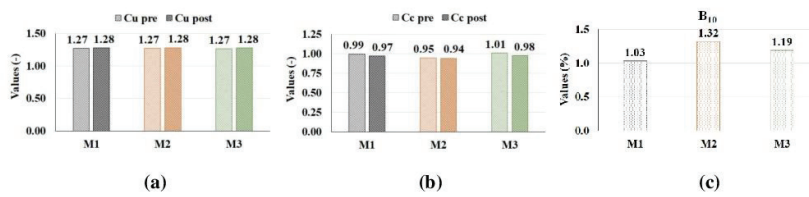


FIG. 18. Coefficient of uniformity (a), coefficient of curvature (b) and particle breakage factor (c) of the sieving curves before and after load

PAPER III

Barbieri, D. M., Mofid, S. A., Hoff, I., and Jelle, B. P. (2018). "Nanoscale technology enhancement of crushed rocks ' mechanical properties for pavement applications." 6th International Symposium on Nanotechnology in Construction.

Nanoscale Technology Enhancement of Crushed Rocks' Mechanical Properties for Pavement Applications

ABSTRACT

The Norwegian Public Roads Administration is currently running the "Ferry-free coastal route E39" project; this highway plan includes the creation of several long tunnels, which will generate a surplus of blasted rocks. They could be used in the road unbound layers close to the place of production providing a sustainable cost-benefit application. A considerable quantity of the excavated rocks does not satisfy the existing code requirements. Two different additive products can enhance the mechanical properties of these "weak" rocks. One additive is polymer-based and the other additive is lignin-based. Los Angeles tests, micro-Deval tests and repeated triaxial load tests thoroughly evaluate the mechanical properties (resilient modulus and permanent deformation) of two investigated "weak" rock types. Scanning electron microscope images display the rock surfaces before and after the treatment. Additive applications show promising positive results.

1. INTRODUCTION AND BACKGROUND

The "Ferry-free coastal route E39" project improves the viability along the Norwegian coast from Trondheim to Kristiansand (NPRA, 2017). The project entails the creation of an extended tunnelling system, which will generate a tremendous quantity of blasted rocks. These rocks could be used as viable aggregates in the road unbound layers close to the production site, which is beneficial from environmental, economical and social points of views (Gomes Correia *et al.*, 2016).

The Norwegian pavement design manual N200 (NPRA, 2014) sets certain requirements regarding unbound layers pavement materials: grain size distribution curve (CEN, 2012), Los Angeles (LA) value (CEN, 2010) and micro-Deval (MDE) value (CEN, 2011).

The major part of the blasted rocks has igneous origin ("strong" rocks) and they could be suitable for the application if they were produced in a quarry. Tunnel blasting induces significant weakening of the rock from microcracks due to the high released energy in a confined situation (Raina *et al.*, 2000): a considerable quantity of the rocks has metamorphic and sedimentary origin and they trespass the limit values connected to the mentioned standard check procedures ("weak" rocks). The goal of the research is to improve the mechanical properties of the "weak" rocks by additive application. LA tests, MDE tests and repeated triaxial load tests (RTLs) thoroughly evaluate the mechanical material properties, which are resilient modulus and permanent

deformation. Scanning electron microscope (SEM) images testify the change of the rocks surface before and after the additive products application.

2. METHODOLOGY

2.1 GEOLOGICAL MATERIAL CHARACTERIZATION

The E39 highway alignment comes across different types of bedrocks (NGU, 2017). The major part of the rocks has igneous origin: they mainly comprise granite, granodiorite and granitic to dioritic gneiss; metamorphic and low-grade metamorphic rocks occur close to Bergen and Stavanger.

Three types of crushed rocks are collected close to Bergen at Lyshorn tunnel. The rocks are selected to properly represent the variety in the geology spread along the entire highway alignment and they are designated as M1, M2, M3 (Barbieri *et al.*, 2018). Since material M1 fulfils the code requirements, this research focuses on materials M2 and M3:

- Material M2: metamorphic origin, fine-grained felsic and micaceous rocks.
- Material M3: metamorphic origin, very fine-grained felsic and micaceous rocks.

2.2 STANDARD TESTS MATERIAL CHARACTERIZATION

Crushed rocks can be used in the road base layer as paved crushed rocks and in the road subbase layer as unsorted crushed rocks if the LA value and the MDE value are low enough (NPRA, 2014). The LA limit values are respectively 30 and 35 for base layer and subbase layer, whereas the MDE limit value is 15 for both of them. Further requirements in terms of upper and lower grain size distribution curve are demanded for the base layer (Figure 1). The distribution curve of the subbase layer must be within 20/120 mm. Figure 1 displays that both materials M2 and M3 have LA values lying close to the limit, and exceed the threshold regarding MDE values: M2 and M3 are designated as "weak" in this research.

The repeated triaxial load test (RTLTL) gives a comprehensive insight into material properties by assessing the stiffness and the resistance to permanent deformation.

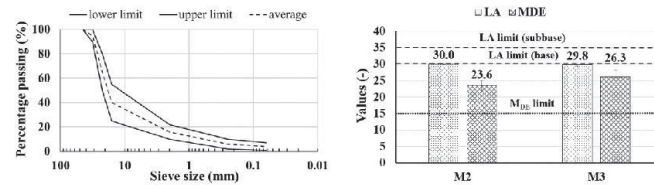


Fig. 1. (left) Grain size distribution limit curves for base layer and (right) Los Angeles and micro-Deval values of the investigated materials (Barbieri *et al.*, 2018).

The preparation of the specimen follows a defined procedure. Firstly, 7300 g of material are prepared according to the grading curve displayed in Figure 1. Consequently, the desired amount of water, and additive if needed by the test, is added. The optimum moisture content (OMC) for materials M2 and M3 is $w=5\%$ in weight. All the samples are compacted with a vibratory hammer; they have a diameter of 150 mm and the height varies between 170 and 190 mm.

RTLTL apparatus exerts a uniform confining pressure in all the directions (σ_i , triaxial or confining stress) and an additional vertical dynamic stress (σ_d , deviatoric stress), which stepwise increases at different levels of σ_i . The RTLTL apparatus performs the multi-stage low stress level (MS LSL) loading procedure: five sequences are associated with five different σ_i values ($\sigma_i = 20, 45, 70, 100, 150$ kPa). In addition, six steps associated to six given σ_d values form each sequence (CEN, 2004). Each load step consists of 10 000 load pulses at 10 Hz frequency. A hydraulic jack exerts σ_d according to a sinusoidal pattern, a minimum value of 5 kPa assures contact between the specimen end plate and the jack. The resilient modulus M_R associated with a change in the dynamic deviatoric stress σ_d^{dyn} and constant σ_i is defined as follows

$$M_R = \frac{\Delta\sigma_d^{dyn}}{\epsilon_a^{el}}, \quad (1)$$

where ϵ_a^{el} is the axial resilient (or elastic) strain. Several non-linear relationships have been proposed to describe M_R with reference to bulk stress θ ; the following k- θ relationship is adopted in this study (Hicks and Monismith, 1971)

$$M_R = k_1 \sigma_a \left(\frac{\theta}{\sigma_a} \right)^{k_2}, \quad (2)$$

where σ_a is a reference pressure (100 kPa) and k_1, k_2 are regression parameters. This study presents the accumulated permanent vertical strain as obtained from the RTLTLs as they clearly highlight the improvement in M2 and M3 performance after the additive application. Replicate specimens are used and average results are displayed: two samples for a MDE test (each MDE test requires a double sample in turn), three samples for a LA test and two samples for a RTLTL are considered for each testing condition described below.

2.3 SEM MATERIAL CHARACTERIZATION

Scanning electron microscopy (SEM, Hitachi S-5500) was employed to characterize the morphology and microstructure of the rocks without any further processing and S(T)EM mode was used to determine the modification in surface after the polymer-based and lignin-based additive application. Analysis with secondary electrons was employed at an acceleration voltage of 10 kV and emission current of 10 μ A while 30 kV was employed for bright field transmission mode in S(T)EM mode.

2.4 ADDITIVE PRODUCTS DESCRIPTION

Two additive products are tested in this research; one is polymer-based, the other one is lignin-based.

The polymer-based additive is water soluble, non-leachable, and UV and heat stable. The additive is a nanoscale technology and is made of two components C1 and C2; the modification taking place at nanoscale dimension entails major changes at a relative larger scale (Paul and Robeson, 2008). Component C1 is an acrylic co-polymer emulsion based on acetic acid and methanol. The particle size is lower than 90 nm and has almost the same number of polymer particles as soil particles. Component C2 is a polymeric dispersion based on propylene glycol and alkoxy-alkyl silyl. It chemically converts the water absorbing silanol groups presented on the rocks

surface to a 4-6 nm layer of water resistant alkyl siloxane. Components C1 and C2 impart water resistance, better lubrication for compaction and bonding action at ambient temperature. The product is mixed at OMC and added to M2 or M3 according to the proportion 10 kg C1 + 10 kg C2 for 200 l water; no special curing procedures are necessary. Materials M2 and M3 enhanced performances are assessed by RTLts. Furthermore, the beneficial coating effect promoted by the additive is evaluated by LA test and wearing MDE test. In this case, materials M2 and M3 are soaked with the additive (50% C1, 50% C2) and tested after 24 hours to let the crushed rocks dry. The lignin-based additive is a product of the pulping industry. Lignosulfonate is an organic polymer that consists of both hydrophilic and hydrophobic groups; it is a non-corrosive and non-toxic chemical (Alazigha *et al.*, 2018). The product is mixed at OMC and added to M2 or M3; the mass percentage of additive added to the crushed rocks is 1.5%. RTLts assess the materials M2 and M3 enhanced performances. Lignosulfonate needs a curing time to dry and attach properly to the material particles. To simulate a long field curing process, each RTL sample is firstly conditioned at 50°C for 24 hours and then at 22°C (room temperature) for 24 hours, whereafter the specimen is finally tested. LA and MDE tests assess the beneficial coating effect provided by the lignosulfonate. Materials M2 and M3 are soaked with the product and undergo the same curing procedure.

3. TEST RESULTS AND DISCUSSION

3.1 POLYMER-BASED ADDITIVE APPLICATION

RTLts assess the stiffness and the deformation properties of the investigated materials at OMC $w=5\%$; the behaviour of non-treated M2 and M3 serves as a comparison basis. Figure 2 shows the resilient moduli of M2 and M3 at OMC with and without additive; black and magenta colours correspond to not-treated and treated materials in the following plots.

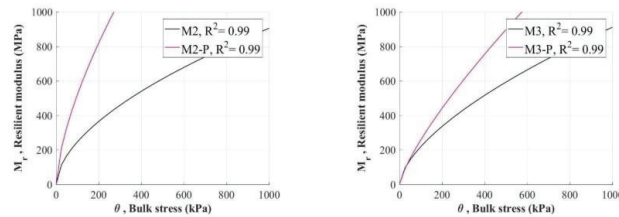


Fig. 2. Resilient modulus (M2, M3) before and (M2-P, M3-P) after polymer-based additive application for (left) M2 and (right) M3.

The materials' resilient moduli increase after the product treatment. Moreover, the results show that the additive is slightly more effective on M2 than M3 due to the rock geological composition, as the product performance is dependent on the quantity of silicate minerals located on the top of the rocks' surfaces.

Figure 3 displays the accumulated vertical permanent (plastic) strain data: the additive entails smaller deformations.

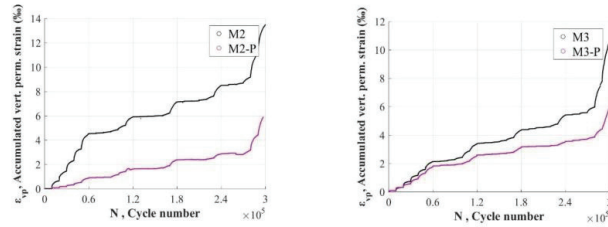


Fig. 3. Permanent vertical deformation (M2, M3) before and (M2-P, M3-P) after polymer-based additive application for (left) M2 and (right) M3.

LA and MDE tests assess the coating effect provided by the additive. Figure 4 shows that the product supplies a significant beneficial effect.

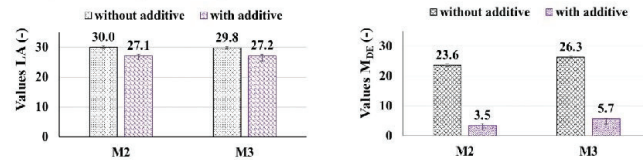


Fig. 4. Coating effect provided by the polymer-based additive assessed by standard procedures: (left) LA test and (right) MDE test.

3.2 LIGNIN-BASED ADDITIVE APPLICATION

RTLs assess the stiffness and the deformation properties of the investigated materials, which are mixed with 1.5% lignin in mass at OMC $w=5\%$; the measured water contents after the curing process are between 2% and 2.5%. The behaviour of the non-treated materials at $w=1\%$ serves as a cautious comparison basis (Erlingsson *et al.*, 2017). Figure 5 shows the resilient moduli for M2 and M3 at $w=1\%$. The materials resilient moduli increase after the product treatment.

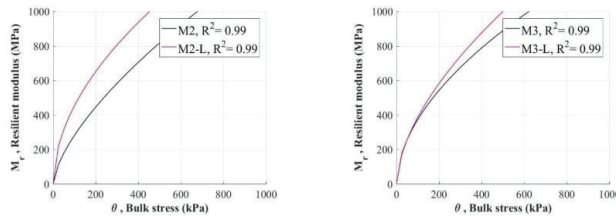


Fig. 5. Resilient modulus (M2, M3) before and (M2-L, M3-L) after lignin-based additive application for (left) M2 and (right) M3.

Figure 6 displays the accumulated vertical permanent (plastic) strain data: the additive entails smaller deformations.

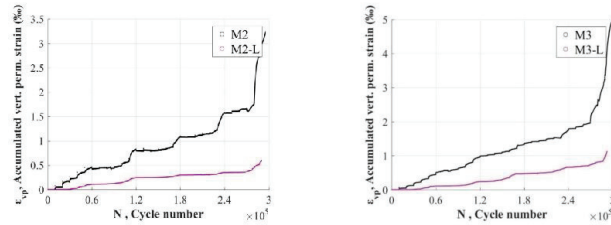


Fig. 6. Permanent vertical deformation (M2, M3) before and (M2-L, M3-L) after lignin-based additive application for (left) M2 and (right) M3.

LA and MDE tests assess the coating effect when soaked with the additive. The improvement in MDE values is not as pronounced as one would expect because lignin is highly susceptible to running water, as in the case of MDE tests.

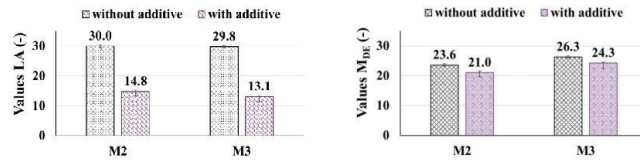


Fig. 7. Coating effect provided by the lignin-based additive assessed by standard procedures: (left) LA test and (right) MDE test.

3.3 SEM IMAGES

Figure 8 displays SEM images of M2 (left) natural surface, change in surface after the (middle) polymer-based and (right) lignin-based additive application. Figure 9 displays SEM images of M3 (left) natural surface, change in surface after the (middle) polymer-based and (right) lignin-based additive application. Both the additives modify the material surface by coating the smaller fragmented particles, which are no longer visible: the products' matrices cover the crushed rocks and promote the formation of a more homogeneous substance.

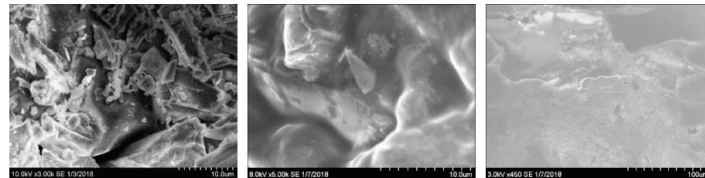


Fig. 8. Surface of material M2 (left, scale bar = 10 μm) without additive, (middle, scale bar = 10 μm) with polymer-based additive and (right, scale bar = 100 μm) with lignin-based additive.

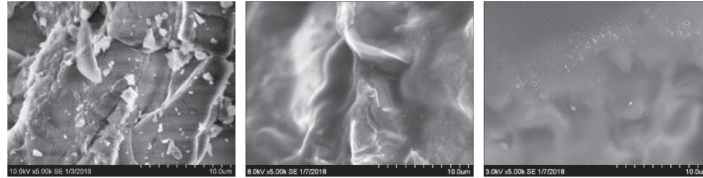


Fig. 9. Surface of material M3 (left, scale bar = 10 µm) without additive, (middle, scale bar = 10 µm) with polymer-based additive and (right, scale bar = 10 µm) with lignin-based additive.

CONCLUSIONS

The use of nanoscale technology additives to enhance the mechanical properties of crushed rocks shows promising results, as both the resilient modulus and vertical permanent deformation parameters testify in this study. The rocks, which do not fulfil the design code requirements, could be used in pavement unbound layers after additive treatment. The following considerations may be drawn:

- (1) Los Angeles (LA) tests, micro-Deval (MDE) tests and repeated triaxial load tests (RTLs) testify the beneficial effect of the additives.
- (2) Both polymer-based additive and lignin-based additive are non-traditional stabilization techniques. Furthermore, the tested additives are environmentally friendly solutions.
- (3) The investigated additives coat and bond the material particles together; the polymer-based product has an immediate effect, the lignin-based product needs a curing time.

The promising results obtained by laboratory tests and discussed in this study should be further investigated, for instance by means of a field-test campaign.

ACKNOWLEDGMENTS

This work was supported by Norwegian Public Roads Administration (grant number 25134404). Polymer-based additive kindly supplied by Zydex Industries, Vadodara, India. Lignin-based additive kindly supplied by Borregaard AS, Sarpsborg, Norway. Furthermore, the Research Council of Norway is acknowledged for the support to the "Norwegian Micro- and Nano-Fabrication Facility" (NorFab, project no. 245963/F50).

REFERENCES

- Alazigha, D. P., Indraratna, B. and Vinod, J. S. (2018) 'Mechanisms of stabilization of expansive soil with lignosulfonate admixture', *Transportation Geotechnics*. Elsevier Ltd, 14, pp. 81–92. doi: 10.1016/J.TRGEO.2017.11.001.
- Barbieri, D. M., Hoff, I. and Mørk, M. B. E. (2018) 'Mechanical assessment of crushed rocks derived from tunnelling operations', in. 5th GeoChina International Conference.

- CEN (2004) *Cyclic load triaxial test for unbound mixture*.
- CEN (2010) *Tests for mechanical and physical properties of aggregates. Part 2: methods for the determination of resistance to fragmentation*.
- CEN (2011) *Tests for mechanical and physical properties of aggregates. Part 1: determination of the resistance to wear (micro-Deval)*.
- CEN (2012) *Tests for geometrical properties of aggregates. Part 1: determination of particle size distribution. Sieving method*.
- Erlingsson, S., Rahman, S. and Salour, F. (2017) 'Characteristic of unbound granular materials and subgrades based on multi stage RLT testing', *Transportation Geotechnics*. The Authors, 13, pp. 28–42. doi: 10.1016/j.trgeo.2017.08.009.
- Gomes Correia, A., Winter, M. G. and Puppala, A. J. (2016) 'A review of sustainable approaches in transport infrastructure geotechnics', *Transportation Geotechnics*. Elsevier Ltd, 7, pp. 21–28. doi: 10.1016/j.trgeo.2016.03.003.
- Hicks, R. G. and Monismith, C. L. (1971) 'Factors influencing the resilient properties of granular materials', in *Highway Research Record*, pp. 15–31.
- NGU (2017) *Norges Geologiske Undersøkelse (Geological Survey of Norway)*. Available at: <http://www.ngu.no/>.
- NPRA (2014) *Håndbok N200 vegbygging*. Vegdirektoratet.
- NPRA (2017) *The E39 coastal highway route*. Available at: <https://www.vegvesen.no/en/roads/Roads+and+bridges/Road+projects/e39coastalhighwayroute;jsessionid=99D143CB28F87A072777C744BBCA31E8?lang=nn>.
- Paul, D. R. and Robeson, L. M. (2008) 'Polymer nanotechnology: nanocomposites', *Polymer*. Elsevier Ltd, 49(15), pp. 3187–3204. doi: 10.1016/j.polymer.2008.04.017.
- Raina, A., Chakraborty, A. and Ramulu, M. (2000) 'Rock mass damage from underground blasting, a literature review, and lab- and full scale tests to estimate crack depth by ultrasonic method', *Fragblast International Journal for Blasting and Fragmentation*, 4(2), pp. 103–125.

PAPER IV

Barbieri, D. M., Hoff, I., and Mørk, M. B. E. “Innovative stabilization techniques for weak crushed rocks used in road unbound layers: a laboratory investigation.” *Transportation Geotechnics*. Submitted.

1 **INNOVATIVE STABILIZATION TECHNIQUES FOR WEAK CRUSHED ROCKS**
2 **USED IN ROAD UNBOUND LAYERS: A LABORATORY INVESTIGATION**

3
4
5 **Diego Maria Barbieri, Corresponding Author**
6 Norwegian University of Science and Technology,
7 Department of Civil and Environmental Engineering,
8 Høgskoleringen 7A, Trondheim, 7491, Trøndelag, Norway
9 Tel: +47 930 02 908; Email: diego.barbieri@ntnu.no

10
11 **Inge Hoff**
12 Norwegian University of Science and Technology,
13 Department of Civil and Environmental Engineering,
14 Høgskoleringen 7A, Trondheim, 7491, Trøndelag, Norway
15 Email: inge.hoff@ntnu.no

16
17 **Mai Britt Engeness Mørk**
18 Norwegian University of Science and Technology,
19 Department of Geosciences and Petroleum,
20 Sem Sæalandsvei 1, Trondheim, 7491, Trøndelag, Norway
21 Email: mai.britt.mork@ntnu.no

22
23
24 Declarations of interest:
25 none

26
27 Submission date:
28 24/09/2018

29
30
31
32
33
34
35
36
37
38
39
40
41
42
43
44
45
46
47

48 **ABSTRACT**

49 The “Ferry-free coastal highway route E39” project includes building several long tunnels
50 along the southwestern Norwegian coast. The tunnelling operations will generate a large
51 quantity of blasted rocks; these could be used in the road unbound layers close to the place of
52 production to provide a sustainable cost-benefit application. The existing design guidelines
53 define strength requirements for road unbound layers in terms of Los Angeles and micro-Deval
54 tests. Even if the major part of the rocks has igneous origin and could potentially fulfil the
55 standard tests, the damage induced by the confined heavy blasting makes the materials fail the
56 check procedures. The research investigates how to enable the use of the “weak” rocks by
57 investigating three possible techniques. The first approach is the mixture between the different
58 types of rocks available in situ. The second approach is additive application; two different non-
59 traditional additive types are examined: one is polymer-based, the other one is lignin-based.
60 The third approach is the attempt to modify the rocks mineralogical structure by overheating.
61 The research test campaign uses both the aforementioned standard tests and repeated triaxial
62 load tests. Rocks mixture and additives application are viable and sustainable methods to
63 improve the mechanical properties of the “weak” crushed metamorphic rocks.

64
65 **Keywords:** Stabilization, Crushed rock, Pavement unbound, Los Angeles test, Micro-Deval
66 test, Repeated triaxial load test.

67
68
69
70
71
72
73
74
75
76
77
78
79
80
81
82
83
84
85
86
87
88
89
90
91
92
93

94 **1 INTRODUCTION AND BACKGROUND**

95

96 Norwegian Public Roads Administration (NPRA) is currently running the “Ferry-free coastal
97 highway route E39” project, which improves the viability along the southwestern Norwegian
98 coast for a total length of about 1100 km from Trondheim to Kristiansand (NPRA, 2017). The
99 project includes the building of several bridges and tunnels, while aiming for creating a
100 sustainable infrastructure. The project is crucial to regional and national development as the
101 industries located along the route generate about half of Norway’s traditional export (Dunham,
102 2016).

103 The extended tunnelling systems will generate a very large quantity of blasted rocks.
104 They could potentially be used as viable substitutes for natural aggregates in the road unbound
105 layers close to the place of production. Previous experience regarding the recycling strategies
106 of tunnel excavation materials highlighted the importance of this challenge for construction
107 management and economics (Burdin and Monin, 2009; Haritonovs et al., 2016; Lieb, 2009;
108 Resch et al., 2009).

109 Using the excavated geomaterials is beneficial from economic, environmental and
110 social points of views (Chittoori et al., 2012; Petkovic, 2005; Riviera et al., 2014); energy
111 consumption reduction and limited greenhouse gas emissions are the most beneficial
112 advantages (Aatheesan et al., 2008; Arulrajah et al., 2013; Gomes Correia et al., 2016; Núñez
113 et al., 2008). The usage of blasted materials in pavement applications is a sustainable solution
114 to minimise the waste while reducing the demand for scarce quarried materials, activity which
115 is resource intensive and consumes large amounts of energy (Fladvad et al., 2017). The
116 transport distance of the blasted and crushed rocks should be within 20 - 30 km to represent a
117 competitive solution compared to the purchase of quarry virgin aggregates (Berger, 1978; Neeb,
118 1992). Furthermore, the concern about environmentally-friendly and sustainable constructions
119 is becoming more and more relevant in Norway, as it pledges to become climate neutral by
120 2030 (Teknologirådet, 2012).

121 The existing strength requirements for road unbound layers are connected to relatively
122 simple tests: the Norwegian pavement design manual N200 (NPRA, 2014a) sets limits in terms
123 of grain shape (CEN, 2012a), flakiness index value (CEN, 2012b), Los Angeles (LA) value
124 (CEN, 2010) and micro-Deval (MDE) value (CEN, 2011). By respecting the specified
125 thresholds, the road is expected to perform adequately without encountering premature damage
126 (Barbieri et al., 2017).

127 The goal of the research is to explore techniques to improve the mechanical properties
128 of the crushed rocks not complying with the standard requirements; the aim is to enable their
129 use in the road unbound layers close to the place of production. This would entail savings on
130 the consumption of natural resources and transport reduction; thus promoting a beneficial
131 impact on sustainability.

132 The research examines mechanical and chemical treatments to make the weak materials
133 suitable for the application. Three types of crushed rocks are chosen and investigated. One type
134 meets the code requirements (“strong” rocks), while the other two do not (“weak” rocks); XRD
135 diffractometer (XRD) analyses describe the mineralogy.

136 The first studied technique is to mix the weak rocks with the strong ones available in
137 situ. The second considered approach is additive application. Currently there are several
138 stabilization methods, i.e. cement, bitumen, lime, fly ash, gypsum (Behnood, 2018; Jiang and
139 Fan, 2013; Myre, 2014; NPRA, 2014b; Siripun et al., 2010). Two non-traditional stabilization
140 techniques are examined: one is polymer-based and the other one is lignin-based. The third

141 investigated method is to overheat the rocks to check for any possible induced changes in the
 142 mineralogical composition, which may strengthen the rocks. Both the standard tests (LA and
 143 MDE) and Repeated Triaxial Load Tests (RTLTs) are used to assess the materials performance.
 144

145 **2 METHODOLOGY**

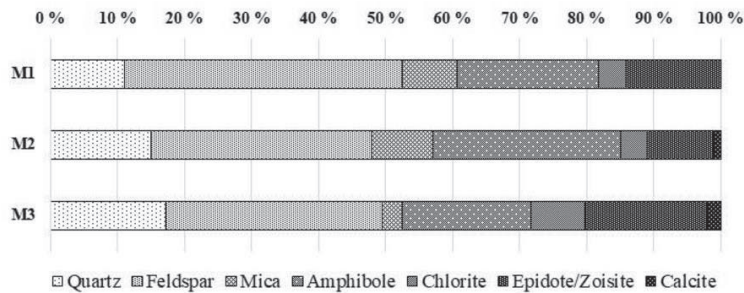
146
 147 **2.1 MATERIALS INVESTIGATED**

148
 149 **2.1.1 GEOLOGICAL CHARACTERIZATION**

150
 151 The E39 highway alignment comes across different types of bedrocks (NGU, 2017; Ramberg
 152 et al., 2013). The major part of the rocks is igneous and supracrustal of Precambrian ages (1700
 153 - 900·10⁶ years) variably influenced by metamorphism and deformation related to the
 154 Caledonian orogeny. They mainly comprise granite, granodiorite and granitic to dioritic gneiss.
 155 There are also areas with Caledonian rocks; these locations are anyway at maximum 20 - 30
 156 km far from the most widespread aforementioned geology. Metamorphic rocks occur close to
 157 Bergen (gabbro and augen gneiss). Zones of foliated Caledonian metamorphic rocks (e.g. mica-
 158 schist and phyllite) are locally present, in particular around Boknafjord area close to Stavanger.
 159 Three types of crushed rocks produced by the current tunnel excavations close to Bergen are
 160 investigated: they properly represent the variety in the geology spread along the entire highway
 161 alignment (Barbieri et al., 2019). The three materials are denominated M1, M2 and M3, all
 162 being mixtures of different local rocks:
 163

- 164 - Material M1. Mafic igneous origin, partly modified by metamorphism (amphibolite), minor
- 165 amounts of felsic gneisses and mica-schist.
- 166 - Material M2. Metamorphic origin, fine-grained felsic and micaceous rocks.
- 167 - Material M3. Metamorphic origin, very fine-grained felsic and micaceous rocks.

168
 169 Batches of each material type are prepared for XRD diffractometer analyses to identify the
 170 main mineralogical compositions according to Rietveld mineral quantification. Samples are
 171 crushed, split, milled to 10µm and analysed as powder prepare in the XRD diffractometer.
 172 Figure 1 displays semi-quantitative weight proportions of the most abundant minerals.
 173



174
 175

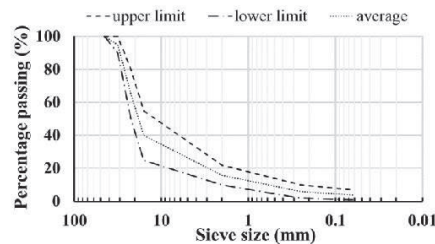
Fig. 1. Bulk mineralogy of the investigated crushed rocks.

176 Quartz, feldspar and amphibole are the predominant minerals in all M1, M2 and M3 mixtures
 177 (and main constituents of amphibolites and gneisses). M3 is richer in chlorite, epidote-zoisite
 178 and calcite compared to M1 and M2. Moreover, M3 has a higher content of foliated felsic rocks:
 179 networks of fine epidote-zoisite particles partly replace feldspars. Igneous rocks M1 are
 180 modified by metamorphism, e.g. amphibolization and replacement of coarse igneous feldspar
 181 by aggregates of fine epidote and feldspar. Finer-grained felsic and micaceous rocks appear
 182 more dominant in M2 and especially in M3.
 183

184 **2.1.2 STANDARD TESTS CHARACTERIZATION**

185
 186 The pavement design manual N200 (NPRA, 2014a) sets requirements for the use of crushed
 187 rocks. It is possible to use this resource in the road base layer as paved crushed rocks and in
 188 the road subbase layer as unsorted crushed rocks if Los-Angeles standard test (LA value) and
 189 micro-Deval standard test (MDE value) are fulfilled. The LA limit values are respectively 30
 190 and 35 for base layer and subbase layer, the MDE limit value is 15 for both of them.

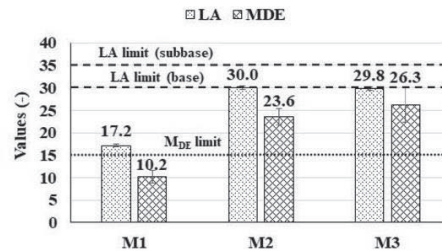
191 Further requirements in terms of upper and lower grain size distribution curve are
 192 demanded for the base layer (Figure 2). The distribution curve of the subbase layer must be
 193 within 20/120 mm.



194 Fig. 2. Grain size distribution limit curves for base layer.

195
 196

197 Figure 3 displays the materials values related to LA and MDE standard check procedures.
 198 Material M1 fulfils the code requirements. Both materials M2 and M3 have LA values lying
 199 close to the limit, and exceed the threshold regarding MDE values. Material M1 is designated
 200 as “strong” and materials M2 and M3 are designated as “weak” in the research.



201
 202

Fig. 3. Los Angeles and micro-Deval values of investigated materials (Barbieri et al., 2019).

203 **2.1.3 REPEATED TRIAXIAL LOAD TEST**

204

205 The Repeated Triaxial Load Test (RTLTL) gives a comprehensive insight into material
206 properties by assessing the stiffness and the resistance to permanent deformation. RTLTL is one
207 of the best methods available for laboratory simulation of traffic loading on unbound granular
208 materials (UGMs); it reproduces the stress conditions in flexible pavements more adequately
209 than other available methods like the CBR test (Barksdale, 1971). UGMs behaviour is
210 connected to the following parameters: stress level, moisture content, dry density, grading and
211 mineralogy, etc. (Lekarp et al., 2000a, 2000b; Uthus et al., 2007).

212 The preparation of the specimen follows a defined procedure. Firstly, 7300 g of material
213 are prepared according to the grading curve displayed in Figure 2. Consequently, the desired
214 amount of water, and additive if needed by the test, is added. The mixture is divided into four
215 parts and rests in as many impermeable bags for 24 h. The operator then compacts the four
216 layers inside a steel mould; the bulk density and dry density are assessed (CEN, 2003).

217 The optimum moisture content (OMC) evaluated for all the materials M1, M2 and M3
218 is $w=5\%$. A Kango 950X vibratory hammer (total weight 35 kg, frequency 25 - 60 Hz,
219 amplitude 5 mm) is used to compact the layers inside the mould, the compaction time is 30 s
220 per layer. All the samples have a diameter of 150 mm and the final height varies between 170
221 and 190 mm. The sample height differs from the indication given by the code, where the height
222 is recommended to be twice the diameter of the sample (CEN, 2004). Research regarding the
223 influence of the height to diameter ratio with respect both to resilient modulus and permanent
224 deformations demonstrates that samples with a ratio ranging from 1:1 to 1.5:1 show little
225 differences (Dongmo-Engeland, 2005).

226 RTLTL apparatus exerts a uniform confining pressure in all the directions (σ_r , triaxial or
227 confining stress) and an additional vertical dynamic stress (σ_d , deviatoric stress), which
228 stepwise increases at different levels of σ_r . The RTLTL apparatus performs the multi-stage low
229 stress level (MS LSL) loading procedure: five sequences are associated with five different σ_r
230 values ($\sigma_r = 20, 45, 70, 100, 150$ kPa). In addition, six steps associated to six given σ_d values
231 form each sequence (CEN, 2004). Figure 4 displays the five loading sequences and the
232 respective loading steps according to bulk stress θ ($\theta = \sigma_1 + \sigma_2 + \sigma_3 = \sigma_d + 3\sigma_r$; $\sigma_1, \sigma_2, \sigma_3$ are
233 principal stresses) and σ_d . Each load step consists of 10,000 load pulses at 10 Hz frequency. A
234 loading sequence is interrupted if the axial permanent deformation reaches 0.5%. Pressurised
235 water is the confining medium; a hydraulic jack exerts σ_d according to a sinusoidal pattern, a
236 minimum value of 5 kPa assures contact between the specimen end plate and the jack.

237

238

239

240

241

242

243

244

245

246

247

248

249

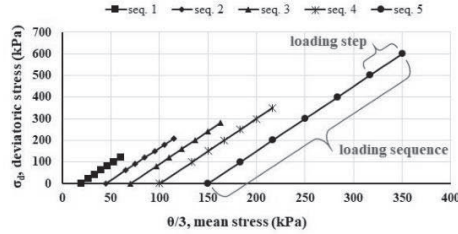


Fig. 4. Loading sequences for the MS LSL procedure.

250
251
252
253
254
255
256

The resilient modulus M_R associated with a change in the dynamic deviatoric stress σ_d^{dyn} and constant σ_i is defined as follows

$$M_R = \frac{\Delta \sigma_d^{dyn}}{\varepsilon_a^{pl}}, \quad (1)$$

257
258
259 where ε_a^{pl} is the axial resilient strain. Several non-linear relationships have been proposed to
260 describe M_R with reference to bulk stress θ (Lekarp et al., 2000a). The following k- θ
261 relationship is adopted (Hicks and Monismith, 1971)
262

$$M_R = k_1 \sigma_a \left(\frac{\theta}{\sigma_a} \right)^{k_2}, \quad (2)$$

263
264 where σ_a is a reference pressure (100 kPa) and k_1, k_2 are regression parameters. The relationship
265 enables a clear comparison in two-dimensional plots between the materials performances.

266 The permanent deformation is investigated through the Coulomb approach (Hoff et al.,
267 2003). The Coulomb criterion relates the mobilized shear strength to the development of
268 permanent deformations and the maximum shear strength to failure. The mobilized angle of
269 friction ρ and the failure angle φ respectively express the degree of mobilized shear strength
270 and the maximum shear strength. The angle of friction and the angle of failure identify three
271 different ranges of material behaviour: elastic, elasto-plastic and failure. The strain rate $\dot{\varepsilon}$ is a
272 measure of the speed of the permanent deformation; this parameter refers to the development
273 of permanent deformation per cycle. Table 1 defines the two boundary lines between the three
274 aforementioned ranges: each load step is categorised considering the average strain rate for the
275 cycles from 5000 to 10,000 (Hoff et al. 2003).
276
277

Permanent strain rate	Range
$\dot{\varepsilon} < 2.5 \cdot 10^{-8}$	elastic zone
$2.5 \cdot 10^{-8} < \dot{\varepsilon} < 1.0 \cdot 10^{-7}$	elasto-plastic zone
$\dot{\varepsilon} > 1.0 \cdot 10^{-7}$	plastic (failure) zone

278
279 Table 1. Permanent strain rate values defining the material range boundary lines.
280

281 The equations defining the elastic limit line and failure line are respectively

282
$$\sigma_d = \frac{2 \sin \rho (\sigma_3 + a)}{1 - \sin \rho}, \quad (3)$$

283
284
$$\sigma_d = \frac{2 \sin \varphi (\sigma_3 + a)}{1 - \sin \varphi}; \quad (4)$$

285
286 a regression analysis is used to assess the boundary lines. As a simplification, the apparent
287 attraction a is assumed to be 20 kPa for all the samples (Uthus et al., 2007).

288 289 **2.2 TECHNIQUES TO IMPROVE THE MECHANICAL PROPERTIES**

290
291 The research investigates different approaches to improve the mechanical properties of the
292 “weak” metamorphic rocks, namely materials M2 and M3. Both standard tests and RLTs
293 evaluate the performance related to the assessed techniques. Replicate specimens are used and
294 average results are estimated: two samples for a MDE test (each MDE test requires a double
295 sample in turn), three samples for a LA test and two samples for a RLT are considered for
296 each testing condition described below.

297 298 **2.2.1 MIXTURE OF THE ROCKS AVAILABLE IN SITU**

299
300 The major part of the rocks spread along the highway alignment have mafic igneous origin and
301 are suitable for road construction; therefore, a convenient solution could be to mix
302 appropriately the different rock types that are available in situ. Material M1 is mixed with
303 materials M2 or M3 according to three proportions in mass (25%, 50%, 75%). LA and MDE
304 tests respectively express resistance against fragmentation and wearing (Erichsen et al., 2011);
305 these standard procedures validate the appropriateness of the mixing approach.

306 307 **2.2.2 POLYMER-BASED ADDITIVE APPLICATION**

308
309 The tested polymer-based additive is water-soluble, non-leachable and UV, heat stable. The
310 additive is a nanoscale technology and is made of two components C1 and C2; the modification
311 taking place at nanoscale dimension entails major changes at a relative larger scale (Huang and
312 Wang, 2016; Paul and Robeson, 2008; Roco, 2003; Sobolev and Shah, 2015).

313 Component C1 is an acrylic co-polymer emulsion based on acetic acid and methanol.
314 The particle size is lower than 90 nm and has almost the same number of polymer particles as
315 soil particles. Component C2 is a polymeric dispersion based on propylene glycol and alkoxy-
316 alkyl silyl. After hydrolysis, the formed silanol (Si-OH) group can condense with another
317 silanol group belonging to the silicate-containing surface of the rocks and form a siloxane
318 linkage (= Si-O-Si=), namely a strong chemical covalent polar bond. Therefore, component C2
319 converts the water absorbing silanol groups presented on the rocks surface to a 4-6 nm layer of
320 hydrophobic alkyl siloxane. Components C1 and C2 impart water resistance, better lubrication
321 for compaction and bonding action bonds at ambient temperature. The existing positive
322 experience refers to silty and clayey soils (Daniels and Hourani, 2009; Ugwu et al., 2013),
323 therefore the research experiments with a new application context. The additive loses its effect
324 in conditions that are seldom achieved in road construction: prolonged exposure to base
325 (Wasserman et al., 1989) or air temperature above 200°C (Kim et al., 2003).

326

327 The product is mixed at OMC and added to M2 or M3. Two different additive
328 proportions are tested: 1 kg C1 + 1 kg C2 for 200 l water (proportion P1) and 10 kg C1 + 10
329 kg C2 for 200 l water (proportion P2), no special curing procedures are necessary. Proportion
330 P2 has been studied after the initial proportion P1 suggested by the product supplier, since the
331 results regarding P1-treated materials have not been too different from the untreated materials
332 (especially for M3). The materials M2 and M3 enhanced performances are assessed by RTLTS.
333 Furthermore, the beneficial coating effect promoted by the additive is evaluated by the standard
334 procedures in terms of resistance against fragmentation (LA test) and wearing (MDE test). In
335 this case, materials M2 and M3 are soaked with the additive (50% C1, 50% C2) and tested after
336 24 hours to let the crushed rocks dry.
337

338 **2.2.3 LIGNIN-BASED ADDITIVE APPLICATION**

339
340 The lignin-based additive (also referred to as lignosulfonate) is a renewable product of pulp
341 and paper industry. It comes from lignin, which is generated by extracting fiber and wood pulp
342 from plant biomass; lignin global annual production is approximately equal to 50 million tons
343 (Angenent et al., 2004). Lignosulfonate is an organic polymer that consists of both hydrophilic
344 and hydrophobic groups; it is a non-corrosive and non-toxic chemical (Alazigha et al., 2018).
345 Previous experiments investigating the strength and density modification of unpaved road
346 using lignosulfonate showed promising outcomes for silty and clayey soils (Alazigha et al.,
347 2018; Chen et al., 2014; Santoni et al., 2002; Ta'neqonbadi and Noorzad, 2018; Zhang et al.,
348 2018). As in the case for the polymer-based additive, the product application to crushed rocks
349 could bring to a wider acceptance of this admixture.

350 The product is mixed at OMC and added to M2 or M3; the mass percentage of
351 lignosulfonate added to the crushed rocks is 1.5%. RTLTS assess the materials M2 and M3
352 enhanced performances. Lignosulfonate needs a curing time to dry in order to become effective
353 and attach properly to the material particles (Santoni et al., 2002). To simulate a long field
354 curing process, each RTLTS sample is firstly conditioned at 50°C for 24 hours and then at 22°C
355 (room temperature) for 24 hours before testing. LA and MDE tests assess the beneficial coating
356 effect provided by the lignin-based additive. Materials M2 and M3 are soaked with the product
357 and undergo the same curing procedure.
358

359 **2.2.4 OVERHEATING**

360
361 The temperature sensitivity of rocks is subject to the geological formation process and
362 mineralogical composition; they can achieve increased mechanical strength by heating (Zhang
363 et al., 2009). Research done on diabase shows an enhanced compressive strength after heating
364 at 190°C and 345°C compared to the investigation results referring to 27°C and 110°C
365 (Simpson and Fergus, 1968). Another study is related to drying six different rocks (marble,
366 limestone, granite, slate and two sandstones) with a temperature higher than 100 °C: an
367 irreversible average 6% increase in the compressive strength properties is attained (Obert et al.,
368 1946). These experiences prove that exposing the materials to high temperatures may change
369 the original mechanical strength. Materials M2 and M3 are conditioned at 175°C and 250°C
370 for 24 hours and 48 hours. After cooling down, micro-Deval standard tests are accomplished.
371
372

373 **3 TEST RESULTS AND DISCUSSION**

374

375 **3.1 MIXTURE OF THE ROCKS AVAILABLE IN SITU**

376

377 Three proportions in mass (25%, 50%, 75%) of “weak” material M2 or M3 are tested in
 378 combination with “strong” material M1. Figure 5a and Figure 5b display the results for M2 and
 379 M3 respectively.

380

381

382

383

384

385

386

387

388

389

390

391

392

393

394

395

396

397

398

399

400

401

402

403

404

405

406

407

408

409

410

411

412

413

414

415

416

417

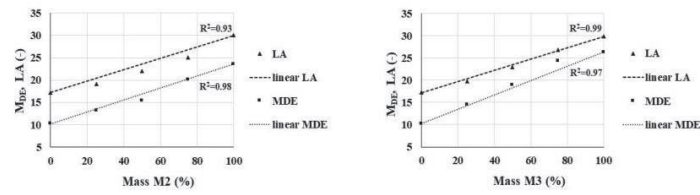


Fig. 5. LA and MDE results and linear trend distributions for mixtures made of M2 and M1 (a), M3 and M1 (b).

The results distribution highlights a linear trend regarding both LA and MDE tests. The following equations describe the observed data in a mixture made of two materials i and j

$$LA_{i+j} = LA_i \frac{m_i}{m_i+m_j} + LA_j \frac{m_j}{m_i+m_j}, \quad (5)$$

$$MDE_{i+j} = MDE_i \frac{m_i}{m_i+m_j} + MDE_j \frac{m_j}{m_i+m_j}; \quad (6)$$

where m_i, m_j are the masses and LA_i, LA_j, MDE_i, MDE_j are the standard test values assessed for materials i, j. A proper mixture of different crushed rocks types is an effective method to meet the code requirements and, possibly, to maximize the use of the “weak” material.

This requires an extra processing step and space to store the two (or more) qualities of rock; on the other hand, the clear linear results for different combinations should bolster a stable production: the economic feasibility has to be evaluated depending on the local specific conditions. The mixed materials are not tested in the RTL device, but it is reasonable to believe that the mechanical properties show similar linear trends.

3.2 POLYMER-BASED ADDITIVE APPLICATION

RTLs assess the stiffness and the deformation properties of the investigated materials at OMC $w=5\%$; the behaviour of untreated M1, M2 and M3 serves as a comparison basis. Figure 6a displays the bulk density and dry density at OMC, Figure 6b illustrates the bulk density after the addition of the polymer-based product according to proportions P1, P2.

418
 419
 420
 421
 422
 423
 424
 425
 426
 427
 428
 429
 430
 431
 432
 433
 434
 435
 436
 437
 438
 439
 440
 441
 442
 443
 444
 445
 446
 447
 448
 449
 450
 451
 452
 453
 454
 455
 456
 457
 458
 459
 460
 461
 462
 463

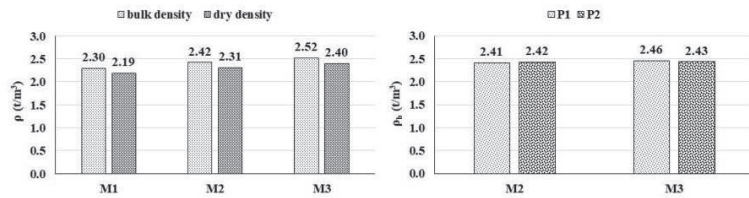


Fig. 6. M1, M2 and M3 bulk density and dry density at OMC w=5% (a), M2 and M3 bulk density after additive application with P1, P2 proportions (b).

Resilient modulus $k-\theta$ relationships are evaluated (equation 2) through data regression, Figure 7 displays the results. Figure 7a shows the performance of M1, M2 and M3 at OMC without additive; material M1 is stiffer than materials M2 and M3. Figure 7b illustrates the enhanced behaviour of M2 and M3; they get stiffer and stiffer when changing from proportion P1 to proportion P2; the “weak” rocks performance becomes comparable with the “strong” rocks behaviour. The results show the product is more effective on M2 than M3 probably because of the geological composition. The additive performance is dependent on the quantity of silicate minerals on the rocks surface. M2 and M3 have similar content of quartz and feldspar, but M2 is richer in amphibole and with a more distinct content of mica. M3 has a higher content of epidote-zoisite, which has lower Si-contents, as well as calcite (CaCO_3) which does not contain silicon.

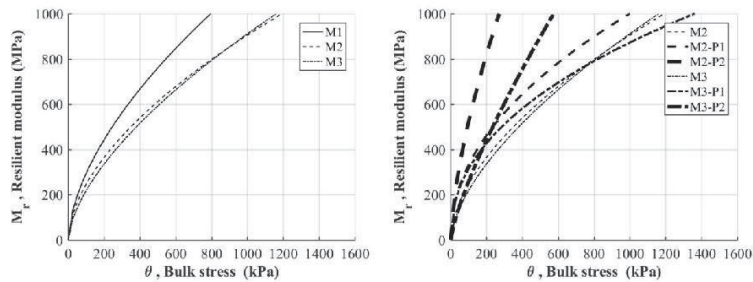


Fig. 7. M1, M2 and M3 resilient modulus at OMC w=5% (a), M2 and M3 resilient modulus after additive application with P1, P2 proportions (b).

The additive effects also pertain to the deformation properties of the materials. Figure 8 depicts the mobilized angle of friction ρ and the failure angle ϕ for the crushed rocks without and with the polymer-based stabilization; the additive application enhances both the angles.

464
465
466
467
468
469
470
471
472
473
474
475
476
477
478
479

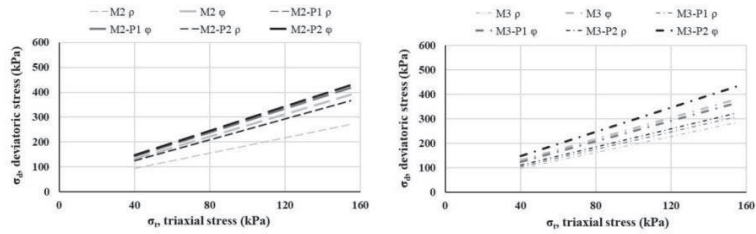


Fig. 8. Mobilized angle of friction ρ and failure angle ϕ of M2 (a) and M3 (b) for untreated and additive-treated conditions.

Table 2 reports the k - θ model regression parameters and the values of the boundary angles.

Material	Model parameters		R^2	Range boundary angles	
	k_1	k_2		ρ	ϕ
M1	2994	0.59	0.99	58.4	64.9
M2	2467	0.56	0.99	57.2	65.8
M2-P1	3314	0.48	0.99	64.4	67.3
M2-P2	5206	0.65	0.99	64.6	67.8
M3	2184	0.62	0.99	58.5	65.3
M3-P1	3142	0.44	0.99	60.4	64.4
M3-P2	2576	0.78	0.99	61.6	68.0

480
481
482
483
484
485
486
487
488
489
490
491
492
493
494
495
496
497
498
499
500

Table 2. Regression parameters of M_R model and ρ , ϕ angles for M1, M2 and M3.

LA and MDE standard tests are used to assess the coating effect provided by the polymer-based product. Figure 9 shows that the additive supplies a significant beneficial effect when it comes to MDE wearing, it also provides a lesser benefit regarding the LA fragmentation. The steel balls used in the LA test imply higher impact loads compared to MDE test; therefore, the thin coating protection is more effective in the latter case.

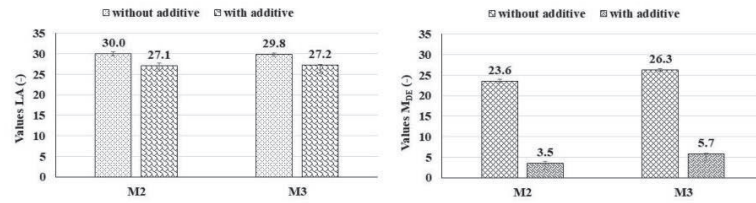
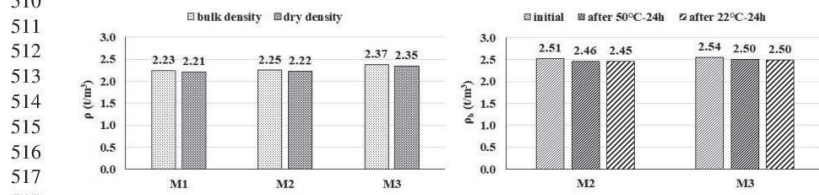


Figure 9. Coating effect provided by the polymer-based additive assessed by standard procedures: LA test (a) and MDE test (b).

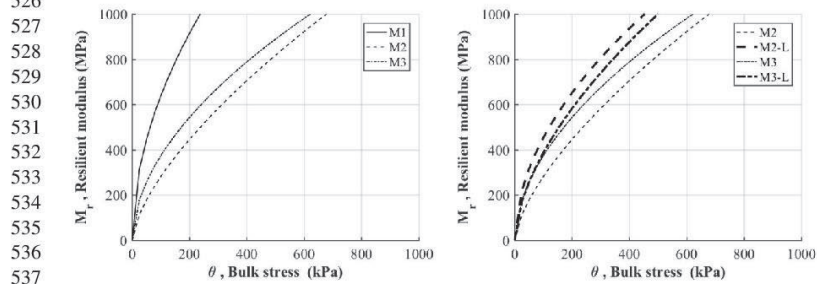
501 **3.3 LIGNIN-BASED ADDITIVE APPLICATION**

502
 503 RTLTs assess the stiffness and the deformation properties of the investigated materials, which
 504 are mixed with 1.5% lignosulfonate in mass at OMC $w=5\%$; the measured water contents after
 505 the curing process are between 2% and 2.5%. The behaviour of the untreated materials at $w=1\%$
 506 serves as a comparison basis, this is a cautious comparison since M_R gradually reduces as w
 507 increases (Erlingsson et al., 2017). Figure 10a displays the bulk density and dry density at
 508 $w=1\%$, Figure 10b illustrates the bulk density relative to the main stages of the curing process
 509 after additive application.



511
 512
 513
 514
 515
 516
 517
 518
 519 Fig. 10. M1, M2 and M3 bulk density and dry density at $w=1\%$ (a),
 520 M2 and M3 bulk density after additive application (b).

521
 522 Resilient modulus k - θ relationships are evaluated (equation 2) through data regression, Figure
 523 11 displays the results. Figure 11a shows the performance for M1, M2 and M3 at $w=1\%$;
 524 material M1 is stiffer than M2 and M3. Figure 11b illustrates the enhanced stiffer resilient
 525 curves of materials M2 and M3.



526
 527
 528
 529
 530
 531
 532
 533
 534
 535
 536
 537
 538
 539 Fig. 11. M1, M2 and M3 resilient modulus at $w=1\%$ (a),
 540 M2 and M3 resilient modulus after additive application (b).

541
 542 The additive effects also pertain to the deformation properties of the materials. Figure 12
 543 depicts the mobilized angle of friction ρ and the failure angle ϕ for the crushed rocks without
 544 and with the lignin-based stabilization; the additive application enhances both the angles.

545
 546
 547

548
549
550
551
552
553
554
555
556
557
558
559
560
561
562

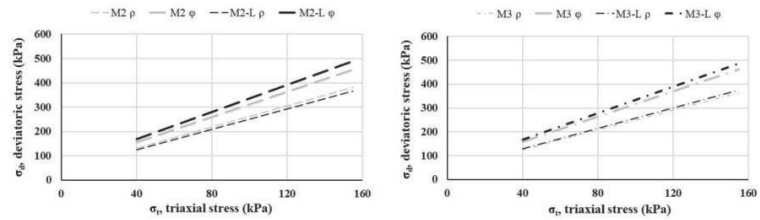


Fig. 12. Mobilized angle of friction ρ and failure angle φ of M2 (a) and M3 (b) for untreated and additive-treated conditions.

Table 3 reports the k - θ model regression parameters and the values of the boundary angles.

Material	Model parameters		R^2	Range boundary angles	
	k_1	k_2		ρ	φ
M1	6378	0.52	0.99	62.1	67.3
M2	2816	0.66	0.99	65.4	68.9
M2-L	4530	0.52	0.99	64.4	70.3
M3	3737	0.54	0.99	64.3	69.2
M3-L	3869	0.59	0.99	65.0	70.2

563
564
565
566
567
568
569
570
571
572

Table 3. Regression parameters of M_R model and ρ , φ angles for M1, M2 and M3.

LA and MDE standard tests are used to assess the coating effect when soaked with the lignin-based additive. Figure 13 shows that the product provides a beneficial effect in terms of LA fragmentation; there is also a small enhancement in terms of MDE wearing. The improvement in MDE values is not as pronounced as one would expect because lignosulfonate is highly moisture susceptible (Santoni et al., 2002); this property is especially relevant when referring to running water, as in the case of MDE test.

573
574
575
576
577
578
579
580
581
582
583
584
585
586
587

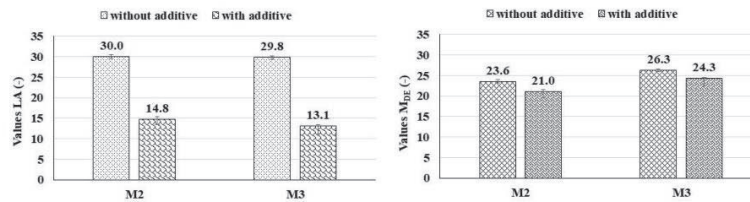


Figure 13. Coating effect provided by the lignin-based additive assessed by standard procedures: LA test (a) and MDE test (b).

588 **3.4 OVERHEATING**

589

590 Materials M2 and M3 are tested with the MDE procedure to assess if the overheating can induce
591 modifications in the mineralogical structure, which may strengthen the rocks and improve the
592 MDE results. The values of the three tested conditioning temperatures (105°C, 175°C, 250°C)
593 do not seem to exert a major influence. On the other hand, the duration of the overheating
594 seems to be a more relevant factor, as the results connected to the 48-hour conditioning are
595 better than those connected to the 24-hour conditioning (Figure 14). Even so, the induced
596 improvement is sensibly limited as the highest observed decrease among the original MDE
597 values is equal to approximately two units. The tested conditioning temperatures do not
598 significantly improve the weak materials to make them meet the code requirements. Anyway,
599 overheating the crushed rocks would demand an intensive energy use even if a small beneficial
600 effect was found.

601

602

603

604

605

606

607

608

609

610

611

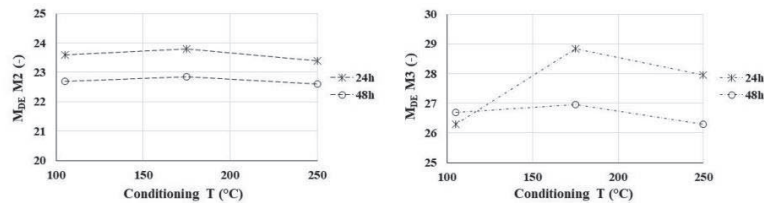


Fig. 14. MDE values after overheating M2 (b) and M3 (b).

612

4 CONCLUSIONS

613

614 The research investigated different approaches to improve the mechanical properties of crushed
615 rocks to serve as construction materials in the road unbound layers. Three types of crushed
616 rocks M1, M2 and M3 were tested; M1 satisfies the code requirements, while M2 and M3 do
617 not meet them. The following conclusions can be drawn, they could be generalized by further
618 testing of more materials:

619

620 (1) Both RLTs and LA, MDE tests identify that material M1 has a better performance than
621 materials M2 and M3. RLTs can also assess the beneficial effect of the additive; on the other
622 hand, there are no standard LA and MDE test procedures concerning an additive application.

623

624 (2) An appropriate mixture of the crushed rocks available in situ is a convenient solution to
625 fulfil LA and MDE requirements. The LA and MDE values of the mixture can be evaluated by
626 a linear relationship based on the mass quantity of each employed material.

627

628 (3) Both polymer-based additive and lignin-based additive are non-traditional stabilization
629 approaches to improve the mechanical properties of crushed rocks and enable their use in the
630 pavement unbound layers.

631

632 (4) The investigated additives coat and bond the material particles closely together; the
633 polymer-based product has a rapid effect, the lignin-based product needs a curing time. The
634 effect of the polymer-based additive is dependent on the silicate content presented on the rocks

635 surface. The lignin-based additive application may need to consider the environmental
636 conditions, as it is water susceptible.

637

638 (5) The attained overheating procedure does not produce a substantial improvement in the
639 materials performance.

640

641 **ACKNOWLEDGMENTS**

642

643 This work has been supported by Norwegian Public Roads Administration (grant number
644 25134404). Polymer-based additive kindly supplied by Sparks AS, Asker, Norway and Zydex
645 Industries, Vadodara, India. Lignin-based additive kindly supplied by Borregaard AS,
646 Sarpsborg, Norway.

647

648

649

650

651

652

653

654

655

656

657

658

659

660

661

662

663

664

665

666

667

668

669

670

671

672

673

674

675

676

677

678

679

680

681

682 **REFERENCES**

- 683
- 684 1. Aatheesan T, Arulrajah A, Wilson J, Bo MW. Beneficial use of brick rubble as
685 pavement sub-base material. *Adv. Transp. Geotech.*, London: Taylor & Francis; 2008,
686 p. 695–9.
- 687 2. Alazigha DP, Indraratna B, Vinod JS. Mechanisms of stabilization of expansive soil
688 with lignosulfonate admixture. *Transp Geotech* 2018;14:81–92.
689 doi:10.1016/J.TRGEO.2017.11.001.
- 690 3. Angenent LT, Karim K, Al-Dahhan MH, Wrenn BA, Domínguez-Espinosa R.
691 Production of bioenergy and biochemicals from industrial and agricultural
692 wastewater. *Trends Biotechnol* 2004;22:477–85. doi:10.1016/j.tibtech.2004.07.001.
- 693 4. Arulrajah A, Piratheepan J, Disfani MM, Bo MW. Geotechnical and
694 geoenvironmental properties of recycled construction and demolition materials in
695 pavement subbase applications. *J Mater Civ Eng* 2013;25:1077–88.
696 doi:10.1061/(ASCE)MT.1943-5533.0000652.
- 697 5. Barbieri DM, Hoff I, Mork H. Laboratory investigation on unbound materials used in
698 a highway with premature damage. 10th Int. Conf. Bear. Capacit. Roads, Railw.
699 Airfields, 2017.
- 700 6. Barbieri DM, Hoff I, Mørk MBE. Mechanical assessment of crushed rocks derived
701 from tunnelling operations. In: Cheng W-C, Yang J, Wang J, editors., Springer; 2019,
702 p. 225–41. doi:https://doi.org/10.1007/978-3-319-95783-8_19.
- 703 7. Barksdale RD. Compressive stress pulse times in flexible pavements for use in
704 dynamic testing. *Highw. Res. Rec.*, 1971, p. 32–44.
- 705 8. Behnood A. Soil and clay stabilization with calcium- and non-calcium-based
706 additives: a state-of-the-art review of challenges, approaches and techniques. *Transp*
707 *Geotech* 2018;17:14–32. doi:10.1016/j.trgeo.2018.08.002.
- 708 9. Berger A. Massedeponering. Beregning av kostnadsminimale tranportmønstre for
709 planering av fjell- og jordmasser ved bygging av veier. Norwegian University of
710 Science and Technology, 1978.
- 711 10. Burdin J, Monin N. The management of excavated materials from the Lyon-Turin rail
712 link project. *Geomech Und Tunnelbau* 2009;2:652–62. doi:10.1002/geot.200900048.
- 713 11. CEN. Tests for geometrical properties of aggregates. Part 1: determination of particle
714 size distribution. Sieving method. 2012a.
- 715 12. CEN. Tests for mechanical and physical properties of aggregates. Part 3:
716 determination of particle shape - flakiness index. 2012b.
- 717 13. CEN. Tests for mechanical and physical properties of aggregates. Part 1:
718 determination of the resistance to wear (micro-Deval). 2011.
- 719 14. CEN. Tests for mechanical and physical properties of aggregates. Part 2: methods for
720 the determination of resistance to fragmentation. 2010.
- 721 15. CEN. Cyclic load triaxial test for unbound mixture. 2004.
- 722 16. CEN. Unbound and hydraulically bound mixtures. Part 4: test methods for laboratory
723 reference density and water content. Vibrating hammer. 2003.
- 724 17. Chen Q, Indraratna B, Carter J, Rujikiatkamjorn C. A theoretical and experimental
725 study on the behaviour of lignosulfonate-treated sandy silt. *Comput Geotech*
726 2014;61:316–27. doi:10.1016/j.compgeo.2014.06.010.
- 727 18. Chittoori B, Puppala AJ, Reddy R, Marshall D. Sustainable reutilization of excavated
728 trench material. *GeoCongress 2012* 2012:4280–9. doi:10.1061/9780784412121.440.
- 729 19. Daniels J, Hourani MS. Soil improvement with organo-silane. U.S.-China Work. Gr.
730 *Improv. Technol.* 2009, Orlando: 2009. doi:doi.org/10.1061/41025(338)23.
- 731 20. Dongmo-Engeland B. GARAP, Influence of sample's height on the development of

- 732 permanent deformation. Trondheim: 2005.
- 733 21. Dunham KK. Coastal Highway Route E39 - Extreme crossings. *Transp Res Procedia*
- 734 2016;14:494–8. doi:10.1016/j.trpro.2016.05.102.
- 735 22. Erichsen E, Ulvik A, Sævik K. Mechanical degradation of aggregate by the Los
- 736 Angeles-, the micro-Deval- and the nordic test methods. *Rock Mech Rock Eng*
- 737 2011;44:333–7. doi:10.1007/s00603-011-0140-y.
- 738 23. Erlingsson S, Rahman MS, Salour F. Characteristic of unbound granular materials and
- 739 subgrades based on multi stage RLT testing. *Transp Geotech* 2017;13:28–42.
- 740 doi:10.1016/j.trgeo.2017.08.009.
- 741 24. Fladvad M, Aurstad J, Wigum BJ. Comparison of practice for aggregate use in road
- 742 construction - results from an international survey. 10th Int. Conf. Bear. Capacit.
- 743 Roads, Railw. Airfields, 2017.
- 744 25. Gomes Correia A, Winter MG, Puppala AJ. A review of sustainable approaches in
- 745 transport infrastructure geotechnics. *Transp Geotech* 2016;7:21–8.
- 746 doi:10.1016/j.trgeo.2016.03.003.
- 747 26. Haritonovs V, Tihonovs J, Smirnovs J. High modulus asphalt concrete with dolomite
- 748 aggregates. *Transp Res Procedia* 2016;14:3485–92. doi:10.1016/j.trpro.2016.05.314.
- 749 27. Hicks RG, Monismith CL. Factors influencing the resilient properties of granular
- 750 materials. *Highw. Res. Rec.*, 1971, p. 15–31.
- 751 28. Hoff I, Bakløkk LJ, Aurstad J. Influence of laboratory compaction method on
- 752 unbound granular materials. 6th Int. Symp. Pavements Unbound, 2003.
- 753 29. Huang Y, Wang L. Experimental studies on nanomaterials for soil improvement: a
- 754 review. *Environ Earth Sci* 2016;75:497. doi:10.1007/s12665-015-5118-8.
- 755 30. Jiang YJ, Fan LF. An investigation of mechanical behavior of cement-stabilized
- 756 crushed rock material using different compaction methods. *Constr Build Mater*
- 757 2013;48:208–515. doi:10.1016/j.conbuildmat.2013.07.017.
- 758 31. Kim HK, Lee JP, Park CR, Kwak HT, Sung MM. Thermal decomposition of
- 759 alkylsiloxane self-assembled monolayers in air. *J Phys Chem B* 2003;107:4348–51.
- 760 doi:10.1021/jp022377s.
- 761 32. Lekarp F, Isacsson U, Dawson A. State of the art. I: resilient response of unbound
- 762 aggregates. *J Transp Eng* 2000a;126:66–75. doi:https://doi.org/10.1061/(ASCE)0733-
- 763 947X(2000)126:1(66).
- 764 33. Lekarp F, Isacsson U, Dawson A. State of the art. II: permanent strain response of
- 765 unbound aggregates. *J Transp Eng* 2000b;126:76–83. doi:10.1061/(ASCE)0733-
- 766 947X(2000)126:1(76).
- 767 34. Lieb R. Materials management at the Gotthard base tunnel - experience from 15 years
- 768 of construction. *Geomech Und Tunnelbau* 2009;2:619–26.
- 769 doi:10.1002/geot.200900032.
- 770 35. Myre J. The use of cold bitumen stabilized base course mixes in Norway 2014:1–14.
- 771 36. Neeb P-R. Byggeråstoff. Trondheim: Tapir; 1992.
- 772 37. NGU. Norges Geologiske Undersøkelse (Geological Survey of Norway) 2017.
- 773 <http://www.ngu.no/> (accessed September 10, 2018).
- 774 38. NPRA. The E39 coastal highway route 2017.
- 775 <https://www.vegvesen.no/en/roads/Roads+and+bridges/Road+projects/e39coastalhighwayroute;jsessionid=99D143CB28F87A072777C744BBCA31E8?lang=nn> (accessed
- 776 September 10, 2018).
- 777 39. NPRA. Håndbok N200 vegbygging. Norway: Vegdirektoratet; 2014a.
- 778 40. NPRA. Kalde bitumen- stabiliserte bærelag. Norway: Vegdirektoratet; 2014b.
- 779 41. Núñez WP, Ceratti JA, Malysz R, Retore TS. Using unbound aggregates resulting
- 780 from amethyst mining in low volume roads. *Adv. Transp. Geotech.*, London: Taylor
- 781

- 782 & Francis; 2008, p. 219–25.
783
784 42. Obert L, Windes SL, Duvall WI. Standardized tests for determining the physical
785 properties of mine rock. 1946.
786 43. Paul DR, Robeson LM. Polymer nanotechnology: nanocomposites. *Polymer (Guildf)*
787 2008;49:3187–204. doi:10.1016/j.polymer.2008.04.017.
788 44. Petkovic G. Recycling in Norwegian conditions. In: Nordal RS, Refsdal G, editors.
789 5th Int. Conf. Bear. Capacit. Roads Airfields, Trondheim: Tapir; 2005.
790 45. Ramberg IB, Bryhni I, Nøttvedt A, Rangnes K. Landet blir til. Trondheim: 2013.
791 46. Resch D, Lassnig K, Galler R, Ebner F. Tunnel excavation material - high value raw
792 material. *Geomech Und Tunnelbau* 2009;2:612–8. doi:10.1002/geot.200900047.
793 47. Riviera PP, Bellopede R, Marini P, Bassani M. Performance-based re-use of tunnel
794 muck as granular material for subgrade and sub-base formation in road construction.
795 *Tunn Undergr Sp Technol* 2014;40:160–73. doi:10.1016/j.tust.2013.10.002.
796 48. Roco MC. Broader societal issues of nanotechnology. *J Nanoparticle Res*
797 2003;5:181–9. doi:10.1023/A:1025548512438.
798 49. Santoni RL, Tingle JS, Webster SL. Stabilization of silty sand with nontraditional
799 additives. *Transp Res Rec* 2002;61–70.
800 50. Simpson DR, Fergus JH. The effect of water on the compressive strength of diabase
801 1968;73:6591–4.
802 51. Siripun K, Jitsangiam P, Nikraz H. Characterization analysis and design of hydrated
803 cement treated crushed rock base as a road base material in Western Australia. *Int J*
804 *Pavement Res Technol* 2010;10:39–47. doi:10.1080/10298430802342682.
805 52. Sobolev K, Shah SP. Nanotechnology in construction. In: Sobolev K, Shah SP,
806 editors. *Proc. NICOM5*, Springer; 2015, p. 509. doi:10.1007/978-3-319-17088-6.
807 53. Ta'neqonbadi B, Noorzad R. Physical and geotechnical long-term properties of
808 lignosulfonate-stabilized clay: An experimental investigation. *Transp Geotech*
809 2018;17:41–50. doi:10.1016/j.trgeo.2018.09.001.
810 54. Teknologirådet. Teknologirådet | Norge 2030 arkiver 2012.
811 <https://teknologiradet.no/norge-2030/> (accessed September 10, 2018).
812 55. Ugwu OO, Arop JB, Nwoji CU, Osadebe NN. Nanotechnology as a preventive
813 engineering solution to highway infrastructure failures. *J Constr Eng Manag*
814 2013;139:987–93. doi:10.1061/(ASCE)CO.1943-7862.0000670.
815 56. Uthus L, Tutumluer E, Horvli I, Hoff I. Influence of grain shape and texture on the
816 deformation properties of unbound aggregates in pavements. *Int J Pavements* 2007;6.
817 57. Wasserman SR, Tao YT, Whitesides GM. Structure and reactivity of alkylsiloxane
818 monolayers formed by reaction of alkyltrichlorosilanes on silicon substrates.
819 *Langmuir* 1989;5:1074–87. doi:10.1021/la00088a035.
820 58. Zhang L, Mao X, Lu A. Experimental study on the mechanical properties of rocks at
821 high temperature. *Sci China, Ser E Technol Sci* 2009;52:641–6. doi:10.1007/s11431-
822 009-0063-y.
823 59. Zhang T, Cai G, Liu S. Application of lignin-stabilized silty soil in highway subgrade:
824 A macroscale laboratory study. *J Mater Civ Eng* 2018;30.
825 doi:10.1061/(ASCE)MT.1943-5533.0002203.
826
827
828
829
830
831

832 **AUTHORS' BIOGRAPHIES**

833
834
835
836
837
838
839
840
841
842
843
844
845
846
847
848
849
850
851
852
853
854
855
856
857
858
859
860
861
862
863
864
865
866
867
868
869
870
871
872
873
874
875
876
877
878
879
880
881



Diego Maria Barbieri is currently Ph.D. Candidate at Norwegian University of Science and Technology, Norway. Before joining the Ph.D. program, he obtained the 2nd level postgraduate master and specialization diploma in railway engineering at La Sapienza University, Italy. He obtained his bachelor and master degree in Civil Engineering at University of Modena and Reggio Emilia, Italy; during this period, he had the opportunity to deepen his studies at Fuzhou University, PRC, as a visiting scholar. His research areas mainly comprise pavement engineering; he is particularly interested in investigating sustainable solutions for infrastructure construction.

Professor **Dr. Inge Hoff** has been doing research on materials for road, railway constructions and pavement design, especially use of unbound granular materials, for more than 20 years. His research interest is both on experimental work in laboratory or field and numerical modelling and design of roads and railways. Before starting to work as professor at NTNU nine years ago, he had been working at the independent research organization SINTEF.

Professor **Dr. Mai Britt E. Mørk** started as professor in geology at NTNU Department of Geology and Mineral Resources Engineering in 2003, now Department of Geoscience and Petroleum. She has geological background from University of Oslo and several years at SINTEF.

Dr. Chun-Hsing Ho is currently an Associate Professor of Civil Engineering at Northern Arizona University, USA. He has over twenty years of work experience spanning in industry and academia. Dr. Ho's research interests lie in construction materials, pavement engineering, and intelligent transportation systems.

PAPER V

Barbieri, D. M., Hoff, I., and Ho, C. S. "Innovative stabilization techniques for weak crushed rocks used in road unbound layers: a numerical investigation." *Construction and Building Materials*. Submitted.

This paper is awaiting publication and is not included in NTNU Open

PAPER VI

Barbieri, D. M., Hoff, I., and Mørk, M. B. E. “Innovative stabilization techniques for weak crushed rocks used in road unbound layers: a field investigation.” *Journal of Transportation Engineering, Part B Pavements*. Submitted.

This paper is awaiting publication and is not included in NTNU Open

APPENDIX A
CONFERENCE POSTERS

THE COASTAL HIGHWAY ROUTE E39 SMART USE OF LOCAL MATERIALS FOR ROAD CONSTRUCTION

Diego Maria Barbieri, Ph.D. candidate, NTNU diego.barbieri@ntnu.no
 Inge Hoff, Professor, NTNU inge.hoff@ntnu.no
 Lillian Mathisen Uthus, Dr. Eng., Veidekke lillian.uthus.mathisen@veidekke.no
 Nils Sigurd Uthus, Dr. Eng., Statens vegvesen nils.uthus@vegvesen.no

REDUCING THE CONSTRUCTION COSTS OF THE ROAD PAVEMENT

The construction plan of the **new E39 highway** improves the viability along the Norwegian coast for a total length of about 1100 km. The infrastructure connects Trondheim to Kristiansand (Fig. 1) linking the major coastal cities.



Fig. 1. E39 highway plan¹

The extended **tunnelling system** (Fig. 2a) is an important part of the infrastructure: the excavations will generate a **surplus of blasted rocks** (Fig. 2b).



Fig. 2a. Tunnel excavation



Fig. 2b. Blasted rocks¹

- Is it possible to **take advantage of these materials** in pavement structures close to the place of production?
- Is it possible to **adjust the design** of layer thicknesses and **construction methods** to enable the **local use** of these materials?

Today the pavement **design manual** sets certain **requirements** for flexible pavement layers. Different **thicknesses of base and subbase** (pavement unbound layers) could be adjusted taking into consideration the different types of rock geology crossed by the highway (Fig. 3).

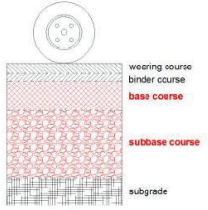


Fig. 3. Flexible pavement structure with unbound layers in evidence

Beneficial goals:

- smart use of environmental resources
- reduce time of material transport
- better economy of the system

LABORATORY TESTING: repeated load triaxial test

Stiffness, resilient modulus and resistance to permanent deformation. Behaviour under repeated loads for different stress state, moisture content and density variation (Fig. 4).



Fig. 4a. Triaxial test apparatus

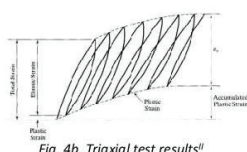


Fig. 4b. Triaxial test results¹¹

FIELD TESTING: static plate load test (SPLT)

Characterize the stiffness of the subgrade (Fig. 5).



Fig. 5a. SPLT apparatus¹¹

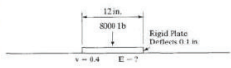


Fig. 5b. SPLT layout testing¹¹

NUMERICAL ANALYSES: FEM modelling

FEM models (Fig. 6) to compare laboratory and field test results.

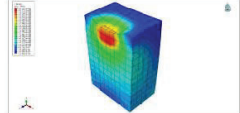


Fig. 6. Example of 3D model of the soil

CREDITS

- I. Statens Vegvesen; <http://www.vegvesen.no/>
 - II. Yang H., Pavement analysis and design, 1997
 - III. Iowa State University; <http://www.ctre.iastate.edu/>
- Via Nordica 2016 NTNU Norwegian University of Science and Technology Statens vegvesen

Via Nordica
8-10 June 2016, Trondheim, Norway

THE COASTAL HIGHWAY ROUTE E39

Laboratory investigation on unbound materials used in a highway with premature damage

Diego Maria Barbieri, Ph.D. candidate, NTNU *diego.barbieri@ntnu.no*

Inge Hoff, Professor, NTNU *inge.hoff@ntnu.no*

Helge Mork, Associate Professor, NTNU *helge.mork@ntnu.no*

The research focuses on a highway section situated in the southern part of Norway. The new road link was built in 2004; the length is about 17.5 km, including a bridge and several tunnels. Damage in form of both alligator cracking and rutting occurred soon after the opening to traffic in 2006: a series of interconnecting cracks developed along the wheel paths. A collaboration comprising Norwegian University of Science and Technology (NTNU), Norwegian Public Roads Administration (NPRA) and the contractor organized a field investigation at five areas. Three locations had clear distresses (Figure 1): site I, site II, site III. Two locations had no visible distresses: site IV, site V.



Figure 1. Investigated sites with visible distresses.

The condition of the road pavement was further inspected according to a pre-set excavation pattern of rectangular size 4 m x 5 m (Figure 2).

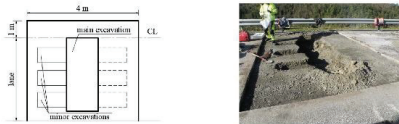


Figure 2. Excavation pattern and fulfillment.

The thickness of each layer was measured and compared to the limits specified by Handbook 018 (NPRA 1998). Table 1 displays the values just for HMA top layer and lower base layer.

Site	Visible status	Rut depth in wheel paths (mm)		HMA top layer measured (mm)	HMA top layer from H018 (mm)	Lower base measured (mm)	Lower base from H018 (mm)
		inner	outer				
I	damage	24	17	80	80	135	150
II	damage	24	20	84	80	158	150
III	damage	13	13	96	80	123	150
IV	no damage	17	15	101	80	95	150
V	no damage	15	16	94	80	148	150

Table 1. Thickness values of HMA top layer and lower base layer.

The unbound lower base course made of crushed rock was investigated. The grain size distribution for sites II and III is very close to the upper limit specified by Handbook 018, moreover the quantity of material smaller than 2 mm is a little higher than the allowed limit (Figure 3).

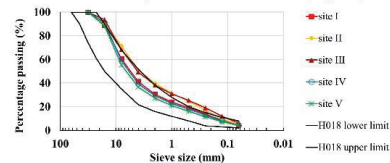


Figure 3. Sieve analysis of the lower base layer.

Repeated Triaxial Load Tests (RTLTL) enables a more careful examination of the materials. The amount of water in the samples varies between 3%, 5% and 7%. A vibratory hammer compacts the specimen layers for $t_c = 20$ s or $t_c = 40$ s leading to different density values.

In the triaxial cell the confining medium applies a uniform constant pressure in all the directions (σ_1); the hydraulic jack exerts an additional sinusoidal vertical dynamic stress (σ_d), which stepwise increases at different levels of confining stress (multistage loading procedure, EN 13286-7 2004). The results showed here just consider $w = 7\%$ because that is sufficient to denote discrepancies in the behaviour among the five sites.

The stiffness is expressed by the resilient modulus M_R . The k- θ non-linear model (Hicks & Monismith, 1971) is adopted.

$$M_R = k_1 \sigma_a \left(\frac{\theta}{\sigma_a} \right)^{k_2}$$

The test results are therefore fitted by the two parameters k_1 and k_2 , Figure 4.

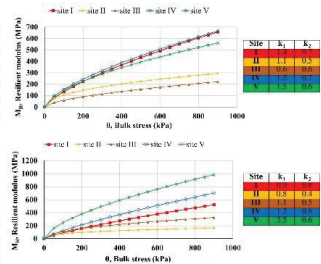


Figure 4. Resilient modulus k- θ regression curves; $w = 7\%$; $t_c = 20$ s (top) and 40 s (bottom).

The permanent deformations are evaluated by the Coulomb approach.

ρ = mobilized friction angle, mobilized shear strength.

ϕ = cyclic failure angle, maximum shear strength.

They identify three different ranges of material behaviour: elastic, elasto-plastic and incremental failure (Figure 5). Sites II and III cannot be displayed because they immediately reach 0.5% deformation limit in the RTLTL.

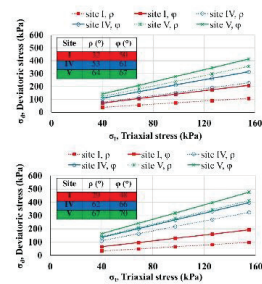


Figure 5. Range boundary lines; $w = 7\%$; $t_c = 20$ s (top) and 40 s (bottom).

The research highlights differences between the areas having visible damage and the areas not having visible damage.

- ❖ **Grading curve:** the damaged sites are much closer to the code limits, site II and III partly exceed the upper limit for material smaller than 2 mm;
- ❖ **Stiffness:** the resilient modulus k- θ regression curves denote that the damaged sites are less stiff than the not damaged ones;
- ❖ **Permanent deformation:** site I has range boundary limits which are significantly lower than those referring to sites IV and V.

This could partly explain the observed damage; other factors could also have contributed, e.g. weak design compared to the real traffic situation.

CREDITS

THE COASTAL HIGHWAY ROUTE E39

SMART USE OF LOCAL MATERIALS FOR ROAD CONSTRUCTION

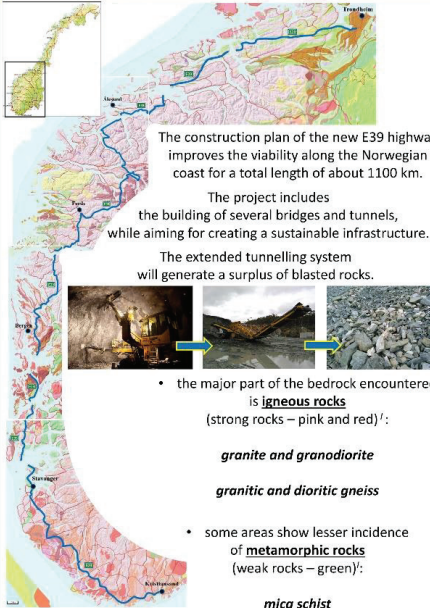
Diego Maria Barbieri, Ph.D. candidate, NTNU diego.barbieri@ntnu.no

Inge Hoff, Professor, NTNU inge.hoff@ntnu.no

Lillian Mathisen Uthus, Dr. Eng., Veidekke lillian.uthus.mathisen@veidekke.no

Nils Sigurd Uthus, Eng., Statens vegvesen nils.uthus@vegvesen.no


FINDING A METHOD TO USE CRUSHED ROCKS: FROM THE TUNNEL TO THE PAVEMENT



The construction plan of the new E39 highway improves the viability along the Norwegian coast for a total length of about 1100 km.

The project includes the building of several bridges and tunnels, while aiming for creating a sustainable infrastructure.

The extended tunnelling system will generate a surplus of blasted rocks.



- the major part of the bedrock encountered is **igneous rocks** (strong rocks – pink and red):
 - granite and granodiorite**
 - granitic and dioritic gneiss**
- some areas show lesser incidence of **metamorphic rocks** (weak rocks – green):
 - mica schist**

➤ Is it possible to **take advantage of these materials** in the **unbound layers** of the pavement structure **close to the place of production**?

Today the pavement **design manual N200** sets certain **requirements** for flexible pavement layers^{II}.

Flakiness index		Los Angeles value	
FI	35	LA	35
Limit requirements for base		Limit requirements for subbase	
LA	30	LA	35
Micro Deval value		Micro Deval value	
M _{DE}	15	M _{DE}	15



The igneous material satisfies these requirements.

➤ How is it possible to enable the use of the weak material as well?

The aim of the research is to **find a method to enable the use of crushed rocks not satisfying the current requirements** in the E39 highway pavement.

Different approaches are now under investigation:

MIXING CRUSHED ROCKS

Mixing strong and weak crushed rocks in order to get the right resource.



Granite and diorite



Mica schist

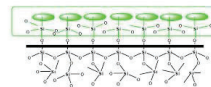
USE THE WEAK MATERIAL IN A BIGGER SIZE

The construction phase can be the most damaging during the road life: the weak material experiences more crushing than the strong one, the former can be used in bigger size.



Compacting the different materials with the same procedure

ADDITIVE STABILIZATION



Aggregate surface silicate structure reaction

Polymeric emulsion coating could enhance properties: resilient modulus and permanent deformation could be improved.

GEOGRID

Geogrids could improve shear transfer (lateral confinement) and reduce deformation and rutting issues.



Geogrid reinforcement



⇒ **smart use of environmental resources**
 ⇒ **reduce time of material transport**
 ⇒ **better economy of the system**



CREDITS

- The Geological Survey of Norway (NGU); www.ngu.no
- Statens Vegvesen; Håndbok N200 Vegbygging, 2014



Norwegian University of Science and Technology



Statens vegvesen

THE COASTAL HIGHWAY ROUTE E39

USE OF LOCAL MATERIALS FOR ROAD CONSTRUCTION

公路建造:使用的本地材料

FINDING A METHOD TO USE CRUSHED ROCKS: FROM THE TUNNEL TO THE PAVEMENT



- ⇒ smart use of environmental resources
- ⇒ reduce time of material transport
- ⇒ better economy of the system

The construction plan of the new E39 highway improves the viability along the Norwegian coast for a total length of about 1100 km.

The project includes the building of several bridges and tunnels, while aiming for creating a sustainable infrastructure.

The extended tunnelling system will generate a surplus of blasted rocks.



- the major part of the bedrock encountered is **igneous rocks** (strong rocks – pink and red):
- some areas show lesser incidence of **metamorphic rocks** (weak rocks – green):

- Is it possible to **take advantage of these materials** in the **unbound layers** of the pavement structure **close to the place of production**?

Today the pavement **design manual N200** sets certain **requirements** for flexible pavement layers.

The igneous material satisfies these requirements.

- How is it possible to enable the use of the weak material as well?



ntnu.no
diego.barbieri@ntnu.no

 **NTNU**
Faculty of Engineering
Department of Civil and
Environmental Engineering


Statens vegvesen

Teknologidagene

23-26 October 2017, Trondheim, Norway

APPENDIX B

EXAMPLE OF MATLAB SCRIPT TO ASSESS RESILIENT MODULUS

```

%RESILIENT MODULUS

clc
clear
close all

%%%%%%%%%%%%%%%%%%%%%%%%%%%%%%%%%%%%%%%%%%%%%%%%%%%%%%%%%%%%%%%%%%%%%%%%

%Input.txt files (---> data in kPa)

load M2.txt;
load ZM2.txt;

%%%%%%%%%%%%%%%%%%%%%%%%%%%%%%%%%%%%%%%%%%%%%%%%%%%%%%%%%%%%%%%%%%%%%%%%

X=M2(:,1); % measured bulk stress, kPa
Y=M2(:,3); % measured deviatoric stress, kPa
Z=M2(:,2); % measured resilient modulus, kPa
T=(X-Y)/3; % measured triaxial stress, kPa
TAU=sqrt( (2/3) * ( -2*T.*(Y+T) - T.^2 + (1/3)*X.^2 )); % measured octahedral stress, kPa

ZX=ZM2(:,1); % measured bulk stress, kPa
ZY=ZM2(:,3); % measured deviatoric stress, kPa
ZZ=ZM2(:,2); % measured resilient modulus, kPa
ZT=(ZX-ZY)/3; % measured triaxial stress, kPa
ZTAU=sqrt( (2/3) * ( -2*ZT.*(ZY+ZT) - ZT.^2 + (1/3)*ZX.^2 )); % measured octahedral stress, kPa

sigmaa=100; % reference stress, kPa

%%%%%%%%%%%%%%%%%%%%%%%%%%%%%%%%%%%%%%%%%%%%%%%%%%%%%%%%%%%%%%%%%%%%%%%%

Cthetabmax=1200; % max bulk stress for computation, kPa
Csigmadmax=600; % max deviatoric stress for computation, kPa
Ctaumax=600; % max octahedral stress for computation, kPa
Cdeltathetab=25; % delta bulk stress for computation, kPa
Cdeltasigmad=25; % delta deviatoric stress for computation, kPa
Cdelтатаu=25; % delta octahedral stress for computation, kPa

Pthetabmax=1000; % max bulk stress for plot, kPa
Psigmadmax=600; % max deviatoric stress for plot, kPa
Ptaumax=600; % max octahedral stress for plot, kPa
Pmodresmax=1000; % max resilient modulus for plot, MPa
Pdeltathetab=200; % delta bulk stress for plot, kPa
Pdeltasigmad=100; % delta deviatoric stress for plot, kPa
Pdeltatau=100; % delta octahedral stress for plot, kPa
Pdeltamodres=200; % delta resilient modulus for plot, MPa

thetab=(0:Cdeltathetab:Cthetabmax)';
sigmad=(0:Cdeltasigmad:Csigmadmax)';
taurange=(0:Cdelтатаu:Ctaumax)';

%%%%%%%%%%%%%%%%%%%%%%%%%%%%%%%%%%%%%%%%%%%%%%%%%%%%%%%%%%%%%%%%%%%%%%%%

x=log10(X/sigmaa);
y=log10(Y/sigmaa);
tau=log10(TAU/sigmaa);
z=log10(Z);

xdim=length(x);
ydim=length(y);
zdim=length(z);

Zx=log10(ZX/sigmaa);
Zy=log10(ZY/sigmaa);
Ztau=log10(ZTAU/sigmaa);
Zz=log10(ZZ);

Zxdim=length(Zx);
Zydim=length(Zy);
Zzdim=length(Zz);

%%%%%%%%%%%%%%%%%%%%%%%%%%%%%%%%%%%%%%%%%%%%%%%%%%%%%%%%%%%%%%%%%%%%%%%%

%Experimental data, 2D

figure(1)
set(gcf, 'DefaultAxesFontName', 'Times New Roman');

hold on
scatter(X,z./1000,10,'k')
scatter(Zx,Zz./1000,10,'MarkerEdgeColor',[0.75, 0, 0.75])
hold off

```



```

xlabel('\theta , Bulk stress (kPa)','FontSize',16,'fontWeight','bold');
ylabel('M_r , Resilient modulus (MPa)','FontSize',16,'fontWeight','bold');
legend({'M2','M2-P'},'Location','northeast','FontSize',18);

grid on
set(gca,'XLim',[0 1200],'XTick',(0:200:1200),'FontSize',16)
set(gca,'YLim',[0 7000],'YTick',(0:1000:7000),'FontSize',16)

print 01_Resilient_modulus_data_2D -djpeg

%%%%%%%%%%%%%%%%%%%%%%%%%%%%%%%%%%%%%%%%%%%%%%%%%%%%%%%%%%%%%%%%%%%%%%%%%%%%%%

%Experimental data, 3D

figure(2);
set(gcf,'DefaultAxesFontName','Times New Roman');
az = 50;
el = 40;
view(az, el);

hold on
scatter3(Y,X,Z./1000,10,'k');
scatter3(ZY,ZX,ZZ./1000,10,'MarkerEdgeColor',[0.75, 0, 0.75]);
hold off

xlabel('\sigma_d , Deviatoric stress (kPa)','FontSize',16,'fontWeight','bold');
ylabel('\theta , Bulk stress (kPa)','FontSize',16,'fontWeight','bold');
zlabel('M_r , Resilient modulus (MPa)','FontSize',16,'fontWeight','bold');
legend({'M2','M2-P'},'Location','northeast','FontSize',18);

grid on
set(gca,'XLim',[0 600],'XTick',(0:100:600),'FontSize',16)
set(gca,'YLim',[0 1000],'YTick',(0:200:1000),'FontSize',16)
set(gca,'ZLim',[0 7000],'ZTick',(0:1000:7000),'FontSize',16)

print 02_Resilient_modulus_data_3D -djpeg

%%%%%%%%%%%%%%%%%%%%%%%%%%%%%%%%%%%%%%%%%%%%%%%%%%%%%%%%%%%%%%%%%%%%%%%%%%%%%%

%Hicks&Monismith model

syms a b

eq1=ones(1,xdim)*(z-a*ones(1,xdim)~-b*x);
eq2=x*(z-a*ones(1,xdim)~-b*x);

[a,b]=solve([eq1==0,eq2==0],[a,b]);

k1=double(10^(a-log10(sigmaa)));
k2=double(b);

syms Za Zb

eq1=ones(1,Zxdim)*(Zz-Za*ones(1,Zxdim)~-Zb*Zx);
eq2=Zx*(Zz-Za*ones(1,Zxdim)~-Zb*Zx);

[Za,Zb]=solve([eq1==0,eq2==0],[Za,Zb]);

Zk1=double(10^(Za-log10(sigmaa)));
Zk2=double(Zb);

HMk=[k1 k2 Zk1 Zk2]

MrHM=k1*sigmaa*(thetab/sigmaa).^k2/1000; %MPa
ZMrHM=Zk1*sigmaa*(thetab/sigmaa).^Zk2/1000; %MPa

figure(3);
set(gcf,'DefaultAxesFontName','Times New Roman');

hold on
plot(thetab,MrHM,'k','Linewidth',1);
plot(thetab,ZMrHM,'color',[0.75, 0, 0.75],'Linewidth',1);
hold off

xlabel('\theta , Bulk stress (kPa)','FontSize',16,'fontWeight','bold');
ylabel('M_r , Resilient modulus (MPa)','FontSize',16,'fontWeight','bold');

grid on
set(gca,'XLim',[0 Pthetabmax],'XTick',(0:Pde1tathetab:Pthetabmax),'FontSize',16)
set(gca,'YLim',[0 Pmodresmax],'YTick',(0:Pde1tamodres:Pmodresmax),'FontSize',16)

%Coefficient of determination

for i=1:xdim

```

```

    AVE(i)=Z(i)^2;
end
SAVE=sum(AVE);
for i=1:xdim
    RSS(i)=(Z(i)-k1*sigmaa*(X(i)/sigmaa).^k2)^2;
    TSS(i)=(Z(i)-SAVE/xdim)^2;
end
R2=1-sum(RSS)/sum(TSS);
for i=1:Zxdim
    ZAVE(i)=ZZ(i)^2;
end
ZSAVE=sum(ZAVE);
for i=1:Zxdim
    ZRSS(i)=(ZZ(i)-Zk1*sigmaa*(ZX(i)/sigmaa).^k2)^2;
    ZTSS(i)=(ZZ(i)-ZSAVE/Zxdim)^2;
end
ZR2=1-sum(ZRSS)/sum(ZTSS);
legend({'M2', R^2= 0.99', 'M2-P', R^2= 0.99'}, 'Location', 'northeast', 'FontSize', 18);
print 03_Resilient_modulus_Hicks&Monismith -djpeg
%%%%%%%%%%%%%%%%%%%%%%%%%%%%%%%%%%%%%%%%%%%%%%%%%%%%%%%%%%%%%%%%%%%%%%%%
%Uzan model
syms a b c
eq1=ones(1,xdim)*(z-a*ones(1,xdim)'+b*x-c*y);
eq2=x'*(z-a*ones(1,xdim)'+b*x-c*y);
eq3=y'*(z-a*ones(1,xdim)'+b*x-c*y);
[a,b,c]=solve([eq1==0,eq2==0,eq3==0],[a,b,c]);
kk1=double(10^(a-log10(sigmaa)));
kk2=double(b);
kk3=double(c);
syms Za Zb Zc
eq1=ones(1,Zxdim)*(Zz-Za*ones(1,Zxdim)'+Zb*Zx-Zc*Zy);
eq2=Zx'*(Zz-Za*ones(1,Zxdim)'+Zb*Zx-Zc*Zy);
eq3=Zy'*(Zz-Za*ones(1,Zxdim)'+Zb*Zx-Zc*Zy);
[Za,Zb,Zc]=solve([eq1==0,eq2==0,eq3==0],[Za,Zb,Zc]);
Zkk1=double(10^(Za-log10(sigmaa)));
Zkk2=double(Zb);
Zkk3=double(Zc);
uzkk=[kk1 kk2 kk3 zkk1 zkk2 zkk3]
MrUZ=kk1*sigmaa*((thetab/sigmaa).^k2)*((sigmad/sigmaa).^k3)/1000; % MPA
ZMrUZ=Zkk1*sigmaa*((thetab/sigmaa).^Zkk2)*((sigmad/sigmaa).^Zkk3)/1000; % MPA
figure(4);
set(gcf,'DefaultAxesFontName','Times New Roman');
[XX,YY]=meshgrid(sigmad,thetab);
az = 50;
el = 40;
view(az, el);
hold on
ss = surf(XX,YY,MrUZ,'FaceAlpha',0.5,'EdgeColor',[0 0 0],'FaceColor',[0 0 0],'Linewidth',0.3);
Zss = surf(XX,YY,ZMrUZ,'FaceAlpha',0.5,'EdgeColor',[0.75, 0, 0.75],'FaceColor',[0.75, 0, 0.75],'Linewidth',0.7);
hold off
xlabel('\sigma_d , Deviatoric stress (kPa)','FontSize',16,'fontWeight','bold');
ylabel('\theta , Bulk stress (kPa)','FontSize',16,'fontWeight','bold');
zlabel('M_r , Resilient modulus (MPa)','FontSize',16,'fontWeight','bold');
grid on
set(gca,'Xlim',[0 Psigmadmax],'XTick',(0:Pdeltasigmad:Psigmadmax),'FontSize',16)
set(gca,'Ylim',[0 Pthetabmax],'YTick',(0:Pdeltathetab:Pthetabmax),'FontSize',16)
set(gca,'Zlim',[0 Pmodresmax],'ZTick',(0:Pdeltamodres:Pmodresmax),'FontSize',16)
%Coefficient of determination

```

```

for i=1:xdim
    AVE(i)=Z(i)^2;
end

SAVE=sum(AVE);

for i=1:xdim
    RSS(i)=(Z(i)-kk1*sigmaa*((X(i)/sigmaa).^kk2)*((Y(i)/sigmaa).^kk3))^2;
    TSS(i)=(Z(i)-SAVE/xdim)^2;
end

R2=1-sum(RSS)/sum(TSS);

for i=1:Zxdim
    ZAVE(i)=ZZ(i)^2;
end

ZSAVE=sum(ZAVE);

for i=1:Zxdim
    ZRSS(i)=(ZZ(i)-zkk1*sigmaa*((ZX(i)/sigmaa).^zkk2)*((ZY(i)/sigmaa).^zkk3))^2;
    ZTSS(i)=(ZZ(i)-ZSAVE/Zxdim)^2;
end

ZR2=1-sum(ZRSS)/sum(ZTSS);

legend({'M2, R^2= 0.99', 'M2-P, R^2= 0.99'}, 'Location', 'northeast', 'FontSize', 18);

print 04_Resilient_modulus_Uzan -djpeg

%%%%%%%%%%%%%%%%%%%%%%%%%%%%%%%%%%%%%%%%%%%%%%%%%%%%%%%%%%%%%%%%%%%%%%%%%%%%%%

%Uzan&Witczak model

syms a b c

eq1=ones(1,xdim)*(z-a*ones(1,xdim)^-b*x-c*tau);
eq2=x*(z-a*ones(1,xdim)^-b*x-c*tau);
eq3=y*(z-a*ones(1,xdim)^-b*x-c*tau);

[a,b,c]=solve([eq1==0,eq2==0,eq3==0],[a,b,c]);

kkk1=double(10^(a-log10(sigmaa)));
kkk2=double(b);
kkk3=double(c);

syms Za Zb Zc

eq1=ones(1,Zxdim)*(Zz-Za*ones(1,Zxdim)^-Zb*Zx-Zc*Ztau);
eq2=Zx*(Zz-Za*ones(1,Zxdim)^-Zb*Zx-Zc*Ztau);
eq3=Zy*(Zz-Za*ones(1,Zxdim)^-Zb*Zx-Zc*Ztau);

[Za,Zb,Zc]=solve([eq1==0,eq2==0,eq3==0],[Za,Zb,Zc]);

zkkk1=double(10^(Za-log10(sigmaa)));
zkkk2=double(Zb);
zkkk3=double(Zc);

uwkkk=[kkk1 kkk2 kkk3 zkkk1 zkkk2 zkkk3]

MrUW=kkk1*sigmaa*((thetab/sigmaa).^kkk2)*((taurange/sigmaa).^kkk3)/1000; % MPa
ZMrUW=zkkk1*sigmaa*((thetab/sigmaa).^zkkk2)*((taurange/sigmaa).^zkkk3)/1000; % MPa

figure(5);
set(gcf,'DefaultAxesFontName','Times New Roman');
[XX,YY]=meshgrid(taurange,thetab);
az = 50;
e1 = 40;
view(az, e1);

hold on
sss = surf(XX,YY,MrUW,'FaceAlpha',0.5,'EdgeColor',[0 0 0],'FaceColor',[0 0 0], 'Linewidth',0.3);
zsss = surf(XX,YY,ZMrUW,'FaceAlpha',0.5,'EdgeColor',[0.75, 0, 0.75],'FaceColor',[0.75, 0, 0.75], 'Linewidth',0.7);
hold off

xlabel('\tau_{oct}, Octahedral stress (kPa)','FontSize',16,'fontweight','bold');
ylabel('\theta, Bulk stress (kPa)','FontSize',16,'fontweight','bold');
zlabel('M_r, Resilient modulus (MPa)','FontSize',16,'fontweight','bold');

grid on
set(gca,'XLim',[100 Ptaumax],'XTick',(0:Pdelтатаu:Ptaumax),'FontSize',16)
set(gca,'YLim',[0 Pthetabmax],'YTick',(0:Pdelatathetab:Pthetabmax),'FontSize',16)

```

```

set(gca,'ZLim',[0 Pmodresmax],'ZTick',(0:Pdeltamodres:Pmodresmax),'FontSize',16)
%Coefficient of determination
for i=1:xdim
    AVE(i)=Z(i)^2;
end
SAVE=sum(AVE);
for i=1:xdim
    RSS(i)=(Z(i)-kkk1*sigmaa*((X(i)/sigmaa).^kkk2) * ((TAU(i)/sigmaa).^kkk3) )^2;
    TSS(i)=(Z(i)-SAVE/xdim)^2;
end
R2=1-sum(RSS)/sum(TSS);
for i=1:Zxdim
    ZAVE(i)=ZZ(i)^2;
end
ZSAVE=sum(ZAVE);
for i=1:Zxdim
    ZRSS(i)=(ZZ(i)-Zkkk1*sigmaa*((ZX(i)/sigmaa).^Zkkk2) * ((ZTAU(i)/sigmaa).^Zkkk3) )^2;
    ZTSS(i)=(ZZ(i)-ZSAVE/Zxdim)^2;
end
ZR2=1-sum(ZRSS)/sum(ZTSS);
Legend({'M2, R^2= 0.99','M2-P, R^2= 0.99'},'Location','northeast','FontSize',18);
print 05_Resilient_modulus_Uzan&Witczak -djpeg

```


APPENDIX C

EXAMPLE OF MATLAB SCRIPT TO ASSESS PERMANENT VERTICAL STRAIN


```

%PERMANENT VERTICAL STRAIN

clc
clear
close all

%%%%%%%%%%%%%%%%%%%%%%%%%%%%%%%%%%%%%%%%%%%%%%%%%%%%%%%%%%%%%%%%%%%%%%%%

%Input.txt files (---> data in kPa)

load M2_11.txt;
load M2_12.txt;
load M2_13.txt;
load M2_14.txt;
load M2_15.txt;
load M2_16.txt;

load M2_21.txt;
load M2_22.txt;
load M2_23.txt;
load M2_24.txt;
load M2_25.txt;
load M2_26.txt;

load M2_31.txt;
load M2_32.txt;
load M2_33.txt;
load M2_34.txt;
load M2_35.txt;
load M2_36.txt;

load M2_41.txt;
load M2_42.txt;
load M2_43.txt;
load M2_44.txt;
load M2_45.txt;
load M2_46.txt;

load M2_51.txt;
load M2_52.txt;
load M2_53.txt;
load M2_54.txt;
load M2_55.txt;
load M2_56.txt;

load ZM2_11.txt;
load ZM2_12.txt;
load ZM2_13.txt;
load ZM2_14.txt;
load ZM2_15.txt;
load ZM2_16.txt;

load ZM2_21.txt;
load ZM2_22.txt;
load ZM2_23.txt;
load ZM2_24.txt;
load ZM2_25.txt;
load ZM2_26.txt;

load ZM2_31.txt;
load ZM2_32.txt;
load ZM2_33.txt;
load ZM2_34.txt;
load ZM2_35.txt;
load ZM2_36.txt;

load ZM2_41.txt;
load ZM2_42.txt;
load ZM2_43.txt;
load ZM2_44.txt;
load ZM2_45.txt;
load ZM2_46.txt;

load ZM2_51.txt;
load ZM2_52.txt;
load ZM2_53.txt;
load ZM2_54.txt;
load ZM2_55.txt;
load ZM2_56.txt;

load AM2_TR_HM.txt;

```

```

M2TRHM=AM2_TR_HM(:,4);
load AM2_TR_UZ.txt;
M2TRUZ=AM2_TR_UZ(:,4);
load AM2_TR_UW.txt;
M2TRUW=AM2_TR_UW(:,4);
load AM2_VM_HM.txt;
M2VMHM=AM2_VM_HM(:,4);
load AM2_VM_UZ.txt;
M2VMUZ=AM2_VM_UZ(:,4);
load AM2_VM_UW.txt;
M2VMUW=AM2_VM_UW(:,4);

load AZM2_TR_HM.txt;
ZM2TRHM=AZM2_TR_HM(:,4);
load AZM2_TR_UZ.txt;
ZM2TRUZ=AZM2_TR_UZ(:,4);
load AZM2_TR_UW.txt;
ZM2TRUW=AZM2_TR_UW(:,4);
load AZM2_VM_HM.txt;
ZM2VMHM=AZM2_VM_HM(:,4);
load AZM2_VM_UZ.txt;
ZM2VMUZ=AZM2_VM_UZ(:,4);
load AZM2_VM_UW.txt;
ZM2VMUW=AZM2_VM_UW(:,4);

load BM2_TR_HM.txt;
M2BTRHM=BM2_TR_HM(:,2);
load BM2_TR_UZ.txt;
M2BTRUZ=BM2_TR_UZ(:,2);
load BM2_TR_UW.txt;
M2BTRUW=BM2_TR_UW(:,2);
load BM2_VM_HM.txt;
M2BVMHM=BM2_VM_HM(:,2);
load BM2_VM_UZ.txt;
M2BVMUZ=BM2_VM_UZ(:,2);
load BM2_VM_UW.txt;
M2BVMUW=BM2_VM_UW(:,2);

load BZM2_TR_HM.txt;
ZM2BTRHM=BZM2_TR_HM(:,2);
load BZM2_TR_UZ.txt;
ZM2BTRUZ=BZM2_TR_UZ(:,2);
load BZM2_TR_UW.txt;
ZM2BTRUW=BZM2_TR_UW(:,2);
load BZM2_VM_HM.txt;
ZM2BVMHM=BZM2_VM_HM(:,2);
load BZM2_VM_UZ.txt;
ZM2BVMUZ=BZM2_VM_UZ(:,2);
load BZM2_VM_UW.txt;
ZM2BVMUW=BZM2_VM_UW(:,2);

load s11.txt;
s11=s11(:,4);

load zS9.txt;
zS9=zS9(:,4);

%%%%%%%%%%%%%%%%%%%%%%%%%%%%%%%%%%%%%%%%%%%%%%%%%%%%%%%%%%%%%%%%%%%%%%%%
sigmaa=100; % reference stress, kPa
%%%%%%%%%%%%%%%%%%%%%%%%%%%%%%%%%%%%%%%%%%%%%%%%%%%%%%%%%%%%%%%%%%%%%%%%

%Number of step first values to be considered for time hardening

SFP11=100;
SFP12=100;
SFP13=100;
SFP14=100;
SFP15=100;
SFP16=100;

matSFP1=[SFP11 SFP12 SFP13 SFP14 SFP15 SFP16];

SFP21=100;
SFP22=100;
SFP23=100;
SFP24=100;
SFP25=100;
SFP26=100;

```

```

matSFP2=[SFP21 SFP22 SFP23 SFP24 SFP25 SFP26];

SFP31=100;
SFP32=100;
SFP33=100;
SFP34=100;
SFP35=100;
SFP36=100;

matSFP3=[SFP31 SFP32 SFP33 SFP34 SFP35 SFP36];

SFP41=100;
SFP42=100;
SFP43=100;
SFP44=100;
SFP45=100;
SFP46=100;

matSFP4=[SFP41 SFP42 SFP43 SFP44 SFP45 SFP46];

SFP51=100;
SFP52=100;
SFP53=100;
SFP54=100;
SFP55=100;
SFP56=100;

matSFP5=[SFP51 SFP52 SFP53 SFP54 SFP55 SFP56];

ZSFP11=100;
ZSFP12=100;
ZSFP13=100;
ZSFP14=100;
ZSFP15=100;
ZSFP16=100;

matZSFP1=[ZSFP11 ZSFP12 ZSFP13 ZSFP14 ZSFP15 ZSFP16];

ZSFP21=100;
ZSFP22=100;
ZSFP23=100;
ZSFP24=100;
ZSFP25=100;
ZSFP26=100;

matZSFP2=[ZSFP21 ZSFP22 ZSFP23 ZSFP24 ZSFP25 ZSFP26];

ZSFP31=100;
ZSFP32=100;
ZSFP33=100;
ZSFP34=100;
ZSFP35=100;
ZSFP36=100;

matZSFP3=[ZSFP31 ZSFP32 ZSFP33 ZSFP34 ZSFP35 ZSFP36];

ZSFP41=100;
ZSFP42=100;
ZSFP43=100;
ZSFP44=100;
ZSFP45=100;
ZSFP46=100;

matZSFP4=[ZSFP41 ZSFP42 ZSFP43 ZSFP44 ZSFP45 ZSFP46];

ZSFP51=100;
ZSFP52=100;
ZSFP53=100;
ZSFP54=100;
ZSFP55=100;
ZSFP56=100;

matZSFP5=[ZSFP51 ZSFP52 ZSFP53 ZSFP54 ZSFP55 ZSFP56];

%%%%%%%%%%%%%%%%%%%%%%%%%%%%%%%%%%%%%%%%%%%%%%%%%%%%%%%%%%%%%%%%%%%%%%%%%%

%Input permanent deformation, each sequence each step

P11=M2_11(:,2);
SP11=size(P11,1);
P12=M2_12(:,2);
SP12=size(P12,1);
P13=M2_13(:,2);
SP13=size(P13,1);

```

```

P14=M2_14(:,2);
SP14=size(P14,1);
P15=M2_15(:,2);
SP15=size(P15,1);
P16=M2_16(:,2);
SP16=size(P16,1);

P1= [P11; P12; P13; P14; P15; P16];
matSP1=[SP11 SP12 SP13 SP14 SP15 SP16];
matCUMSP1=[SP11 SP11+SP12 SP11+SP12+SP13 SP11+SP12+SP13+SP14 SP11+SP12+SP13+SP14+SP15
SP11+SP12+SP13+SP14+SP15+SP16];
matcumSP1=[0 SP11 SP11+SP12 SP11+SP12+SP13 SP11+SP12+SP13+SP14 SP11+SP12+SP13+SP14+SP15];

P21=M2_21(:,2);
SP21=size(P21,1);
P22=M2_22(:,2);
SP22=size(P22,1);
P23=M2_23(:,2);
SP23=size(P23,1);
P24=M2_24(:,2);
SP24=size(P24,1);
P25=M2_25(:,2);
SP25=size(P25,1);
P26=M2_26(:,2);
SP26=size(P26,1);

P2= [P21; P22; P23; P24; P25; P26];
matSP2=[SP21 SP22 SP23 SP24 SP25 SP26];
matCUMSP2=[SP21 SP21+SP22 SP21+SP22+SP23 SP21+SP22+SP23+SP24 SP21+SP22+SP23+SP24+SP25
SP21+SP22+SP23+SP24+SP25+SP26];
matcumSP2=[0 SP21 SP21+SP22 SP21+SP22+SP23 SP21+SP22+SP23+SP24 SP21+SP22+SP23+SP24+SP25];

P31=M2_31(:,2);
SP31=size(P31,1);
P32=M2_32(:,2);
SP32=size(P32,1);
P33=M2_33(:,2);
SP33=size(P33,1);
P34=M2_34(:,2);
SP34=size(P34,1);
P35=M2_35(:,2);
SP35=size(P35,1);
P36=M2_36(:,2);
SP36=size(P36,1);

P3= [P31; P32; P33; P34; P35; P36];
matSP3=[SP31 SP32 SP33 SP34 SP35 SP36];
matCUMSP3=[SP31 SP31+SP32 SP31+SP32+SP33 SP31+SP32+SP33+SP34 SP31+SP32+SP33+SP34+SP35
SP31+SP32+SP33+SP34+SP35+SP36];
matcumSP3=[0 SP31 SP31+SP32 SP31+SP32+SP33 SP31+SP32+SP33+SP34 SP31+SP32+SP33+SP34+SP35];

P41=M2_41(:,2);
SP41=size(P41,1);
P42=M2_42(:,2);
SP42=size(P42,1);
P43=M2_43(:,2);
SP43=size(P43,1);
P44=M2_44(:,2);
SP44=size(P44,1);
P45=M2_45(:,2);
SP45=size(P45,1);
P46=M2_46(:,2);
SP46=size(P46,1);

P4= [P41; P42; P43; P44; P45; P46];
matSP4=[SP41 SP42 SP43 SP44 SP45 SP46];
matCUMSP4=[SP41 SP41+SP42 SP41+SP42+SP43 SP41+SP42+SP43+SP44 SP41+SP42+SP43+SP44+SP45
SP41+SP42+SP43+SP44+SP45+SP46];
matcumSP4=[0 SP41 SP41+SP42 SP41+SP42+SP43 SP41+SP42+SP43+SP44 SP41+SP42+SP43+SP44+SP45];

P51=M2_51(:,2);
SP51=size(P51,1);
P52=M2_52(:,2);
SP52=size(P52,1);
P53=M2_53(:,2);
SP53=size(P53,1);
P54=M2_54(:,2);
SP54=size(P54,1);
P55=M2_55(:,2);
SP55=size(P55,1);
P56=M2_56(:,2);
SP56=size(P56,1);

P5= [P51; P52; P53; P54; P55; P56];
matSP5=[SP51 SP52 SP53 SP54 SP55 SP56];

```

```

matCUMSP5=[SP51 SP51+SP52 SP51+SP52+SP53 SP51+SP52+SP53+SP54 SP51+SP52+SP53+SP54+SP55
SP51+SP52+SP53+SP54+SP55+SP56];
matcumSP5=[0 SP51 SP51+SP52 SP51+SP52+SP53 SP51+SP52+SP53+SP54 SP51+SP52+SP53+SP54+SP55];

matCUMSP=[length(P1) length(P1)+length(P2) length(P1)+length(P2)+length(P3)
length(P1)+length(P2)+length(P3)+length(P4)
length(P1)+length(P2)+length(P3)+length(P4)+length(P5)];
matcumSP=[0 length(P1) length(P1)+length(P2) length(P1)+length(P2)+length(P3)
length(P1)+length(P2)+length(P3)+length(P4)];

ZP11=ZM2_11(:,2);
ZSP11=size(ZP11,1);
ZP12=ZM2_12(:,2);
ZSP12=size(ZP12,1);
ZP13=ZM2_13(:,2);
ZSP13=size(ZP13,1);
ZP14=ZM2_14(:,2);
ZSP14=size(ZP14,1);
ZP15=ZM2_15(:,2);
ZSP15=size(ZP15,1);
ZP16=ZM2_16(:,2);
ZSP16=size(ZP16,1);

ZP1= [ZP11; ZP12; ZP13; ZP14; ZP15; ZP16];
matZSP1=[ZSP11 ZSP12 ZSP13 ZSP14 ZSP15 ZSP16];
matCUMZSP1=[ZSP11 ZSP11+ZSP12 ZSP11+ZSP12+ZSP13 ZSP11+ZSP12+ZSP13+ZSP14
ZSP11+ZSP12+ZSP13+ZSP14+ZSP15 ZSP11+ZSP12+ZSP13+ZSP14+ZSP15+ZSP16];
matcumZSP1=[0 ZSP11 ZSP11+ZSP12 ZSP11+ZSP12+ZSP13 ZSP11+ZSP12+ZSP13+ZSP14
ZSP11+ZSP12+ZSP13+ZSP14+ZSP15];

ZP21=ZM2_21(:,2);
ZSP21=size(ZP21,1);
ZP22=ZM2_22(:,2);
ZSP22=size(ZP22,1);
ZP23=ZM2_23(:,2);
ZSP23=size(ZP23,1);
ZP24=ZM2_24(:,2);
ZSP24=size(ZP24,1);
ZP25=ZM2_25(:,2);
ZSP25=size(ZP25,1);
ZP26=ZM2_26(:,2);
ZSP26=size(ZP26,1);

ZP2= [ZP21; ZP22; ZP23; ZP24; ZP25; ZP26];
matZSP2=[ZSP21 ZSP22 ZSP23 ZSP24 ZSP25 ZSP26];
matCUMZSP2=[ZSP21 ZSP21+ZSP22 ZSP21+ZSP22+ZSP23 ZSP21+ZSP22+ZSP23+ZSP24
ZSP21+ZSP22+ZSP23+ZSP24+ZSP25 ZSP21+ZSP22+ZSP23+ZSP24+ZSP25+ZSP26];
matcumZSP2=[0 ZSP21 ZSP21+ZSP22 ZSP21+ZSP22+ZSP23 ZSP21+ZSP22+ZSP23+ZSP24
ZSP21+ZSP22+ZSP23+ZSP24+ZSP25];

ZP31=ZM2_31(:,2);
ZSP31=size(ZP31,1);
ZP32=ZM2_32(:,2);
ZSP32=size(ZP32,1);
ZP33=ZM2_33(:,2);
ZSP33=size(ZP33,1);
ZP34=ZM2_34(:,2);
ZSP34=size(ZP34,1);
ZP35=ZM2_35(:,2);
ZSP35=size(ZP35,1);
ZP36=ZM2_36(:,2);
ZSP36=size(ZP36,1);

ZP3= [ZP31; ZP32; ZP33; ZP34; ZP35; ZP36];
matZSP3=[ZSP31 ZSP32 ZSP33 ZSP34 ZSP35 ZSP36];
matCUMZSP3=[ZSP31 ZSP31+ZSP32 ZSP31+ZSP32+ZSP33 ZSP31+ZSP32+ZSP33+ZSP34
ZSP31+ZSP32+ZSP33+ZSP34+ZSP35 ZSP31+ZSP32+ZSP33+ZSP34+ZSP35+ZSP36];
matcumZSP3=[0 ZSP31 ZSP31+ZSP32 ZSP31+ZSP32+ZSP33 ZSP31+ZSP32+ZSP33+ZSP34
ZSP31+ZSP32+ZSP33+ZSP34+ZSP35];

ZP41=ZM2_41(:,2);
ZSP41=size(ZP41,1);
ZP42=ZM2_42(:,2);
ZSP42=size(ZP42,1);
ZP43=ZM2_43(:,2);
ZSP43=size(ZP43,1);
ZP44=ZM2_44(:,2);
ZSP44=size(ZP44,1);
ZP45=ZM2_45(:,2);
ZSP45=size(ZP45,1);
ZP46=ZM2_46(:,2);
ZSP46=size(ZP46,1);

ZP4= [ZP41; ZP42; ZP43; ZP44; ZP45; ZP46];

```

```

matZSP4=[ZSP41 ZSP42 ZSP43 ZSP44 ZSP45 ZSP46];
matCUMZSP4=[ZSP41 ZSP41+ZSP42 ZSP41+ZSP42+ZSP43 ZSP41+ZSP42+ZSP43+ZSP44
ZSP41+ZSP42+ZSP43+ZSP44+ZSP45 ZSP41+ZSP42+ZSP43+ZSP44+ZSP45+ZSP46];
matcumZSP4=[0 ZSP41 ZSP41+ZSP42 ZSP41+ZSP42+ZSP43 ZSP41+ZSP42+ZSP43+ZSP44
ZSP41+ZSP42+ZSP43+ZSP44+ZSP45];

ZP51=ZM2_51(:,2);
ZSP51=size(ZP51,1);
ZP52=ZM2_52(:,2);
ZSP52=size(ZP52,1);
ZP53=ZM2_53(:,2);
ZSP53=size(ZP53,1);
ZP54=ZM2_54(:,2);
ZSP54=size(ZP54,1);
ZP55=ZM2_55(:,2);
ZSP55=size(ZP55,1);
ZP56=ZM2_56(:,2);
ZSP56=size(ZP56,1);

ZP5= [ZP51; ZP52; ZP53; ZP54; ZP55; ZP56];
matZSP5=[ZSP51 ZSP52 ZSP53 ZSP54 ZSP55 ZSP56];
matCUMZSP5=[ZSP51 ZSP51+ZSP52 ZSP51+ZSP52+ZSP53 ZSP51+ZSP52+ZSP53+ZSP54
ZSP51+ZSP52+ZSP53+ZSP54+ZSP55 ZSP51+ZSP52+ZSP53+ZSP54+ZSP55+ZSP56];
matcumZSP5=[0 ZSP51 ZSP51+ZSP52 ZSP51+ZSP52+ZSP53 ZSP51+ZSP52+ZSP53+ZSP54
ZSP51+ZSP52+ZSP53+ZSP54+ZSP55];

matCUMZSP=[length(ZP1) length(ZP1)+length(ZP2) length(ZP1)+length(ZP2)+length(ZP3)
length(ZP1)+length(ZP2)+length(ZP3)+length(ZP4)
length(ZP1)+length(ZP2)+length(ZP3)+length(ZP4)+length(ZP5)];
matcumZSP=[0 length(ZP1) length(ZP1)+length(ZP2) length(ZP1)+length(ZP2)+length(ZP3)
length(ZP1)+length(ZP2)+length(ZP3)+length(ZP4)];

%%%%%%%%%%%%%%%%%%%%%%%%%%%%%%%%%%%%%%%%%%%%%%%%%%%%%%%%%%%%%%%%%%%%%%%%

PP = [P1; P1(end)+P2; P1(end)+P2(end)+P3; P1(end)+P2(end)+P3(end)+P4;
P1(end)+P2(end)+P3(end)+P4(end)+P5];

ZP = [ZP1; ZP1(end)+ZP2; ZP1(end)+ZP2(end)+ZP3; ZP1(end)+ZP2(end)+ZP3(end)+ZP4;
ZP1(end)+ZP2(end)+ZP3(end)+ZP4(end)+ZP5];

%%%%%%%%%%%%%%%%%%%%%%%%%%%%%%%%%%%%%%%%%%%%%%%%%%%%%%%%%%%%%%%%%%%%%%%%

%Input cycle number, each sequence each step

NP11=M2_11(:,1);
NP12=M2_12(:,1);
NP13=M2_13(:,1);
NP14=M2_14(:,1);
NP15=M2_15(:,1);
NP16=M2_16(:,1);

NP1= [NP11; NP12; NP13; NP14; NP15; NP16];
modNP1= [NP11(end); NP12(end); NP13(end); NP14(end); NP15(end); NP16(end)];

NP21=M2_21(:,1);
NP22=M2_22(:,1);
NP23=M2_23(:,1);
NP24=M2_24(:,1);
NP25=M2_25(:,1);
NP26=M2_26(:,1);

NP2= [NP21; NP22; NP23; NP24; NP25; NP26];
modNP2= [NP21(end); NP22(end); NP23(end); NP24(end); NP25(end); NP26(end)];

NP31=M2_31(:,1);
NP32=M2_32(:,1);
NP33=M2_33(:,1);
NP34=M2_34(:,1);
NP35=M2_35(:,1);
NP36=M2_36(:,1);

NP3= [NP31; NP32; NP33; NP34; NP35; NP36];
modNP3= [NP31(end); NP32(end); NP33(end); NP34(end); NP35(end); NP36(end)];

NP41=M2_41(:,1);
NP42=M2_42(:,1);
NP43=M2_43(:,1);
NP44=M2_44(:,1);
NP45=M2_45(:,1);
NP46=M2_46(:,1);

NP4= [NP41; NP42; NP43; NP44; NP45; NP46];
modNP4= [NP41(end); NP42(end); NP43(end); NP44(end); NP45(end); NP46(end)];

NP51=M2_51(:,1);

```

```

NP52=M2_52(:,1);
NP53=M2_53(:,1);
NP54=M2_54(:,1);
NP55=M2_55(:,1);
NP56=M2_56(:,1);

NP5= [NP51; NP52; NP53; NP54; NP55; NP56];
modNP5= [NP51(end); NP52(end); NP53(end); NP54(end); NP55(end); NP56(end)];

ZNP11=ZM2_11(:,1);
ZNP12=ZM2_12(:,1);
ZNP13=ZM2_13(:,1);
ZNP14=ZM2_14(:,1);
ZNP15=ZM2_15(:,1);
ZNP16=ZM2_16(:,1);

ZNP1= [ZNP11; ZNP12; ZNP13; ZNP14; ZNP15; ZNP16];
modZNP1= [ZNP11(end); ZNP12(end); ZNP13(end); ZNP14(end); ZNP15(end); ZNP16(end)];

ZNP21=ZM2_21(:,1);
ZNP22=ZM2_22(:,1);
ZNP23=ZM2_23(:,1);
ZNP24=ZM2_24(:,1);
ZNP25=ZM2_25(:,1);
ZNP26=ZM2_26(:,1);

ZNP2= [ZNP21; ZNP22; ZNP23; ZNP24; ZNP25; ZNP26];
modZNP2= [ZNP21(end); ZNP22(end); ZNP23(end); ZNP24(end); ZNP25(end); ZNP26(end)];

ZNP31=ZM2_31(:,1);
ZNP32=ZM2_32(:,1);
ZNP33=ZM2_33(:,1);
ZNP34=ZM2_34(:,1);
ZNP35=ZM2_35(:,1);
ZNP36=ZM2_36(:,1);

ZNP3= [ZNP31; ZNP32; ZNP33; ZNP34; ZNP35; ZNP36];
modZNP3= [ZNP31(end); ZNP32(end); ZNP33(end); ZNP34(end); ZNP35(end); ZNP36(end)];

ZNP41=ZM2_41(:,1);
ZNP42=ZM2_42(:,1);
ZNP43=ZM2_43(:,1);
ZNP44=ZM2_44(:,1);
ZNP45=ZM2_45(:,1);
ZNP46=ZM2_46(:,1);

ZNP4= [ZNP41; ZNP42; ZNP43; ZNP44; ZNP45; ZNP46];
modZNP4= [ZNP41(end); ZNP42(end); ZNP43(end); ZNP44(end); ZNP45(end); ZNP46(end)];

ZNP51=ZM2_51(:,1);
ZNP52=ZM2_52(:,1);
ZNP53=ZM2_53(:,1);
ZNP54=ZM2_54(:,1);
ZNP55=ZM2_55(:,1);
ZNP56=ZM2_56(:,1);

ZNP5= [ZNP51; ZNP52; ZNP53; ZNP54; ZNP55; ZNP56];
modZNP5= [ZNP51(end); ZNP52(end); ZNP53(end); ZNP54(end); ZNP55(end); ZNP56(end)];

%%%%%%%%%%%%%%%%%%%%%%%%%%%%%%%%%%%%%%%%%%%%%%%%%%%%%%%%%%%%%%%%%%%%%%%%

NP = [NP1; NP1(end)+NP2; NP1(end)+NP2(end)+NP3; NP1(end)+NP2(end)+NP3(end)+NP4;
NP1(end)+NP2(end)+NP3(end)+NP4(end)+NP5];

ZNP = [ZNP1; ZNP1(end)+ZNP2; ZNP1(end)+ZNP2(end)+ZNP3; ZNP1(end)+ZNP2(end)+ZNP3(end)+ZNP4;
ZNP1(end)+ZNP2(end)+ZNP3(end)+ZNP4(end)+ZNP5];

modNP = [modNP1; modNP1(end)+modNP2; modNP1(end)+modNP2(end)+modNP3;
modNP1(end)+modNP2(end)+modNP3(end)+modNP4;
modNP1(end)+modNP2(end)+modNP3(end)+modNP4(end)+modNP5];

modZNP = [modZNP1; modZNP1(end)+modZNP2; modZNP1(end)+modZNP2(end)+modZNP3;
modZNP1(end)+modZNP2(end)+modZNP3(end)+modZNP4;
modZNP1(end)+modZNP2(end)+modZNP3(end)+modZNP4(end)+modZNP5];

%%%%%%%%%%%%%%%%%%%%%%%%%%%%%%%%%%%%%%%%%%%%%%%%%%%%%%%%%%%%%%%%%%%%%%%%

%Input p and q stresses, each sequence each step

pP11=M2_11(:,3);
qP11=M2_11(:,4);
maxpP11=max(pP11);
maxqP11=max(qP11);
pP12=M2_12(:,3);

```



```

qp12=M2_12(:,4);
maxpp12=max(pp12);
maxqp12=max(qp12);
pp13=M2_13(:,3);
qp13=M2_13(:,4);
maxpp13=max(pp13);
maxqp13=max(qp13);
pp14=M2_14(:,3);
qp14=M2_14(:,4);
maxpp14=max(pp14);
maxqp14=max(qp14);
pp15=M2_15(:,3);
qp15=M2_15(:,4);
maxpp15=max(pp15);
maxqp15=max(qp15);
pp16=M2_16(:,3);
qp16=M2_16(:,4);
maxpp16=max(pp16);
maxqp16=max(qp16);

pp1=[ pp11 ; pp12 ; pp13 ; pp14 ; pp15 ; pp16];
qp1=[ qp11 ; qp12 ; qp13 ; qp14 ; qp15 ; qp16];
maxpP1=[ maxpP11 ; maxpP12 ; maxpP13 ; maxpP14 ; maxpP15 ; maxpP16];
maxqP1=[ maxqP11 ; maxqP12 ; maxqP13 ; maxqP14 ; maxqP15 ; maxqP16];

pp21=M2_21(:,3);
qp21=M2_21(:,4);
maxpp21=max(pp21);
maxqp21=max(qp21);
pp22=M2_22(:,3);
qp22=M2_22(:,4);
maxpp22=max(pp22);
maxqp22=max(qp22);
pp23=M2_23(:,3);
qp23=M2_23(:,4);
maxpp23=max(pp23);
maxqp23=max(qp23);
pp24=M2_24(:,3);
qp24=M2_24(:,4);
maxpp24=max(pp24);
maxqp24=max(qp24);
pp25=M2_25(:,3);
qp25=M2_25(:,4);
maxpp25=max(pp25);
maxqp25=max(qp25);
pp26=M2_26(:,3);
qp26=M2_26(:,4);
maxpp26=max(pp26);
maxqp26=max(qp26);

pp2=[ pp21 ; pp22 ; pp23 ; pp24 ; pp25 ; pp26];
qp2=[ qp21 ; qp22 ; qp23 ; qp24 ; qp25 ; qp26];
maxpP2=[ maxpP21 ; maxpP22 ; maxpP23 ; maxpP24 ; maxpP25 ; maxpP26];
maxqP2=[ maxqP21 ; maxqP22 ; maxqP23 ; maxqP24 ; maxqP25 ; maxqP26];

pp31=M2_31(:,3);
qp31=M2_31(:,4);
maxpp31=max(pp31);
maxqp31=max(qp31);
pp32=M2_32(:,3);
qp32=M2_32(:,4);
maxpp32=max(pp32);
maxqp32=max(qp32);
pp33=M2_33(:,3);
qp33=M2_33(:,4);
maxpp33=max(pp33);
maxqp33=max(qp33);
pp34=M2_34(:,3);
qp34=M2_34(:,4);
maxpp34=max(pp34);
maxqp34=max(qp34);
pp35=M2_35(:,3);
qp35=M2_35(:,4);
maxpp35=max(pp35);
maxqp35=max(qp35);
pp36=M2_36(:,3);
qp36=M2_36(:,4);
maxpp36=max(pp36);
maxqp36=max(qp36);

pp3=[ pp31 ; pp32 ; pp33 ; pp34 ; pp35 ; pp36];
qp3=[ qp31 ; qp32 ; qp33 ; qp34 ; qp35 ; qp36];
maxpP3=[ maxpP31 ; maxpP32 ; maxpP33 ; maxpP34 ; maxpP35 ; maxpP36];
maxqP3=[ maxqP31 ; maxqP32 ; maxqP33 ; maxqP34 ; maxqP35 ; maxqP36];

```

```

pP41=M2_41(:,3);
qP41=M2_41(:,4);
maxpP41=max(pP41);
maxqP41=max(qP41);
pP42=M2_42(:,3);
qP42=M2_42(:,4);
maxpP42=max(pP42);
maxqP42=max(qP42);
pP43=M2_43(:,3);
qP43=M2_43(:,4);
maxpP43=max(pP43);
maxqP43=max(qP43);
pP44=M2_44(:,3);
qP44=M2_44(:,4);
maxpP44=max(pP44);
maxqP44=max(qP44);
pP45=M2_45(:,3);
qP45=M2_45(:,4);
maxpP45=max(pP45);
maxqP45=max(qP45);
pP46=M2_46(:,3);
qP46=M2_46(:,4);
maxpP46=max(pP46);
maxqP46=max(qP46);

pP4=[ pP41 ; pP42 ; pP43 ; pP44 ; pP45 ; pP46];
qP4=[ qP41 ; qP42 ; qP43 ; qP44 ; qP45 ; qP46];
maxpP4=[ maxpP41 ; maxpP42 ; maxpP43 ; maxpP44 ; maxpP45 ; maxpP46];
maxqP4=[ maxqP41 ; maxqP42 ; maxqP43 ; maxqP44 ; maxqP45 ; maxqP46];

pP51=M2_51(:,3);
qP51=M2_51(:,4);
maxpP51=max(pP51);
maxqP51=max(qP51);
pP52=M2_52(:,3);
qP52=M2_52(:,4);
maxpP52=max(pP52);
maxqP52=max(qP52);
pP53=M2_53(:,3);
qP53=M2_53(:,4);
maxpP53=max(pP53);
maxqP53=max(qP53);
pP54=M2_54(:,3);
qP54=M2_54(:,4);
maxpP54=max(pP54);
maxqP54=max(qP54);
pP55=M2_55(:,3);
qP55=M2_55(:,4);
maxpP55=max(pP55);
maxqP55=max(qP55);
pP56=M2_56(:,3);
qP56=M2_56(:,4);
maxpP56=max(pP56);
maxqP56=max(qP56);

pP5=[ pP51 ; pP52 ; pP53 ; pP54 ; pP55 ; pP56];
qP5=[ qP51 ; qP52 ; qP53 ; qP54 ; qP55 ; qP56];
maxpP5=[ maxpP51 ; maxpP52 ; maxpP53 ; maxpP54 ; maxpP55 ; maxpP56];
maxqP5=[ maxqP51 ; maxqP52 ; maxqP53 ; maxqP54 ; maxqP55 ; maxqP56];

ZpP11=ZM2_11(:,3);
ZqP11=ZM2_11(:,4);
maxZpP11=max(ZpP11);
maxZqP11=max(ZqP11);
ZpP12=ZM2_12(:,3);
ZqP12=ZM2_12(:,4);
maxZpP12=max(ZpP12);
maxZqP12=max(ZqP12);
ZpP13=ZM2_13(:,3);
ZqP13=ZM2_13(:,4);
maxZpP13=max(ZpP13);
maxZqP13=max(ZqP13);
ZpP14=ZM2_14(:,3);
ZqP14=ZM2_14(:,4);
maxZpP14=max(ZpP14);
maxZqP14=max(ZqP14);
ZpP15=ZM2_15(:,3);
ZqP15=ZM2_15(:,4);
maxZpP15=max(ZpP15);
maxZqP15=max(ZqP15);
ZpP16=ZM2_16(:,3);
ZqP16=ZM2_16(:,4);
maxZpP16=max(ZpP16);
maxZqP16=max(ZqP16);

```

```

ZpP1=[ ZpP11 ; ZpP12 ; ZpP13 ; ZpP14 ; ZpP15 ; ZpP16];
ZqP1=[ ZqP11 ; ZqP12 ; ZqP13 ; ZqP14 ; ZqP15 ; ZqP16];
maxZpP1=[ maxZpP11 ; maxZpP12 ; maxZpP13 ; maxZpP14 ; maxZpP15 ; maxZpP16];
maxZqP1=[ maxZqP11 ; maxZqP12 ; maxZqP13 ; maxZqP14 ; maxZqP15 ; maxZqP16];

ZpP21=ZM2_21(:, 3);
ZqP21=ZM2_21(:, 4);
maxZpP21=max(ZpP21);
maxZqP21=max(ZqP21);
ZpP22=ZM2_22(:, 3);
ZqP22=ZM2_22(:, 4);
maxZpP22=max(ZpP22);
maxZqP22=max(ZqP22);
ZpP23=ZM2_23(:, 3);
ZqP23=ZM2_23(:, 4);
maxZpP23=max(ZpP23);
maxZqP23=max(ZqP23);
ZpP24=ZM2_24(:, 3);
ZqP24=ZM2_24(:, 4);
maxZpP24=max(ZpP24);
maxZqP24=max(ZqP24);
ZpP25=ZM2_25(:, 3);
ZqP25=ZM2_25(:, 4);
maxZpP25=max(ZpP25);
maxZqP25=max(ZqP25);
ZpP26=ZM2_26(:, 3);
ZqP26=ZM2_26(:, 4);
maxZpP26=max(ZpP26);
maxZqP26=max(ZqP26);

ZpP2=[ ZpP21 ; ZpP22 ; ZpP23 ; ZpP24 ; ZpP25 ; ZpP26];
ZqP2=[ ZqP21 ; ZqP22 ; ZqP23 ; ZqP24 ; ZqP25 ; ZqP26];
maxZpP2=[ maxZpP21 ; maxZpP22 ; maxZpP23 ; maxZpP24 ; maxZpP25 ; maxZpP26];
maxZqP2=[ maxZqP21 ; maxZqP22 ; maxZqP23 ; maxZqP24 ; maxZqP25 ; maxZqP26];

ZpP31=ZM2_31(:, 3);
ZqP31=ZM2_31(:, 4);
maxZpP31=max(ZpP31);
maxZqP31=max(ZqP31);
ZpP32=ZM2_32(:, 3);
ZqP32=ZM2_32(:, 4);
maxZpP32=max(ZpP32);
maxZqP32=max(ZqP32);
ZpP33=ZM2_33(:, 3);
ZqP33=ZM2_33(:, 4);
maxZpP33=max(ZpP33);
maxZqP33=max(ZqP33);
ZpP34=ZM2_34(:, 3);
ZqP34=ZM2_34(:, 4);
maxZpP34=max(ZpP34);
maxZqP34=max(ZqP34);
ZpP35=ZM2_35(:, 3);
ZqP35=ZM2_35(:, 4);
maxZpP35=max(ZpP35);
maxZqP35=max(ZqP35);
ZpP36=ZM2_36(:, 3);
ZqP36=ZM2_36(:, 4);
maxZpP36=max(ZpP36);
maxZqP36=max(ZqP36);

ZpP3=[ ZpP31 ; ZpP32 ; ZpP33 ; ZpP34 ; ZpP35 ; ZpP36];
ZqP3=[ ZqP31 ; ZqP32 ; ZqP33 ; ZqP34 ; ZqP35 ; ZqP36];
maxZpP3=[ maxZpP31 ; maxZpP32 ; maxZpP33 ; maxZpP34 ; maxZpP35 ; maxZpP36];
maxZqP3=[ maxZqP31 ; maxZqP32 ; maxZqP33 ; maxZqP34 ; maxZqP35 ; maxZqP36];

ZpP41=ZM2_41(:, 3);
ZqP41=ZM2_41(:, 4);
maxZpP41=max(ZpP41);
maxZqP41=max(ZqP41);
ZpP42=ZM2_42(:, 3);
ZqP42=ZM2_42(:, 4);
maxZpP42=max(ZpP42);
maxZqP42=max(ZqP42);
ZpP43=ZM2_43(:, 3);
ZqP43=ZM2_43(:, 4);
maxZpP43=max(ZpP43);
maxZqP43=max(ZqP43);
ZpP44=ZM2_44(:, 3);
ZqP44=ZM2_44(:, 4);
maxZpP44=max(ZpP44);
maxZqP44=max(ZqP44);
ZpP45=ZM2_45(:, 3);
ZqP45=ZM2_45(:, 4);
maxZpP45=max(ZpP45);

```

```

maxZqP45=max(ZqP45);
ZpP46=ZM2_46(:,3);
ZqP46=ZM2_46(:,4);
maxZpP46=max(ZpP46);
maxZqP46=max(ZqP46);

ZpP4=[ ZpP41 ; ZpP42 ; ZpP43 ; ZpP44 ; ZpP45 ; ZpP46];
ZqP4=[ ZqP41 ; ZqP42 ; ZqP43 ; ZqP44 ; ZqP45 ; ZqP46];
maxZpP4=[ maxZpP41 ; maxZpP42 ; maxZpP43 ; maxZpP44 ; maxZpP45 ; maxZpP46];
maxZqP4=[ maxZqP41 ; maxZqP42 ; maxZqP43 ; maxZqP44 ; maxZqP45 ; maxZqP46];

ZpP51=ZM2_51(:,3);
ZqP51=ZM2_51(:,4);
maxZpP51=max(ZpP51);
maxZqP51=max(ZqP51);
ZpP52=ZM2_52(:,3);
ZqP52=ZM2_52(:,4);
maxZpP52=max(ZpP52);
maxZqP52=max(ZqP52);
ZpP53=ZM2_53(:,3);
ZqP53=ZM2_53(:,4);
maxZpP53=max(ZpP53);
maxZqP53=max(ZqP53);
ZpP54=ZM2_54(:,3);
ZqP54=ZM2_54(:,4);
maxZpP54=max(ZpP54);
maxZqP54=max(ZqP54);
ZpP55=ZM2_55(:,3);
ZqP55=ZM2_55(:,4);
maxZpP55=max(ZpP55);
maxZqP55=max(ZqP55);
ZpP56=ZM2_56(:,3);
ZqP56=ZM2_56(:,4);
maxZpP56=max(ZpP56);
maxZqP56=max(ZqP56);

ZpP5=[ ZpP51 ; ZpP52 ; ZpP53 ; ZpP54 ; ZpP55 ; ZpP56];
ZqP5=[ ZqP51 ; ZqP52 ; ZqP53 ; ZqP54 ; ZqP55 ; ZqP56];
maxZpP5=[ maxZpP51 ; maxZpP52 ; maxZpP53 ; maxZpP54 ; maxZpP55 ; maxZpP56];
maxZqP5=[ maxZqP51 ; maxZqP52 ; maxZqP53 ; maxZqP54 ; maxZqP55 ; maxZqP56];

%%%%%%%%%%%%%%%%%%%%%%%%%%%%%%%%%%%%%%%%%%%%%%%%%%%%%%%%%%%%%%%%%%%%%%%%

pP = [pP1; pP2; pP3; pP4; pP5];
qP = [qP1; qP2; qP3; qP4; qP5];

ZpP = [ZpP1; ZpP2; ZpP3; ZpP4; ZpP5];
ZqP = [ZqP1; ZqP2; ZqP3; ZqP4; ZqP5];

%%%%%%%%%%%%%%%%%%%%%%%%%%%%%%%%%%%%%%%%%%%%%%%%%%%%%%%%%%%%%%%%%%%%%%%%

%Experimental data, N cycles

figure(1);
set(gcf, 'DefaultAxesFontName', 'Times New Roman');

hold on
scatter(NP,PP,1,'k');
scatter(ZNP,ZP,1,'MarkerEdgeColor',[0.75, 0, 0.75]);

xlabel('N , Cycle number','FontSize',16,'fontWeight','bold');
ylabel([char(949) , '_{vp}'; Accumulated vert. perm. strain
(char(8240) , ')'],'FontSize',16,'fontWeight','bold');
legend({'M2','M2-P'},'Location','northwest','FontSize',18);

grid on
set(gca,'XLim',[0 300000],'XTick',(0:60000:300000),'FontSize',16)
set(gca,'YLim',[0 14],'YTick',(0:2:14),'FontSize',16)
hold off

print 01_Permanent_deformation_curves_N_cycles -djpeg

figure(2);
set(gcf, 'DefaultAxesFontName', 'Times New Roman');

hold on
scatter(NP,PP,1,'k');
scatter(modNP,M2TRHM,24,'s','k');
scatter(modNP,M2TRUZ,24,'d','k');
scatter(modNP,M2TRUW,24,'p','k');
scatter(ZNP,ZP,1,'MarkerEdgeColor',[0.75, 0, 0.75]);
scatter(modZNP,M2TRHM,24,'s','MarkerEdgeColor',[0.75, 0, 0.75]);
scatter(modZNP,M2TRUZ,24,'d','MarkerEdgeColor',[0.75, 0, 0.75]);
scatter(modZNP,M2TRUW,24,'p','MarkerEdgeColor',[0.75, 0, 0.75]);

```

```

xlabel('N, Cycle number','FontSize',16,'fontWeight','bold');
ylabel([char(949), '_{vp} Accumulated vert. perm. strain
(char(8240), ')'], 'FontSize',16,'fontWeight','bold');
legend({'M2', M2 Hicks&Monismith, 'M2 Uzan', 'M2 Uzan&Witczak', 'M2-P', 'M2-P
Hicks&Monismith', 'M2-P Uzan', 'M2-P Uzan&Witczak'}, 'Location', 'northwest', 'FontSize',14);

grid on
set(gca, 'XLim', [0 300000], 'XTick', (0:60000:300000), 'FontSize',16)
set(gca, 'YLim', [0 20], 'YTick', (0:2:20), 'FontSize',16)
hold off

print 02_Permanent_deformation_curves_N_cycles_stationary_Tresca -djpeg

figure(3);
set(gcf, 'DefaultAxesFontName', 'Times New Roman');

hold on
scatter(NP, PP, 1, 'k');
scatter(modNP, M2VMHM, 24, 's', 'k');
scatter(modNP, M2VMUZ, 24, 'd', 'k');
scatter(modNP, M2VMUW, 24, 'p', 'k');
scatter(ZNP, ZP, 1, 'MarkerEdgeColor', [0.75, 0, 0.75]);
scatter(modZNP, ZM2VMHM, 24, 's', 'MarkerEdgeColor', [0.75, 0, 0.75]);
scatter(modZNP, ZM2VMUZ, 24, 'd', 'MarkerEdgeColor', [0.75, 0, 0.75]);
scatter(modZNP, ZM2VMUW, 24, 'p', 'MarkerEdgeColor', [0.75, 0, 0.75]);

xlabel('N, Cycle number','FontSize',16,'fontWeight','bold');
ylabel([char(949), '_{vp} Accumulated vert. perm. strain
(char(8240), ')'], 'FontSize',16,'fontWeight','bold');
legend({'M2', M2 Hicks&Monismith, 'M2 Uzan', 'M2 Uzan&Witczak', 'M2-P', 'M2-P
Hicks&Monismith', 'M2-P Uzan', 'M2-P Uzan&Witczak'}, 'Location', 'northwest', 'FontSize',14);

grid on
set(gca, 'XLim', [0 300000], 'XTick', (0:60000:300000), 'FontSize',16)
set(gca, 'YLim', [0 20], 'YTick', (0:2:20), 'FontSize',16)
hold off

print 03_Permanent_deformation_curves_N_cycles_stationary_Von_Mises -djpeg

figure(4);
set(gcf, 'DefaultAxesFontName', 'Times New Roman');

hold on
scatter(NP, PP, 1, 'k');
scatter([0:10000:300000], M2BTRHM, 24, 's', 'k');
scatter([0:10000:300000], M2BTRUZ, 24, 'd', 'k');
scatter([0:10000:300000], M2BTRUW, 24, 'p', 'k');
scatter(ZNP, ZP, 1, 'MarkerEdgeColor', [0.75, 0, 0.75]);
scatter([0:10000:300000], ZM2BTRHM, 24, 's', 'MarkerEdgeColor', [0.75, 0, 0.75]);
scatter([0:10000:300000], ZM2BTRUZ, 24, 'd', 'MarkerEdgeColor', [0.75, 0, 0.75]);
scatter([0:10000:300000], ZM2BTRUW, 24, 'p', 'MarkerEdgeColor', [0.75, 0, 0.75]);

xlabel('N, Cycle number','FontSize',16,'fontWeight','bold');
ylabel([char(949), '_{vp} Accumulated vert. perm. strain
(char(8240), ')'], 'FontSize',16,'fontWeight','bold');
legend({'M2', M2 Hicks&Monismith, 'M2 Uzan', 'M2 Uzan&Witczak', 'M2-P', 'M2-P
Hicks&Monismith', 'M2-P Uzan', 'M2-P Uzan&Witczak'}, 'Location', 'northwest', 'FontSize',14);

grid on
set(gca, 'XLim', [0 300000], 'XTick', (0:60000:300000), 'FontSize',16)
set(gca, 'YLim', [0 22], 'YTick', (0:2:22), 'FontSize',16)
hold off

print 04_Permanent_deformation_curves_N_cycles_time_dependent_Tresca -djpeg

figure(5);
set(gcf, 'DefaultAxesFontName', 'Times New Roman');

hold on
scatter(NP, PP, 1, 'k');
scatter([0:10000:300000], M2BVMHM, 24, 's', 'k');
scatter([0:10000:300000], M2BVMUZ, 24, 'd', 'k');
scatter([0:10000:300000], M2BVMUW, 24, 'p', 'k');
scatter(ZNP, ZP, 1, 'MarkerEdgeColor', [0.75, 0, 0.75]);
scatter([0:10000:300000], ZM2BVMHM, 24, 's', 'MarkerEdgeColor', [0.75, 0, 0.75]);
scatter([0:10000:300000], ZM2BVMUZ, 24, 'd', 'MarkerEdgeColor', [0.75, 0, 0.75]);
scatter([0:10000:300000], ZM2BVMUW, 24, 'p', 'MarkerEdgeColor', [0.75, 0, 0.75]);

xlabel('N, Cycle number','FontSize',16,'fontWeight','bold');
ylabel([char(949), '_{vp} Accumulated vert. perm. strain
(char(8240), ')'], 'FontSize',16,'fontWeight','bold');
legend({'M2', M2 Hicks&Monismith, 'M2 Uzan', 'M2 Uzan&Witczak', 'M2-P', 'M2-P
Hicks&Monismith', 'M2-P Uzan', 'M2-P Uzan&Witczak'}, 'Location', 'northwest', 'FontSize',14);

grid on

```

```

set(gca,'xLim',[0 300000],'xTick',(0:60000:300000),'FontSize',16)
set(gca,'yLim',[0 22],'yTick',(0:2:22),'FontSize',16)
hold off

print 05_Permanent_deformation_curves_N_cycles_time_dependent_Von_Mises -djpeg

figure(6);
set(gcf,'DefaultAxesFontName','Times New Roman');

hold on
scatter(NP,PP,1,'k');
scatter([0:10000:300000],M2BVMHM,24,'s','k');
scatter([0:10000:300000],M2BVMHM+S11,24,'h','k');
scatter(ZNP,ZP,1,'MarkerEdgeColor',[0.75 0 0.75]);
scatter([0:10000:300000],ZM2BVMHM,24,'s','MarkerEdgeColor',[0.75 0 0.75]);
scatter([0:10000:300000],ZM2BVMHM+ZS9,24,'h','MarkerEdgeColor',[0.75 0 0.75]);

xlabel('N, Cycle number','FontSize',16,'fontWeight','bold');
ylabel([char(949) '_{vp}'; Accumulated vert. perm. strain
(char(8240) ' ')], 'FontSize',16,'fontWeight','bold');
legend({'M2',M2 Hicks&Monismith,'M2-P',M2-P
Hicks&Monismith,'M2-P Hicks&Monismith, creep'},'Location','northwest','FontSize',14);

grid on
set(gca,'xLim',[0 300000],'xTick',(0:60000:300000),'FontSize',16)
set(gca,'yLim',[0 22],'yTick',(0:2:22),'FontSize',16)
hold off

print 06_Permanent_deformation_curves_N_cycles_time_dependent_creep_Von_Mises -djpeg

%%%%%%%%%%%%%%%%%%%%%%%%%%%%%%%%%%%%%%%%%%%%%%%%%%%%%%%%%%%%%%%%%%%%%%%%
%Experimental data, q stress

figure(7);
set(gcf,'DefaultAxesFontName','Times New Roman');

hold on
scatter(qP./(pP-qP),PP,10,'k');
scatter(ZqP./(ZpP-ZqP),ZP,10,'MarkerEdgeColor',[0.75 0 0.75]);

xlabel('q/\sigma_t (-)','FontSize',16,'fontWeight','bold');
ylabel([char(949) '_{vp}'; Accumulated vert. perm. strain
(char(8240) ' ')], 'FontSize',16,'fontWeight','bold');
legend({'M2',M2-P'},'Location','northwest','FontSize',18);

grid on
set(gca,'xLim',[0 2.2],'xTick',(0:0.2:2.2),'FontSize',16)
set(gca,'yLim',[0 14],'yTick',(0:2:14),'FontSize',16)
hold off

print 07_Permanent_deformation_curves_q_p_stress -djpeg

figure(8);
set(gcf,'DefaultAxesFontName','Times New Roman');

hold on

for j=1:5;

WP=PP(matcumSP(1,j)+1:matCUMSP(1,j));
wpP=pP(matcumSP(1,j)+1:matCUMSP(1,j));
wqP=qP(matcumSP(1,j)+1:matCUMSP(1,j));
[wqPmax, loc]=max(wqP);

wZP=ZP(matcumZSP(1,j)+1:matCUMZSP(1,j));
wZpP=ZpP(matcumZSP(1,j)+1:matCUMZSP(1,j));
wZqP=ZqP(matcumZSP(1,j)+1:matCUMZSP(1,j));
[wZqPmax, Zloc]=max(wZqP);

scatter(wqPmax./(wpP-wqP),wP,10,'k');
scatter(wZqPmax./(wZpP-wZqP),wZP,10,'MarkerEdgeColor',[0.75 0 0.75]);
end

xlabel('q_{max}/\sigma_t (-)','FontSize',16,'fontWeight','bold');
ylabel([char(949) '_{vp}'; Accumulated vert. perm. strain
(char(8240) ' ')], 'FontSize',16,'fontWeight','bold');
legend({'M2',M2-P'},'Location','northwest','FontSize',18);

grid on
set(gca,'xLim',[1 2.2],'xTick',(1:0.2:2.2),'FontSize',16)
set(gca,'yLim',[0 14],'yTick',(0:2:14),'FontSize',16)
hold off

print 08_Permanent_deformation_curves_qmax_p_stress -djpeg

```

```

%%%%%%%%%%%%%%%%%%%%%%%%%%%%%%%%%%%%%%%%%%%%%%%%%%%%%%%%%%%%%%%%%%%%%%%%
% Tresca model, plastic tangent modulus

syms a b

yTR=qP;
SyTR=size(yTR,1);
xTR=PP;

eq1=ones(1,SyTR)*(yTR-a*ones(1,SyTR)'+b*xTR);
eq2=xTR'*(yTR-a*ones(1,SyTR)'+b*xTR);

[a,b]=solve([eq1==0,eq2==0],[a,b]);
aTR=double(a)
bTR=double(b)

syms a b

yTR=ZqP;
SyTR=size(yTR,1);
xTR=ZP;

eq1=ones(1,SyTR)*(yTR-a*ones(1,SyTR)'+b*xTR);
eq2=xTR'*(yTR-a*ones(1,SyTR)'+b*xTR);

[a,b]=solve([eq1==0,eq2==0],[a,b]);
ZaTR=double(a)
ZbTR=double(b)

syms a b

yTR=qP1;
SyTR=size(yTR,1);
xTR=P1/1000;

eq1=ones(1,SyTR)*(yTR-a*ones(1,SyTR)'+b*xTR);
eq2=xTR'*(yTR-a*ones(1,SyTR)'+b*xTR);

[a,b]=solve([eq1==0,eq2==0],[a,b]);
bTR1=double(b)

syms a b

yTR=qP2;
SyTR=size(yTR,1);
xTR=P2/1000;

eq1=ones(1,SyTR)*(yTR-a*ones(1,SyTR)'+b*xTR);
eq2=xTR'*(yTR-a*ones(1,SyTR)'+b*xTR);

[a,b]=solve([eq1==0,eq2==0],[a,b]);
bTR2=double(b)

syms a b

yTR=qP3;
SyTR=size(yTR,1);
xTR=P3/1000;

eq1=ones(1,SyTR)*(yTR-a*ones(1,SyTR)'+b*xTR);
eq2=xTR'*(yTR-a*ones(1,SyTR)'+b*xTR);

[a,b]=solve([eq1==0,eq2==0],[a,b]);
bTR3=double(b)

syms a b

yTR=qP4;
SyTR=size(yTR,1);
xTR=P4/1000;

eq1=ones(1,SyTR)*(yTR-a*ones(1,SyTR)'+b*xTR);
eq2=xTR'*(yTR-a*ones(1,SyTR)'+b*xTR);

[a,b]=solve([eq1==0,eq2==0],[a,b]);
bTR4=double(b)

syms a b

yTR=qP5;
SyTR=size(yTR,1);
xTR=P5/1000;

```



```

eq1=ones(1,SyTR)*(yTR-a*ones(1,SyTR)'-b*xTR);
eq2=xTR'(yTR-a*ones(1,SyTR)'-b*xTR);

[a,b]=solve([eq1==0,eq2==0],[a,b]);
bTR5=double(b)

syms a b
yTR=ZqP1;
SyTR=size(yTR,1);
xTR=ZP1/1000;

eq1=ones(1,SyTR)*(yTR-a*ones(1,SyTR)'-b*xTR);
eq2=xTR'(yTR-a*ones(1,SyTR)'-b*xTR);

[a,b]=solve([eq1==0,eq2==0],[a,b]);
ZbTR1=double(b)

syms a b
yTR=ZqP2;
SyTR=size(yTR,1);
xTR=ZP2/1000;

eq1=ones(1,SyTR)*(yTR-a*ones(1,SyTR)'-b*xTR);
eq2=xTR'(yTR-a*ones(1,SyTR)'-b*xTR);

[a,b]=solve([eq1==0,eq2==0],[a,b]);
ZbTR2=double(b)

syms a b
yTR=ZqP3;
SyTR=size(yTR,1);
xTR=ZP3/1000;

eq1=ones(1,SyTR)*(yTR-a*ones(1,SyTR)'-b*xTR);
eq2=xTR'(yTR-a*ones(1,SyTR)'-b*xTR);

[a,b]=solve([eq1==0,eq2==0],[a,b]);
ZbTR3=double(b)

syms a b
yTR=ZqP4;
SyTR=size(yTR,1);
xTR=ZP4/1000;

eq1=ones(1,SyTR)*(yTR-a*ones(1,SyTR)'-b*xTR);
eq2=xTR'(yTR-a*ones(1,SyTR)'-b*xTR);

[a,b]=solve([eq1==0,eq2==0],[a,b]);
ZbTR4=double(b)

syms a b
yTR=ZqP5;
SyTR=size(yTR,1);
xTR=ZP5/1000;

eq1=ones(1,SyTR)*(yTR-a*ones(1,SyTR)'-b*xTR);
eq2=xTR'(yTR-a*ones(1,SyTR)'-b*xTR);

[a,b]=solve([eq1==0,eq2==0],[a,b]);
ZbTR5=double(b)

%%%%%%%%%%%%%%%%%%%%%%%%%%%%%%%%%%%%%%%%%%%%%%%%%%%%%%%%%%%%%%%%%%%%%%%%
% Von Mises model, plastic tangent modulus

syms a b
yVM=qP;
SyVM=size(yVM,1);
xVM=(2/3)*PP;

eq1=ones(1,SyVM)*(yVM-a*ones(1,SyVM)'-b*xVM);
eq2=xVM'(yVM-a*ones(1,SyVM)'-b*xVM);

[a,b]=solve([eq1==0,eq2==0],[a,b]);
aVM=double(a)
bVM=double(b)

```

```

syms a b

yVM=ZqP;
SyVM=size(yVM,1);
xVM=(2/3)*ZP;

eq1=ones(1,SyVM)*(yVM-a*ones(1,SyVM)'+b*xVM);
eq2=xVM*(yVM-a*ones(1,SyVM)'+b*xVM);

[a,b]=solve([eq1==0,eq2==0],[a,b]);
ZaVM=double(a)
ZbVM=double(b)

syms a b

yVM=qP1;
SyVM=size(yVM,1);
xVM=(2/3)*P1/1000;

eq1=ones(1,SyVM)*(yVM-a*ones(1,SyVM)'+b*xVM);
eq2=xVM*(yVM-a*ones(1,SyVM)'+b*xVM);

[a,b]=solve([eq1==0,eq2==0],[a,b]);
bVM1=double(b)

syms a b

yVM=qP2;
SyVM=size(yVM,1);
xVM=(2/3)*P2/1000;

eq1=ones(1,SyVM)*(yVM-a*ones(1,SyVM)'+b*xVM);
eq2=xVM*(yVM-a*ones(1,SyVM)'+b*xVM);

[a,b]=solve([eq1==0,eq2==0],[a,b]);
bVM2=double(b)

syms a b

yVM=qP3;
SyVM=size(yVM,1);
xVM=(2/3)*P3/1000;

eq1=ones(1,SyVM)*(yVM-a*ones(1,SyVM)'+b*xVM);
eq2=xVM*(yVM-a*ones(1,SyVM)'+b*xVM);

[a,b]=solve([eq1==0,eq2==0],[a,b]);
bVM3=double(b)

syms a b

yVM=qP4;
SyVM=size(yVM,1);
xVM=(2/3)*P4/1000;

eq1=ones(1,SyVM)*(yVM-a*ones(1,SyVM)'+b*xVM);
eq2=xVM*(yVM-a*ones(1,SyVM)'+b*xVM);

[a,b]=solve([eq1==0,eq2==0],[a,b]);
bVM4=double(b)

syms a b

yVM=qP5;
SyVM=size(yVM,1);
xVM=(2/3)*P5/1000;

eq1=ones(1,SyVM)*(yVM-a*ones(1,SyVM)'+b*xVM);
eq2=xVM*(yVM-a*ones(1,SyVM)'+b*xVM);

[a,b]=solve([eq1==0,eq2==0],[a,b]);
bVM5=double(b)

syms a b

yVM=ZqP1;
SyVM=size(yVM,1);
xVM=(2/3)*ZP1/1000;

eq1=ones(1,SyVM)*(yVM-a*ones(1,SyVM)'+b*xVM);
eq2=xVM*(yVM-a*ones(1,SyVM)'+b*xVM);

[a,b]=solve([eq1==0,eq2==0],[a,b]);

```

```

ZbVM1=double(b)

syms a b

yVM=ZqP2;
SyVM=size(yVM,1);
xVM=(2/3)*ZP2/1000;

eq1=ones(1,SyVM)*(yVM-a*ones(1,SyVM)'+b*xVM);
eq2=xVM*(yVM-a*ones(1,SyVM)'+b*xVM);

[a,b]=solve([eq1==0,eq2==0],[a,b]);
ZbVM2=double(b)

syms a b

yVM=ZqP3;
SyVM=size(yVM,1);
xVM=(2/3)*ZP3/1000;

eq1=ones(1,SyVM)*(yVM-a*ones(1,SyVM)'+b*xVM);
eq2=xVM*(yVM-a*ones(1,SyVM)'+b*xVM);

[a,b]=solve([eq1==0,eq2==0],[a,b]);
ZbVM3=double(b)

syms a b

yVM=ZqP4;
SyVM=size(yVM,1);
xVM=(2/3)*ZP4/1000;

eq1=ones(1,SyVM)*(yVM-a*ones(1,SyVM)'+b*xVM);
eq2=xVM*(yVM-a*ones(1,SyVM)'+b*xVM);

[a,b]=solve([eq1==0,eq2==0],[a,b]);
ZbVM4=double(b)

syms a b

yVM=ZqP5;
SyVM=size(yVM,1);
xVM=(2/3)*ZP5/1000;

eq1=ones(1,SyVM)*(yVM-a*ones(1,SyVM)'+b*xVM);
eq2=xVM*(yVM-a*ones(1,SyVM)'+b*xVM);

[a,b]=solve([eq1==0,eq2==0],[a,b]);
ZbVM5=double(b)

%%%%%%%%%%%%%%%%%%%%%%%%%%%%%%%%%%%%%%%%%%%%%%%%%%%%%%%%%%%%%%%%%%%%%%%%

%Barksdale model

figure(09)
set(gcf,'DefaultAxesFontName','Times New Roman');

hold on
xlabel('N , Cycle number','FontSize',16,'fontWeight','bold');
ylabel(['char(949)_{vp} , Accumulated vert. perm. strain',
(char(8240),')'],'FontSize',16,'fontWeight','bold');

grid on
set(gca,'Xlim',[0 300000],'XTick',(0:60000:300000),'FontSize',16)
set(gca,'Ylim',[0 14],'YTick',(0:2:14),'FontSize',16)

for j=1:6;

P=P1(matcumSP1(1,j)+1:matcumSP1(1,j));
FP=P1(matcumSP1(1,j)+1:matcumSP1(1,j)+matSFP1(1,j));
NP=NP1(matcumSP1(1,j)+1:matcumSP1(1,j));
FNP=NP1(matcumSP1(1,j)+1:matcumSP1(1,j)+matSFP1(1,j));

syms Fa Fb Fc

eq1=FNP.^2*(FP-Fa*FNP.^2-Fb*FNP.^2-Fc*ones(1,size(FNP,1)))';
eq2=FNP.^1*(FP-Fa*FNP.^2-Fb*FNP.^2-Fc*ones(1,size(FNP,1)))';
eq3=ones(1,size(FNP,1))*(FP-Fa*FNP.^2-Fb*FNP.^2-Fc*ones(1,size(FNP,1)))';

[Fa,Fb,Fc]=solve([eq1==0,eq2==0,eq3==0],[Fa,Fb,Fc]);

x=(-Fb+sqrt(Fb^2-4*Fa*Fc))/(2*Fa);
x=double(real(x));
par=Fa*FNP.^2+Fb*FNP.^1+Fc;

```

```

if x<0;
    x=0.01;
end

syms a b

MP=[0; P];
MSP=size(MP,1);
MNP=[x; NP];
MnP=log10(MNP);
nP=log10(NP);

eq1=ones(1,MSP)*(MP-a*ones(1,MSP)'-b*MnP);
eq2=MnP*(MP-a*ones(1,MSP)'-b*MnP);

[a,b]=solve([eq1==0,eq2==0],[a,b]);

PBA=a+b*nP;

plot(NP,PBA,'-k','Linewidth',1.2);

R2_1=1-(sum(MP(:,1)-(a+b*MnP(:,1)))^2)/(sum(MP(:,1)-sum(MP(:,1),MSP))^2);
%
P=ZP1(matcumZSP1(1,j)+1:matCUMZSP1(1,j));
FP=ZP1(matcumZSP1(1,j)+1:matcumZSP1(1,j)+matZSFP1(1,j));
NP=ZNP1(matcumZSP1(1,j)+1:matcumZSP1(1,j));
FNP=ZNP1(matcumZSP1(1,j)+1:matcumZSP1(1,j)+matZSFP1(1,j));

syms Fa Fb Fc

eq1=FNP'.^2*(FP-Fa*FNP.^2-Fb*FNP.^1-Fc*ones(1,size(FNP,1)))';
eq2=FNP'.^1*(FP-Fa*FNP.^2-Fb*FNP.^1-Fc*ones(1,size(FNP,1)))';
eq3=ones(1,size(FNP,1))*(FP-Fa*FNP.^2-Fb*FNP.^1-Fc*ones(1,size(FNP,1)))';

[Fa,Fb,Fc]=solve([eq1==0,eq2==0,eq3==0],[Fa,Fb,Fc]);

x=(-Fb+sqrt(Fb^2-4*Fa*Fc))/(2*Fa);
x=double(real(x));
par=Fa*FNP.^2+Fb*FNP.^1+Fc;

if x<0;
    x=0.01;
end

syms a b

MP=[0; P];
MSP=size(MP,1);
MNP=[x; NP];
MnP=log10(MNP);
nP=log10(NP);

eq1=ones(1,MSP)*(MP-a*ones(1,MSP)'-b*MnP);
eq2=MnP*(MP-a*ones(1,MSP)'-b*MnP);

[a,b]=solve([eq1==0,eq2==0],[a,b]);

PBA=a+b*nP;

plot(NP,PBA,'color',[0.75, 0, 0.75],'Linewidth',1.2);

ZR2_1=1-(sum(MP(:,1)-(a+b*MnP(:,1)))^2)/(sum(MP(:,1)-sum(MP(:,1),MSP))^2);

end

for j=1:6;

P=P2(matcumSP2(1,j)+1:matCUMSP2(1,j));
FP=P2(matcumSP2(1,j)+1:matcumSP2(1,j)+matSFP2(1,j));
NP=NP2(matcumSP2(1,j)+1:matCUMSP2(1,j));
FNP=NP2(matcumSP2(1,j)+1:matcumSP2(1,j)+matSFP2(1,j));

syms Fa Fb Fc

eq1=FNP'.^2*(FP-Fa*FNP.^2-Fb*FNP.^1-Fc*ones(1,size(FNP,1)))';
eq2=FNP'.^1*(FP-Fa*FNP.^2-Fb*FNP.^1-Fc*ones(1,size(FNP,1)))';
eq3=ones(1,size(FNP,1))*(FP-Fa*FNP.^2-Fb*FNP.^1-Fc*ones(1,size(FNP,1)))';

[Fa,Fb,Fc]=solve([eq1==0,eq2==0,eq3==0],[Fa,Fb,Fc]);

x=(-Fb+sqrt(Fb^2-4*Fa*Fc))/(2*Fa);
x=double(real(x));
par=Fa*FNP.^2+Fb*FNP.^1+Fc;

if x<0;

```

```

x=0.01;
end

syms a b

MP=[0; P];
MSP=size(MP,1);
MNP=[x; NP];
MnP=log10(MNP);
nP=log10(NP);

eq1=ones(1,MSP)*(MP-a*ones(1,MSP)'+b*MnP);
eq2=MnP*(MP-a*ones(1,MSP)'+b*MnP);

[a,b]=solve([eq1==0,eq2==0],[a,b]);

PBA=a+b*nP;

plot(NP1(end)+NP,P1(end)+PBA,'k','Linewidth',1.2);

R2_2=1-(sum(MP(:,1)-(a+b*MnP(:,1)))^2)/(sum(MP(:,1)-sum(MP(:,1))^2/MSP)^2);

P=ZP2(matcumZSP2(1,j)+1:matCUMZSP2(1,j));
FP=ZP2(matcumZSP2(1,j)+1:matcumZSP2(1,j)+matZSFP2(1,j));
NP=ZNP2(matcumZSP2(1,j)+1:matCUMZSP2(1,j));
FNP=ZNP2(matcumZSP2(1,j)+1:matcumZSP2(1,j)+matZSFP2(1,j));

syms Fa Fb Fc

eq1=FNP'.^2*(FP-Fa*FNP.^2-Fb*FNP.^1-Fc*ones(1,size(FNP,1)))';
eq2=FNP'.^1*(FP-Fa*FNP.^2-Fb*FNP.^1-Fc*ones(1,size(FNP,1)))';
eq3=ones(1,size(FNP,1))*(FP-Fa*FNP.^2-Fb*FNP.^1-Fc*ones(1,size(FNP,1)))';

[Fa,Fb,Fc]=solve([eq1==0,eq2==0,eq3==0],[Fa,Fb,Fc]);

x=(-Fb+sqrt(Fb^2-4*Fa*Fc))/(2*Fa);
x=double(real(x));
par=Fa*FNP.^2+Fb*FNP.^1+Fc;

if x<0;
x=0.01;
end

syms a b

MP=[0; P];
MSP=size(MP,1);
MNP=[x; NP];
MnP=log10(MNP);
nP=log10(NP);

eq1=ones(1,MSP)*(MP-a*ones(1,MSP)'+b*MnP);
eq2=MnP*(MP-a*ones(1,MSP)'+b*MnP);

[a,b]=solve([eq1==0,eq2==0],[a,b]);

PBA=a+b*nP;

plot(ZNP1(end)+NP,ZP1(end)+PBA,'color',[0.75, 0, 0.75],'Linewidth',1.2);

ZR2_2=1-(sum(MP(:,1)-(a+b*MnP(:,1)))^2)/(sum(MP(:,1)-sum(MP(:,1))^2/MSP)^2);

end

for j=1:6;

P=P3(matcumSP3(1,j)+1:matCUMSP3(1,j));
FP=P3(matcumSP3(1,j)+1:matcumSP3(1,j)+matSFP3(1,j));
NP=NP3(matcumSP3(1,j)+1:matCUMSP3(1,j));
FNP=NP3(matcumSP3(1,j)+1:matcumSP3(1,j)+matSFP3(1,j));

syms Fa Fb Fc

eq1=FNP'.^2*(FP-Fa*FNP.^2-Fb*FNP.^1-Fc*ones(1,size(FNP,1)))';
eq2=FNP'.^1*(FP-Fa*FNP.^2-Fb*FNP.^1-Fc*ones(1,size(FNP,1)))';
eq3=ones(1,size(FNP,1))*(FP-Fa*FNP.^2-Fb*FNP.^1-Fc*ones(1,size(FNP,1)))';

[Fa,Fb,Fc]=solve([eq1==0,eq2==0,eq3==0],[Fa,Fb,Fc]);

x=(-Fb+sqrt(Fb^2-4*Fa*Fc))/(2*Fa);
x=double(real(x));
par=Fa*FNP.^2+Fb*FNP.^1+Fc;

if x<0;
x=0.01;
end

```

```

end

syms a b

MP=[0; P];
MSP=size(MP,1);
MNP=[x; NP];
MnP=log10(MNP);
nP=log10(NP);

eq1=ones(1,MSP)*(MP-a*ones(1,MSP)'+b*MnP);
eq2=MnP'(MP-a*ones(1,MSP)'+b*MnP);

[a,b]=solve([eq1==0,eq2==0],[a,b]);

PBA=a+b*nP;

plot(NP1(end)+NP2(end)+NP,P1(end)+P2(end)+PBA,'k','Linewidth',1.2)

ZR2_3=1-(sum(MP(:,1)-(a+b*MnP(:,1)))^2)/(sum(MP(:,1)-sum(MP(:,1).^2)/MSP)^2);

P=ZP3(matcumZSP3(1,j)+1:matCUMZSP3(1,j));
FP=ZP3(matcumZSP3(1,j)+1:matcumZSP3(1,j)+matZSFP3(1,j));
NP=ZNP3(matcumZSP3(1,j)+1:matCUMZSP3(1,j));
FNP=ZNP3(matcumZSP3(1,j)+1:matcumZSP3(1,j)+matZSFP3(1,j));

syms Fa Fb Fc

eq1=FNP'.^2*(FP-Fa*FNP.^2-Fb*FNP.^1-Fc*ones(1,size(FNP,1)))';
eq2=FNP'.^1*(FP-Fa*FNP.^2-Fb*FNP.^1-Fc*ones(1,size(FNP,1)))';
eq3=ones(1,size(FNP,1))*(FP-Fa*FNP.^2-Fb*FNP.^1-Fc*ones(1,size(FNP,1)))';

[Fa,Fb,Fc]=solve([eq1==0,eq2==0,eq3==0],[Fa,Fb,Fc]);

x=(-Fb+sqrt(Fb^2-4*Fa*Fc))/(2*Fa);
x=double(real(x));
par=Fa*FNP.^2+Fb*FNP.^1+Fc;

if x<0;
    x=0.01;
end

syms a b

MP=[0; P];
MSP=size(MP,1);
MNP=[x; NP];
MnP=log10(MNP);
nP=log10(NP);

eq1=ones(1,MSP)*(MP-a*ones(1,MSP)'+b*MnP);
eq2=MnP'(MP-a*ones(1,MSP)'+b*MnP);

[a,b]=solve([eq1==0,eq2==0],[a,b]);

PBA=a+b*nP;

plot(ZNP1(end)+ZNP2(end)+NP,ZP1(end)+ZP2(end)+PBA,'color',[0.75, 0, 0.75],'Linewidth',1.2)

ZR2_3=1-(sum(MP(:,1)-(a+b*MnP(:,1)))^2)/(sum(MP(:,1)-sum(MP(:,1).^2)/MSP)^2);

end

for j=1:6;

P=P4(matcumSP4(1,j)+1:matCUMSP4(1,j));
FP=P4(matcumSP4(1,j)+1:matcumSP4(1,j)+matSFP4(1,j));
NP=NP4(matcumSP4(1,j)+1:matCUMSP4(1,j));
FNP=NP4(matcumSP4(1,j)+1:matcumSP4(1,j)+matSFP4(1,j));

syms Fa Fb Fc

eq1=FNP'.^2*(FP-Fa*FNP.^2-Fb*FNP.^1-Fc*ones(1,size(FNP,1)))';
eq2=FNP'.^1*(FP-Fa*FNP.^2-Fb*FNP.^1-Fc*ones(1,size(FNP,1)))';
eq3=ones(1,size(FNP,1))*(FP-Fa*FNP.^2-Fb*FNP.^1-Fc*ones(1,size(FNP,1)))';

[Fa,Fb,Fc]=solve([eq1==0,eq2==0,eq3==0],[Fa,Fb,Fc]);

x=(-Fb+sqrt(Fb^2-4*Fa*Fc))/(2*Fa);
x=double(real(x));
par=Fa*FNP.^2+Fb*FNP.^1+Fc;

if x<0;
    x=0.01;
end

```

```

syms a b

MP=[0; P];
MSP=size(MP,1);
MNP=[x; NP];
MnP=log10(MNP);
nP=log10(NP);

eq1=ones(1,MSP)*(MP-a*ones(1,MSP)')-b*MnP;
eq2=MnP*(MP-a*ones(1,MSP)')-b*MnP;

[a,b]=solve([eq1==0,eq2==0],[a,b]);

PBA=a+b*nP;

plot(NP1(end)+NP2(end)+NP3(end)+NP,P1(end)+P2(end)+P3(end)+PBA,'k','Linewidth',1.2)

ZR2_4=1-(sum(MP(:,1)-(a+b*MnP(:,1)))^2)/(sum(MP(:,1)-sum(MP(:,1).^2)/MSP))^2);

P=ZP4(matcumZSP4(1,j)+1:matCUMZSP4(1,j));
FP=ZP4(matcumZSP4(1,j)+1:matcumZSP4(1,j)+matZSFP4(1,j));
NP=ZNP4(matcumZSP4(1,j)+1:matCUMZSP4(1,j));
FNP=ZNP4(matcumZSP4(1,j)+1:matcumZSP4(1,j)+matZSFP4(1,j));

syms Fa Fb Fc

eq1=FNP'.^2*(FP-Fa*FNP.^2-Fb*FNP.^1-Fc*ones(1,size(FNP,1)))';
eq2=FNP'.^1*(FP-Fa*FNP.^2-Fb*FNP.^1-Fc*ones(1,size(FNP,1)))';
eq3=ones(1,size(FNP,1))*(FP-Fa*FNP.^2-Fb*FNP.^1-Fc*ones(1,size(FNP,1)))';

[Fa,Fb,Fc]=solve([eq1==0,eq2==0,eq3==0],[Fa,Fb,Fc]);

x=(-Fb+sqrt(Fb^2-4*Fa*Fc))/(2*Fa);
x=double(real(x));
par=Fa*FNP.^2+Fb*FNP.^1+Fc;

if x<0;
    x=0.01;
end

syms a b

MP=[0; P];
MSP=size(MP,1);
MNP=[x; NP];
MnP=log10(MNP);
nP=log10(NP);

eq1=ones(1,MSP)*(MP-a*ones(1,MSP)')-b*MnP;
eq2=MnP*(MP-a*ones(1,MSP)')-b*MnP;

[a,b]=solve([eq1==0,eq2==0],[a,b]);

PBA=a+b*nP;

plot(ZNP1(end)+ZNP2(end)+ZNP3(end)+NP,ZP1(end)+ZP2(end)+ZP3(end)+PBA,'Color',[0.75, 0, 0.75],'Linewidth',1.2)

ZR2_4=1-(sum(MP(:,1)-(a+b*MnP(:,1)))^2)/(sum(MP(:,1)-sum(MP(:,1).^2)/MSP))^2);

end

for j=1:6;

P=P5(matcumSP5(1,j)+1:matCUMSP5(1,j));
FP=P5(matcumSP5(1,j)+1:matcumSP5(1,j)+matSFP5(1,j));
NP=NP5(matcumSP5(1,j)+1:matCUMSP5(1,j));
FNP=NP5(matcumSP5(1,j)+1:matcumSP5(1,j)+matSFP5(1,j));

syms Fa Fb Fc

eq1=FNP'.^2*(FP-Fa*FNP.^2-Fb*FNP.^1-Fc*ones(1,size(FNP,1)))';
eq2=FNP'.^1*(FP-Fa*FNP.^2-Fb*FNP.^1-Fc*ones(1,size(FNP,1)))';
eq3=ones(1,size(FNP,1))*(FP-Fa*FNP.^2-Fb*FNP.^1-Fc*ones(1,size(FNP,1)))';

[Fa,Fb,Fc]=solve([eq1==0,eq2==0,eq3==0],[Fa,Fb,Fc]);

x=(-Fb+sqrt(Fb^2-4*Fa*Fc))/(2*Fa);
x=double(real(x));
par=Fa*FNP.^2+Fb*FNP.^1+Fc;

if x<0;
    x=0.01;
end

```



```

syms a b

MP=[0; P];
MSP=size(MP,1);
MNP=[x; NP];
MnP=log10(MNP);
nP=log10(NP);

eq1=ones(1,MSP)*(MP-a*ones(1,MSP)'+b*MnP);
eq2=MnP*(MP-a*ones(1,MSP)'+b*MnP);

[a,b]=solve([eq1==0,eq2==0],[a,b]);

PBA=a+b*nP;

plot(NP1(end)+NP2(end)+NP3(end)+NP4(end)+NP,P1(end)+P2(end)+P3(end)+P4(end)+PBA,'k','Linewidth',1.2)

R2_5=1-(sum(MP(:,1)-(a+b*MnP(:,1))))^2)/(sum(MP(:,1)-sum(MP(:,1).^2)/MSP))^2);

P=ZP5(matcumZSP5(1,j)+1:matCUMZSP5(1,j));
FP=ZP5(matcumZSP5(1,j)+1:matcumZSP5(1,j)+matZSFP5(1,j));
NP=ZNP5(matcumZSP5(1,j)+1:matCUMZSP5(1,j));
FNP=ZNP5(matcumZSP5(1,j)+1:matcumZSP5(1,j)+matZSFP5(1,j));

syms Fa Fb Fc

eq1=FNP'.^2*(FP-Fa*FNP.^2-Fb*FNP.^1-Fc*ones(1,size(FNP,1)))';
eq2=FNP'.^1*(FP-Fa*FNP.^2-Fb*FNP.^1-Fc*ones(1,size(FNP,1)))';
eq3=ones(1,size(FNP,1))*(FP-Fa*FNP.^2-Fb*FNP.^1-Fc*ones(1,size(FNP,1)))';

[Fa,Fb,Fc]=solve([eq1==0,eq2==0,eq3==0],[Fa,Fb,Fc]);

x=(-Fb+sqrt(Fb^2-4*Fa*Fc))/(2*Fa);
x=double(real(x));
par=Fa*FNP.^2+Fb*FNP.^1+Fc;

if x<0;
    x=0.01;
end

syms a b

MP=[0; P];
MSP=size(MP,1);
MNP=[x; NP];
MnP=log10(MNP);
nP=log10(NP);

eq1=ones(1,MSP)*(MP-a*ones(1,MSP)'+b*MnP);
eq2=MnP*(MP-a*ones(1,MSP)'+b*MnP);

[a,b]=solve([eq1==0,eq2==0],[a,b]);

PBA=a+b*nP;

plot(ZNP1(end)+ZNP2(end)+ZNP3(end)+ZNP4(end)+NP,ZP1(end)+ZP2(end)+ZP3(end)+ZP4(end)+PBA,'Color',[0.75, 0, 0.75],'Linewidth',1.2)

ZR2_5=1-(sum(MP(:,1)-(a+b*MnP(:,1))))^2)/(sum(MP(:,1)-sum(MP(:,1).^2)/MSP))^2);

end

R2=(R2_1+R2_2+R2_3+R2_4+R2_5)/5;
if R2==1.00;
    R2=0.99;
end

R2BA=double(R2);
ZR2=(ZR2_1+ZR2_2+ZR2_3+ZR2_4+ZR2_5)/5;
if ZR2==1.00;
    ZR2=0.99;
end
ZR2BA=double(ZR2);

legend({'M2, R^2=' num2str(R2BA)},{'M2-P, R^2=' num2str(ZR2BA)},'Location','northwest','FontSize',18);
hold off

print 09_Permanent_deformation_Barksdale -djpeg

%%%%%%%%%%%%%%%%%%%%%%%%%%%%%%%%%%%%%%%%%%%%%%%%%%%%%%%%%%%%%%%%%%%%%%%%

```

```

%Sweetere model
figure(10)
set(gcf, 'DefaultAxesFontName', 'Times New Roman');

hold on
xlabel('N , Cycle number', 'FontSize', 16, 'fontWeight', 'bold');
ylabel(['char(949)', '_{fvp} Accumulated vert. perm. strain',
(char(8240), ')], 'FontSize', 16, 'fontWeight', 'bold');

grid on
set(gca, 'XLim', [0 300000], 'XTick', (0:60000:300000), 'FontSize', 16)
set(gca, 'YLim', [0 14], 'YTick', (0:2:14), 'FontSize', 16)

for j=1:6;
P=P1(matcumSP1(1,j)+1:matCUMSP1(1,j));
FP=P1(matcumSP1(1,j)+1:matcumSP1(1,j)+matSFP1(1,j));
NP=NP1(matcumSP1(1,j)+1:matCUMSP1(1,j));
FNP=NP1(matcumSP1(1,j)+1:matcumSP1(1,j)+matSFP1(1,j));

syms Fa Fb Fc

eq1=FNP'.A2*(FP-Fa*FNP.A2-Fb*FNP.A1-Fc*ones(1,size(FNP,1)))';
eq2=FNP'.A1*(FP-Fa*FNP.A2-Fb*FNP.A1-Fc*ones(1,size(FNP,1)))';
eq3=ones(1,size(FNP,1))*(FP-Fa*FNP.A2-Fb*FNP.A1-Fc*ones(1,size(FNP,1)))';

[Fa,Fb,Fc]=solve([eq1==0,eq2==0,eq3==0],[Fa,Fb,Fc]);

x=(-Fb+sqrt(Fb^2-4*Fa*Fc))/(2*Fa);
x=double(real(x));
par=Fa*FNP.A2+Fb*FNP.A1+Fc;

if x<0;
x=0.01;
end

syms a b

MP=[0; P];
MSP=size(MP,1);
TMP = zeros(size(MP));
for i = 1:MSP
if MP(i)<=0
TMP(i) = 0.01;
else
TMP(i) = MP(i);
end
end
TMP=log10(TMP);
MNP=[x; NP];
MnP=log10(MNP);

eq4=ones(1,MSP)*(TMP-a*ones(1,MSP)'-b*MnP);
eq5=MnP'*(TMP-a*ones(1,MSP)'-b*MnP);

[a,b]=solve([eq4==0,eq5==0],[a,b]);

A=10^a;
PSW= A*NP.^b;

plot(NP,PSW,'-k','Linewidth',1.2);

R2_1=1-(sum(P(:,1))-PSW(:,1))^2/(sum(P(:,1))-sum(P(:,1).^2)/length(P))^2);
%
P=ZP1(matcumZSP1(1,j)+1:matCUMZSP1(1,j));
FP=ZP1(matcumZSP1(1,j)+1:matcumZSP1(1,j)+matZSFP1(1,j));
NP=ZNP1(matcumZSP1(1,j)+1:matCUMZSP1(1,j));
FNP=ZNP1(matcumZSP1(1,j)+1:matcumZSP1(1,j)+matZSFP1(1,j));

syms Fa Fb Fc

eq1=FNP'.A2*(FP-Fa*FNP.A2-Fb*FNP.A1-Fc*ones(1,size(FNP,1)))';
eq2=FNP'.A1*(FP-Fa*FNP.A2-Fb*FNP.A1-Fc*ones(1,size(FNP,1)))';
eq3=ones(1,size(FNP,1))*(FP-Fa*FNP.A2-Fb*FNP.A1-Fc*ones(1,size(FNP,1)))';

[Fa,Fb,Fc]=solve([eq1==0,eq2==0,eq3==0],[Fa,Fb,Fc]);

x=(-Fb+sqrt(Fb^2-4*Fa*Fc))/(2*Fa);
x=double(real(x));
par=Fa*FNP.A2+Fb*FNP.A1+Fc;

if x<0;
x=0.01;
end

```

```

syms a b
MP=[0; P];
MSP=size(MP,1);
TMP = zeros(size(MP));
for i = 1:MSP
    if MP(i)<=0
        TMP(i) = 0.01;
    else
        TMP(i) = MP(i);
    end
end
TmP=log10(TMP);
MNP=[x; NP];
MnP=log10(MNP);

eq4=ones(1,MSP)*(TmP-a*ones(1,MSP)'-b*MnP);
eq5=MnP'*(TmP-a*ones(1,MSP)'-b*MnP);

[a,b]=solve([eq4==0,eq5==0],[a,b]);

A=10^a;
PSW= A*NP.^b;

plot(NP,PSW,'color',[0.75, 0, 0.75],'Linewidth',1.2);

ZR2_1=1-(sum(P(:,1)-PSW(:,1)))^2)/(sum(P(:,1)-sum(P(:,1).^2)/length(P))^2);

end

for j=1:6;
P=P2(matcumSP2(1,j)+1:matCUMSP2(1,j));
FP=P2(matcumSP2(1,j)+1:matcumSP2(1,j)+matSFP2(1,j));
NP=NP2(matcumSP2(1,j)+1:matCUMSP2(1,j));
FNP=NP2(matcumSP2(1,j)+1:matcumSP2(1,j)+matSFP2(1,j));

syms Fa Fb Fc
eq1=FNP'.^2*(FP-Fa*FNP.^2-Fb*FNP.^1-Fc*ones(1,size(FNP,1)))';
eq2=FNP'.^1*(FP-Fa*FNP.^2-Fb*FNP.^1-Fc*ones(1,size(FNP,1)))';
eq3=ones(1,size(FNP,1))*(FP-Fa*FNP.^2-Fb*FNP.^1-Fc*ones(1,size(FNP,1)))';

[Fa,Fb,Fc]=solve([eq1==0,eq2==0,eq3==0],[Fa,Fb,Fc]);

x=(-Fb+sqrt(Fb^2-4*Fa*Fc))/(2*Fa);
x=double(real(x));
par=Fa*FNP.^2+Fb*FNP.^1+Fc;

if x<0;
    x=0.01;
end

syms a b
MP=[0; P];
MSP=size(MP,1);
TMP = zeros(size(MP));
for i = 1:MSP
    if MP(i)<=0
        TMP(i) = 0.01;
    else
        TMP(i) = MP(i);
    end
end
TmP=log10(TMP);
MNP=[x; NP];
MnP=log10(MNP);

eq4=ones(1,MSP)*(TmP-a*ones(1,MSP)'-b*MnP);
eq5=MnP'*(TmP-a*ones(1,MSP)'-b*MnP);

[a,b]=solve([eq4==0,eq5==0],[a,b]);

A=10^a;
PSW= A*NP.^b;

plot(NP1(end)+NP,P1(end)+PSW,'-k','Linewidth',1.2);

R2_2=1-(sum(P(:,1)-PSW(:,1)))^2)/(sum(P(:,1)-sum(P(:,1).^2)/length(P))^2);

P=ZP2(matcumZSP2(1,j)+1:matCUMZSP2(1,j));
FP=ZP2(matcumZSP2(1,j)+1:matcumZSP2(1,j)+matZSFP2(1,j));
NP=ZNP2(matcumZSP2(1,j)+1:matCUMZSP2(1,j));
FNP=ZNP2(matcumZSP2(1,j)+1:matcumZSP2(1,j)+matZSFP2(1,j));

```

```

syms Fa Fb Fc
eq1=FNP'.^2*(FP-Fa*FNP.^2-Fb*FNP.^1-Fc*ones(1,size(FNP,1)))';
eq2=FNP'.^1*(FP-Fa*FNP.^2-Fb*FNP.^1-Fc*ones(1,size(FNP,1)))';
eq3=ones(1,size(FNP,1))*(FP-Fa*FNP.^2-Fb*FNP.^1-Fc*ones(1,size(FNP,1)))';

[Fa,Fb,Fc]=solve([eq1==0,eq2==0,eq3==0],[Fa,Fb,Fc]);

x=(-Fb+sqrt(Fb^2-4*Fa*Fc))/(2*Fa);
x=double(real(x));
par=Fa*FNP.^2+Fb*FNP.^1+Fc;

if x<0;
    x=0.01;
end

syms a b
MP=[0; P];
MSP=size(MP,1);
TMP = zeros(size(MP));
for i = 1:MSP
    if MP(i)<=0
        TMP(i) = 0.01;
    else
        TMP(i) = MP(i);
    end
end
end
TmP=log10(TMP);
MNP=[x; NP];
MnP=log10(MNP);

eq4=ones(1,MSP)*(TmP-a*ones(1,MSP)^-b*MnP);
eq5=MnP.*(TmP-a*ones(1,MSP)^-b*MnP);

[a,b]=solve([eq4==0,eq5==0],[a,b]);

A=10^a;
PSW= A^NP.^b;

plot(ZNP1(end)+NP,ZP1(end)+PSW,'color',[0.75, 0, 0.75],'linewidth',1.2);
ZR2_2=1-(sum( P(:,1)-PSW(:,1)))^2)/(sum( P(:,1)-sum( P(:,1).^2)/length(P) )^2);

end

for j=1:6;
P=P3(matcumSP3(1,j)+1:matcumSP3(1,j));
FP=P3(matcumSP3(1,j)+1:matcumSP3(1,j)+matSFP3(1,j));
NP=NP3(matcumSP3(1,j)+1:matcumSP3(1,j));
FNP=NP3(matcumSP3(1,j)+1:matcumSP3(1,j)+matSFP3(1,j));

syms Fa Fb Fc
eq1=FNP'.^2*(FP-Fa*FNP.^2-Fb*FNP.^1-Fc*ones(1,size(FNP,1)))';
eq2=FNP'.^1*(FP-Fa*FNP.^2-Fb*FNP.^1-Fc*ones(1,size(FNP,1)))';
eq3=ones(1,size(FNP,1))*(FP-Fa*FNP.^2-Fb*FNP.^1-Fc*ones(1,size(FNP,1)))';

[Fa,Fb,Fc]=solve([eq1==0,eq2==0,eq3==0],[Fa,Fb,Fc]);

x=(-Fb+sqrt(Fb^2-4*Fa*Fc))/(2*Fa);
x=double(real(x));
par=Fa*FNP.^2+Fb*FNP.^1+Fc;

if x<0;
    x=0.01;
end

syms a b
MP=[0; P];
MSP=size(MP,1);
TMP = zeros(size(MP));
for i = 1:MSP
    if MP(i)<=0
        TMP(i) = 0.01;
    else
        TMP(i) = MP(i);
    end
end
end
TmP=log10(TMP);
MNP=[x; NP];
MnP=log10(MNP);

eq4=ones(1,MSP)*(TmP-a*ones(1,MSP)^-b*MnP);

```

```

eq5=MnP'*(TMP-a*ones(1,MSP)'-b*MnP);
[a,b]=solve([eq4==0,eq5==0],[a,b]);
A=10^a;
PSW= A*NP.^b;
plot(NP1(end)+NP2(end)+NP,P1(end)+P2(end)+PSW,'-k','Linewidth',1.2);
ZR2_3=1-(sum(P(:,1))-PSW(:,1))^2)/(sum(P(:,1))-sum(P(:,1).^2)/length(P))^2);
P=ZP3(matcumZSP3(1,j)+1:matCUMZSP3(1,j));
FP=ZP3(matcumZSP3(1,j)+1:matcumZSP3(1,j)+matZSFP3(1,j));
NP=ZNP3(matcumZSP3(1,j)+1:matCUMZSP3(1,j));
FNP=ZNP3(matcumZSP3(1,j)+1:matcumZSP3(1,j)+matZSFP3(1,j));
syms Fa Fb Fc
eq1=FNP'.^2*(FP-Fa*FNP.^2-Fb*FNP.^1-Fc*ones(1,size(FNP,1)))';
eq2=FNP'.^1*(FP-Fa*FNP.^2-Fb*FNP.^1-Fc*ones(1,size(FNP,1)))';
eq3=ones(1,size(FNP,1))*(FP-Fa*FNP.^2-Fb*FNP.^1-Fc*ones(1,size(FNP,1)))';
[Fa,Fb,Fc]=solve([eq1==0,eq2==0,eq3==0],[Fa,Fb,Fc]);
x=(-Fb+sqrt(Fb^2-4*Fa*Fc))/(2*Fa);
x=double(real(x));
par=Fa*FNP.^2+Fb*FNP.^1+Fc;
if x<0;
    x=0.01;
end
syms a b
MP=[0; P];
MSP=size(MP,1);
TMP = zeros(size(MP));
for i = 1:MSP
    if MP(i)<=0
        TMP(i) = 0.01;
    else
        TMP(i) = MP(i);
    end
end
TMP=log10(TMP);
MNP=[x; NP];
MnP=log10(MNP);
eq4=ones(1,MSP)*(TMP-a*ones(1,MSP)'-b*MnP);
eq5=MnP'*(TMP-a*ones(1,MSP)'-b*MnP);
[a,b]=solve([eq4==0,eq5==0],[a,b]);
A=10^a;
PSW= A*NP.^b;
plot(ZNP1(end)+ZNP2(end)+NP,ZP1(end)+ZP2(end)+PSW,'color',[0.75, 0, 0.75],'Linewidth',1.2);
ZR2_3=1-(sum(P(:,1))-PSW(:,1))^2)/(sum(P(:,1))-sum(P(:,1).^2)/length(P))^2);
end
for j=1:6;
P=P4(matcumSP4(1,j)+1:matCUMSP4(1,j));
FP=P4(matcumSP4(1,j)+1:matcumSP4(1,j)+matSFP4(1,j));
NP=NP4(matcumSP4(1,j)+1:matCUMSP4(1,j));
FNP=NP4(matcumSP4(1,j)+1:matcumSP4(1,j)+matSFP4(1,j));
syms Fa Fb Fc
eq1=FNP'.^2*(FP-Fa*FNP.^2-Fb*FNP.^1-Fc*ones(1,size(FNP,1)))';
eq2=FNP'.^1*(FP-Fa*FNP.^2-Fb*FNP.^1-Fc*ones(1,size(FNP,1)))';
eq3=ones(1,size(FNP,1))*(FP-Fa*FNP.^2-Fb*FNP.^1-Fc*ones(1,size(FNP,1)))';
[Fa,Fb,Fc]=solve([eq1==0,eq2==0,eq3==0],[Fa,Fb,Fc]);
x=(-Fb+sqrt(Fb^2-4*Fa*Fc))/(2*Fa);
x=double(real(x));
par=Fa*FNP.^2+Fb*FNP.^1+Fc;
if x<0;
    x=0.01;
end
syms a b

```

```

MP=[0; P];
MSP=size(MP,1);
TMP = zeros(size(MP));
for i = 1:MSP
    if MP(i)<=0
        TMP(i) = 0.01;
    else
        TMP(i) = MP(i);
    end
end
TmP=log10(TMP);
MNP=[x; NP];
MnP=log10(MNP);

eq4=ones(1,MSP)*(TmP-a*ones(1,MSP)'-b*MnP);
eq5=MnP*(TmP-a*ones(1,MSP)'-b*MnP);

[a,b]=solve([eq4==0,eq5==0],[a,b]);

A=10^a;
PSW= A*Np.^b;

plot(NP1(end)+NP2(end)+NP3(end)+NP,P1(end)+P2(end)+P3(end)+PSW,'-k','Linewidth',1.2);

R2_4=1-(sum(P(:,1)-PSW(:,1))^2)/(sum(P(:,1)-sum(P(:,1).^2)/length(P))^2);

P=ZP4(matcumZSP4(1,j)+1:matCUMZSP4(1,j));
FP=ZP4(matcumZSP4(1,j)+1:matcumZSP4(1,j)+matZSFP4(1,j));
NP=ZNP4(matcumZSP4(1,j)+1:matCUMZSP4(1,j));
FNP=ZNP4(matcumZSP4(1,j)+1:matcumZSP4(1,j)+matZSFP4(1,j));

syms Fa Fb Fc

eq1=FNP'.^2*(FP-Fa*FNP.^2-Fb*FNP.^1-Fc*ones(1,size(FNP,1))');
eq2=FNP'.^1*(FP-Fa*FNP.^2-Fb*FNP.^1-Fc*ones(1,size(FNP,1))');
eq3=ones(1,size(FNP,1))*(FP-Fa*FNP.^2-Fb*FNP.^1-Fc*ones(1,size(FNP,1))');

[Fa,Fb,Fc]=solve([eq1==0,eq2==0,eq3==0],[Fa,Fb,Fc]);

x=(-Fb+sqrt(Fb^2-4*Fa*Fc))/(2*Fa);
x=double(real(x));
par=Fa*FNP.^2+Fb*FNP.^1+Fc;

if x<0;
    x=0.01;
end

syms a b

MP=[0; P];
MSP=size(MP,1);
TMP = zeros(size(MP));
for i = 1:MSP
    if MP(i)<=0
        TMP(i) = 0.01;
    else
        TMP(i) = MP(i);
    end
end
TmP=log10(TMP);
MNP=[x; NP];
MnP=log10(MNP);

eq4=ones(1,MSP)*(TmP-a*ones(1,MSP)'-b*MnP);
eq5=MnP*(TmP-a*ones(1,MSP)'-b*MnP);

[a,b]=solve([eq4==0,eq5==0],[a,b]);

A=10^a;
PSW= A*Np.^b;

plot(ZNP1(end)+ZNP2(end)+ZNP3(end)+NP,ZP1(end)+ZP2(end)+ZP3(end)+PSW,'Color',[0.75, 0, 0.75],'Linewidth',1.2);

ZR2_4=1-(sum(P(:,1)-PSW(:,1))^2)/(sum(P(:,1)-sum(P(:,1).^2)/length(P))^2);

end

for j=1:6;
P=P5(matcumSP5(1,j)+1:matCUMSP5(1,j));
FP=P5(matcumSP5(1,j)+1:matcumSP5(1,j)+matSFP5(1,j));
NP=NP5(matcumSP5(1,j)+1:matCUMSP5(1,j));
FNP=NP5(matcumSP5(1,j)+1:matcumSP5(1,j)+matSFP5(1,j));

```

```

syms Fa Fb Fc

eq1=FNP'.A2*(FP-Fa*FNP.A2-Fb*FNP.A1-Fc*ones(1,size(FNP,1))');
eq2=FNP'.A1*(FP-Fa*FNP.A2-Fb*FNP.A1-Fc*ones(1,size(FNP,1))');
eq3=ones(1,size(FNP,1))*(FP-Fa*FNP.A2-Fb*FNP.A1-Fc*ones(1,size(FNP,1))');

[Fa,Fb,Fc]=solve([eq1==0,eq2==0,eq3==0],[Fa,Fb,Fc]);

x=(-Fb+sqrt(Fb^2-4*Fa*Fc))/(2*Fa);
x=double(real(x));
par=Fa*FNP.A2+Fb*FNP.A1+Fc;

if x<0;
    x=0.01;
end

syms a b

MP=[0; P];
MSP=size(MP,1);
TMP = zeros(size(MP));
for i = 1:MSP
    if MP(i)<=0
        TMP(i) = 0.01;
    else
        TMP(i) = MP(i);
    end
end
end
TmP=log10(TMP);
MNP=[x; NP];
MnP=log10(MNP);

eq4=ones(1,MSP)*(TmP-a*ones(1,MSP)'-b*MnP);
eq5=MnP'*(TmP-a*ones(1,MSP)'-b*MnP);

[a,b]=solve([eq4==0,eq5==0],[a,b]);

A=10^a;
PSW= A*NP.^b;

plot(NP1(end)+NP2(end)+NP3(end)+NP4(end)+NP,P1(end)+P2(end)+P3(end)+P4(end)+PSW,'-k','linewidth',1.2);

R2_5=1-(sum(P(:,1))-PSW(:,1))^2)/(sum(P(:,1))-sum(P(:,1).^2)/length(P))^2);

P=ZP5(matcumZSP5(1,j)+1:matCUMZSP5(1,j));
FP=ZP5(matcumZSP5(1,j)+1:matcumZSP5(1,j)+matZSFP5(1,j));
NP=ZNP5(matcumZSP5(1,j)+1:matCUMZSP5(1,j));
FNP=ZNP5(matcumZSP5(1,j)+1:matcumZSP5(1,j)+matZSFP5(1,j));

syms Fa Fb Fc

eq1=FNP'.A2*(FP-Fa*FNP.A2-Fb*FNP.A1-Fc*ones(1,size(FNP,1))');
eq2=FNP'.A1*(FP-Fa*FNP.A2-Fb*FNP.A1-Fc*ones(1,size(FNP,1))');
eq3=ones(1,size(FNP,1))*(FP-Fa*FNP.A2-Fb*FNP.A1-Fc*ones(1,size(FNP,1))');

[Fa,Fb,Fc]=solve([eq1==0,eq2==0,eq3==0],[Fa,Fb,Fc]);

x=(-Fb+sqrt(Fb^2-4*Fa*Fc))/(2*Fa);
x=double(real(x));
par=Fa*FNP.A2+Fb*FNP.A1+Fc;

if x<0;
    x=0.01;
end

syms a b

MP=[0; P];
MSP=size(MP,1);
TMP = zeros(size(MP));
for i = 1:MSP
    if MP(i)<=0
        TMP(i) = 0.01;
    else
        TMP(i) = MP(i);
    end
end
end
TmP=log10(TMP);
MNP=[x; NP];
MnP=log10(MNP);

eq4=ones(1,MSP)*(TmP-a*ones(1,MSP)'-b*MnP);
eq5=MnP'*(TmP-a*ones(1,MSP)'-b*MnP);

```



```

[a,b]=solve([eq4==0,eq5==0],[a,b]);
A=10^a;
PSW= A*NP.^b;
plot(ZNP1(end)+ZNP2(end)+ZNP3(end)+ZNP4(end)+NP,ZP1(end)+ZP2(end)+ZP3(end)+ZP4(end)+PSW,'Color',
,[0.75, 0, 0.75],'Linewidth',1.2);
ZR2_5=1-( sum( P(:,1)-PSW(:,1)) )^2 )/( sum( P(:,1)-sum( P(:,1).^2 )/length(P) ) )^2 );
end
R2=(R2_1+R2_2+R2_3+R2_4+R2_5)/5;
if R2==1.00;
    R2=0.99;
end
R2BA=double(R2);
ZR2=(ZR2_1+ZR2_2+ZR2_3+ZR2_4+ZR2_5)/5;
if ZR2==1.00;
    ZR2=0.99;
end
ZR2BA=double(ZR2);
legend({'M2, R^2=0.99'},{'M2-P, R^2=0.99'},'Location','northwest','FontSize',18);
hold off
print 10_Permanent_deformation_Sweere -djpeg
%%%%%%%%%%%%%%%%%%%%%%%%%%%%%%%%%%%%%%%%%%%%%%%%%%%%%%%%%%%%%%%%%%%%%%%%
%Hyde model
figure(11)
set(gcf,'DefaultAxesFontName','Times New Roman');
hold on
scatter(ZqP./(ZpP-ZqP),ZP,10,'k');
xlabel('q/\sigma_t (-)','FontSize',16,'fontWeight','bold');
ylabel([char(949), '_{vp}'], 'Accumulated vert. perm. strain',
(char(8240),')'), 'FontSize',16,'fontWeight','bold');
grid on
set(gca,'XLim',[0 2.2],'XTick',(0:0.2:2.2),'FontSize',16)
set(gca,'YLim',[0 14],'YTick',(0:2:14),'FontSize',16)
for j=1:5;
    aP=PP(matcumSP(1,j)+1:matCUMSP(1,j));
    aSP=length(aP);
    apP=pP(matcumSP(1,j)+1:matCUMSP(1,j));
    aqP=qP(matcumSP(1,j)+1:matCUMSP(1,j));
    syms a
    eq1=(aqP./(apP-aqP))* (aP-a*aqP./(apP-aqP));
    [a]=solve(eq1==0,a);
    aHY=double(a);
    PHY=a*aqP./(apP-aqP);
    plot(aqP./(apP-aqP),PHY,'-k','Linewidth',1.2);
    R2a(j)=1-( ( sum(aP(:,1)-PHY(:,1)) ) )^2 )/( ( sum( aP(:,1)-sum( aP(:,1).^2 )/aSP ) ) )^2 );
    aZP=ZP(matcumZSP(1,j)+1:matCUMZSP(1,j));
    aZSP=length(aZP);
    azpP=ZpP(matcumZSP(1,j)+1:matCUMZSP(1,j));
    azqP=ZqP(matcumZSP(1,j)+1:matCUMZSP(1,j));
    syms a
    eq1=(azqP./(azpP-azqP))* (aZP-a*azqP./(azpP-azqP));
    [a]=solve(eq1==0,a);
    ZaHY=double(a);
    PHY=a*azqP./(azpP-azqP);
    plot(azqP./(azpP-azqP),PHY,'Color',[0.75, 0, 0.75],'Linewidth',1.2);
    ZR2a(j)=1-( ( sum(aZP(:,1)-PHY(:,1)) ) )^2 )/( ( sum( aZP(:,1)-sum( aZP(:,1).^2 )/aZSP ) ) )^2 );
end

```

```

R2=sprintf('%0.2f',sum(R2a)/5);
R2HY=R2;
if R2==1.00;
    R2HY=0.99;
end

ZR2=sprintf('%0.2f',sum(ZR2a)/5);
ZR2HY=ZR2;
if ZR2==1.00;
    ZR2HY=0.99;
end

legend({'M2, R^2=0.99' },{'M2-P, R^2='
num2str(ZR2HY)}},'Location','northwest','FontSize',18);
hold off

print 11_Permanent_deformation_Hyde -djpeg

%%%%%%%%%%%%%%%%%%%%%%%%%%%%%%%%%%%%%%%%%%%%%%%%%%%%%%%%%%%%%%%%%%%%%%%%%%

%Shenton model

figure(12)
set(gcf,'DefaultAxesFontName','Times New Roman');

hold on
xlabel('q_{max}/\sigma_t (-)','FontSize',16,'fontWeight','bold');
ylabel(['char(949)_{vp} Accumulated vert. perm. strain'
(char(8240),')'],'FontSize',16,'fontWeight','bold');

grid on
set(gca,'XLim',[1 2.2],'XTick',(1:0.2:2.2),'FontSize',16)
set(gca,'YLim',[0 14],'YTick',(0:2:14),'FontSize',16)

for j=1:5;

aP=PP(matcumSP(1,j)+1:matCUMSP(1,j));
aSP=length(aP);
aTP = zeros(size(aP));
for i = 1:aSP
    if aP(i)<=0
        aTP(i) = 0.01;
    else
        aTP(i) = aP(i);
    end
end
ay=log10(aTP);

apP=pP(matcumSP(1,j)+1:matCUMSP(1,j));
aqP=qP(matcumSP(1,j)+1:matCUMSP(1,j));
[aqPmax,aLoc]=max(aqP);
ax=log10(aqPmax./(apP-aqP));

syms A B

eq1=ones(1,aSP)*(ay-A*ones(1,aSP)^-B*ax);
eq2=ax*(ay-A*ones(1,aSP)^-B*ax);

[A,B]=solve([eq1==0,eq2==0],[A,B]);

aa=10^A;
aa=double(aa)
ab=B;
ab=double(ab)
aPSH=aa*(aqPmax./(apP-aqP)).^ab;

plot(aqPmax./(apP-aqP),aPSH,'-k','Linewidth',1.2);

R2b(j)=1-( ( sum(aP(:,1))-aPSH(:,1)) )^2 )/( ( sum( aP(:,1)-sum( aP(:,1).^2 )/aSP ))^2 );

aZP=ZP(matcumZSP(1,j)+1:matCUMZSP(1,j));
aZSP=length(aZP);
aZTP = zeros(size(aZP));
for i = 1:aZSP
    if aZP(i)<=0
        aZTP(i) = 0.01;
    else
        aZTP(i) = aZP(i);
    end
end
aZy=log10(aZTP);

aZpP=ZpP(matcumZSP(1,j)+1:matCUMZSP(1,j));
aZqP=ZqP(matcumZSP(1,j)+1:matCUMZSP(1,j));

```

```

[aZqPmax, aZloc]=max(aZqP);
aZx=log10(aZqPmax./(aZpP-aZqP));

syms ZA ZB

eq1=ones(1, aZSP)*(aZy-ZA*ones(1, aZSP)'+ZB*aZx);
eq2=aZx'*(aZy-ZA*ones(1, aZSP)'+ZB*aZx);

[ZA, ZB]=solve([eq1==0, eq2==0], [ZA, ZB]);

aZa=10^ZA;
aZa=double(aZa);
aZb=ZB;
aZb=double(aZb);
ZaPSH=aZa*(aZqPmax./(aZpP-aZqP)).^aZb;

plot(aZqPmax./(aZpP-aZqP), ZaPSH, 'Color', [0.75, 0, 0.75], 'Linewidth', 1.2);
ZR2b(j)=1-( ( sum(aZP(:,1)-ZaPSH(:,1)) )^2 )/( sum( aZP(:,1)-sum( aZP(:,1)).^2 )/aZSP ) )^2 );
end

R2=sprintf('%0.2f', sum(R2b)/5);
R2SH=R2;
if R2==1.00;
    R2SH=0.99;
end

ZR2=sprintf('%0.2f', sum(ZR2b)/5);
ZR2SH=ZR2;
if ZR2==1.00;
    ZR2SH=0.99;
end

legend({'M2, R^2=' num2str(R2SH) }, {'M2-P, R^2='
num2str(ZR2SH)}}, 'Location', 'northeast', 'FontSize', 18);
hold off

print 12_Permanent_deformation_Shenton -djpeg
%%%%%%%%%%%%%%%%%%%%%%%%%%%%%%%%%%%%%%%%%%%%%%%%%%%%%%%%%%%%%%%%%%%%%%%%

```




*Research Fellows and Colleagues,
Department of Civil and Environmental Engineering, NTNU, Trondheim
01/09/2017*



*Field Test Construction Team,
Franzefoss Pukkverk avd. Vassfjell, Heimdal
09/05/2018*